Performance Assessment and Retrofit Strategies for Unreinforced Masonry Structures

MINA PEZESHKI

A THESIS SUBMITTED TO THE FACULTY OF GRADUATE STUDIES IN PARTIAL FULFILLMENT OF THE REQUIREMENTS FOR THE DEGREE OF MASTER OF APPLIED SCIENCE

GRADUATE PROGRAM IN CIVIL ENGINEERING

YORK UNIVERSITY

TORONTO, ONTARIO

JANUARY 2024

Abstract

This thesis presents a comprehensive study on the seismic assessment and retrofitting of unreinforced masonry (URM) structures, with a particular emphasis on intervention methods that are compatible with restoration of URM structures with heritage importance. The research investigates the mechanical behavior of masonry and applies advanced numerical modeling techniques to understand the dynamic response of URM buildings under seismic loads. Key aspects such as natural frequencies, mass participation, deformation patterns, and their correlation with actual damage patterns are examined. A pivotal contribution of this work is the evaluation of advanced seismic assessment methodologies, offering a nuanced understanding of URM structures' failure modes. This enhances prediction accuracy and contributes to improvements in seismic codes and seismic evaluation guidelines for existing URM structures. The thesis also pioneers in analyzing various retrofitting techniques, balancing the need for seismic resilience with heritage conservation, ensuring international standards compatibility. Further advancements are made in nonlinear modeling, specifically in addressing challenges in material behavior representation and simulation convergence. These advancements are validated through practical applications using SAP2000, including sensitivity analyses. The thesis highlights how the effectiveness of these models is influenced by the presence of stiff diaphragms in URM structures, a crucial factor in retrofitting buildings with timber floors prevalent in heritage construction. A significant portion of the study demonstrates the effectiveness of three-dimensional finite element modeling with shell-type elements. This approach is pivotal in evaluating URM structures' dynamic response and capturing the common occurrence of out-of-plane failures in the absence of stiff diaphragms. The research leads to important practical conclusions regarding the applicability and idealization of the established method of analysis used till now in seismic evaluation of URM constructions, which is based on the Equivalent Frame Idealization. It is illustrated that with the advent of modern nonlinear shell element analysis methods it is possible to leap to a new paradigm in the seismic evaluation of URM structures that no longer requires unrealistic idealization of surface components into linear beam-column elements as is the case with the Equivalent Frame Analysis.

Acknowledgements

I would like to express my sincere and deepest gratitude to my supervisor, Dr. Stavroula Pantazopoulou, for her guidance and support, and for providing me with the opportunity to have such a valuable experience at York University for my Master's degree. Learning from her has been an honor, and without her guidance, this thesis would not have been possible.

Special thanks go to Ms. Sindy Mahal for all her help and kind support. I also want to extend my gratitude to all my friends and colleagues who supported me throughout my graduate studies: Malihe, Behnam, Siamak, Farah, Zoie, Roberto, and Sina.

I am forever grateful to my parents especially to my husband, Farhad, for always being there and supporting me in achieving my goals.

Table of Contents

List of Figures

List of Tables

1. Introduction

1.1 Research Motivation

Heritage structures serve as custodians of past civilizations, safeguarding cultural legacies. Unreinforced masonry (URM) was a prevalent construction method from ancient times through the 19th and early 20th centuries. Despite their historical significance, URM buildings proved susceptible to earthquakes, resulting in significant economic and cultural losses.

Contemporary earthquake engineering highlights the importance of URM seismic evaluation, recognizing the inherent lack of seismic resistance in unreinforced masonry as a risk to human life and heritage. Utilizing advanced software and modeling techniques becomes imperative for assessing URM structures' seismic performance and predicting their resistance to seismic hazards.

Recent earthquakes have emphasized the financial toll of physical damage, particularly in regions with URM buildings. Masonry restoration demands expertise and costly materials. Despite technical and scientific awareness, public and political attention to this issue remains limited in some areas.

Due to their unique characteristics, heritage structures with URM pose distinct challenges in seismic assessment and restoration. This project focuses on methods of assessment of existing URM (Unreinforced Masonry) structures against earthquakes and explores the effectiveness of the most prevalent approaches used for seismic upgrading of such structures. It explores the limitations of computer modeling in carrying out comprehensive seismic evaluation, with the intent to improve seismic performance, identify the pertinent modelling approaches to represent the dynamic characteristics of composite masonry, and assess various strengthening strategies. Challenges include the distributed stiffness and mass of heritage buildings, along with the absence of diaphragm action, complicating conventional nonlinear analysis.

Additionally, the thesis will delve into the maintenance and repair issues of heritage buildings, offering recommendations for their sustained upkeep and management that are compatible with International Conventions and Treaties as to the preservation of the built heritage, such as principles of reversibility and non-invasiveness as outlined by the International Council on Monuments and Sites in the Venice Charter (1964). In navigating the complexity of heritage structures and considering these limitations on the extent of plausible intervention techniques, it is essential to fully understand the seismic protection effectiveness of selected scenarios used in preservation, restoration, and strengthening. These issues are explored in the thesis in a computational context using 3-D finite element modelling methods.

Heritage structures act as tangible testaments to bygone civilizations, embodying technological advancements, aesthetics, customs, religious practices, art, defense, or governance. They play a pivotal role in the historical evolution of their respective societies. However, the materials in these historic buildings degrade over time due to exposure to the elements, risking the integrity of this cultural asset. The potential impact of a seismic hazard compatible with the seismicity of the region where the heritage URM is located, and the ensuing cultural losses is inherently fraught with a great degree of uncertainty (Pantazopoulou, 2013).

Presently, there is a scarcity of sophisticated software capable of effectively analyzing certain performance limit states that are associated with a significant degree of damage (e.g. repairable condition). This limitation is attributed to the complex nature of material behavior under mechanical stresses and the inherent uncertainty in defining the load paths in the structural system of URM buildings on account of the massive walls and the frequent absence of diaphragms. Industry focus currently revolves around implementing modeling methodologies to create a versatile procedure for assessing various types of URM structures and materials (Valadao, 2021).

Recent seismic disasters underscore the substantial economic losses incurred from physical damage, especially when a significant portion of a community's building stock comprises unreinforced masonry (URM) buildings. URMs are often considered highly susceptible to seismic forces, and the subsequent need for skilled builders to undertake costly and time-consuming repair procedures further compounds the issue. Despite acknowledgment within the International Scientific Committee on Structures of Architectural Heritage (e.g., ISCARSAH) societal and political awareness of these problems remains relatively low (ISCARSAH GUIDELINES 2005). Efficient seismic risk reduction requires the analytical quantification of decision factors, such as monetary loss, for communication with stakeholders like building owners, policymakers, and insurance companies. To address this demand, new assessment techniques have been incorporated into technical recommendations in some regions where built cultural heritage is considered a high priority (e.g. parts of Europe, https://iscarsah.org/); but there is significant difference in approaches taken in different codes, to conduct the assessment. There are several reasons for this state of practice, one being that the types of URM structures, the materials and methods of construction vary vastly from one region to the next, rendering the experience and knowledge collected from field observation very region specific. In this thesis the most prevalent and Codified method used for assessment, known as frame approach, which involves significant degree of simplification and idealization of the structural system is compared against detailed finite element modeling – this is intended to identify the limitations of the Assessment code procedures and to illustrate ways to bypass these limitations by taking advantage of currently available modelling tools in the Finite Element context.

1.2 Current State of Art

The methodology followed in this thesis comprises the comparative evaluation of different computational modelling methods used in seismic assessment of URM structures such as the detailed seismic evaluation procedures prescribed in ASCE/SEI 41 (2017). To identify the differences in the performance of different approaches, a test structure is used as benchmark. The structure is a two-storey brick house, built at ½ scale of a reference full scale prototype, with flexible diaphragms (Bothara, Dhakal and Mander, 2010). The building was tested on a shaking table to a suite of strong ground motions of increasing intensity whereas damage accumulation is reflected by the gradual change of the fundamental dynamic characteristics of the building. Approaches for seismic assessment that are recommended by seismic evaluation Codes such as the ASCE/SEI 41 (2017) are studied while highlighting limitations of existing modeling approaches. It is noted that the recommended code method is the so-called Equivalent Frame Analysis whereas a prevalent alternative is the Detailed 3-D shell nonlinear analysis that is used in research. It is shown that the URM buildings' distributed stiffness, mass, and lack of diaphragm action pose challenges to conventional nonlinear analysis.

Once the corresponding models are calibrated to match the experimental evidence, they are used to study the knowledge gaps outlined in the following paragraph, through a series of parametric studies.

Another aspect is the evaluation through numerical modelling, of sustainable retrofitting strategies, addressing issues such as the low material strengths of the masonry joints, and the complex behavior of the masonry composite to lateral shear.

1.3 Problem Statement

This research endeavors to bridge a significant knowledge gap within seismic assessment for Unreinforced Masonry (URM) structures. The focal point revolves around the intrinsic uncertainty entailing the dynamic, nonlinear behavior of these structures during seismic events.

- Spatial Mass Distribution and Diaphragm Absence: The origin of this uncertainty lies in the height-wise distribution of mass and continuous stiffness, coupled with the prevalent absence of diaphragm action across floors and roofs. These attributes distinctly characterize heritage masonry structures, differentiating them from contemporary reinforced concrete buildings and therefore require specialized computational idealization methods.
- Vulnerability Arising from Mass Concentration in Masonry Walls: A notable portion of the mass encased within masonry walls diverges from the conventional floor and roof distribution. Consequently, untied and unreinforced masonry walls face susceptibility to out-of-plane forces propelled by substantial lateral inertia forces. Their resistance against out-of-plane flexural action remains minimal, reliant upon pre-compression derived from vertical loads.
- Challenges Inherent in Material Nonlinearity and Modeling: The intricate material nonlinearity and modeling uncertainties inherent in URM structures have given rise to a scarcity of viable seismic assessment methods and there is practically no background training in engineering disciplines in this area, so that they can be used with confidence by practitioners.
- Nonlinear Nature of Masonry Wall Behavior: Masonry walls function as continuous shells, showcasing nonlinear behavior under both in-plane and out-of-plane actions, thereby introducing complexity of mechanistic response.
- Convergence Issues and Limited Simulations: The intricacy of material behavior and the stark brittleness of masonry in tension in the absence of reinforcement, poses significant challenges when it comes to achieving convergence under the influence of reversed cyclic loading. Only a limited number of nonlinear simulations have hitherto addressed this intricate representation.

1.4 Research Objective

The study encompasses computational modeling, dynamic analysis, and detailed numerical investigation. This holistic approach aims to develop reliable seismic assessment techniques for heritage structures with unreinforced masonry, contributing to a comprehensive understanding of URM behavior and effective seismic risk mitigation strategies for culturally significant buildings. The methodology employed in this research comprises three primary components, each addressing crucial aspects of the study: 1) Calibration and Validation of Computational Models, 2) Analysis of Dynamic Response and Failure Characteristics, and 3) Numerical parametric investigation of the effect of diaphragms in reducing the damage and vulnerability of masonry, along with other retrofitting procedures such as repointing of joints to enhance material stiffness and strength. A detailed breakdown of each component is presented below:

1.4.1 Calibration and Validation of Computational Models

This phase begins with the calibration of a computational model of a brick masonry building previously tested on a shake table by Bothara and Mander in 2010. Utilizing the SAP2000 program, the lateral load analysis employs two distinct approaches:

a) Equivalent Frame Analysis: This method involves substituting walls and spandrels with equivalent beam/column elements, following ASCE/SEI-41 guidelines. Nonlinear hinge elements in SAP2000, with properties specified in ASCE/SEI-41 tables for URM buildings, are incorporated.
b) Shell Idealization: Shell elements are used to model building walls, with floors and roofs adopting an approach from Ryan Valadao's NIKER project thesis. The analysis begins with linear elastic response, transitioning to nonlinear response when needed. It covers gravity loads, lateral pushover analysis, and nonlinear modal analysis.

1.4.2 Analysis of Dynamic Response and Failure Characteristics

Field evidence from past earthquakes establishes practical criteria for assessing masonry structures, particularly out-of-plane failure modes. The numerical investigation aims to provide insights into nonlinear masonry modeling, estimating critical properties such as the effective modulus of elasticity, compressive and composite shear strength, and deformation capacities. Comparisons with ASCE-SEI 41 empirical equations are used to check the relevance of the code acceptance criteria. The study also validates a seismic assessment methodology for structures lacking diaphragm action, correlating deformation demand with measured lateral deformation profiles.

1.5 Organization of the Thesis

This thesis marks the completion of a study delving into the mechanical characteristics of masonry, with a specific emphasis on relevant numerical modeling methods for both masonry and unreinforced masonry (URM) structures. It is organized in Six chapters supported with supplementary material added in Appendices. The contents of each chapter - following the current one, are outlined below.

1.5.1 Chapter 2: State of the Art and Literature Review

This section delves into retrofitting Canada's historic URM buildings, referencing frameworks like Venice Charter, ASCE/SEI 41-17, and UNESCO guidelines. It underscores URM challenges and advanced modeling for seismic performance, leaning on past research and disaster insights.

1.5.2 Chapter3: Numerical Modelling of Two-Storey Unreinforced Masonry Building in SAP2000

Analyzing a two-story URM structure using SAP2000, this chapter validates material properties and structural responses. Employing EFA and Shell Element Modeling, it assesses seismic behavior through modal analysis, aiming to enhance understanding and validate experimental data.

1.5.3 Chapter 4: Nonlinear Modelling of the Two-Storey URM Building

Shifting to nonlinear modeling, this chapter gauges URM building's seismic reactions, emphasizing masonry's semi-brittle nonlinear stress-strain behavior. With a 3D model, techniques like pushover analysis spotlight structural limits and resilience, analyzing the seismic response.

1.5.4 Chapter 5: Various Ways to Strengthening the Building

This section assesses reinforcement methods for Canadian URM heritage buildings against quakes. Techniques like repointing and jacketing are discussed, aiming to boost seismic resistance.

Selection criteria consider structural state, heritage value, and seismic risks, guiding resilience enhancement.

1.5.5 Chapter 6: Conclusion and Future Work

Summarizing research findings on seismic assessment methods, this chapter reviews retrofitting techniques' efficacy, noting challenges in heritage conservation. Emphasis is on refining methods with advanced materials and addressing climate change's seismic implications, aiming for both safety and preservation.

2. Chapter 2: State of the Art and Literature Review

2.1 Unreinforced Masonry Structures Background

In the late 18th century, working-class neighborhoods emerged around historic Old Montreal, marked by unplanned urbanization and comprising mostly timber construction. Unfortunately, a significant portion of these houses were devastated by fire in 1852, prompting the City of Montreal to mandate masonry construction as a prevention measure. Between 1860 and 1915 Unreinforced Masonry (URM) residential houses became common in Montreal and generally in Canada (Kraiem et al., 2019), (Auger et al., 1999), (SIM 2018).

Common residential Unreinforced Masonry (URM) clay structures are rooted in the architectural history of the past two centuries, dictated by the need to address the need of housing for a growing population. During this period, the construction of dwellings and other amenities was guided using traditional building methods and easily accessible materials such as stone, fired brick, or adobe.

Historically, older unreinforced masonry buildings had massive vertical walls with diminishing thickness in upper floors. These structures rarely exceeded four or five stories in height and featured vaulted basements or lower floors, while upper stories utilized timber floors and roofs. Simple folk dwellings were limited to one or two stories, with timber beams and sheathing as the primary floor system and timber roof diaphragms (Karantoni, Papadopoulos, and Pantazopoulou, 2016). In former centuries, buildings in Canada's oldest cities like Montreal, Quebec, Ottawa, and Toronto, as well as in the U.S. (in cities like Boston), and various European locations, were commonly constructed using unreinforced masonry. These historical structures, predating 1950, showcase the use of masonry as a composite material, formed by laying masonry blocks or units (made of stone, clay, or other materials) in courses and binding them together with mortar (Lourenco, 2015).

The dramatic vulnerability of unreinforced masonry structures to seismic events was highlighted in reconnaissance reports. Significant damage and collapse of URM structures are frequent in earthquakes through unique failure mechanisms. A key challenge in unreinforced masonry construction is the absence of kinematic restraint in the form of stiff diaphragms -which is the common characteristic of frame structures - on the lateral movement of vertical structural components. Diaphragms, typically provided by floors and roofing systems, connect load-bearing masonry walls if they are properly anchored in the ends, which enables them to take a share of the lateral load according to their lateral stiffness (Hendry, Sinha, and Davies, 2017).

Understanding this background is essential in addressing the seismic vulnerabilities and unique characteristics associated with URM structures in historical and heritage contexts. For one thing, it is often hard to figure out how the structures work because they're made of different kinds of materials and have a lot of different interfaces and undefined paths for forces to be carried through the long, solid walls. These problems are exacerbated by material aging and degradation – either by corrosion of metal connectors or by weathering of mortars and building blocks since these materials are naturally brittle. Limited test experience exists due to the wide range of materials used (e.g., stones with different strengths and finishes, clay tiles, adobe, wood, lime-based mortar, and mud mortar). This complexity is transferred to the modeling assumptions for breaking up a continuous system into separate structural members and the constitutive models used to represent the mechanistic behavior of the materials under stress. Thus, analysis of heritage structures may push the current state of the art in terms of computer simulation to its limits, particularly if the analysis accounts for the connectivity of the system, and the nonlinearity and brittleness of the materials. Analysis is an essential requirement for seismic assessment not only to determine the trajectory of internal actions but also to find the locations of stress concentrations and potential failure points and to eventually guide design of retrofitting and rehabilitation (Pantazopoulou, 2013).

2.2 Standards for Retrofitting Historical Unreinforced Masonry Buildings

In Canada, retrofitting unreinforced masonry heritage buildings requires structural civil engineers to adhere to both national and provincial regulations, codes, and standards to maintain the building's structural integrity and historical value. Key frameworks include, The Venice Charter for heritage conservation, and the ICOMOS Guidelines for cultural heritage conservation; when it comes to seismic evaluation, frameworks used include the American ASCE/SEI 41-17 standard for seismic retrofitting – Chapter 11 which includes clauses for URM structures, the UNESCO World Heritage Centre Guidelines for preserving world heritage sites, and local heritage conservation guidelines specific to regional architectural styles. Additionally, the National Building Code of Canada and Canadian Standards Association provide comprehensive guidelines for design, construction, and seismic safety of new masonry structures, including some provisions for URM.

The retrofitting process encompasses assessing the building's historical value, conducting detailed structural analyses, and were deemed necessary by international conventions on the built heritage, applying minimal intervention and reversible techniques, ensuring material and technique compatibility with those used in the existing structure, and collaborating with historians, conservationists, and local authorities to ensure the preservation of both structural integrity and historical value.

2.2.1 Overview of the Venice Charter: Fundamental Principles and Impact on Cultural Heritage Preservation

The Venice Charter, created in 1964, is a foundational document in cultural heritage preservation. It defines monuments as culturally significant structures, advocating for their minimal intervention while maintaining historical and aesthetic values. The Charter emphasizes the use of original materials and historical documentation, requiring restoration work to be discernible, reversible, and based on scientific evidence. It has significantly influenced global conservation practices and led to the establishment of the International Council on Monuments and Sites (ICOMOS). The Charter outlines several principles: continuous maintenance of monuments, allowing their social use without altering architectural integrity, controlled environments for security, and the possibility of relocating monuments under specific conditions. It permits the removal of artworks for preservation, emphasizes the importance of archaeological and historical research, and supports using modern technologies in restoration. The aim of restoration is to respect a monument's historical development, ensuring any replacements do not diminish its value. Changes must not compromise the monument’s beauty, setting, or relationship with its surroundings, and archaeological excavations should follow scientific standards. Comprehensive documentation of all restoration processes is mandated.

2.2.2 ISCARSAH Guidelines

“Architectural heritage preservation requires a collaborative, multidisciplinary approach, valuing the cultural context of physical heritage. Authenticity and value are dynamic, extending beyond aesthetics to include all structural elements. Genuine preservation demands more than mere facade maintenance; modifications must respect conservation standards and safety. Restoration prioritizes holistic preservation, with research and strategy formulation: compiling information, diagnosing damage causes, selecting restoration methods, and ongoing monitoring for efficiency and minimal impact. Non-urgent actions should balance benefits and risks, minimizing irreversible changes. Comprehensive knowledge of a structure's history, architecture, and materials is key, especially in archaeological settings. Diagnosis involves historical understanding, qualitative (direct observation, historical/archaeological studies) and quantitative (material tests, structural assessments) methods, identifying root damage causes and safety evaluation. Restoration plans should respect architectural significance, structural integrity, and functionality, prioritizing preservation of historic elements and favoring repair over replacement. Temporary safety measures during restoration should be non-intrusive and reversible, with continuous evaluation and monitoring to ensure effectiveness. All actions should be thoroughly documented for historical records." (ISCARSAH GUIDELINES 2005)

2.2.3 The NIKER Project

The NIKER project (Figure 2.1), funded by the European Commission under the 7th Framework Programed from 2009 to 2012, aimed to develop innovative seismic protection methods for cultural heritage buildings, especially unreinforced masonry (URM) structures. It focused on balancing seismic protection with the preservation of cultural and historical values. Key aspects included seismic risk assessment for heritage buildings, developing non-invasive seismic retrofitting techniques, interdisciplinary collaboration across engineering, architecture, materials science, and heritage conservation, and conducting pilot studies on actual heritage buildings to validate the methods.

The NIKER project, featured for evaluating numerical modeling, involved testing two half-scale masonry buildings at the Technical University of Athens. These two-story structures had dimensions of 3.65 meters by 2.30 meters, and a height of 3.2 meters. One building was unreinforced, and the other included timber elements. These structures were composed of limestone, mortar, and rubble and tested against seismic events like the 1986 Kalamata and 1980 Irpinia earthquakes. After initial tests, the unreinforced structure was reinforced, leading to improved resistance to seismic activity. This project demonstrates the effectiveness of transitioning from flexible to rigid diaphragms in enhancing the performance of masonry buildings under earthquake loading.

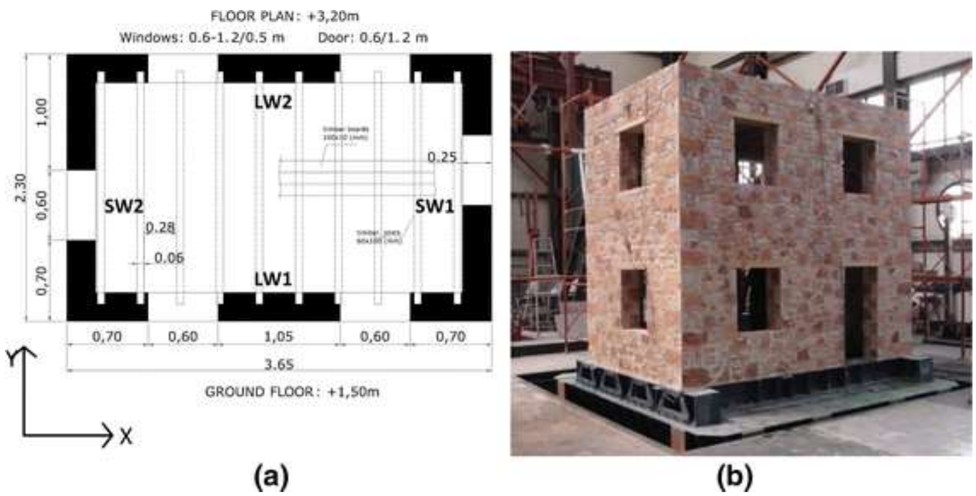

Figure 2.1. The Niker Project, (Vintzileou et al., 2015)

2.3 The CSA S304.1-04 "Design of Masonry Structures" (Re-affirmed 2010)

2.3.1 Definitions and Standard Notation

The CSA S304.1-04 standard's definitions are meant to guide the safe design and construction of masonry. The reference made to URM structures is rather limited on account of the fact that in modern structures, URM is not a recommended method of construction except for veneers which are used in non-bearing facades, and single masonry layers (wythes) that are connected against out of plane displacement with tie backs. In this context, anchors are recommended for connecting masonry walls, beams for supporting vertical loads, and bonding units for structural or aesthetic unity. Bond beams provide reinforced support, while cavity walls have a gap between layers. Clay and concrete masonry units are specific types of bricks or blocks, and collar joints are connecting units between wall layers. Column piers are vertical load-bearing elements, and composite walls combine different materials. Connectors include various ties and fasteners, and cross-sectional area calculations vary based on the inclusion of materials. Grout is used to fill masonry voids, where hollow units (like cinder blocks) have less net load bearing area. Loadbearing elements support additional loads apart from their self-weight, where the limiting parameter is the allowable compressive stress acting on the member. This is measured from masonry wallettes tested in compression and therefore representing the composite masonry strength. Reinforced masonry includes steel reinforcement for strength and stiffness; lateral force resistance is provided by shear walls.

In the case of unreinforced masonry, the sole source of strength is provided by the brick and mortar, so there is no resistance to tension. Considering that the lateral strength is only provided by the axial load N, acting over a lever arm from the centroid of the cross section (Fig. 2.2), evidently the use of solid brick and block units with a large solid area are more appropriate to provide axial load strength for load bearing action (f_d); however, the solid bricks also have a large mass – and this compromises the seismic response because of the large out of plane inertia pressures developed as a result.

Flexural resistance in the absence of reinforcement (URM walls) is only provided by the overbearing axial load. If no axial load acts on the section, its lateral strength is zero.

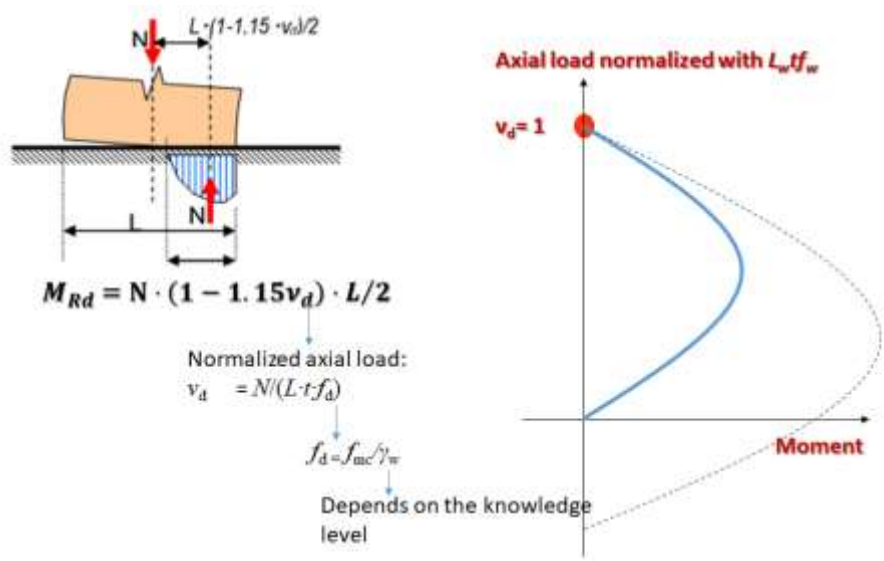

Figure 2.2. Flexural Behavior of Unreinforced Masonry Walls Under Axial Loads
(Pantazopoulou, S.J, 2022)

A knowledge factor is used in the case of existing structures, in the same role as a material safety factor that design codes use for new structures. So, whereas in new construction the material strength fm is multiplied by 0.65 to produce the design value fd, in existing structures factor γ_w - a number greater than 1, is used to reduce the strength value obtained from in situ tests of the existing material strength in order to determine the allowable value used in the necessary calculations for assessment.

2.3.2 CSA S304.1-04: Unreinforced Masonry

CSA S304.1-04 was an earlier code to the current version, and therefore provisions were not as detailed. For unreinforced masonry an eccentricity tolerance of axial loads is defined, equal to 10% of the wall's thickness at both top and bottom, and if lateral forces or specific axial load eccentricities exceed these limits, the resulting moment resistances are neglected. The standard limits the maximum compressive axial stress in unreinforced masonry (URM) to 80% of the uniaxial compressive stress, calculated based on effective cross-sectional area, which accounts for mortar and grouted voids and adjusts for imperfections like raked joints and recesses. However, reductions are not required for small voids or shallowly tooled mortar joints.

Section 8.2 provides guidelines for designing URM to handle tensile stresses, emphasizing that masonry should remain intact under normal loads, including those caused by environmental factors. It advises using joints and construction methods to manage these stresses. For URM design calculations, reinforcement for movement control or seismic strengthening is not considered. The design assumptions include proportionate strain distribution, a direct relationship between flexural stress and strain, and the exclusion of reinforcement stresses in load-bearing capacity calculations. Section 8.2.4.1 introduces a unity interaction equation for designing masonry under axial and flexural compressive stresses, adaptable for biaxial bending but excluding secondary bending effects from axial loads.

URM design typically does not consider axial tension resistance, and walls experiencing uplift, such as the case of overturning seismic moments, would require reinforcement. Section 8.2.6 discusses shear failure in URM, with three potential modes and specific guidelines for calculating shear stresses. The Code addresses the effective width of the flange in URM and sets deflection limits for materials supporting URM. A material safety factor of 0.60 (=φ) is stipulated for URM under flexure or axial load. The design criteria and assumptions emphasize that URM elements should be engineered to remain uncracked and behave elastically under expected loads. As mentioned earlier, the nominal strength for combined flexure and axial loads is calculated to ensure compressive stress doesn't exceed 0.80 f_m', with specific guidelines for nominal axial strength calculations.

2.3.3 National Building Code (NBCC-1941)

The National Building Code's guidelines for masonry construction have evolved over the years – the earliest version available being the one issued in 1941. Older masonry structures have been built to various earlier code versions, so it is of interest to review the salient points of past guidelines as they represent the method and provisions of construction at the time when an existing structure was built.

The 1941 version mandated adherence to specific production standards for bricks, classified into grades like SW, MW, and NW, each suited for different environmental exposure. SW is ideal for cold, moist environments, MW for less water-saturated cold areas, and NW for internal use or mild climates. Reclaimed bricks, limited to 10% fragmented pieces, must be thoroughly cleaned. Mortar bonding strength depends on non-organic elements, with types like lime, lime-cement, cement, and gypsum requiring different component mixes. Masonry joints need a minimum 3-inch depth, matching the facing's thickness for thinner facings. A slight inward splay in joints is allowed in some masonry types. Structural integrity is maintained by setting a minimum bearing pressure of 10% of a unit's highest compressive strength. Horizontal shear strength can be taken equal to one-third of the vertical stress calculated from the structure's weight. Compressive stresses for solid units are classified by minimum compressive strength, with specific limits for soft brick in unreinforced walls or piers. Hollow masonry stresses are based on effective net cross-sectional area. Working stresses can increase by 50% with authority approval for solid masonry walls with specific construction and inspection criteria. Walls with mixed-strength units should follow the lowest strength from the group's allowable stresses. Shearing strength is set at different fractions of compressive strength for hollow and solid unit walls. Unreinforced gypsum masonry is limited to non-load bearing uses. Masonry work must be straight, vertical, and fully mortar covered. Vertical and interior joints need solid mortar filling, and masonry must directly support joists, beams, and girders without shims or blocks. Wood components like joists, plugs, bricks, strips, continuous strips in 3-story walls, nailing blocks, plates, and boarding are permissible in masonry walls and parapets with certain conditions.

Table 2.1 Allowable Compression Stresses for Unit Masonry (NBCC-1941)

Type of Masonry	Nominal Min. Compressive Strength (lb/sq. in.)	Cement Mortar	Lime-Cement Mortar	Lime Mortar
Solid, composed of any solid unit except rubble stone	10,000	500	350	100
	8,000	400	300	100
	4,500	250	200	100
	2,500	175	140	75
	1,500	125	100	50
Hollow, composed of any solid unit except rubble stone	2,500	125	100	50
Hollow composed of any hollow unit	-	80	70	-

2.3.4 National Building Code of Canada - 1953

The 1953 National Building Code of Canada outlined comprehensive guidelines for masonry construction, focusing on the bearing of structural members, support and bonding requirements, wall thickness, and use of timber. Columns had to have a minimum 12-inch-thick concrete cap or pad for support. Flexural members should assume eccentric axial load application, and concentrated loads on hollow masonry units had to have a solid unit bearing. Masonry should not be supported by combustible materials and had to be properly anchored. Bonding rules varied for different wall types, including rubble stone, solid brick, block walls, and cavity walls, with specific bonding requirements for each. Wall thickness was determined based on the wall's top section, with varying height limits for non-load-bearing partitions. Parapet walls and balustrades should comprise solid masonry units, meet minimum thickness and height requirements, and have specific capping and back face protection. Wood use in masonry was limited and regulated, including for structural members' ends, plugs, blocks, strips, continuous nailing strips, and cambered wood lintels. These guidelines ensured structural integrity, fire safety, and proper support mechanisms in masonry construction.

2.3.5 Building Standards (1954)

The 1954 Building Standards specified additional guidelines for various aspects of masonry construction. Load-bearing basement or cellar walls made of unit masonry had to be bonded or tied into exterior foundation walls using overlapping masonry courses or metal ties, with specific dimensions and spacing for the ties and brick or block columns. Mortar materials required clean sand or similar aggregates, clean water, and cementitious materials stored so as to be protected from weather. Different mortar types were specified, including lime mortar, lime-cement mortar, cement mortar, and cement grout, each with precise composition requirements. The permissible stresses in unreinforced masonry were clearly defined: allowable compressive and shear stresses should not be exceeded, and bearing pressure on unit masonry under concentrated loads should adhere to specified limits. Additionally, the allowable transverse shear stress could be increased under certain conditions, and specific maximum unit stress limits were set for sound natural stone used in various construction elements. These standards ensured the structural integrity and safety of masonry construction.

Table 2.2. Maximum Allowable Stresses in Masonry Elements. CSA 304-78, (Pantazopoulou, S.J, 2022)

Type of Stress or Modulus	Designation	Brick Masonry	Concrete Masonry: Units with no voids or filled hollow units. Use gross area	Concrete Masonry: Units with Voids. Use Net cross-sectional area
Axial compression, walls columns	f_m	0.25 f_m 0.2 f_m	0.2 f_m 0.18 f_m	0.225 f_m 0.2 f_m
Flexural Compression, Walls columns	f_m	0.32 f_m 0.26 f_m	0.3 f_m 0.24 f_m	0.3 f_m 0.24 f_m
Tensile, Flexural; to bed joints _M or S mortar _ N mortar	f_t	0.25 (36) 0.19 (28)	0.25 (36) 0.19 (28)	0.16 (23) 0.11 (16)
Tensile, Flexural; II to bed joints _M or S mortar _N mortar	f_t	0.5 (72) 0.39 (56)	0.5 (72) 0.39 (56)	0.32 (46) 0.22(32)
Shear _M or S mortar _N mortar	V_m	$0.083f_m < 0.35$ ($f_m < 50$) $0.083f_m < 0.24$ ($f_m < 35$)	0.23 (34) 0.16 (23)	0.23 (34) 0.16 (23)
Bearing on masonry	f_b	0.25 f_m		
Modulus of elasticity	E_m	1000 f_m < 20 GPa (3000ksi)		
Modulus of rigidity	E_v	400 f_m < 8 GPa (1200ksi)		

2.4 Brick Varieties and Colors in Canada's Historic Unreinforced Masonry Structures.

Unreinforced masonry (URM) structures in Canada typically were constructed using traditional materials such as brick, stone, mortar, timber, and terracotta, with brick types and colors varying by region and construction era. These variations reflect local materials and architectural styles, influencing the building's character. Brick colors range from light tan to deep reds and browns, depending on local clay and firing processes. Bricks are categorized into adobe or brick units, differing in shape, size, and manufacturing methods. Older bricks, usually wood/coal kiln-fired and handmade, have high porosity (20-35%), moderate compressive strength (4-32 MPa), and densities of 1,200 to 1,900 kg/m3. Tensile strength tests for bricks, including splitting-tensile or flexural tests, show variable strength ratios, with an Elasticity modulus typically between 1 and 18 GPa. Adobe units, made from clay and earth mixtures often reinforced with straw in the role of fibers, vary greatly in size, have low compressive strength (1.0 to 3.0 MPa), low Elasticity modulus (0.4 to 2.0 GPa), and very high porosity (up to 50%), making them sensitive to moisture changes. (Costa, Guedes and Varum, 2014), (Canadian Historic Sites: Occasional Papers in Archaeology and History). Specific details are as follows:

- Red Clay Bricks: These are the most common brick type found in historic Canadian buildings. They are typically made from natural clay that has a high iron oxide content, giving them a distinctive red color.
- Yellow Bricks: Also known as buff bricks, these are less common than red bricks. They are made from clay with lower iron content and often fired at a lower temperature, resulting in a lighter, yellowish color.
- Cream City Bricks: Named for their cream or light-yellow color, these bricks were made from a type of clay found in some regions. While more associated with the Milwaukee area in the United States, similar bricks were also used in parts of Canada.
- Black Bricks: Less common in historic structures, black bricks were usually created by adding manganese to the clay. These were often used for decorative purposes or to create detailed patterns in masonry work.

- Sand-Lime Bricks: These are a type of brick made from sand and lime, as opposed to clay. They can come in a range of colors, including white, grey, or light yellow, depending on the mix and the pigments used.
- Handmade Bricks: In many older buildings, bricks were handmade, leading to a variety of shapes, sizes, and colors.

Figure 2.3. Samples of Bricks Representing the Four Historical Periods of Canadian Brick Masonry Construction. (Harun, 2021)

2.5 Background on Analysis Methods for URM Structures

Buildings classified as cultural heritage are valued for their historical significance, architectural complexity, and impact on urban environments. A priority in conservation of these structures is their condition assessment with emphasis on the evaluation of their seismic resistance or other extreme events. To predict the behavior of such structures during seismic events and to plan appropriate restoration and reinforcement strategies, pertinent analytical modeling procedures that are compatible with current software capabilities are needed. These are discussed in detail in (Pantazopoulou, 2013). Seismic safety evaluation of URM structures using modern nonlinear analysis techniques is a challenging endeavor on account of the unique structural characteristics they have, like non-uniform stiffness, spatial mass distribution, and limited diaphragm action. International conventions dictate minimally invasive and reversible restoration measures, especially for repurposed buildings, while the fragility of masonry and a lack of comprehensive understanding further complicate seismic evaluation and restoration.

Heritage structures symbolize significant technological, artistic, cultural, religious, defensive, and administrative achievements throughout history, representing various architectural styles. Examples include the Acropolis of Athens, Arg-e Bam, the Pyramids of Giza, the Colosseum, the

Great Wall of China, the Alhambra, Angkor Wat, Hagia Sophia, and the Western Wall, all protected under international treaties. Despite structural wear, these monuments remain operational. Restoration of these sites is guided by international agreements favoring non-intrusive and reversible methods, anticipating future advances in materials and techniques. Societal commitment to preserving cultural heritage has resulted in guidelines and standards to ensure conservation without irreversible changes to their design, decorative elements, original materials, structural systems, and historical construction techniques. Balancing historical authenticity with practical restoration is a significant engineering challenge.

Figure 2.4. Acropolis of Athens in Greece, https://en.wikipedia.org/wiki/Acropolis_of_Athens

Figure 2.5. Arg-e Bam in Iran. https://whc.unesco.org/en/list/1208/

Figure 2.6. Great Pyramids of Giza in Egypt.
https://en.wikipedia.org/wiki/Great_Pyramid_of_Giza

Figure 2.7. Colosseum in Italy. https://en.wikipedia.org/wiki/Colosseum

Figure 2.8. Hagia Sophia in Turkey. https://en.wikipedia.org/wiki/Hagia_Sophia

Figure 2.9. Great Wall of China. https://en.wikipedia.org/wiki/Great_Wall_of_China

Figure 2.10. Alhambra in Spain. https://en.wikipedia.org/wiki/Alhambra

Figure 2.11. Angkor Wat in Cambodia. https://en.wikipedia.org/wiki/Angkor_Wat

Figure 2.12. Western Wall in Israel. https://en.wikipedia.org/wiki/Western_Wall

2.6 Stiffness, Strength, and Drift Capacity of Stone Masonry Walls

Recent attempts to adopt performance-based design principles in the seismic evaluation of existing structures have highlighted the greatest challenges associated with quantification of the effects of earthquakes in URM structures. Properties that may be well defined for other materials (e.g. Steel), such as the modulus of Elasticity of masonry, introduces great uncertainty in the analysis of any masonry component under lateral loads. For example, in the Canadian masonry design practice, the modulus of Elasticity of masonry is taken 850 times the compressive strength of the masonry wallette – the factor is 1000 in the US Masonry Code. Many researchers, however, recommend using less than half these values on account of cracking (Vanin et al. 2017).

Uncertainty in the modulus of elasticity of masonry also creates significant uncertainty regarding the estimation of seismic demands, because of the effect it has on structural fundamental period, and through that, on the Spectral Response Acceleration for a given earthquake. For one, the many interfaces between brick/stone and mortar create significant inhomogeneity in the properties of the composite masonry. In addition, most masonry material tests are conducted on walletes under compression (i.e., under normal clamping stress on the bed joints) and then, all other mechanical characteristics are linked to the compressive strength of the composite. However, earthquakes induce lateral forces where the typical pier's lateral response depends on the strength in diagonal tension and the occurrence of horizontal sliding over joints.

Apart from being remarkably brittle, because their stiffness and strength depend on the extend of cracking and the original properties of a vastly complex component such as a URM pier or wall (e.g. Fig. 2.13), any attempt at modelling in order to estimate the design forces that would need to be checked against component strengths and drift capacity are fraught with great uncertainty. For this reason, a systematic effort to quantify the parameters that affect the modelling parameters and the limiting conditions associated with specific levels of permanent damage in masonry was undertaken both in N.A. (as reflected in Chapter 11 of the ASCE/SEI 41-2017) as well as in Europe (e.g. (Vanin et al., 2017), KADET (2018), and Eurocode 8-III (2005)). The former focused particularly in reinforced walls, whereas the latter focused in URM constructions aiming to evaluate the drift limits at specific damage states, in order to supplement the respective sections of Eurocode 8, Part 3 (EC8-3). The salient points are reviewed in this section on account of its relevance with the objectives and the scope of the present thesis.

Figure 2.13, illustrates three different configurations of brick masonry wallette specimens. The first shows a neat and orderly arrangement with even mortar joints. The second figure emphasizes the mortar joints more. The bonding between bricks is not strong enough compared to other shapes. The third, however, presents a highly irregular and complex pattern with varied brick sizes, non-uniform placement, and misalignments. In this figure joints and other components have a stronger connection.

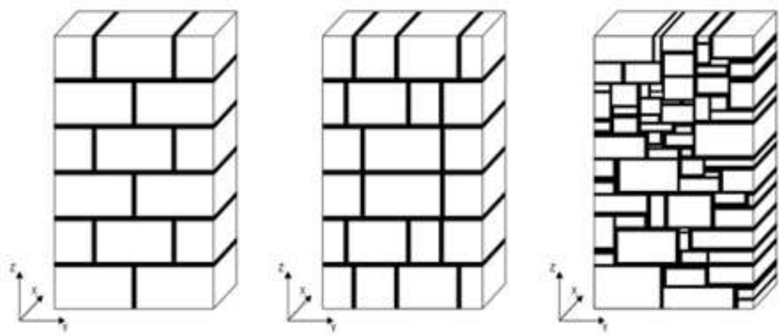

Figure 2.13. Typical Form of Wallette Specimens

An important knowledge gap encountered in seismic evaluation of URM structures are the deformation limits that may be considered to define the level of damage under a specific earthquake. It is noted here that throughout the literature, seismic damage in masonry wall piers is defined in terms of drift ratio - to avoid dimensional bias; drift ratio is obtained by dividing the lateral displacement of a pier to the height over which deformation takes place. Because drift ratio is a measure of damage, both seismic demands and member capacities are quantified in terms of drift ratio – understanding its magnitude and the relevance it has in quantifying damage are considered essential for evaluating how structures respond to lateral forces.

The Hellenic Code (KADET 2018) recommends the following limit states: An unreinforced masonry wall cracks and therefore it is considered to undergo “notional yielding” at a drift ratio of 0.15% for in-plane lateral loads and 0.2% for out of plane actions (see Figure 2.14); for walls dominated by flexural behavior, it is postulated that the structural component may develop a drift of 0.8%, whereas for walls dominated by shear, the drift capacity is only 0.4% (the drift capacities are increased by 50% in the case of secondary elements).

To conduct an evaluation of a structure, performance limit states are defined by the visible damage that a structure has developed during a seismic event – this requires a field assessment by an architect or an engineer following the seismic event. The commonly accepted limits for an unreinforced masonry structure are described below; the notional yielding or wall cracking described in Figure 2.14, but also in all other relevant codes, refer to IO (immediate occupancy). Ultimate drift capacity refers to Life-Safety (LS/SD) where damage may still be repaired. CP refers to 33% exceedance of the drift limits provided above for LS.

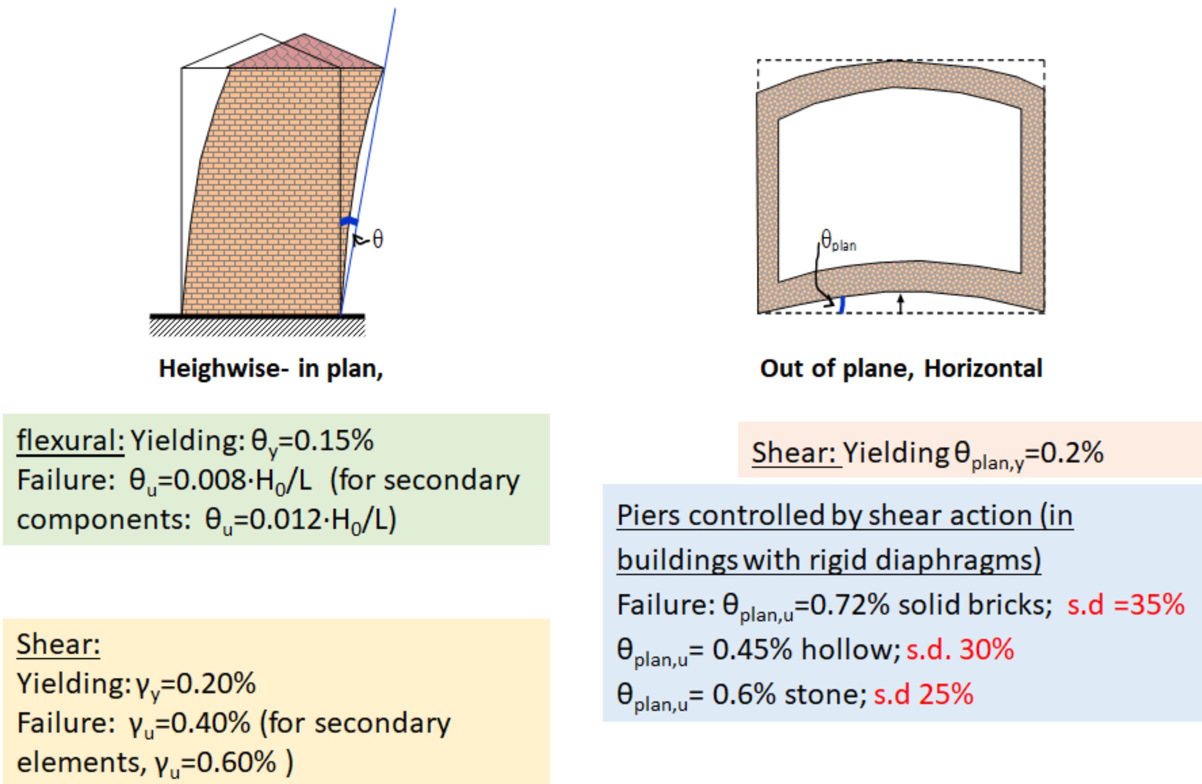

Figure 2.14. Drift Limits for Walls According to KADET (2018).

Table 2.3. Definition of Visible Damage at Reference Limit States for Visual Evaluation

Type	Structural Performance Levels		
	Immediate Occupancy: A: IO / DL (Limited Damage)	Life Safety: B: LS / SD (Repairable Damage)	Collapse Prevention: C: CP / NC (Avoid Collapse)
Primary Elements	Minor cracking of veneers. Minor spalling in veneers at a few corner openings. No observable out-of-plane offsets.	Major cracking. Noticeable in-plane offsets of masonry. Minor out-of-plane offsets	Extensive cracking; face course and veneer might peel off. Noticeable in-plane and out-of-plane offsets
Secondary Elements	Same as for primary elements	Same as for primary elements	Non-bearing panels dislodge

Type	Structural Performance Levels		
	Immediate Occupancy: A: IO / DL (Limited Damage)	Life Safety: B: LS / SD (Repairable Damage)	Collapse Prevention: C: CP / NC (Avoid Collapse)
Drift	Transient drift that causes minor or no non-structural damage. Negligible permanent drift.	Transient drift sufficient to cause non-structural damage. Noticeable permanent drift.	Transient drift sufficient to cause extensive non-structural damage. Extensive permanent drift.

The corresponding limits for the ASCE/SEI 41-2017 and the Eurocode 8-III are given in the following table: The various Q terms represent lateral strength of the masonry pier at flexural failure, toe crushing failure, wall rocking about a lower corner that acts as pivot, and sliding (see respective subscripts). It is noted that regardless of the mode of wall deformation that prevails, in the ASCE Code the Immediate occupancy corresponds to a drift ratio of 0.1% - which means damage that has exceeded that limit is already into the range of Life Safety limit state (i.e., the building has to be evaluated in order to be repaired and strengthened). In EC8-III the notional drift at yielding, θ_y, refered to as "elastic limit" is taken the same with the values used in KADET 2018.

Table 2.4. Limiting Values for Drift Capacity of Unreinforced Masonry Walls According with ASCE/SEI - 41 (2017) Chapter 11, and According with the EC8-III (2005)

Limiting Behavior Mode for URM Walls/Piers	Modelling Parameters			
	c	d	e	f
Rocking	$Q_{toe,L}/Q_{roc,E}$	Δ_c/H_e %	Δ_c/H_e %	$\frac{\Delta_c+\Delta_y}{H_e}$ %
Bed-joint sliding	$Q_{c,E,F}/Q_{slid,E}$	0.4%	1.0%	$1.0+\frac{\Delta_y}{H_e}$ %
Δ_c= Lateral displacement associated with the onset of toe crushing $V_{tc,r}$,				

Limiting Behavior Mode		Drift Ratio Limits		
		IO : A	LS : B	CP: C
Rocking	Simplified	0.1%	$0.4h_{eff}/L\leq1.5\%$	$0.6h_{eff}/L\leq2.25\%$
	Comprehensive	0.1%	$0.6h_{eff}/L\leq2.25\%$	$\delta_{c,u}/h_{eff}\leq2.5\%$
Bed-joint Sliding		0.1%	0.75%	1.0%

Flexural (Rocking)			Bed-joint Shear Sliding			Diagonal Shear Cracking		
θ_{DL}	$\theta_{SD}=\theta_{f,u}$	$\theta_{NC}=\theta_{f,u2}$	θ_{DL}	$\theta_{SD}=\theta_{s,u}$	$\theta_{NC}=\theta_{s,u2}$	θ_{DL}	$\theta_{SD}=\theta_{d,u}$	$\theta_{NC}=\theta_{d,u2}$
elastic limit θ_y	(1-ν)%	$\left(\frac{4}{3}\right)\theta_{f,u}$	elastic limit θ_y	0.4% (solid bricks) 0.5% (hollow bricks) 0.8% (stone)	$\left(\frac{4}{3}\right)\theta_{s,u}$	elastic limit θ_y	0.5%• or 0.6%▲	$\left(\frac{4}{3}\right)\theta_{d,u}$

Eurocode 8 Part 3 (EC8-3, 2005) which refers to existing structures, does not differentiate between masonry construction typologies in assessing drift capacity, a measure of a structure's ability to endure lateral displacement. Drift capacity is determined based on failure mode (shear vs. flexure) and the Shear Span Ratio (H_o/L), which is the height of zero moment measured from the critical section at the base, to wall length ratio. Assessing in-plane shear force capacity of masonry walls involves the hierarchy of the results obtained from different equations estimating the lateral resistance of a number of failure mechanisms to which there is evidence of wall susceptibility different failure modes such as rocking failure with compressed toe crushing and shear failure with diagonal cracking or sliding along bed joints, as per Magenes and Calvi (1997). A parametric sensitivity analysis highlighted an overestimation of shear strength in shear-governed failures. It was noted that walls restrained at the top are more prone to brittle shear failure ($H_o/H<1$). Additionally, it was found that existing code expressions often overestimate shear resistance in overly stocky walls, pointing to the need for refined modeling approaches. The research defined notional yield and ultimate points by linearizing lateral load resistance curves, providing crucial data on yield displacement and ultimate deformation capacity. Limiting drift ratios for masonry walls and piers at the onset of failure were defined as follows:

Shear failure: $\delta_{SD} = 0.4\%$

Flexural failure: $\delta_{SD} = 0.8\% \, . \frac{H_0}{L}$ (2.1)

This comprehensive understanding of URM wall behavior underscores the need for accurate modeling, considering factors like shear strength, wall restraint, and aspect ratio. These insights are essential for improving the design and assessment of URM structures, enhancing their safety and resilience. (Vanin et al., 2017), (Pantazopoulou, S.J, 2022)

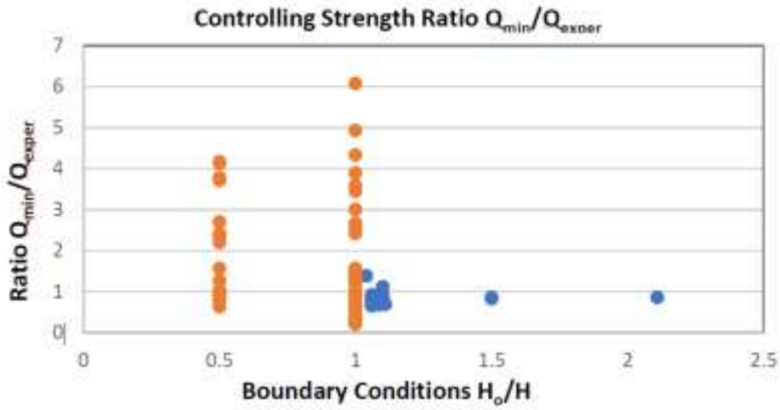

Figure 2.15. The Effect of Boundary Conditions on Mode of Failure (Pantazopoulou, S.J, 2022)

The general discord and ambiguity between codes regarding drift limits prompted a collective review of the available experimental evidence. To this end, a database of 123 quasi-static, in plane shear-compression tests on masonry walls from 16 test campaigns was assembled in the reference study of Vanin et al., (2017). The goal was to provide data for displacement-based evaluations of masonry structures, assessing lateral strength and stiffness, and proposing improvements to current procedures. The research evaluated drift capacity across six limit states and calculated median values and CoVs, factoring in the natural variability of stone and brick masonry. It also examined the effects of mortar injections and load history (monotonic vs cyclic) on the walls' stiffness, strength, and drift capacities. The results led to new or enhanced expressions for stiffness, friction coefficients, tensile strength, and drift capacity models. These include new expressions for the effective Elastic modulus of URM piers based on masonry typology, compressive strength, and axial load ratio, as well as updated values for friction coefficient against sliding and composite masonry tensile strength. The study differentiated between stone masonry typologies and addressed variabilities in stiffness, strength, and drift limits, considering load history and retrofit interventions.

The collection of data revealed deviations in testing configurations, including ancient stone masonry and shaking table tests, and the incorporation of elements like FRP strips, necessitating dataset expansion from international literature. A vetting procedure ensured that lateral strength in tests did not exceed rocking resistance, Q_{rock}, by more than 10% as given by Eq. 2.1, where (P_d+P_W) is the dead load and self-weight of the wall pier, respectively, L_w is the wall length, and H_o is the distance from the critical section of the pier to the position of zero moment (the critical section usually occurs in the base of a wall for example). This comprehensive analysis provides valuable insights for enhancing assessment procedures for stone masonry structures (Vanin et al., 2017).

Lateral Strength < $1.1 \cdot Q_{rock}$, where, $Q_{rock} = (P_d+P_W) \cdot L_w/2H_o$ (2.2)

Results of the database analysis are presented in Table 2.3 in the forthcoming review.

2.6.1 Summary of Proposed Median Values and Coefficients of Variations for Stone Masonry Assessment

This paper presents a detailed analysis of the mechanical properties of stone masonry walls, contributing to earthquake engineering and structural assessment. It identifies distinct characteristics and performance metrics for six stone masonry classes (A, B, C, D, E, and E1), each with unique features:

- Type A: Irregular stone masonry with pebbles and stones of varying shapes and sizes.
- Type B: Uncut stone masonry with external thin layers and a core of infill, typical of three-leaf structures.
- Type C: Masonry from well-bonded cut stones.
- Type D: Masonry using softer stones, like tuff or sandstone blocks.
- Type E: Ashlar masonry with blocks more resistant than Type D, further divided into regular squared block masonry with mortar joints (E) and ashlar masonry with dry joints (E1).

The study proposes two drift capacity models based on masonry typology, failure mode, shear span, and axial load ratio for a detailed understanding of drift capacities at six limit states. It explores aleatoric variability in stone masonry through replicate tests, emphasizing uncertainties in stiffness, strength, and drift limits. Retrofit interventions like mortar injections show improvements in drift capacity, suggesting potential for mechanical models to predict retrofit effects. The impact of loading history (monotonic vs cyclic) on stone masonry is also analyzed for seismic assessments.

Table 2.5. Summary of Proposed Median Values and Coefficients of Variations for Stone Masonry Assessment. (Vanin et al., 2017)

MASONRY TYPOLOGIES

A	B	C	D	E	E1

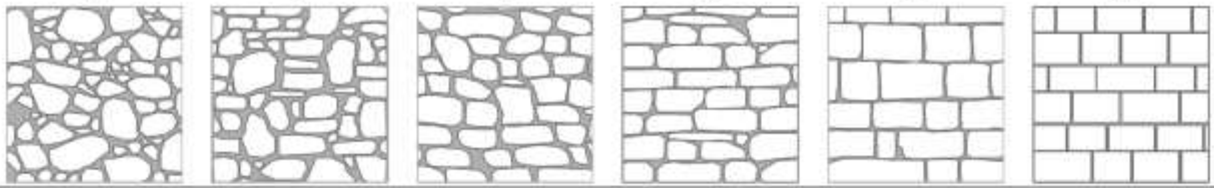

FORCE CAPACITY

Flexure: $V_{fl} = \frac{L^2 t}{2H_0}\sigma_0\left(1 - 1.15\frac{\sigma_0}{f_c}\right)$, f_c from (1)

Shear: $V_{sh} = \frac{Lt}{b} f_t \sqrt{1 + \frac{\sigma_0}{f_t}}$

$f_t \cong 0.015 + 0.006 \cdot MQI^{1.5}$, or from (3)

If a Mohr Coulomb criterion is preferred: values and CoVs for the friction angle in (4), $c = 2\mu f_t$

	A	B	C	D	E-E1
1. f_c [MPa] [1]	1.40	2.50	3.20	1.90	7.00
CoV [1]	0.30	0.20	0.19	0.27	0.14
2. f_t code [MPa] [1]	0.039	0.065	0.098	0.053	0.158
CoV	0.24	0.19	0.14	0.20	0.14
3. f_t exp. [MPa]	0.045	0.045	0.110	0.050	0.130
CoV	0.80	0.30	0.20	0.50	0.40
4. Friction coeff.	0.45	0.20	0.25	0.25	0.30
CoV	0.20	0.15	0.15	0.10	0.10

[1] from MIT (2009); coefficient of variation derived from CNR (2013)

EFFECTIVE STIFFNESS

$E_{eff} \cong \left(\frac{E}{f_c}\right)_{ref} f_c \cdot \frac{\sigma_0/f_c}{0.30}$ or from (1-2).

$K_{eff} = \frac{1}{\frac{H^3}{3E_{eff}I}\left(\frac{H_0}{H} - \frac{1}{3}\right) + \frac{6H}{5G_{eff}Lt}}$ with $\frac{G_{eff}}{E_{eff}} = 0.33$

	A	B	C	D	E-E1
1. E_{eff} code [MPa] [1]	430	610	870	540	1400
CoV [1]	0.20	0.20	0.15	0.20	0.15
2. E_{eff} exp. [MPa]	320	(2240)	900	430	500-650
CoV	0.50	(0.25)	0.40	0.40	0.50
3. $(E/f_c)_{ref}$	400	(700)	300	250	200-250
CoV	0.40	0.40	0.40	0.40	0.40

[1] from MIT (2009); coefficient of variation derived from CNR (2013)

DISPLACEMENT CAPACITY

Drift at cracking: $\delta_{cr} = 0.20\%$

Yielding drift:

- shear $\delta_y = 1/4 \cdot \delta_u$
- flexure $\delta_y = 1/6.5 \cdot \delta_u$

Drift at SD limit state $\delta_{SD} = 0.50 \cdot \delta_u$

Drift at max. force: $\delta_{max} = 0.70 \cdot \delta_u$

Drift at collapse $\delta_c = 1.15 \cdot \delta_u$

	A-B-C-D		E-E1	
	Shear failure	Flexural failure	Shear failure	Flexural failure
Model 1: δ_u	0.60	0.90	1.50	2.25
CoV	0.50	0.50	0.50	0.50

Ultimate drift:

- Model 1: reference values from table
- Model 2: $\delta_u = \max(1.5\% - 4\% \cdot \frac{\sigma_{0,tot}}{f_c}, 0.3\%) \cdot \frac{H_0}{\min(H,L)}$ (typologies A-B-C-D)

$\delta_u = \max(2.25\% - 6\% \cdot \frac{\sigma_{0,tot}}{f_c}, 0.3\%) \cdot \frac{H_0}{\min(H,L)}$ (typologies E-E1)

ALEATORIC VARIABILITY	Suggested coefficients of variation							
	K_{eff}	V_u	δ_{cr}	δ_y	δ_{SD}	δ_{max}	δ_u	δ_c
A-E1	0.20	0.10	0.10	0.20	0.30	0.30	0.30	-

The research finds that codes like EC8-3 often overestimate stone masonry's shear strength using the Mohr–Coulomb criterion. It proposes adjustments in friction coefficients for each typology based on experimental data. The Turnšek–Čačovič criterion, considering masonry’s tensile strength, offered more accurate predictions. Estimating stone masonry walls' effective stiffness was complex, with the effective-to-elastic stiffness ratio around 0.5, influenced by shear deformations. A new expression for calculating effective E-modulus was introduced, accounting for masonry typology, compressive strength, and axial load ratio, diverging from existing codes linking E-modulus solely to compressive strength.

2.6.2 Lateral Strength of Masonry Piers that Exhibit Hybrid or Shear Failure Modes

It was seen in the preceding that the hierarchy of flexural to shear strength of masonry piers is an important criterion in determining the mode of failure and drift capacity of the components. It was illustrated in Fig. 2.2 that flexural strength is only owing to the overbearing axial force – in the absence of an axial load the wall has practically negligible flexural resistance. (For out of plane action, the very slender form of the walls would render any consideration for shear strength redundant – failure occurs flexural in the out of plane actions of walls). However, for in-plane action, the shear strength is determined by the least of two strength components: (a) Sliding shear along bed joints, and (b) Diagonal tension failure, as depicted in Figure 2.16 The last figure below represents the strength increase obtained when reinforcement in the form of timber lacing is also included in the wall construction.

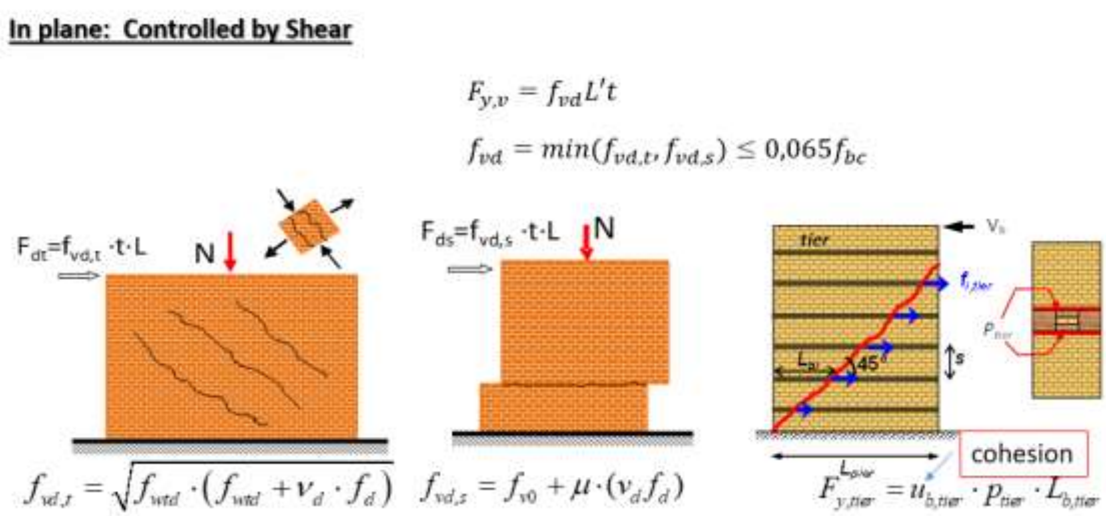

Figure 2.16. Analysis of Shear Strength in Masonry Piers

Figure 2.16 illustrates the Shear strength (MPa) of masonry piers (Strength would be obtained by the product of the stress value at failure times the cross-sectional area of the wall, L_{wt}): (a) Shear stress at diagonal tension failure, where f_d' is the design compressive strength of masonry and f'_{wtd}

is the tensile strength; (b) Shear stress at sliding failure, where f_{v0} is the cohesion and μ is the coefficient of friction.

The shear strength associated with sliding is based on a frictional model – so it relates to a Mohr-Coulomb criterion. Recent research (Pantazopoulou, S.J, 2022) has suggested that a variation of the above, known as Turnšek–Čačovič failure criterion is found to provide more accurate predictions of force capacity compared to the Mohr–Coulomb criterion (EC8-3) with a friction coefficient set at 0.4 (see Figure 2.16 (b)). This improvement is observed regardless of how the tensile strength (f_{wtd}) is estimated. However, a similar level of accuracy can be achieved by optimizing the parameters of a Mohr–Coulomb criterion, with the friction coefficient being identified as the most influential parameter. In essence, the Turnšek–Čačovič criterion generally performs well in predicting lateral strength, but alternative adjustments to the parameters of the Mohr–Coulomb criterion can also yield comparable accuracy.

2.6.2.1 Turnšek–Čačovič (1971) Criterion

The Turnšek–Čačovič failure criterion is a theoretical model used in material science and engineering. It's designed to predict the failure of materials under complex stress conditions. This criterion was developed by Franc Turnšek and Peter Čačovič, researchers in the field of material science (Turnšek V, Čačovič F ,1971). The criterion is particularly useful for analyzing materials subjected to multi-axial stress states, which means when the material experiences stresses in multiple directions simultaneously.

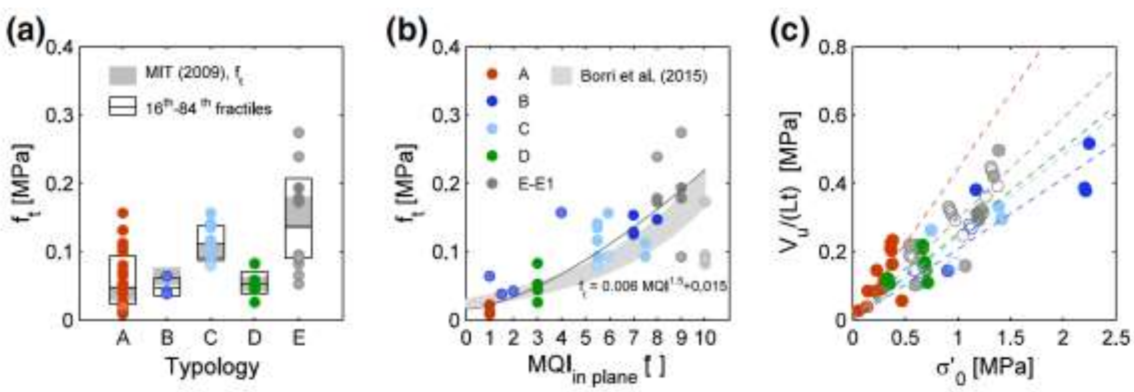

Figure 2.17. Masonry Tensile Strength According to Turnšek-Čačovič Criterion

Figure 2.17 (a) represents the tensile strength of Masonry (in MPa) according to the Italian Code, MIT (2009): The plot shows the tensile strength distribution across different typologies of masonry, labeled A to E (see Vanin et al. 2017, also summarized in the preceding section). The grey boxes represent ranges suggested in the Italian code (MIT 2009), and the individual points represent fracture data. The box plot elements represent the interquartile range, median, and range of the data excluding outliers. Figure 2.17 (b) plots the experimental tensile strength estimate: This scatter plot correlates the Masonry Quality Index (MQI) in the plane with the tensile strength (f_t) The data points are color-coded by typology and the curve represents a regression analysis with the formula provided:

$$f_t = 0.0006 \, . \; MQI_{in\,plane}^{1.5} + 0.015 \qquad (2.3)$$

which models the relationship between MQI and f_t. In the last part of Fig. 2.17 (c), regression analysis for friction coefficient estimation is shown, as the relationship between normalized shear stress (σ_c') and the normalized lateral shear strength (V_u/L_{wt}). Different regression lines are plotted, suggesting the analysis of multiple data sets or models, with dashed lines indicating confidence intervals or bounds and presenting empirical data supporting a particular model or criterion for predicting material failure, in this case, masonry under tension and shear stresses.

A general equation for shear strength, where V_u is the ultimate shear strength, μ is the friction coefficient, σ_0' is the normalized shear stress is of the form:

$$V_u = \mu \cdot \sigma_o' \cdot (L_w t) \qquad (2.4)$$

2.7 Material Mechanical Properties and It’s Impact on Seismic Assessment

The Seismic Evaluation Guideline framework aims to accurately determine seismic demands for structures, focusing on maximum deformations in components based on stiffness estimations of the masonry components. It was stated earlier that errors in evaluating stiffness can result in incorrect distribution of seismic forces across the structural system, influenced by factors like material inhomogeneity, simplifications in modeling, and stress state differences during material testing compared to lateral loading conditions. Masonry design codes provide a practical estimate range for the modulus of elasticity of masonry ($750f'_m$ to $1000f'_m$), where f'_m denotes the masonry's compressive strength. However, there are concerns that this range might be too high for performance-based design and assessment, potentially leading to an underestimation of displacement demands and unsafe conclusions about structural performance. Conservative stiffness estimation is crucial, with a recommendation by Tomazevic (1999) suggesting that the effective Elastic modulus of masonry in lateral load analysis not to exceed 300 times f'_m for seismic evaluation. This highlights the importance of avoiding overestimation of lateral stiffness, as it significantly impacts the reliability of seismic assessments. (Pantazopoulou, Recommending Modelling to NRC, 2022)

Table 2.6. Analyzing the Relationship Between Modulus of Elasticity and Masonry Compressive Strength in Various Codes and Relevant Literature (Vanin et al. 2017).

Model Number	Reference Document	Elastic Modulus of Masonry in Compression
1	NEHRP 2000	Clay Bricks: $E_m = 750f_m$'
2	Tomazevic, 1999	Clay Bricks: $200f_{cb} \leq E_m \leq 2000f_{cb}$'
3	FEMA 273, 1997	Clay Bricks: $E_m = 550f_m$'
4	Sahlin 1971, Crisafulli et al, 1995	Clay Bricks: $E_m = 300f_m$'
5	Drysdale et al, 1994	Concrete Blocks: $E_m = 750f_{m'}$ Clay Bricks: $E_m = 500\text{-}600f_{m'}$
6	Paulay & Priestley, 1992	Concrete Blocks: $E_m = 1000f_{m'}$ Clay Bricks: $E_m = 750f_{m'}$
7	EC8-III (2005)	Clay Bricks: $E_m = 1000f_{m'}$

2.8 Suggested Material Property Values for Seismic Evaluation and Assessment of Existing Structures

Due to the substantial spread of the data, suggested adjustments to the examined ASCE-SEI 41 (2017) procedures are proposed, drawing from the research conducted by (Vanin et al., 2017), Pantazopoulou, (Recommending Modelling to NRC, 2022), (Salmanpour, Mojsilović and Schwartz, 2015).

Table 2.7. Modelling Parameters of URM Walls Proposed for Review per ASCE-SEI 41 Procedures

Parameter	Value
Stiffness (E_m)	$250 \cdot f'_m$
Shear Modulus (G_m)	$0.35 \cdot E_m$

Table 2.8. Modelling Parameters of URM Walls Proposed for Review per ASCE-SEI 41 Procedures

Drift Capacity	Value
Cracking	ϑ_{cr}=0.2%
Yielding and Ultimate	Flexure: θ_y=0.15×θ_u, where θ_u =2.25% (CoV = 0.5%)
Yielding and Ultimate	Shear: θ_y=0.25×θ_u, where θ_u=1.5% (CoV = 0.5%)

2.9 Open Issues in Seismic Analysis and Assessment of URM Structures

The development of unreinforced masonry (URM) buildings in the past centuries involved materials like stone, fired brick, and adobe, and methods like massive vertical walls with timber floors and roof diaphragms. As was discussed in the preceding sections, these structures depend on the overbearing weights and friction to resist lateral loads, and their capacity for lateral deformation is extremely limited. Owing to their large mass which is spatially distributed, and the absence of diaphragm action in case of timber floors, URM structures are particularly sensitive to seismic events. Because the built heritage comprises in its entirety structures that are completely or partially made of unreinforced masonry, there is a global need for improved understanding and modeling of URM structures, especially for earthquake susceptibility. Improved nonlinear models are essential for the design, evaluation, and retrofitting of URM buildings, focusing on performance-based evaluation. Tools for reinforced concrete and steel structures are not easily adaptable to URM structures, due to different structural behaviors and material properties.

Advanced modeling and analysis techniques, such as using SAP2000 software, are vital for addressing challenges in seismic evaluation and retrofitting of URM structures. Current software limitations in performance analysis in seismic zones highlight the need for new modeling methodologies for various URM types and materials. Considering the large part of world population that is currently residing in URM buildings, their high susceptibility to seismic forces leads to significant economic and recovery challenges after seismic events – many recent earthquakes have highlighted this vulnerability and disaster risk in many areas where URM construction abounds (e.g. Gorkha Earthquake, Nepal, April 2015). The research aims to identify knowledge gaps and to develop insights regarding the ability of the existing methods for seismic evaluation of URM structures using different computer modeling approaches. Another objective is to understand how various alternative retrofitting scenarios may be used to upgrade these structures considering the degree of invasiveness of these methods with reference to their applicability in URM structures with heritage value which are governed by the Venice Charter. The investigation includes extensive numerical analysis of simulated URM buildings that model a shake-table tested real URM structure using Linear and Nonlinear models in SAP2000, focusing on various structural features and interfacial contact models. Effective modulus of elasticity and failure criteria are essential study variables, as are discretization methods and structural model creation for accurate building representation.

2.9.1 Available Modelling Techniques

The complexity of unreinforced masonry (URM) structures necessitates advanced modeling techniques for seismic assessment (Valadao 2021). Traditional tools for reinforced concrete and steel structures face challenges with URM due to the absence of reinforcement for ductility in post-elastic responses. Various methods have been developed:

- Equivalent Frame Analysis: Simplifies complex masonry into elements like piers and spandrels, modeled as beam/column components. This method, popular due to its adaptability and ease of use, has limitations in addressing out-of-plane failure modes, especially in seismic analysis.
- Finite Element Analysis (FEM): Offers a detailed view of masonry structures, combining micro and macro modeling. Despite providing nuanced understanding, FEM faces challenges due to high computational demands and lack of precise experimental data on masonry materials.
- Discrete Element Modeling (DEM): Suitable for simulating dynamic failure mechanisms in URM, DEM represents elements as interacting blocks but is limited in accurately analyzing stress states in deformable blocks.
- Shell Type Finite Element Analysis: Used in software like SAP2000, this method enables detailed three-dimensional modeling, crucial for analyzing URM brick walls. However, most commercial software lacks capabilities for 3-D nonlinear analysis with shell elements, often relying on one-dimensional elements for simplification (CSi Inc. (2021), Pantazopoulou, (2013), Valadao, 2021).

2.10 A Review of Canada's Unreinforced Masonry Heritage Categories

In Canada, a range of heritage structures have been constructed using unreinforced masonry (URM) techniques, reflecting the country's immigration history and diverse architectural influences. These URM heritage structures include:

2.10.1 Historic Residential Buildings

Many older neighborhoods in cities like Montreal, Quebec City, and parts of Toronto feature historic homes and apartments built with URM. These often exhibit unique architectural styles like Victorian, Edwardian, or Arts and Crafts. The Distillery District in Toronto, Ontario, is a notable example. This area is known for its well-preserved Victorian industrial architecture, primarily made of brick masonry, and now serves as a popular cultural and residential area.

Figure 2.18. Distillery District in Toronto. https://en.wikipedia.org/wiki/Distillery_District

2.10.2 Religious Structures

Canada has a variety of historic churches, cathedrals, and other religious buildings constructed with unreinforced masonry. Notable examples include the Notre-Dame Basilica in Montreal and the Cathedral-Basilica of Notre-Dame de Québec. This stunning Gothic Revival church, built in the 1820s, is renowned for its intricate interior and impressive masonry work.

Figure 2.19 Notre-Dame Basilica in Montrealhttps://en.wikipedia.org/wiki/Notre-Dame_Basilica_(Montreal)

2.10.3 Educational Institutions

Some of Canada's oldest universities and colleges have URM buildings on their campuses. These structures often include original university halls and libraries with significant architectural and historical value. The University of Toronto's St. George campus features several historic URM buildings. One such building is University College, an exemplary Gothic Revival structure built in the mid-19th century, known for its distinctive masonry.

Figure 2.20 The University of Toronto's St. George Campus. https://www.toronto.ca/city-government/planning-development/planning-studies-initiatives/university-of-toronto-st-george-campus-secondary-plan/

2.10.4 Commercial Buildings

In many Canadian cities, especially within historic districts, you'll find old warehouses, shops, and offices built with URM. These buildings often feature detailed masonry work and are integral parts of the urban historical fabric. The historic Gastown neighborhood in Vancouver, British Columbia, is lined with URM commercial buildings. These structures, dating back to the late 19th and early 20th centuries, have been restored and now house a variety of shops, restaurants, and galleries.

Figure 2.21. Gastown in Vancouver, British Columbia. https://en.wikipedia.org/wiki/Gastown

2.10.5 Government Buildings

Several provincial and municipal buildings, including legislatures and city halls, were traditionally constructed with URM techniques. These structures not only hold historical significance but also often represent important examples of Canadian civic architecture. The Saskatchewan Legislative Building in Regina is an iconic URM structure. Built in the early 20th century, this Beaux-Arts building is constructed of Manitoba Tyndall stone, a type of limestone.

Figure 2.22. The Legislative Building in Saskatchewan.
https://en.wikipedia.org/wiki/Saskatchewan_Legislative_Building

Figure 2.23. Centre Block & Parliament Hill in Ottawa
https://en.wikipedia.org/wiki/Parliament_Hill#/media/File:Ottawa_-_ON_-_Stadtansicht.jpg /
https://en.wikipedia.org/wiki/Centre_Block

Figure 2.24. The Ontario Legislative Building in Toronto.
https://en.wikipedia.org/wiki/Ontario_Legislative_Building

2.10.6 Cultural and Public Spaces

Heritage structures like theaters, museums, and old train stations, many of which are made from unreinforced masonry, can be found across Canada. These buildings are significant both for their architectural beauty and their roles in Canadian cultural history. The Place Royale in Quebec City, often considered the birthplace of French America, features several URM buildings, including the Notre-Dame-des-Victoires Church, one of the oldest stone churches in North America, dating back to the late 17th century.

Figure 2.25. Place Royale in Quebec City.
https://fr.wikipedia.org/wiki/Place_Royale_(Qu%C3%A9bec)

2.10.7 Industrial Sites

Some historic industrial facilities, such as old factories or mills, are URM structures. While many have been repurposed, they retain their original masonry construction. The Alton Mill Arts Centre in Caledon, Ontario, is a fine example of adaptive reuse of an industrial URM site. Originally a woolen and knitting mill in the 19th century, the complex now serves as an arts center while retaining its historic masonry architecture.

Figure 2.26. Alton Mill Centre in Caledon. https://altonmill.ca/

These URM heritage structures are spread across various regions of Canada, each telling a part of the story of the country's development and cultural evolution. Preservation and conservation efforts are key to maintaining these structures, given their vulnerability to environmental factors and the challenges posed by modern urban development.

3 Chapter 3: Numerical Modelling of Two-Storey Unreinforced Masonry Building in SAP2000

3.1 Introduction

Unreinforced masonry (URM) construction, widespread worldwide, often lacks proper engineering and code compliance. URM buildings frequently suffer severe earthquake damage, particularly in developing nations. Recent decades have seen increased experimental studies on URM components and buildings, shedding light on their seismic performance, but certain aspects remain poorly understood due to construction diversity, lack of engineering oversight, non-standard designs, regional variations, and aging structures.

This chapter discusses the numerical model developed to represent a test URM structure which was built in half scale relative to a realistic prototype and tested to a series of earthquake motions. The experimental evidence regarding this structure and its computer models are used in the present work as a testbed of the seismic evaluation and modelling methodologies used in practice to assess the performance of the building in anticipated future events. Such procedures are prescribed by the American Code for Seismic Assessment (ASCE/SEI-41 2017) - Chapter 11, and by Eurocode 8-III (2005 and 2022) for structures of this kind. The experimental details and seismic response of the physical specimen was presented in the referenced project by Bothara, Dhakal, and Mander (2010). The numerical model was created in SAP2000, using identical material properties, and loading conditions as the original physical specimen, both at full scale and half scale. Within this chapter, we will delve into the assessment and retrofit strategies applied during the model's development, alongside the presentation of preliminary analysis results.

In SAP2000, a widely used structural engineering software, frame analysis refers to the process of simulating and analyzing the behavior of framed structures, such as buildings. Frame analysis in SAP2000 involves creating a mathematical model of the structure, representing it as an interconnected system of beams, columns, and other structural elements. The first step in frame analysis is defining the geometry of the structure. This includes specifying the dimensions, locations, and orientations of all structural components, by idealizing them as beams and columns. SAP2000 allows users to model different types of structural elements, including beams (members that resist bending), columns or Piers (members that resist axial and lateral loads), and shells (elements that represent surfaces such as slabs and walls). Support Conditions are defined as boundary conditions, representing how the structure is supported at its base or connections. Supports can include fixed supports, rollers, and hinges, among others. SAP2000 allows the user to define different load cases and load combinations to simulate different loading scenarios. Users may choose from different analysis types, including linear static analysis (for determining the response under static loads), modal analysis (for finding natural frequencies and mode shapes), response spectrum analysis (for seismic analysis), and nonlinear analysis (for capturing nonlinear behavior of materials and connections). Once the model is defined and loads are applied, SAP2000 performs the analysis to calculate the structural response. The software provides various output results such as member forces, displacements and stresses, to assess the structural performance.

3.2 Graphical Representation and Damage Classification of an Unreinforced Masonry Building According to EMS-98 (Grünthal and Levret, 1998)

The table shows the need for scientific studies to understand the general reasons for damage before repair, retrofit, and reconstruction activities are carried out. The study categorizes damage levels and types in monumental masonry structures and relates them to their wall geometry, construction quality, and material properties. It aims to provide a systematic correlation between these aspects, which could inform detailed modeling efforts for predicting the behavior of historic masonry buildings during earthquakes.

Table 3.1. Graphical Representation and Damage Classification of an Unreinforced Masonry Building

Graphical Representation	Damage Classification
	Grade 1: Minimal Impact • No impact on structural integrity; minor cosmetic damage • Very fine cracks on a limited number of walls • Only small plaster pieces dislodge • Occasional falling of loose stones from the highest parts of some buildings
	Grade 2: Limited Harm • Minor structural damage; more significant non-structural effects • Visible cracking across several walls • Larger plaster sections may come loose • Some chimneys might partially collapse

	Grade 3: Considerable Damage • Noticeable structural damage; serious non-structural issues • Broad and deep cracking in most walls • Roof tiles may come loose and fall • Chimneys may break at the point where they meet the roof • Non-structural elements like partitions and gable walls may fail
	Grade 4: Severe Damage • Major structural damage; extensive non-structural failure • Walls may fail significantly • Roofs and floors could have substantial structural failure
	Grade 5: Complete Destruction • Extremely severe structural damage • Buildings may be completely or almost entirely collapsed

3.3 The Methodology of Assessing the Damage to the Buildings

The image below provides a key to interpreting the impact of earthquakes on buildings, EMS-98 (Grünthal and Levret, 1998). These classifications help differentiate the types of buildings studied, as different types of construction may respond differently to seismic activity. Here is an explanation of its components:

Figure 3.1. The categories of Damage to the Buildings

- <u>Monumental Class</u>: This part identifies types of structures that have been assessed for damage. The four types of structures are:
- <u>Church</u>: Represented by an icon of a Christian church, characterized by a cross on top of the structure.
- <u>Mosque</u>: Depicted with a crescent, found on mosques representing Islamic architecture.

- Public: Indicated by a building with columns, signifying government or public buildings like museums, libraries, etc.
- Residential: Shown as a simple house icon, representing where people live.

Damage Grade: Next to the building icons is a scale labeled "Damage Grade" with numbers 1 to 5, each with a distinct color. This is a simplified representation of the European Macroseismic Scale (EMS-98) or a similar scale used to classify the extent of damage to structures after an earthquake. Here's what each grade generally signifies:

- Blue - Grade 1: Negligible to slight damage. This might include minor cracks or cosmetic damage that doesn't affect the structure's integrity.
- Green - Grade 2: Moderate damage. Small structural issues may be present, along with more significant non-structural damage.
- Yellow - Grade 3: Substantial to heavy damage. At this level, the building may have serious structural issues that could compromise its integrity or safety.
- Orange - Grade 4: Very heavy damage. This likely includes severe structural compromise, with a high risk of partial collapse.
- Red - Grade 5: Destruction. This indicates that the building has been destroyed or is near total collapse.
- The arrow on the right side emphasizes the increasing severity of damage from bottom to top.

Such scales are critical for rapid assessment of infrastructure after seismic events, for prioritizing emergency response, and for subsequent rebuilding and strengthening efforts.

The majority of the unreinforced buildings lack the necessary wall strength to withstand the tremors. Notably, insufficiency in in-plane wall strength is a significant factor in structural failures. Moreover, even though some walls reported in past post-earthquake reconnaisances were of adequate thickness, the disintegration of masonry diminished their effective resistance to seismic forces, leading to collapses. The Masonry Quality Index (MQI) assesses the buildings' conditions and it is known that a large percentage fell into a lower quality category, suggesting a susceptibility to damage from seismic activity, attributed mainly to the irregular stonework and substandard materials used. The array of compressive strengths through on-site non-destructive testing methods like the Ultrasonic Pulse Velocity and Schmidt Hammer have indicated not only a broad range of stone and mortar qualities but also generally poor mortar quality, especially in walls with irregular stone masonry. It is suggested that the methods should be updated to better reflect the true strength of a building by considering things like how well the building parts stick together and how heavy the building is. These rules for judging the safety of buildings ought not to be used when the stonework is falling apart. Instead, the Masonry Quality Index should be used as a guilding variable, because it seems to show the chance of damage more than it predicts it. It is necessary to use more detailed computer studies to look at other important things like how the ground and buildings interact, how multiple earthquakes affect buildings, and the influence of vertical shaking (when the epicenter is near, the vertical component of the earthquake may be significant). This is all to make sure old buildings can better survive earthquakes.

3.4 Values of the Displacements in Terms of Out of Plane Motion for Spectral Analysis, (Frame Model)

Spectral Analysis is a method used in structural engineering for assessing the response of structures to dynamic loads, especially seismic activity. Spectral analysis provides insights as to how different frequencies of ground motion, as might be experienced during an earthquake, affect the structure. In the context of spectral analysis using a frame model in SAP2000, the "values of the displacements in terms of out of plane motion" refer to the quantified measurements of how much points or elements in the structure move perpendicular to their main plane. This is particularly relevant in seismic analysis, where the out of plane motions can significantly impact the integrity and safety of a structure.

3.4.1 The Earthquake is Acting Parallel to the Short (i.e., X) Direction, Affecting Mainly the Long Walls.

When an earthquake acts parallel to the short direction (X-axis) of a building, the primary impact is on the long walls of the structure. Long walls are generally more vulnerable. This scenario presents specific challenges and considerations in structural engineering and seismic analysis:

1. Direction of Seismic Forces: Earthquake forces acting parallel to the short direction of the building (along the X-axis) means that the long walls (typically oriented perpendicular to the X-axis) will experience the most significant impact. These walls are subjected to out-of-plane bending moments due to the seismic waves.

2. In-Plane and Out-of-Plane Responses: The long walls will have two primary types of responses:

    - In-Plane Response: This refers to the shear forces that the walls will experience within their plane. The long walls will tend to shear in the direction of the earthquake force.

    - Out-of-Plane Response: This is critical for long walls as they are susceptible to bending and buckling perpendicular to their plane (out-of-plane) due to the lateral forces.

3.5 Model Dimensions

The SAP2000 model for the project by Bothara, Dhakal, and Mander (2010) was created based on the dimensions illustrated in Figure 3-1, which refer to the half scale model of a full scale prototype, which was a two-story unreinforced masonry (URM) building located in Christchurch, New Zealand, representing a typical URM house from the previous century in the region. Thus, any geometric dimensions of the model represent 50% of the respective values of the prototype. To better understand URM building dynamics of New Zealand's typical URM houses, the model represents a two-story brick house with flexible floor and roof, comprising fired clay bricks made to scale. Modifications were made to the roof type and roofing material to observe the behavior of gable walls and clay roofing tiles.

In plan, the scaled model is 1920mm long along the X-axis and 2880mm long along the Y-axis. Additionally, the height of each story was 1340 and 1140 mm respectively, with a gabled roof extending vertically by 875 mm. The total model height was 3295mm. Windows were positioned on all three walls. The structural system included supplementary components such as the wood floor system and roof. This system included timber floor joists measuring 35mm in width, and 125mm in depth, and spanning a total of 1920 mm (short plan dimension), being equally spaced at 180 mm in the Y-axis. These joists supported a system of timber floor planks, measuring 23mm in width and 11mm in depth, which covered the entire floor area, extending over 2880mm along the Y-axis. Twin-wythe cavity walls in the original building were replicated using single wythe walls with an average mortar thickness of 12mm. The same materials as the original were used to maintain similitude, with scale factors.

To achieve structural similitude in a building, a meticulous approach to mass distribution was employed. A total of 4.2 tons of additional mass was added to the gable walls at both the floor and eaves levels, with this mass evenly divided between two floors, amounting to 2.1 tons per floor. In the model, each floor was segmented into 24 nodes, and each node was allocated a mass of 0.0875 tons. This precise distribution of mass was deemed crucial for maintaining the laws of similitude between the model and its prototype structure.

It's worth noting that load-bearing masonry buildings with timber floor and roof structures are primarily distributed mass systems, with the floors and roofs contributing to less than 10-20% of the building's mass. The lumped addition of mass, necessary for geometric similitude, may result in different response mechanisms compared to a real prototype, potentially affecting model performance during excitation. Additionally, the use of full-sized bricks for the walls, while providing appropriate in-plane shear stress and stiffness, led to higher out-of-plane flexural stiffness and strength compared to half-scale bricks, presenting another limitation of the experimental work.

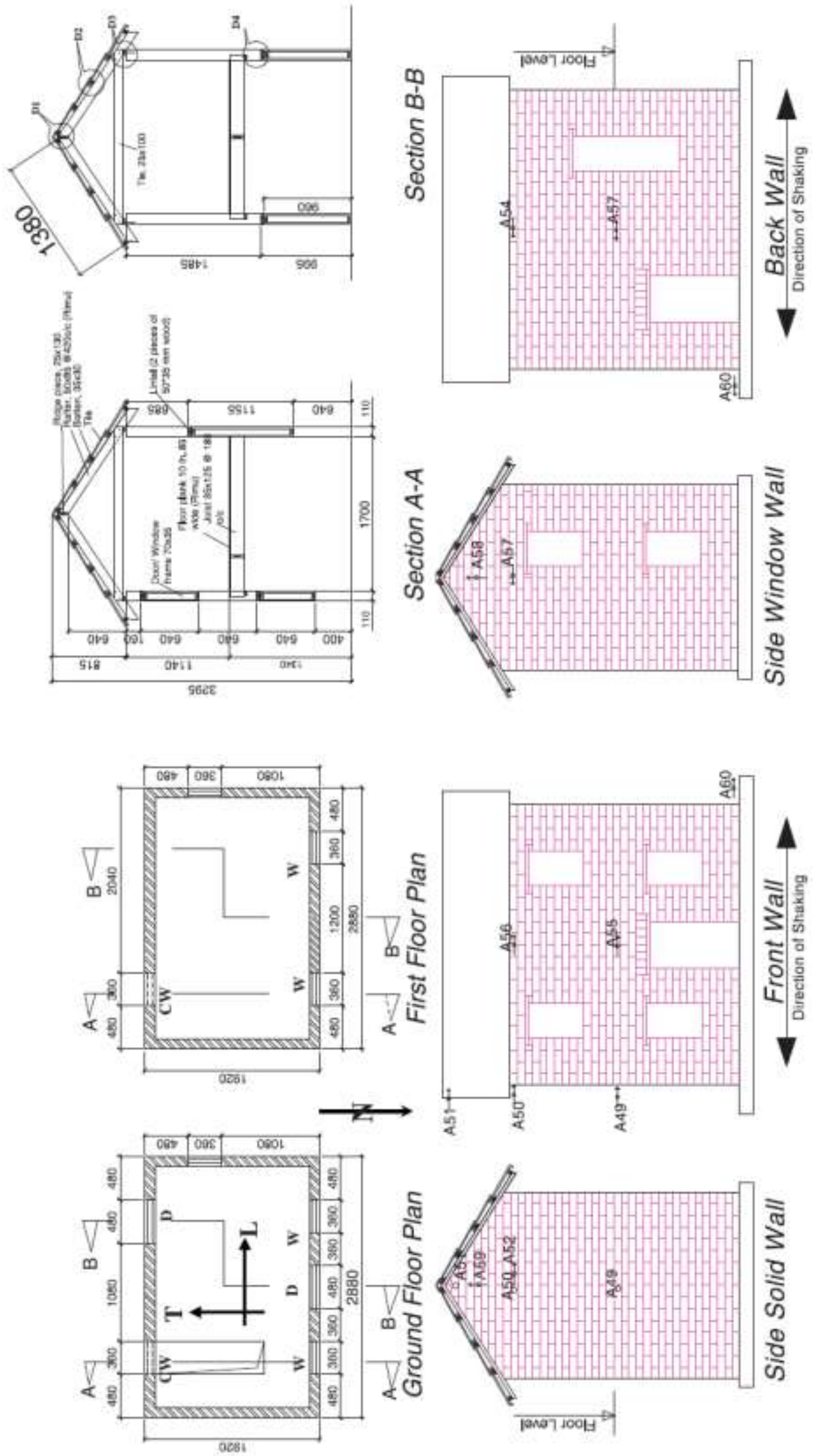

Figure 3.2 Elevation and Plan of the Model by Bothara, Dhakal, and Mander (2010)

3.6 Material Properties

The reference building case study comprised two main materials: masonry bricks and timber. Specific material properties for both materials were defined in SAP2000 by creating custom materials. During the model building's construction, extensive tests had been done to characterize the material properties. Bricks were tested in compression and for moisture absorption, whereas cubes were used for measuring the compressive strength of mortar. Masonry prisms, made at different brickwork layers and time intervals, were tested under compression, flexural bond, and shear tests. Results, detailed in Table I for material strengths likely surpass those of existing masonry buildings.

Table 3.2. Average Material Properties Used by Bothara, Dhakal, and Mander (2010).

Material	Test type	Test result	CoV (%)	Remarks
Brick Masonry	Compressive strength	26.6 MPa	17	
Brick Masonry	Initial rate of absorption (IRA)	63.6 g	7.4	
Mortar cubes	Compressive strength	7.6 MPa	10.6	
Masonry prism	Compressive strength	16.2 MPa	19.7	At strain 0.0035
Masonry prism	Young's modulus, E	6100 MPa	45.2	At strain 0.0016
Masonry prism	Shear strength	τ_0 =0.93 MPa	38.6	
Masonry prism	Shear strength	Φ=44.4°	13.4	
Masonry prism	Flexural bond	0.42 MPa	35	
Masonry prism	Split bond	0.41 MPa	38	

The analysis was carried out using SAP2000 software, considering various load cases such as dead loads and lateral loads simulating seismic effects. Live loads were omitted in estimating the added mass per the laws of similitude, as they typically contribute less than 5-6% of the total mass in this type of building, as specified by building codes. In the present chapter, linear elastic materials were used in the finite element shell and equivalent frame analysis models, with linear elements for specific components like beams and joists which were used in the alternative approaches taken in simulating the floor and roof of the structure. To represent the building's interaction with the ground, fixed supports were employed at the foundation level of the model building, restricting both lateral and vertical movements at the base of columns and walls. This choice aimed to simulate real-world boundary conditions during testing.

Timber was utilized for the portable pitched roof and floor, while masonry was employed for the walls. This choice of materials reflects the real-world prototype. Table 3.3 shows the Materials properties data and the introduction of these values in the program material definition tables. (Figure 3.3, Figure 3.4, Figure 3.5)

Table 3.3. Materials Properties Data.

Material	Weight (kN/m3)	Modulus of Elasticity (MPa)	Poisson's Ratio
Masonry	18.63	840 MPa	0.2
Masonry Rigid Zones	18.63	840,000 MPa (1000 times higher than Modulus of Elasticity of Masonry)	0.2
Timber	15	10 GPa	0.3

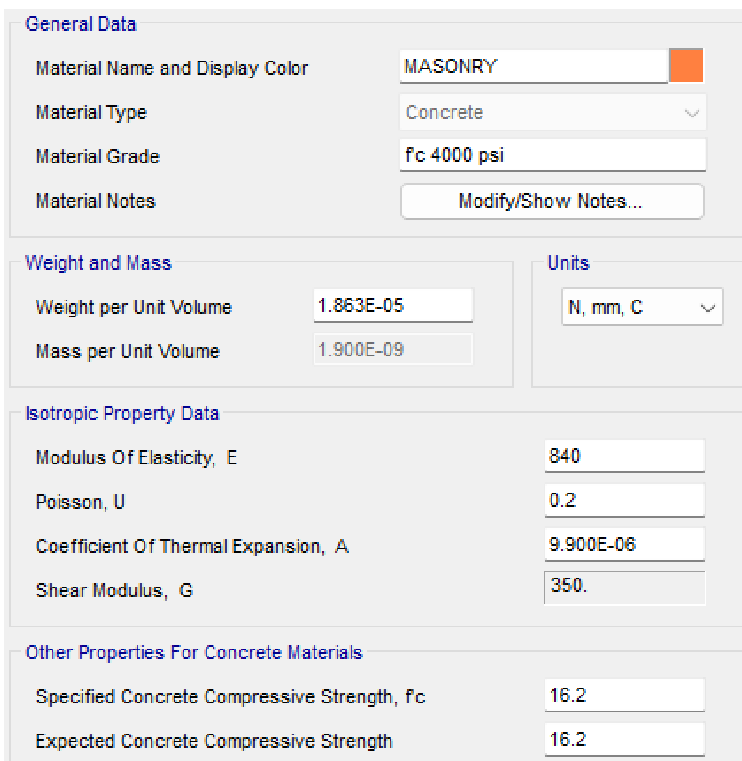

Figure 3.3. Material Properties for Masonry

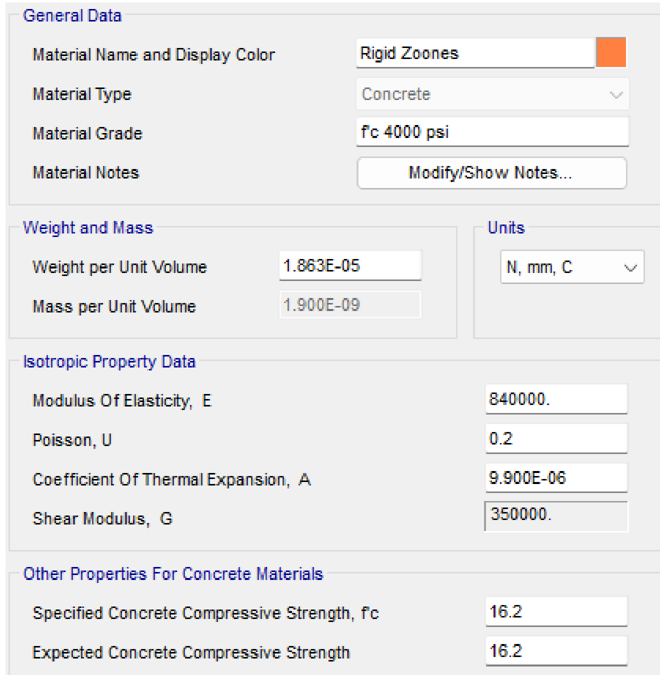

Figure 3.4. Material Properties for Rigid Zones

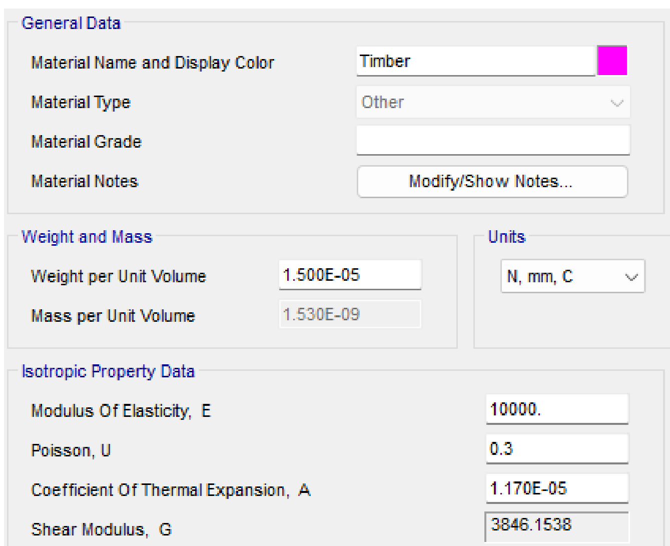

Figure 3.5. Material Properties for Timber

3.6.1 Masonry

The material properties for Masonry used in the SAP2000 models were obtained using the Code expressions for the relationship between modulus of elasticity and masonry compressive strength.

3.6.2 Modulus of Elasticity for the Original Masonry Structure

This mechanical property is crucial for understanding how unreinforced masonry (URM), typically comprising brick, stone, or clay, responds to stress, particularly under seismic loads. The modulus of Elasticity influences stress distribution, seismic vulnerability, and the effectiveness of retrofitting strategies. For URM structures, known for their limited tensile strength and flexibility. according to the experimental results of Bothara, Dhakal, and Mander (2010) building, the theoretical value of the modulus of Elasticity for the original structure was estimated as follows:

- f_{jc}, represents the compressive strength of the mortar joints and is taken equal to 7.6 MPa according to experimental characterization tests conducted by Bothara, Dhakal, and Mander, (2010). However, this value was obtained through cube mortar testing. To find the normal strength, we need to determine the compressive strength of cylinder mortar, which is typically 85% of the cube mortar compressive strength, reducing the above value to 6.46 MPa.
- $7.6 \times 85\% = 6.46 \ MPa$
- f_{bc}, is the compressive strength of the masonry unit, which is 26.6 MPa, as per the experimental report (Bothara, Dhakal and Mander, 2010)
- f'_m, is the homogenized compressive strength of masonry as a composite.
- k, is a function of the mortar thickness, varying from 0.55 for 6mm joints to 0.35 for 15mm joints. In this case the mortar thickness was kept 12mm on average according to (Bothara, Dhakal and Mander, 2010), so the coefficient k is estimated by interpolation equal to 0.42.
- According to Clause 6.5.2, in the CSA S304-14 the modulus of Elasticity is ($850 \cdot f'_m$) MPa but < 20 GPa.

$$f'_{mc} = K \cdot f_{bc}^{0.7} \cdot f_{jc}^{0.3} \quad MPa \tag{3.1}$$

$f'_{mc} = 0.42 \times 26.6^{0.7} \times 6.46^{0.3}$

$f'_{mc} = 7.3 \quad MPa$

$E_m = 850 \times f'_m$

$E_m = 850 \times 7.3 = 6{,}205 \ MPa.$

According to the earlier discussion presented in Chapter 2, this theoretical value represents an unconservative upper limit (higher stiffness underestimates the displacements that the structure is likely to develop during strong earthquakes. A 50% reduction is recommended to account for cracking, reducing the above nominal value to 3100 MPa; for type E typology, which represents the present structure in the Table 2.5, this value is probably excessive and will not correlate well the seismic test results. Lower values are recommended in Table 2.5 based on the collective experimental evidence, suggesting that the anticipated value should be,

$E_m = 200\, f'_m = 1240\ MPa$; whereas based on the experimental values a mean value of 500 MPa was recommended with a coefficient of variation of 0.5. A reference analysis was made using $E_m = 840\ MPa$ as an average value between the above recommended limits.

Table 3.4 Material Properties for Masonry Used in the SAP2000

Property	Value
Weight	18.63 kN/m³
Modulus of Elasticity	6205 MPa
Compressive Strength of Masonry prism	16.2 MPa
Compressive Strength of Masonry Brick	26.6 MPa
Poisson's Ratio	0.2
Shear Modulus	2585 MPa

Figure 3.6. Theoretical Material Properties for Masonry

3.6.3 Timber

In Table 3-1 below, the material properties for timber were selected from the research conducted by Karapitta et al. (2012) and Engineering ToolBox (2004), as documented in the study by Vintzileou et al. (2015). These specific properties were subsequently employed in the SAP2000 models.

Table 3.5. Material Properties for Timber Used in the SAP2000

Property	Value
Density	4.413 kN/m³
Modulus of Elasticity	10 GPa
Poisson's Ratio	0.3
Shear Modulus	3.58 Pa

3.7 Model Elements

Unreinforced Masonry (URM), which is typically encountered in older construction prior to the widespread adoption of steel reinforcement in masonry, is discussed in Section 3.4.2 of the ASCE/SEI-41 (2017) Recommendations. As was mentioned in the Introduction and in Section 2.10, some older Canadian URM constructions have been standing in major cities for almost two centuries. While auxiliary materials like iron ties and timber may be incorporated, these buildings are not considered Reinforced Masonry (RM). In the absence of steel reinforcement, the strength of URM masonry is based on frictional action along the bed joints, where the presence of overbearing axial load was shown to be critical in Fig. 2.2. These mechanisms of resistance deteriorate quickly during cyclic displacement reversals, whereas URM's overall response is brittle even if some individual members may possess some ductility. URM structures may be made from two or three wythe walls that work as a single component with semi-composite action even without cavity filling if header courses are present. It is noted here that despite the practicality of nonlinear modeling, particularly in static pushover analysis, results from this modeling may be non-dependable on account of the variability of material characteristics caused by aging, weathering, and the original masonry construction.

In URM constructions, timber is a commonly used flooring material. Timber floors typically consist of tongue and groove planks nailed to joists, which are supported either on URM walls or on bearers resting on internal columns. (Russell and Ingham, 2010)

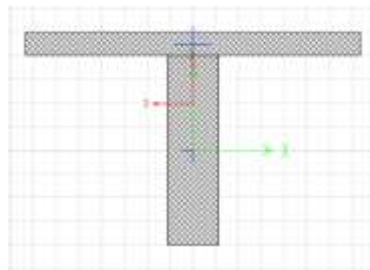

Figure 3.7. SAP2000 Section Designer Joist and Participating Slab

3.8 Case One: Equivalent Frame Analysis

Equivalent Frame Analysis (EFA) was chosen as the modeling approach for the building since it is the Code-recommended method for modelling the behavior of unreinforced masonry structures and it is known for its computational efficiency; but its accuracy and relevance to the true building behavior under seismic loads is not well documented.

Equivalent Frame Modeling is an analysis method in structural engineering, idealizing complex continuous structures into interconnected beams and columns as shown in Fig. 3.7 for an example wall pier and spandrel. This method replaces walls, slabs, and shells with beam and column elements.

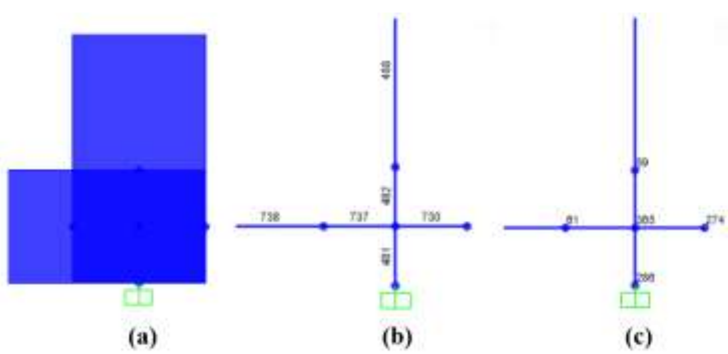

Figure 3.8. (a) The Frame Model of Structure, (b) Label of Frames, and (c) Label of Joints

The Equivalent Frame Analysis method described in the FEMA / SEI 41 (2017) and the NRC (2021) report, simplifies complex structures such as walls, piers, and spandrels into idealized, beam-column linear elements. This approach considers nodal rotations and transverse displacements as degrees of freedom, with considerations for reinforcement slip. It utilizes elastic flexural and shear rigidities, along with cracked properties. End plastic hinge zones are represented by lumped rotational springs or distributed plasticity. Reinforcement slip and dowel action are factored-in using rotational and translational springs, while gap elements are used to deal with imperfect connections between components. Careful selection of hysteresis rules is crucial to accurately model member responses in cyclic displacement analyses. The backbone curves, essential for analysis, are determined based on characteristic points, shaping the system's behavior.

The behavior of masonry walls and spandrels is influenced by factors like the axial load ratio, longitudinal and transverse reinforcement ratios, and aspect ratio. Different modes of failure can occur based on these factors, and understanding their hierarchy is vital in determining how brittle the structural response might be. Failure modes dominated by compression toe crushing, compression bar buckling, local instability of the compression zone of the diagonal strut, or diagonal shear failure are considered brittle because they are limited by the force capacity of the component. If sliding shear occurs along bed joints within the wall plane, it represents a more ductile failure mode. In the out-of-plane direction, potential failures include weak-axis bending, local instability of the wall in the compression zone, and global instability due to out-of-plane rocking influenced by lateral earthquake pressure (Pantazopoulou (2022), ASCE/SEI-41 (2017)).

Frame-models are tailored to represent assemblies of linear elements like beams and columns. They are ideal in modeling structures where primary deformation occurs along a single axis. Particularly suitable for components undergoing axial and bending deformations, frame elements simplify intricate 3D structures into computationally efficient 1D representations, especially in straightforward structures. However, frame elements have limitations when dealing with thin surface structures such as slabs or shells, where significant out-of-plane deformations (bending) come into play. Their accuracy diminishes notably when structures exhibit simultaneous and substantial membrane (in-plane) and bending (out-of-plane) behaviors. In such cases, frame elements may not provide precise results.

Shell elements, in contrast, are two-dimensional constructs adept at capturing both in-plane (membrane) and out-of-plane (bending) deformations. They find application in modeling thin-walled structures like slabs, walls, and shells. Vital for accurately representing surface structures, shell elements excel in scenarios where both in-plane and out-of-plane deformations are crucial, as seen in roofs, walls, and slabs. Shell elements offer a more precise depiction of actual structural behavior, especially when both membrane and bending deformations are substantial. In seismic or dynamic analyses, shell elements provide superior accuracy in predicting the structure's response due to their ability to capture multiple types of deformation. However, their higher complexity means that shell element analyses can be more computationally intensive than frame element analyses. Proper meshing and discretization play pivotal roles in obtaining accurate results with shell elements, especially in areas around openings and irregularities. Careful attention to these factors ensures the reliability of analyses involving shell elements in SAP2000.

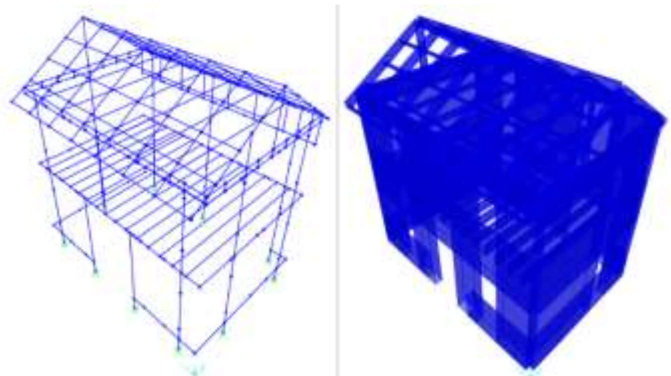

Figure 3.9. Equivalent Frame Analysis

3.8.1 Geometry of the EFA Model Per Façade

In SAP2000, the geometry of an Equivalent Frame Analysis (EFA) model for each building façade is structured to simulate the building's seismic behavior accurately. This involves dividing each façade into vertical lines or frames that represent the primary lateral load-resisting elements, such as columns, walls and spandrels, while incorporating horizontal elements like floors and roofs as rigid or semi-rigid diaphragms to distribute lateral loads. The model also accounts for rigid zones as the areas where spandrels and wall/piers overlap, by adjusting the stiffness of the frames and includes stiffer structural properties for these areas.

Table 3.6. The Geometry of the EFA Model Per Façade on SAP2000

	(EFA) model XZ façade	(EFA) model YZ façade	(EFA) model XZ façade	(EFA) model YZ façade
Standard	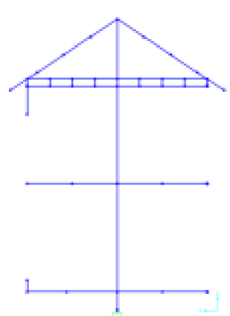	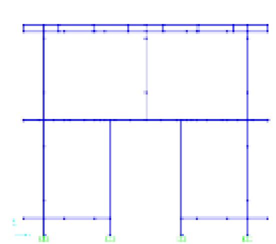	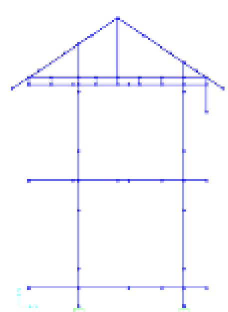	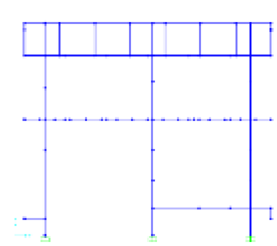

	(EFA) model XZ façade	(EFA) model YZ façade	(EFA) model XZ façade	(EFA) model YZ façade
Extrude	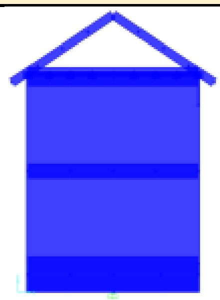	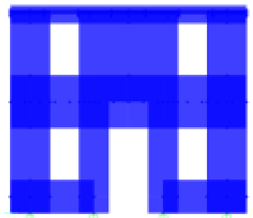	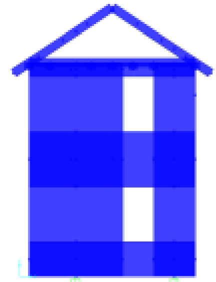	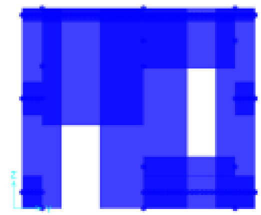

3.8.2 Equivalent Frame Analysis Scope

The scope of Equivalent Frame Analysis (EFA) in SAP2000, focuses on a comprehensive evaluation of a building's structural response under various load conditions. The analysis is methodically segmented into distinct phases, each addressing critical aspects of structural behavior.

- Gravity Load Analysis: The analysis begins by solving for the building's response to gravity loads. This involves modeling the structure with fixed supports at the foundation level and studying its behavior under self-weight and other gravity-induced loads.
- Lateral Load Analysis: The analysis investigates the building's response to lateral loads induced by seismic forces. Equivalent frame analysis will be used, where walls and spandrels are replaced with equivalent beam/column elements. Nonlinear hinge elements specified in ASCE/SEI-41 tables for URM buildings will be used to model the nonlinear response of the members.
- Load Cases: The different load cases considered include dead loads and lateral loads due to seismic forces. Live loads will be ignored due to their minimal contribution to the building's total mass.
- Boundary Conditions: The model is equipped with fixed supports at the foundation level to represent real-world constraints.
- Modeling Assumptions: Assumptions made during the modeling process includes using rigid zones with a modulus of Elasticity 1000 times higher than that of masonry for the flexible components. In the present chapter, materials are approximated as linear elastic.

- Experimental Validation: The elastic analysis aims to validate the modelling procedure by correlating the initial elastic period of the experimental structure obtained in the early tests on the half-scale model of the URM building on the shake table.
- Performance Levels: The analysis will assess the building's response in both elastic and in the following Chapter 4, into the inelastic range, to evaluate its seismic performance under various levels of seismic excitation.
- Displacement Analysis: The analysis will include evaluating the maximum displacements at the middle of the short and long walls during lateral load analysis to understand the out-of-plane effects created by the flexible diaphragms at floor and roof level.
- Damage Assessment: The analysis will assess potential damage locations and severity based on the modeled response, helping to identify vulnerable areas and potential failure modes during seismic events.

Considering these factors (Modeling Assumptions, Cracking and Structural Degradation, Excitation Conditions, Measurement Errors, Model Validation, and Dynamic Damping) it is crucial to carefully review the modeling assumptions, boundary conditions, material properties, and excitation parameters used in both the experimental and numerical analyses to identify the reasons for the differences in the obtained period ranges. Additionally, validating the numerical model against experimental data can help improve its accuracy and reliability in predicting the dynamic behavior of the structure.

3.8.2.1 Load Input

The following load patterns have been used in the EFA of the experimental building. The dead load represents the permanent and constant weight of the building components, such as walls, floors, and roofs. It is applied as a linear static load to account for the structure's self-weight; dead and permanent loads are used for calculating the mass of the structure which is subsequently used in modal analysis.

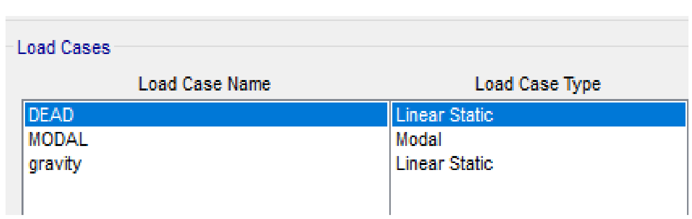

Figure 3.10. Define Loads

3.8.2.2 Additional Mass

During the shake table test, the specimen under examination was reduced in size to a 1:2 scale to align with the test facility's limitations. Scaling down the length units by half, denoted as $\lambda = 1/2$ resulted in a reduction of the structure's volume and weight by the third power of the scaling factor, i.e., the weight (and mass) of the model was only 1/8 of the prototype. However, to maintain consistent material strength, stresses must be equal between the model and the full scale reference – thus, forces needed to be scaled down by ¼ (which is the ratio reduction of the areas) in order to ensure comparable stress levels with the full-scale model. As weight is a force, it was necessary to add external weights, to compensate for the absence of the model's self-weight. To achieve similitude with a scaled ratio of 1:2 in both mass and dimensions, 4.2 tons of additional mass were added to the gable walls at both floor and eaves levels. This equated to 2.1-ton masses distributed among 24 nodes on the first-floor level, with an equal amount applied at the top on eaves levels and gable walls, following the assignment of mass to joints in the global coordinate system, including translations in the X, Y, and Z directions. Additionally, extra mass related to the tile weight on the portable pitched roof was included.

In the experiment, the additional masses were fixed to the floor joists and roof ties to load the long walls (Bothara, Dhakal, and Mander (2010)). For the short walls, platforms were constructed, one end of which was rigidly tied to the short wall, and the other end rested on sliding joints supported on floor joists or roof ties. The additional weights were attached as close as possible to the walls to minimize amplifying effects due to diaphragms. However, there were constraints in the modeling process. For example, the concentrated additional mass used to achieve stress similarity, while essential for the experiment, might have altered the response mechanism in a manner distinct from a genuine prototype. Furthermore, the decision to substitute twin wythe cavity walls with single wythe full-sized brick walls posed a limitation, affecting the flexural stiffness and strength of the walls in the out-of-plane direction. Table 3.8 and Table 3.9 provided a clear overview of the roof weight distribution and the impact of additional masses on different sections of the roof and gable walls.

Table 3.7. Additional Distributed Mass

Item	Additional Mass (tons)	Mass on Each Floor (tons)	Number of Nodes on Each Floor	Mass on Each Node (ton)
Additional Mass on Gable Walls and eaves level	4.2	2.1	24	0.0875

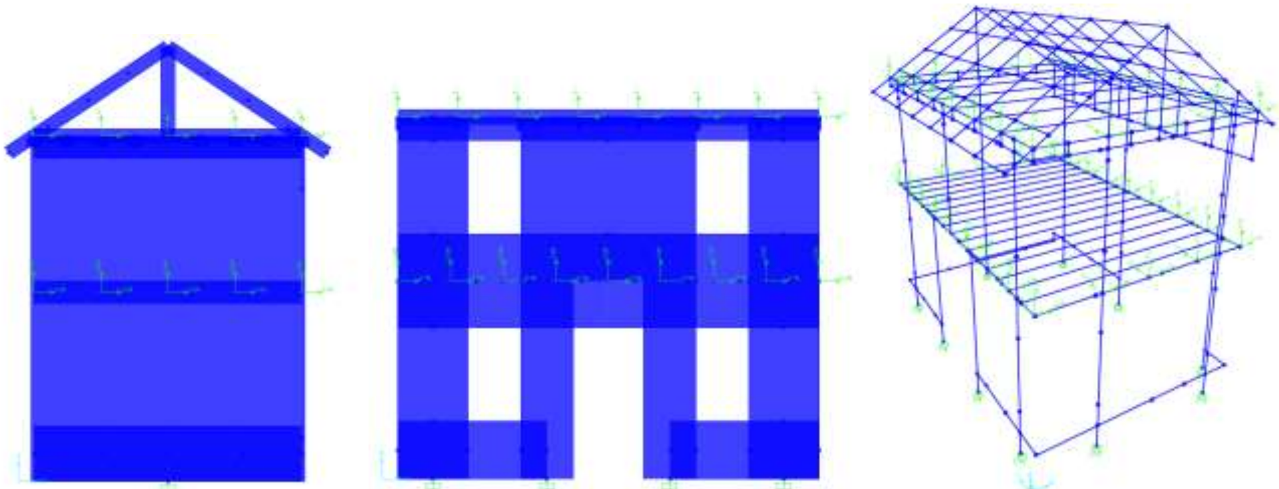

Figure 3.11. Distributed Mass on Half Scale Frame Model

Table 3.8. Additional Mass on the Roof

Node Type	Number of Nodes
Middle and Top	42
Eaves Level	26
Edges	4

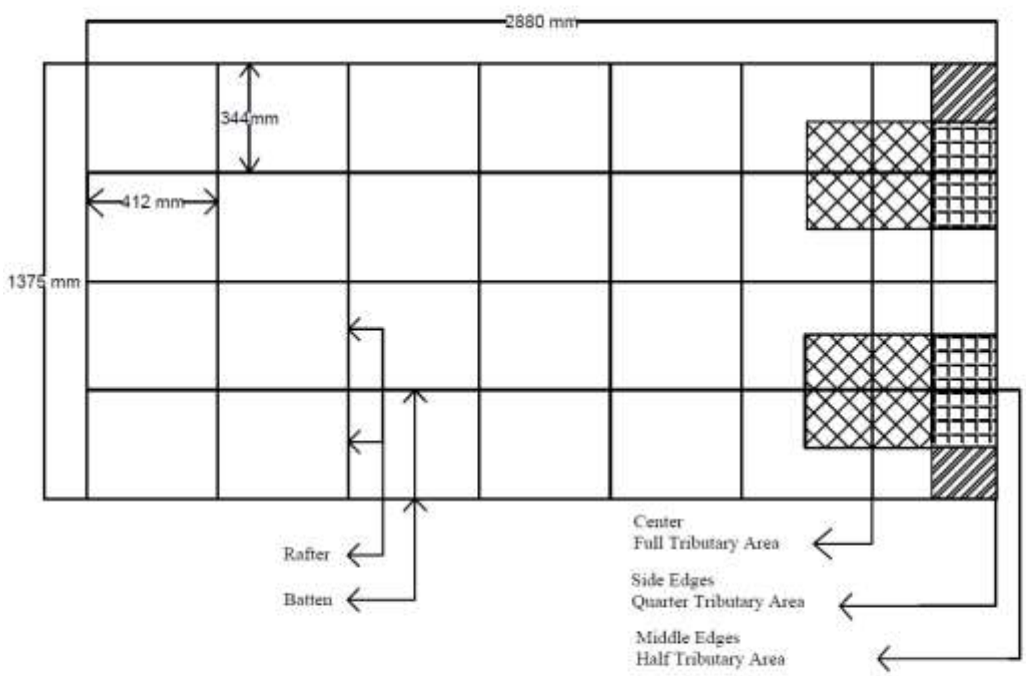

Figure 3.12. Distributed Mass on the Portable Pitched Roof

The weight of the tiles was taken equal to 0.2 kN/m². Each tributary area square of the Batten and Rafter on the pitched roof (Figure 3.12) had dimensions of 344mm × 412 mm (about 1.13 f_t ×1.35 f_t). Consequently, the distributed mass for each center node, calculated based on the full tributary area, amounted to 28.46 N.

$$0.2kN/m^2 \times 0.344\ m\ \times 0.412 = 0.02846\ kN$$

Table 3.9. Roof Weight and Tile Analysis

Section	Tile Weight (kN/m^2)	Tributary Area	Distributed Weight (N)
Center (Ridge Board)	0.2	Full	28.46
Middle Edges	0.2	Half	14.23
Side Edges	0.2	Quarter	7.11

To estimate the weight of the model, the perimeter wall volume was determined:

(2.88x2 + 1.92x2) × 2.48 × 0.11 = 2.61 m^3 of masonry, which, when multiplied by the density of 18.63 kN/m³, leads to 48.6 kN; this is the part of the building weight that is owing to the brickwork, without any additional components and excluding the roof's weight. Consequently, the building has a mass of 4.8 tons. To this, 4.2 tons were added at the gables and eaves, and an additional 2 tons is the mass of portable pitched roof itself, totaling 11 tons.

Table 3.10. Assembled Joint Masses

TABLE: Assembled Joint Masses										
Joint	MassSource	U1	U2	U3	R1	R2	R3	CenterX	CenterY	CenterZ
Text	Text	KN-s2/m	KN-s2/m	KN-s2/m	KN-m-s2	KN-m-s2	KN-m-s2	m	m	m
6	MSSSRC1	0.04096	0.04096	0.04096	0	0	0	1.07	2.99	0
267	MSSSRC1	0.01003	0.01003	0.01003	0	0	0	0.11	0.35	0
286	MSSSRC1	0.01003	0.01003	0.01003	0	0	0	0.11	2.75	0
288	MSSSRC1	0.00952	0.00952	0.00952	0	0	0	0.11	1.97	0
293	MSSSRC1	0.00952	0.00952	0.00952	0	0	0	0.11	1.13	0
334	MSSSRC1	0.01003	0.01003	0.01003	0	0	0	1.79	0.11	0
341	MSSSRC1	0.02257	0.02257	0.02257	0	0	0	0.65	0.11	0
396	MSSSRC1	0.01003	0.01003	0.01003	0	0	0	2.03	0.35	0
399	MSSSRC1	0.01605	0.01605	0.01605	0	0	0	2.03	2.75	0
410	MSSSRC1	0.03611	0.03611	0.03611	0	0	0	2.03	1.61	0
SumAccelUX	MSSSRC1	11.3	0	0	0	0	0	1.1063	1.56441	1.56671
SumAccelUY	MSSSRC1	0	11.3	0	0	0	0	1.1063	1.56441	1.56671
SumAccelUZ	MSSSRC1	0	0	11.3	0	0	0	1.1063	1.56441	1.56671

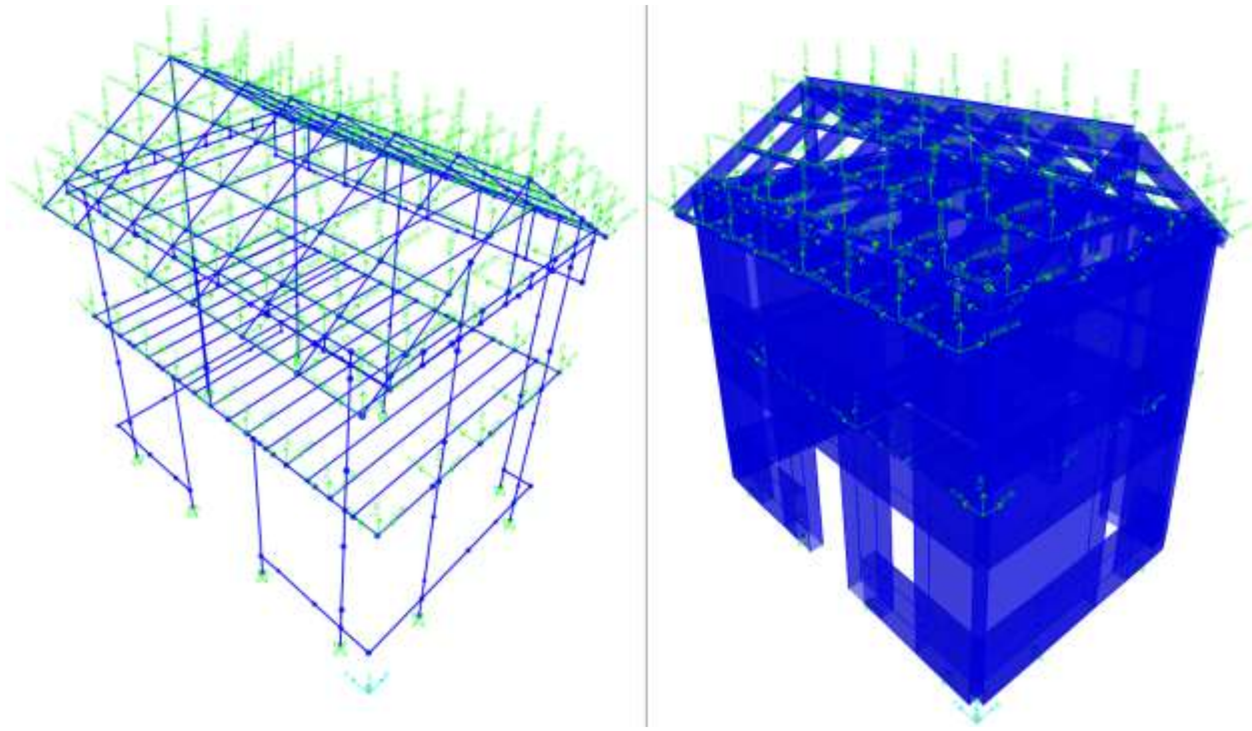

Figure 3.13. Additional Mass Distributed Load

3.8.3 Modal Participating Mass Ratios

Modal analysis was performed to determine the natural frequencies and mode shapes of the structure. In the context of unreinforced masonry structures, these analyses become intricate due to the numerous degrees of freedom. Therefore, a substantial number of modes must be considered to sufficiently excite an appropriate fraction of the total mass in the lateral directions, making the process more complex (Pantazopoulou, 2013). This was done in order to calibrate the material properties of the elastic model with the experiment, and to validate the EFA model. Results are listed in Figure 3.11 which is organized as follows:

- Output Case: This column indicates that the results are from a modal analysis.
- Step Type: Indicates the type of analysis step, which is "Mode" in this case.
- Step Num: Represents the mode number corresponding to the natural vibration mode of the structure.
- Period (Sec): Represents the period of vibration in seconds for each mode. It is the reciprocal of the natural frequency and indicates how many seconds it takes for one complete cycle of vibration.

- UX, UY, UZ: These columns indicate the fractions of the total mass of the building that are actively involved or 'working' in each specific mode of vibration. They do not represent displacements but rather demonstrate how the mass of the building is distributed across different modes when the structure is subjected to dynamic excitation, such as during seismic events.
- SumUX, SumUY, SumUZ: Represent the total modal mass participation factors in the X, Y, and Z directions respectively, summarizing how much of the building's mass contributes to its dynamic response in each of these directions across all vibration modes. RX, RY, RZ: These columns represent the modal participation to rotational modes of vibration about the X, Y, and Z axes respectively.

Table 3.11. Modal Participating Mass Ratios for Frame Model

TABLE: Modal Participating Mass Ratios															
OutputCase	StepType	StepNum	Period	UX	UY	UZ	SumUX	SumUY	SumUZ	RX	RY	RZ	SumRX	SumRY	SumRZ
Text	Text	Unitless	Sec	Unitless	Unitless	Unitless	Unitless	Unitless	Unitless	Unitless	Unitless	Unitless	Unitless	Unitless	Unitless
MODAL	Mode	1	0.2227	0.005614	0.17	4.997E-07	0.00561	0.17	4.997E-07	0.02093	0.001553	6.718E-06	0.02093	0.00155	6.718E-06
MODAL	Mode	2	0.1877	0.52	0.00415	3.618E-06	0.52	0.17	4.117E-06	0.000512	0.12	0.006063	0.02144	0.12	0.006069
MODAL	Mode	3	0.13145	0.002254	0.29	6.788E-06	0.53	0.46	0.00001091	0.04422	0.0004124	0.001575	0.06566	0.12	0.007644
MODAL	Mode	4	0.10899	0.001317	0.02341	1.524E-07	0.53	0.48	0.00001106	0.01451	2.418E-05	0.0272	0.08017	0.12	0.03484
MODAL	Mode	5	0.10675	0.009588	0.00143	6.794E-06	0.54	0.49	0.00001785	0.002111	3.848E-05	0.45	0.08228	0.12	0.49
MODAL	Mode	6	0.09677	0.02614	0.12	0.00002141	0.56	0.61	0.00003926	0.0126	0.0007691	0.08334	0.09487	0.12	0.57
MODAL	Mode	7	0.09232	0.17	0.00525	2.541E-06	0.73	0.61	0.00004181	0.002753	0.03756	0.001825	0.09763	0.16	0.57
MODAL	Mode	8	0.09033	0.000646	0.00128	6.516E-08	0.73	0.61	0.00004187	0.00485	0.0000446	0.0003943	0.1	0.16	0.57
MODAL	Mode	9	0.08377	0.003327	0.00322	4.697E-06	0.73	0.62	0.00004657	0.05061	0.0001765	0.008131	0.15	0.16	0.58
MODAL	Mode	10	0.07998	0.003972	0.15	0.00001404	0.74	0.77	0.00006061	0.01351	0.0007979	0.09435	0.17	0.16	0.68

In this analysis of two two-story experimental building using SAP2000, Modal Participating Mass Ratios (MPMR) were computed to understand the structure's dynamic behavior. Modal Participating Mass Ratios indicate the engagement of mass across different modes of vibration.

Considering the tabulated data, certain outcomes have been observed:

- Mode 1: The structure has a period of 0.222703 seconds. The dominant displacement occurs in the Y direction with a value of 0.17, indicating lateral translation. There is very little rotation.
- Mode 2: The period is 0.187699 seconds. Significant lateral displacement occurs in the X direction (0.52) and some rotation around the Z axis (0.006069).
- Mode 3: The period is 0.13145 seconds. Lateral mass participation is significant in the Y direction (0.29) and about the Z axis (0.0015).
- Mode 5: The period for this specific mode is 0.106749 seconds, and it exhibits a modal mass participation of 0.45 in twisting about the Z-axis, identifying it as the primary

rotational mode. This value represents the mass participation of this mode alone, without summing contributions from previous modes. In the present analysis, multiple modes are included to ensure a comprehensive sum of total mass participation, reflecting the contribution from all the modes considered, not just a single one. These results were obtained from the modulus of elasticity of 840 MPa.

3.8.4 Building Period

In structural dynamics, the period of a building refers to the time needed for a structure to complete one full cycle of vibration. It is a fundamental property that characterizes the dynamic response of a building. The period of the building depends on various factors such as its height, mass distribution, stiffness, and structural system. Taller buildings typically have longer periods compared to shorter buildings, while buildings with flexible or less stiff structures tend to have longer periods as well. In the context of unreinforced masonry buildings, factors like the height-to-width aspect ratio, masonry strength, and mass density can influence their period properties. Generally, heavier buildings tend to have larger periods. These factors affect the overall stiffness and response of the building under seismic loading.

Experimentally, the frequency analysis was conducted on the model using various longitudinal and transverse excitations, which included white-noise tests (Bothara, Dhakal and Mander, 2010). In the longitudinal direction, the frequency decreased from 11.7 to 8.6 Hz (0.085s to 0.116s in terms of Period) due to reduced stiffness (caused by cracking) and the piers' inelastic rocking behavior. Remarkably, during specific excitations (Wn 0.05, Taft 0.2g, Taft 0.3g), the frequency remained stable despite the observed damage and softening in the time history of the displacement response. Damping increased from 4.7% to 10.3% with the damage progression after successive testing with gradually increasing ground motion intensity. In the short direction, where the building was more flexible due to its long aspect ratio, the fundamental frequency dropped from 9.8 to 6.8 Hz (a period shift from 0.1s to 0.147s) as the model underwent more intense excitations. The shift in the fundamental period was also accompanied with an increase in the second mode frequency from 17 to 14 Hz (second mode period shift from 0.059 s to 0.071 s) as the model became more compliant with increasing extent of damage. Damping increased from 8% to 20% during these tests, indicating hysteretic activity dues to damage particularly for ground motions acting in the short direction of the plan.

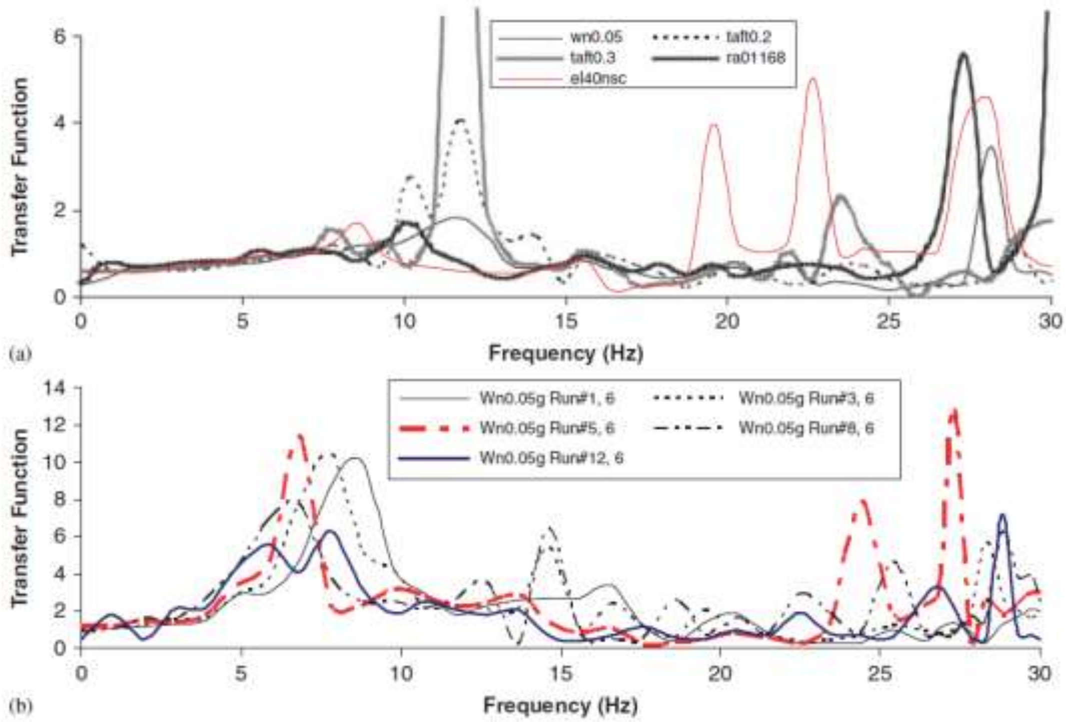

Figure 3.14. Transfer Functions for the Eaves Level Response Acceleration: (a) Longitudinal Shaking and (b) Transverse Shaking.(Bothara, Dhakal and Mander, 2010)

In the table below, the initial test conducted in the long direction displayed a frequency of 13.7 Hz at an intensity of 0.02g, corresponding to a period of 0.072 seconds. As the test intensities increased, this frequency decreased. By the final test (the El-Centro earthquake), due to the building's increased flexibility caused by damage, the frequency in the longitudinal direction was reduced to 8.6 Hz, equating to a period of 0.116 seconds.

Table 3.12. Dynamic Characteristics of the Model (Longitudinal Shaking).

Test	Frequency fi (Hz)	Mode shapes Φij	Stiffness Ki j (kN/m)
White noise (0.02g)	(13.7)	(1 0.82)	(56 922)
White noise (0.05g)	(11.7)	(1 0.81)	(41 516)
Taft (0.2g)	(11.7)	(1 0.71)	(41 516)
Taft (0.3g)	(11.7)	(1 0.8)	(41 516)
RA01.68 (0.5g)	(10.1)	(1 0.93)	(30 937)
ELA01NSC	(8.6)	(1 0.91)	(22 430)

It is crucial to note that the values above apply to the long direction, where the earthquake occurs perpendicular to the short walls and parallel to the long walls. Significantly, this orientation is more stiff, leading to a shorter period.

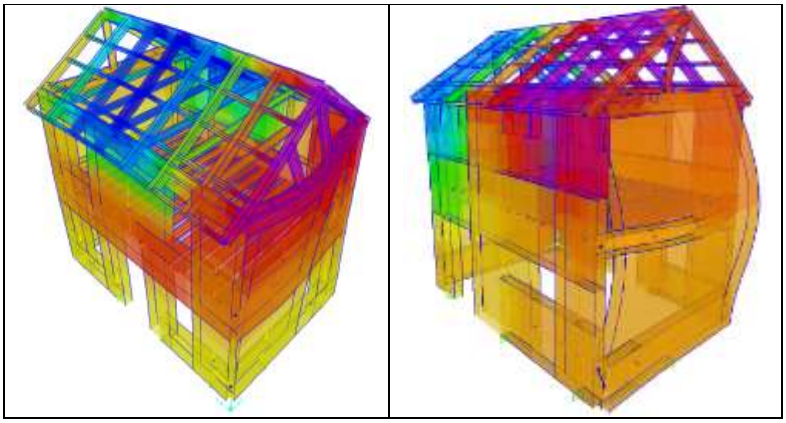

Figure 3.15. Longitudinal Shaking

In the subsequent table, comparable data is presented for shaking in the flexible, Transverse direction. In this configuration, the fundamental frequency diminished from 9.8 to 6.8 Hz as the model underwent more intense excitations. Initially, in the Transverse direction, the frequency was 9.8 Hz under an intensity of 0.05g, corresponding to a period of 0.1 seconds. With escalating test intensities, this frequency declined. In the final test, due to structural damage that enhanced the building's flexibility, the frequency in the Transverse direction dropped to 6.83 Hz, equivalent to a period of 0.146 seconds. This shift highlights a substantial reduction in the fundamental frequency from its initial value of 9.8 Hz to approximately 6.0 Hz, indicating a significant softening of the model under the applied conditions.

In the half-scaled designed equivalent frame model, structure based on the preceding analysis with SAP2000 the fundamental period of building was estimated at 0.22 s, and the frequency was 4.49 Hz. (Table.3.15)

Table 3.13. Dynamic Characteristics of the Model (Transverse Shaking)

Test	Frequency fi (Hz)	Mode shapes	Stiffness Kij (kN/m)
White noise (0.05g) Run#1	9.8	1 0.49	29 733
White noise (0.05g) Run#3	8.8	1 0.77	23 974

Test	Frequency fi (Hz)	Mode shapes	Stiffness Kij (kN/m)
White noise (0.05g) Run#5	7.8	1 0.52	18 835
White noise (0.05g) Run#8	7.8	1 0.69	18 835
White noise (0.05g) Run#12	6.83	1 0.79	14 442

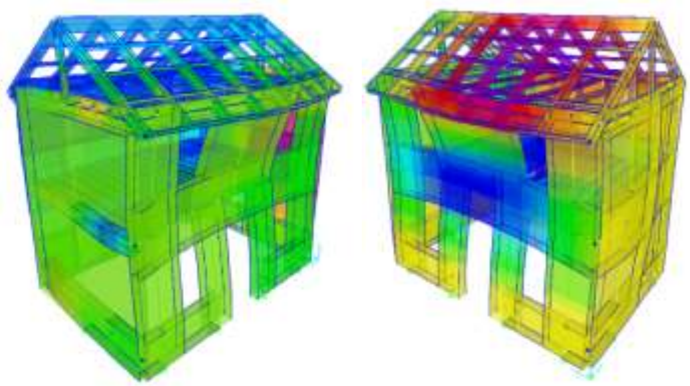

Figure 3.16. Transverse Shaking

Table 3.14. Model Longitudinal and Transverse Shaking Direction - Frequency Range

Direction	Frequency Range (Hz)	Period Range (seconds)
Longitudinal	11.7 to 8.6	0.08 to 0.11
Transverse	9.8 to 6.8 (shift to ~6.0)	0.1 to 0.16

Table 3.15. Deformed Shape (MODAL) Period Results

Aspect	Value
Model Type	Half-scaled Designed Frame
Software	SAP2000
Period	0.22 seconds
Frequency	4.49 Hz

Evidently, the equivalent frame element model, assembled as recommended by the NRC Code, yielded a significantly longer building period than what was measured in the experiment. Ideally, a well-designed building should exhibit a smaller period, achieved by either maintaining a fixed mass or increasing stiffness. Increasing stiffness reduces the period, while adding mass results in elongating the period.

3.9 Case Two: Half Scale Shell Element Model

It is evident from the model of the preceding section, that the EFA does away with the intrinsic continuity of masonry by representing surface elements with linear beam-columns. Although it is the recommended approach in Codes, alternative modelling approaches where the continuity is accounted for explicitly, have also been proposed (Valadao, 2021). This calls for the use of surface finite elements – classified as shell elements in SAP2000 software. Shell elements are designed to represent slabs and shear walls within structures. A rectangular mesh was used to model the structure studied in this work.

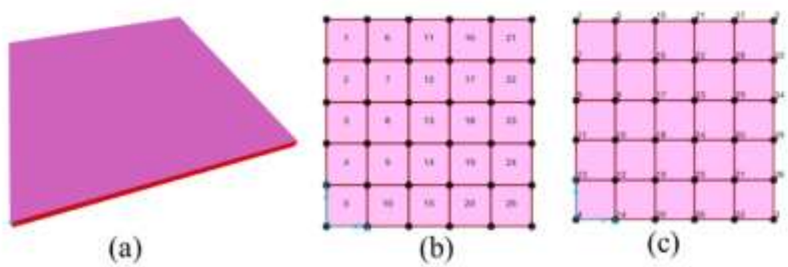

Figure 3.17. (a) 3D model of Square Thin-Shell Structure, (b) The Labels of Shell Elements, and (c) the Labels of Nodes. (Minh *et al.*, 2022)

Shell elements in SAP2000 are constructed by combining two-dimensional plate bending and membrane actions, as depicted in Figure 3.16. The plate bending elements in SAP2000 are available in two formulations: "thin-plate" and "thick-plate." The "thin-plate" formulation, following Kirchhoff principles, neglects transverse shear deformation, while the "thick-plate" formulation, based on Mindlin/Reissner principles, accounts for the effects of shear deformation. In Figure 3.17, the plate bending element features three degrees of freedom (DOF) per node, including one for out-of-plane displacement and two for rotations. Similarly, the membrane element includes two in-plane displacement components and a normal rotation, summing up to 12 DOF. This choice allows consideration of transverse shear deformations in the analysis. Shell elements prove invaluable in analyzing thin-walled structures such as slabs and shear walls, delivering precise results across a broad spectrum of engineering challenges. (Minh *et al.*, 2022)

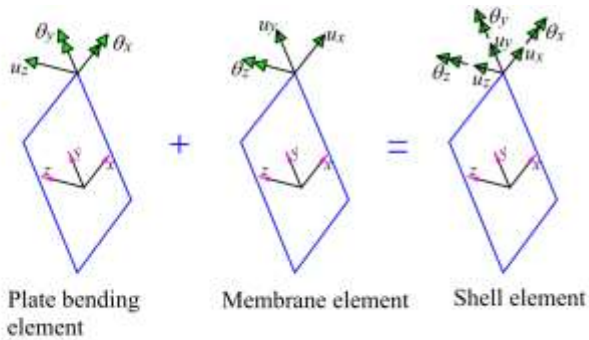

Figure 3.18. Formation of Shell Element (Oscier, Bosley and Milner, 2008)

3.9.1 Wall Element Designs & Dimensions

Again, the properties of masonry and timber were used to model the building specimen. The dimensions and material properties used for unreinforced Masonry brick structures in the SAP2000 models were the same as frame model and were obtained from (Bothara, Dhakal and Mander, 2010) and the (Vintzileou et al., 2015) projects. Wall elements were modeled using a half-scale model and meshed into divided area objects with a maximum size of 50×50mm (about 1.97 in) and the wall thickness was 110 cm (about 3.61 f_t).

3.9.2 Finite Element Mesh

To enhance result accuracy and to visualize deflection changes across the structure's height, the finite element mesh was designed following the structural geometry in detail. Distorted elements were avoided by maintaining an aspect ratio below 2:1. Element size was set at approximately 50mm × 50mm, corresponding to the walls' thickness of 110mm (this mattered at the intersection between orthogonal walls). Adjustments were made at midspan and along window locations for proper placement of floor joists. This dimension choice facilitated efficient insertion of windows and doors while ensuring complete coverage around openings. The resulting mesh was connected using the pertinent option (Enforce Edge Constraints) of the program where different surfaces overlapped to ensure numerical robustness in the computed results.

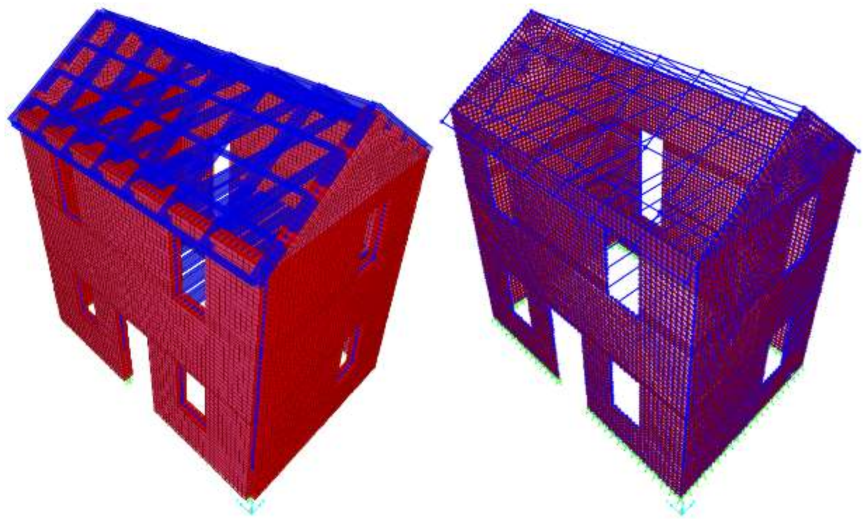

Figure 3.19. 3D View of Shell Element Model of the Test Structure

3.9.2.1 Geometry of the Shell Model Per Façade

In SAP2000, the geometry of a shell model per façade is a comprehensive representation that utilizes planar elements, or 'shells', to simulate the structural geometry of a building's façade. The shell elements are defined by their thickness, material properties, and were carefully meshed into smaller segments to capture the façade's complexity accurately. The model incorporates detailed boundary conditions that reflect how the façade integrates with the overall building structure, including supports and connections. It allows for the precise application of various loads and seismic forces, ensuring a realistic distribution of these forces across the façade.

Table 3.16. Geometry of the Shell Model Per Façade

	Shell model XZ Side Wall	Shell model YZ Front Wall	Shell model XZ Side Wall	Shell model YZ Back Wall
Stan dard	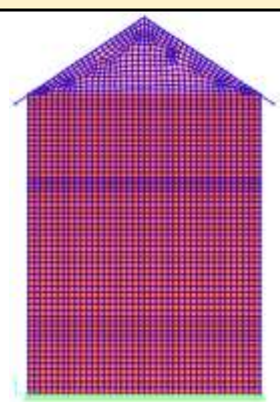	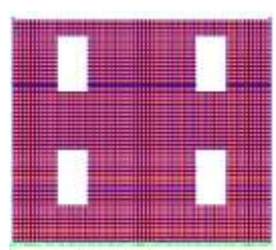	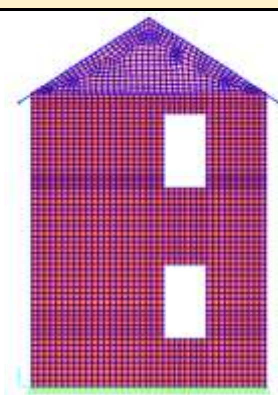	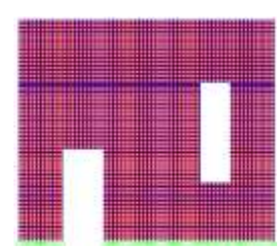

The Table 3.18, Specified geometry specifications of the shell model are based on the half-scale experimental building used in the project conducted by Bothara, Dhakal, and Mander (2010)

Table 3.17. Shell Model Geometry Specifications Per Façade for Seismic Analysis in SAP2000

Façade	Width (mm)	Height (mm)	Thickness (mm)	Notes
Front Wall, YZ	2880	2480	110	Includes door and window openings on both floors.
Side Solid Wall, XZ	1920	3295	110	Solid wall with no openings; height is wall with gable
Side Wall, XZ	1950	3295	110	Includes window openings as per section view.
Back Wall, YZ	2880	2480	110	Similar to the front wall with door and window openings.

3.9.2.2 Additional Mass

It was mentioned earlier that an additional mass of 4.2 tons was added to the gable walls at both floor and eaves levels to achieve a scaled ratio of 1:2 in both mass and dimensions. The initial 2.1 tons were allocated across 195 nodes of the model located on the first-floor level. Likewise, an equivalent mass of 2.1 tons was distributed among 232 nodes of the model located on the eave's levels and gable walls. The table below illustrates the distribution of the total 4.2 tons between the two floors:

Table 3.18. Allocation of Mass on Shell Model

Description	Total Weight (tons)	Number of Nodes	Weight per Node (tons)
Allocation on first-floor level	2.1	195	0.0107
Allocation on gable walls at top floor and eaves level	2.1	232	0.0091

This allocation ensures consistency between the EFA model with the shell models in both mass and dimensions across the specified nodes on the first-floor level and the gable walls at the floor and eaves levels.

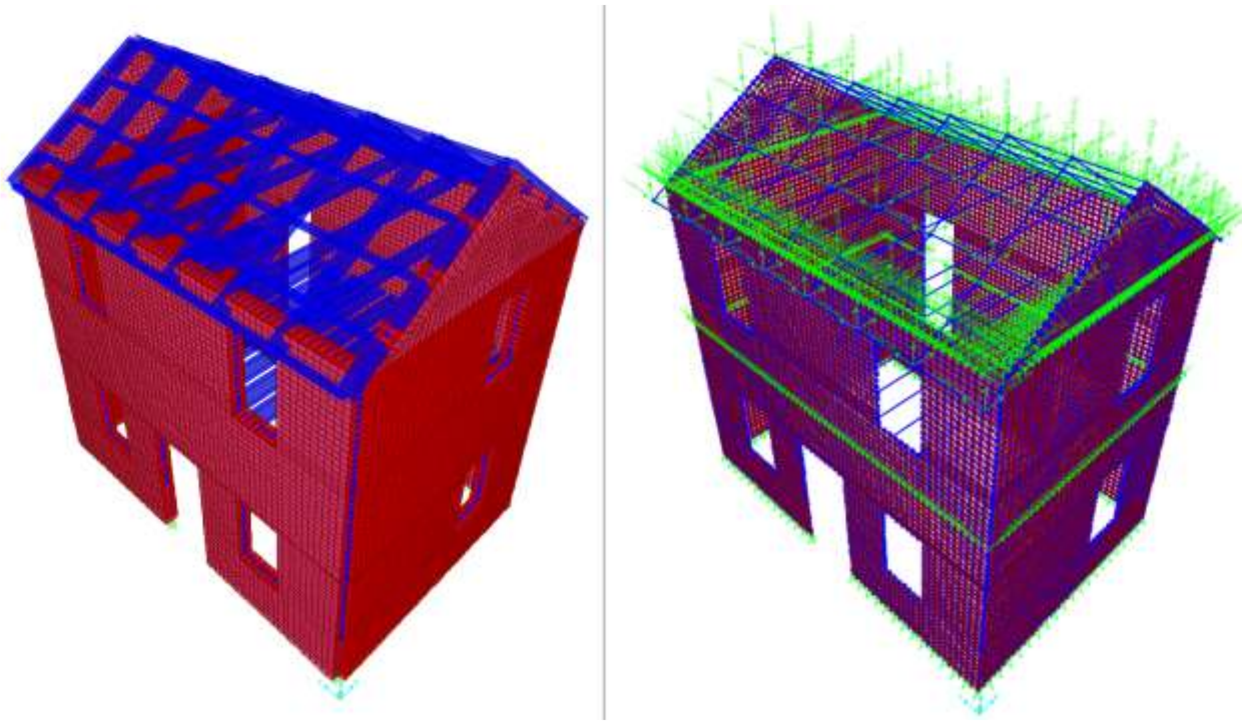

Figure 3.20. Additional Mass

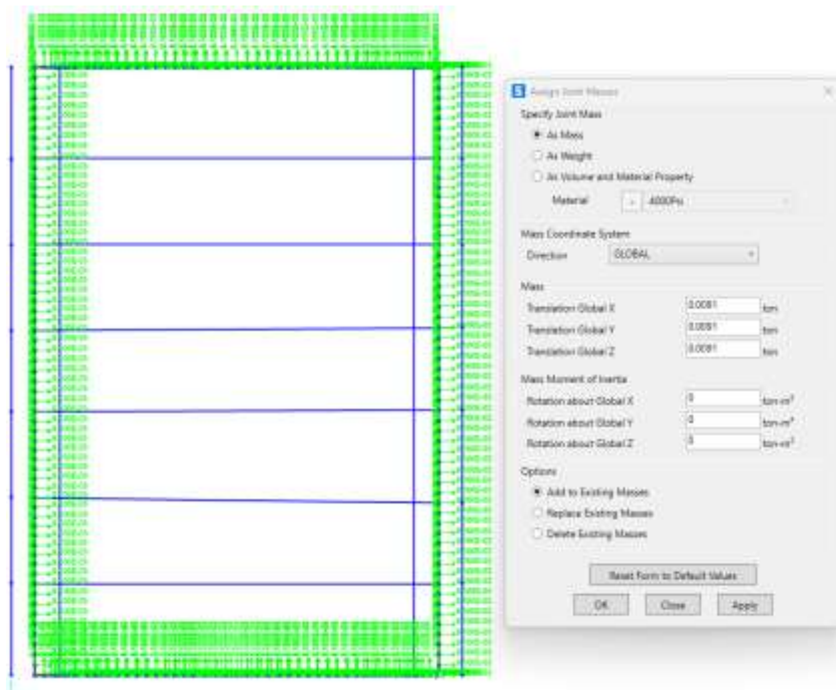

Figure 3.21. Eaves Levels and Gable Walls Assign Joint Masses.

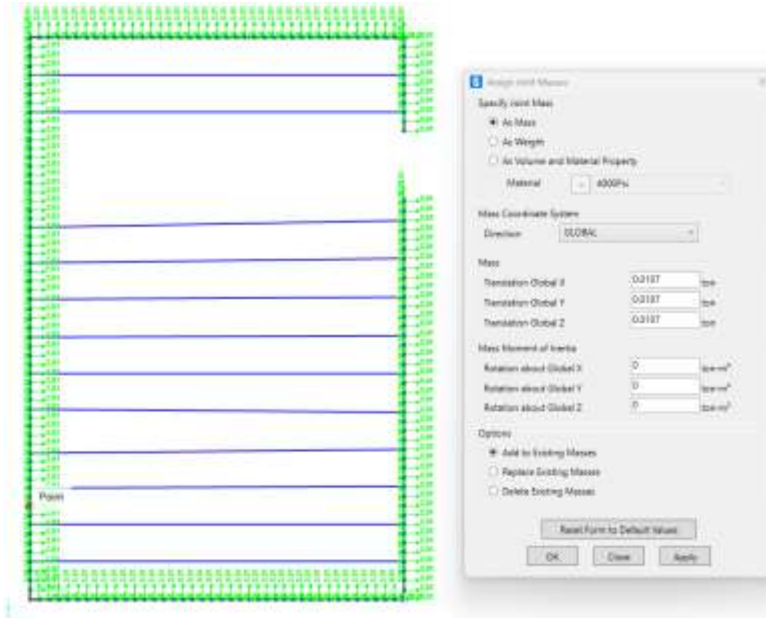

Figure 3.22. First-Floor Level Assign Joint Masses

3.9.2.3 Building Period

The data used in this analysis was sourced from a project by Bothara, Dhakal, and Mander (2010), which is identical to the data applied in the frame model. Despite this consistency, the results obtained differ significantly. Hence, we explore the same dataset to understand the disparities.

Table 3.19. Experimental Model Longitudinal and Transverse Direction Frequency Range

Direction	Frequency Range (Hz)	Period Range (seconds)
X Direction	11.7 to 8.6	0.08 to 0.11
Y Direction	9.8 to 6.8 (shift to ~6.0)	0.1 to 0.16

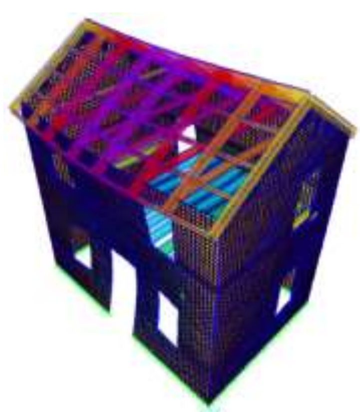

Figure 3.23. Translational Mode for Excitation Parallel to the Short (X) -Direction

3.9.2.4 Modal Participating Mass Ratios

Table 3.20, presents the periods and Modal Participation Mass Ratios for the studied building model based on the shell-F.E. approach. Below the most significant modes in the X, the Y and about the Z axis are discussed:

- Mode 1:

Period: 0.147577 seconds

Mass participation: Predominant translation in the X-direction (mass participation =0.57). Rotation: Minimal rotation about the Z-axis (rotational mass participation = 0.001987). This suggests significant lateral movement with minimal twisting, indicating a primary mode of horizontal vibration.

- Mode 2:

Period: 0.103127 seconds; this is a translational mode in the Y-direction (mass participation = 0.67) with a minimal contribution by twisting (rotational mass participation by 0.052 about the X axis).

- Mode 4:

Period: 0.083796 seconds; this is a twisting mode about the Z-axis with a rotational mass participation by 12%.

It is noted that the period values are substantially closer to the experimental results at an advanced stage of testing. Evidently, for the same input, same structure, the Equivalent Frame Analysis model produces significantly different results from the shell element model.

Table 3.20. Modal Participating Mass Ratios for Shell Model Half Scale

TABLE: Modal Participating Mass Ratios

OutputCase	StepType	StepNum	Period	UX	UY	UZ	SumUX	SumUY	SumUZ	RX	RY	RZ	SumRX	SumRY	SumRZ
Text	Text	Unitless	Sec	Unitless	Unitless	Unitless	Unitless	Unitless	Unitless	Unitless	Unitless	Unitless	Unitless	Unitless	Unitless
MODAL	Mode	1	0.14758	0.57	2.28E-08	1.731E-09	0.57	2.28E-08	1.73E-09	4.147E-06	0.04235	0.001987	4.147E-06	0.04235	0.00199
MODAL	Mode	2	0.10313	3.02E-07	0.67	0.0001099	0.57	0.67	0.00011	0.05203	0.0003129	0.000887	0.05203	0.04267	0.00287
MODAL	Mode	3	0.09313	0.005166	0.001378	6.231E-06	0.58	0.68	0.000116	0.0001116	0.15	9.33E-08	0.05214	0.19	0.00287
MODAL	Mode	4	0.0838	0.004331	0.003299	0.00006814	0.58	0.68	0.000184	0.0006364	0.008584	0.12	0.05278	0.2	0.13
MODAL	Mode	5	0.07311	0.000394	0.11	0.00003865	0.58	0.79	0.000223	0.0003522	0.00001831	0.01944	0.05313	0.2	0.15
MODAL	Mode	6	0.06638	0.0034	0.000242	5.936E-06	0.58	0.79	0.000229	0.08721	0.0005517	0.04733	0.14	0.2	0.19
MODAL	Mode	7	0.06301	0.06175	0.005056	0.00005891	0.65	0.79	0.000288	0.01335	0.01121	0.34	0.15	0.21	0.53
MODAL	Mode	8	0.05997	0.19	0.000116	0.00002581	0.84	0.79	0.000314	0.0006714	0.06031	0.14	0.15	0.27	0.68
MODAL	Mode	9	0.05391	0.0001883	0.08049	0.0006593	0.84	0.87	0.000973	0.01289	5.795E-06	0.009499	0.17	0.27	0.69
MODAL	Mode	10	0.04736	0.001359	0.000766	8.761E-07	0.84	0.87	0.000974	0.0007859	4.736E-06	0.007537	0.17	0.27	0.69

3.10 Case Three: Full Scale Shell Element Model

The Full-Scale Shell Element Model is exactly similar in geometry with the test specimen of (Bothara, Dhakal and Mander, 2010) however the dimensions correspond to the full-scale reference structure. The geometry difference would render the period of the model √2 times larger than the ½ scale shell model; however, because there is no need for adding masses now, it is examined whether the geometry of the mode shapes would differ from that of the scaled model since the building mass in the full scale is spatially distributed.

3.10.1 Additional Mass

In shell model for seismic analysis or other dynamic simulations, it is essential to accurately account for the mass of the structure because it affects the inertia forces during dynamic loading. Normally, the self-weight of the structure is automatically included in the mass calculations, which includes the weight of the materials used in the construction of the building. However, there are cases where additional masses need to be specified manually if they are not inherently part of the analyzed structure or if they are movable or temporary, as in the case of the roof tiles. The weight of the roof tiles is considered an additional mass in the analysis of a full-scale building. The tiles, with a weight of 0.2 kN/m², add to the overall mass of the structure. For the pitched roof in the shell model, the weight of the tiles affects the batten and rafter elements. The tiles' weight is distributed based on the tributary area that each rafter and batten supports, which, in this case, is a rectangle with dimensions of 688mm by 824mm. The mass distribution is calculated and then applied to the nodes representing the center, middle edges, and side edges of the roof in the SAP2000 model. For instance, a center node on the ridge board receives a full tributary area's worth of mass, resulting in 110 N of additional mass at that node. The middle edges and side edges receive half and a quarter of this mass, respectively, reflecting the portion of the roof area they are responsible for supporting.

$$0.2kN/m^2 \times 0.688\,m\ \times 0.824 = 0.11\,kN$$

Table 3.21. Tile Weights Shell Model Full Scale

Section	Tile Weight (kN/m^2)	Tributary Area	Distributed Weight (N)
Center (Ridge Board)	0.2	Full	110
Middle Edges	0.2	Half	55
Side Edges	0.2	Quarter	27.5

Table 3.22. Distributed Tile Mass on the Roof

Node Type	Number of Nodes
Middle and Top	42
Eaves Level	26
Edges	4

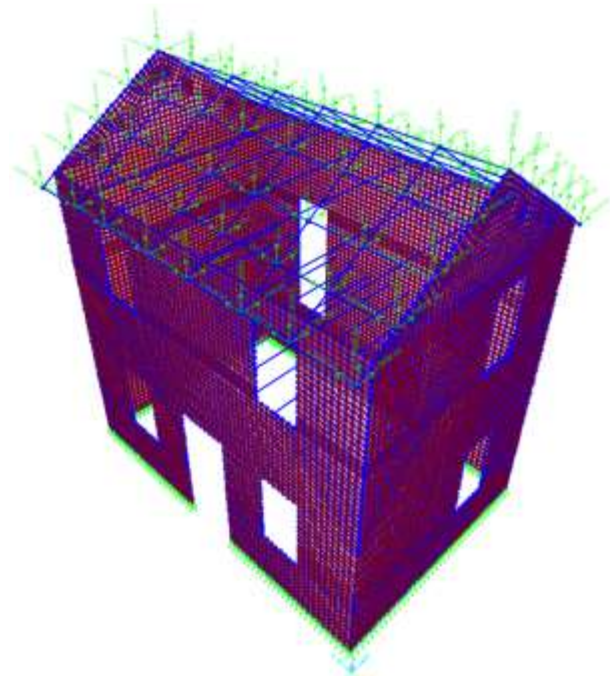

Figure 3.24. Additional Mass Shell Model Full Scale

3.10.1.1 Modal Participating Mass Ratios of the Full Scale Shell Element Model

- Results from the modal analysis are summarized in

Table 3.23. Modal Participating Mass Ratios for Shell Model Full Scale. For the same modes considered in the ½ shell model, the following are obtained:

- Mode 1 (Period: 0.212993 seconds): Significant mass participation in the X direction (mass participation = 0.5) with minimal twisting action about the Z-axis.
- Mode 2 (Period: 0.152784 seconds): Significant mass participation in the Y direction (=60%).
- Mode 4 (Period: 0.11204 seconds), a twisting mode, with rotational mass participation about Z axis of 12%.

Table 3.23. Modal Participating Mass Ratios for Shell Model Full Scale

TABLE: Modal Participating Mass Ratios																		
OutputCase	StepType	StepNum	Period	UX	UY	UZ	SumUX	SumUY	SumUZ	RX	RY	RZ	SumRX	SumRY	SumRZ
Text	Text	Unitless	Sec	Unitless	Unitless	Unitless	Unitless	Unitless	Unitless	Unitless	Unitless	Unitless	Unitless	Unitless	Unitless
MODAL	Mode	1	0.21299	0.5	3.348E-07	5.254E-07	0.5	3.35E-07	5.254E-07	6.387E-06	0.0598	0.001604	6.387E-06	0.0598	0.0016
MODAL	Mode	2	0.15278	5.147E-06	0.6	0.00001518	0.5	0.6	0.0000157	0.1	8.728E-05	0.001365	0.1	0.05989	0.00297
MODAL	Mode	3	0.1288	0.008214	0.0002858	6.451E-07	0.51	0.6	1.635E-05	8.831E-06	0.15	2.118E-05	0.1	0.21	0.00299
MODAL	Mode	4	0.11204	0.0002198	0.000858	0.00005059	0.51	0.6	6.694E-05	0.001884	0.001689	0.12	0.1	0.22	0.12
MODAL	Mode	5	0.10846	3.513E-06	7.236E-05	0.0001416	0.51	0.6	0.0002085	0.00003611	0.0001162	0.001122	0.1	0.22	0.12
MODAL	Mode	6	0.10125	0.00001736	0.05493	2.187E-06	0.51	0.66	0.0002107	0.07532	2.179E-05	0.006672	0.18	0.22	0.13
MODAL	Mode	7	0.08959	0.01302	0.0002749	0.00002791	0.52	0.66	0.0002386	6.786E-08	0.002006	0.4	0.18	0.22	0.52
MODAL	Mode	8	0.08217	0.27	0.0000141	9.458E-08	0.79	0.66	0.0002387	0.00005925	0.08781	0.01802	0.18	0.31	0.54
MODAL	Mode	9	0.07798	0.002254	0.0007873	0.00004987	0.8	0.66	0.0002886	0.0001232	0.000842	5.163E-05	0.18	0.31	0.54
MODAL	Mode	10	0.07342	0.0005842	0.12	0.0001743	0.8	0.78	0.0004629	0.0192	0.0000296	0.0008525	0.2	0.31	0.54

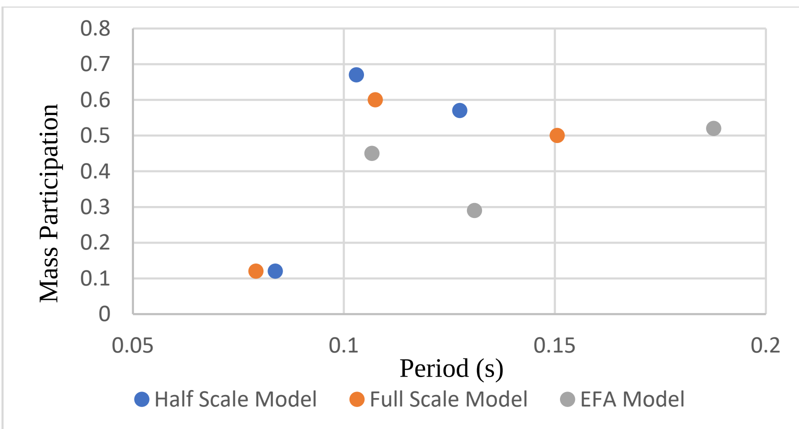

Figure 3.25. Comparison of Period/Mass Participation Fraction for the First 3 Modes. To Facilitate Comparison, the Period Values of the Full Scale Model have been Divided by √2

Figure 3.25 illustrates that even with an identical modeling procedure the full scale and the corresponding half scale model differ, particularly in the Y-mode and the Z-twisting mode; the mass participation in the scaled model is higher than the corresponding ratios of mass participation obtained for the full scale model – most likely because of the lumped mass addition at the floor and roof model to satisfy mass similitude. It is noted that the EFA model has a marked difference from the two Shell Models. In addition, the EFA model presents one more mode with a significant mode participation in the Y axis (17%) with a period of 0.22 s. This implies that the approach of idealization of the continuous structure in the form of an equivalent frame is not representative of the actual behavior of the structure.

3.10.1.2 Parametric Investigation for the Modulus of Elasticity (E)

The objective of the present section is to obtain results that match closely those of the experimental study at the start of the experiment, before the onset of damage accumulation that led to period lengthening. The full-scale building's period should ideally be equivalent to that of the small building multiplied by the square root of 2. Applying this principle, the period of the larger structure is calculated as 0.115 seconds (the period of the small building) multiplied by $\sqrt{2}$ (approximately 1.41), resulting in 0.16 seconds. To achieve this it is imperative to use a similar or closely related value for the material's elastic modulus (E) in both the small and large building designs. Table 3.23 lists the Elastic Modulus values that match the experimental results for the different modelling approaches. The stark difference in the obtained values between EFA and Shell element models underlines the level of uncertainty that hampers the field of modeling URM structures. The half scale and full-scale models yielded close, comparative values for the modulus of Elasticity, the small difference being attributed to the different concentration of mass in the half scale structural model as compared to the full scale prototype.

Table 3.24. Full Scale Shell Model Period and Frequency

Model	Modulus of Elasticity (E)	Period and Frequency
Frame model half scale	6450	Mode 1; T=0.1153 s. ; f= 8.672 Hz.
Shell model half scale	1800	Mode 1; T=0.1154 s. ; f= 8.659 Hz.
Shell model full scale	1900	Mode 1; T=0.1590 s. ; f= 6.288 Hz.

3.11 Element Selection in SAP2000: Impact on Modulus of Elasticity and Structural Behavior

The choice of elements in SAP2000 (frame vs. shell) significantly impacts the required modulus of elasticity to achieve a specific period. This difference arises from the varying abilities of these elements to capture several types of deformations. Shell elements, accounting for all the modes of deformation, can achieve the desired behavior with a lower modulus of elasticity, providing a more accurate representation of the structural response. On the other hand, frame elements, being inherently flexible, require the imposition of external restraints by means of an increased modulus to meet the effect of continuity of the shell model on the resulting response. The choice between these elements should be made considering the specific structural system, however, it is clear that extensive calibrations with other published tests would be needed in order to vet the selection of the elastic Modulus as a determining parameter of stiffness, and therefore seismic demand, depending on the method of idealization selected for structural analysis.

3.12 Differences due to Mass Scaling for the Half and Full-Scale Structures

This research critically examined the compatibility between frame and shell approaches and rigorously evaluated the chosen scaling method to ensure it accurately mimics the behavior of a full-scale structure. This comprehensive analysis aims to bridge the gap between simulation and reality, considering factors such as mass distribution and various deformations in both thin and complex structures. The research implemented a scaling method that concentrated masses at the top of the building to simulate full-scale behavior. However, a challenge arose due to the nonlinear reduction in material mass concerning quantity, deviating from the simulated law. To compensate, additional masses were added at the top and intermediate floor levels. Frame elements might lack accuracy in capturing the complexities of surface structures such as wall piers, particularly when both in-plane and out-of-plane deformations are significant. Shell elements, being two-dimensional, can accurately represent both in-plane (membrane) and out-of-plane (bending) deformations and are essential for modeling thin-walled structures where both deformations are vital. The study aimed to determine whether this scaling method, including mass concentration at the top and at the middle floor levels, aligns with the behavior of a full-scale structure. The hypothesis being tested suggested that if similitude is perfect, the periods of the scaled model should align with the square root of the scaling factor times the period of the full-scale model. By analyzing the difference in behavior due to this scaling method, the research would illustrate how well the scaled model represents a real-world scenario. This evaluation is crucial to ensure that the simulation is accurate, especially considering the distribution of mass in actual buildings and how this concentration at the top affects the overall structural response.

3.13 Comparing the Results of Shell Model and Frame Model

The frame model simplifies the structure into one-dimensional elements, potentially missing some complex deformations, while the shell model considers a broader range of deformations due to its two-dimensional nature that combines both membrane and out of plane (slab) action. As a result, the shell model captures more realistically the detailed structural behavior, leading to a shorter period compared to that obtained from the frame model for the same Elastic Modulus.

Table 3.25. Comparing the Period of Shell and Frame Model, (Modulus of Elasticity - E: 840)

Model Type	Scale	Mode	Displacement	Highest Mass Participation (%)	Period
Frame	Half Scale	2	UX	52	T= 0.1877
Frame	Half Scale	3	UY	29	T= 0.1314
Frame	Half Scale	5	RZ	45	T= 1067
Shell	Half Scale	1	UX	57	T= 0.1475
Shell	Half Scale	2	UY	67	T= 0.1031
Shell	Half Scale	7	RZ	34	T= 0.0631
Shell	Full Scale	1	UX	50	T= 0.2129
Shell	Full Scale	2	UY	60	T= 0.1527
Shell	Full Scale	7	RZ	40	T= 0.0895

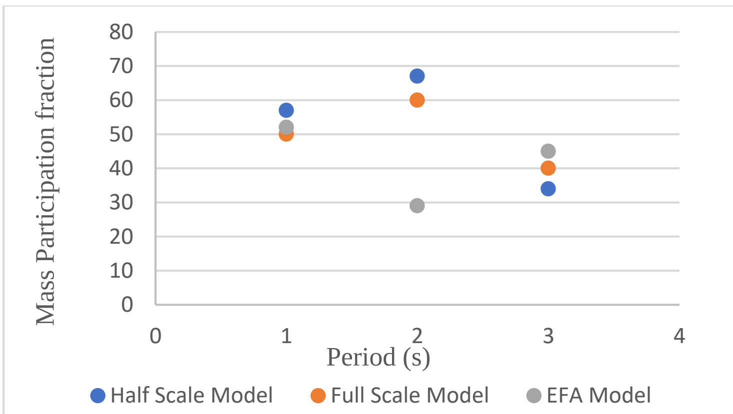

Figure 3.26.Comparison of Period/Mass Participation Fraction for the Two Translational Modes in the Short Direction (X), in the Long Direction (Y), and for the first Rotational Mode. (Modulus of Elasticity - *E*: 840)

3.13.1 Model Comparison (Modulus of Elasticity - *E*: 840)

In the frame model at half-scale, Mode 2 exhibits the highest mass participation in the UX direction at 52%, Mode 3 shows the highest mass participation in the UY direction at 29%, and Mode 5 demonstrates the highest mass participation in the RZ direction at 45%. In the half-scale shell model, Mode 1 displays the highest mass participation in the UX direction at 57%, Mode 2 exhibits the highest mass participation in the UY direction at 67%, and Mode 7 demonstrates the highest mass participation in the RZ direction at 34%. Furthermore, in the full-scale shell model, Mode 1 shows the highest mass participation in the UX direction at 50%, Mode 2 exhibits the highest mass participation in the UY direction at 60%, and Mode 7 demonstrates the highest mass participation in the RZ direction at 40%.

3.13.2 Model Comparison After Setting Modulus of Elasticity to the Values of Table 3.23

In the half-scale frame model, Mode 1 exhibits the highest mass participation with 37% in the UX (translation in the short) direction. Mode 10 shows the highest mass participation with 36% in the UY (longitudinal) direction, while Mode 8 demonstrates the highest mass participation with 22% in the RZ (rotation about Z-axis) direction. In the half-scale shell model, Mode 1 displays the highest mass participation with 51% in the UX direction, Mode 2 exhibits the highest mass participation with 61% in the UY direction. Furthermore, Mode 7 demonstrates the highest mass participation with 29% in the RZ (rotation about Z-axis) direction. Moving on to the full-scale shell model, Mode 1 shows the highest mass participation with 46% in the UX (horizontal) direction. Mode 2 exhibits the highest mass participation with 47% in the UY (vertical) direction. Similarly, Mode 7 demonstrates the highest mass participation with 29% in the RZ (rotation about Z-axis) direction.

Table 3.26. Model Mass Participation Comparison After Changing Modulus of Elasticity to the respective values listed in Table 3.23

Model Type	Scale	Mode	Direction	Highest Mass Participation (%)	Period
Frame	Half Scale	1	UX	37	T= 0.1153
Frame	Half Scale	10	UY	36	T= 0.0369
Frame	Half Scale	8	RZ	22	T= 0.0449
Shell	Half Scale	1	UX	51	T= 0.1154
Shell	Half Scale	2	UY	61	T= 0.0731
Shell	Half Scale	7	RZ	29	T= 0.0449
Shell	Full Scale	1	UX	46	T= 0.1590
Shell	Full Scale	2	UY	47	T= 0.1107
Shell	Full Scale	7	RZ	29	T= 0.0618

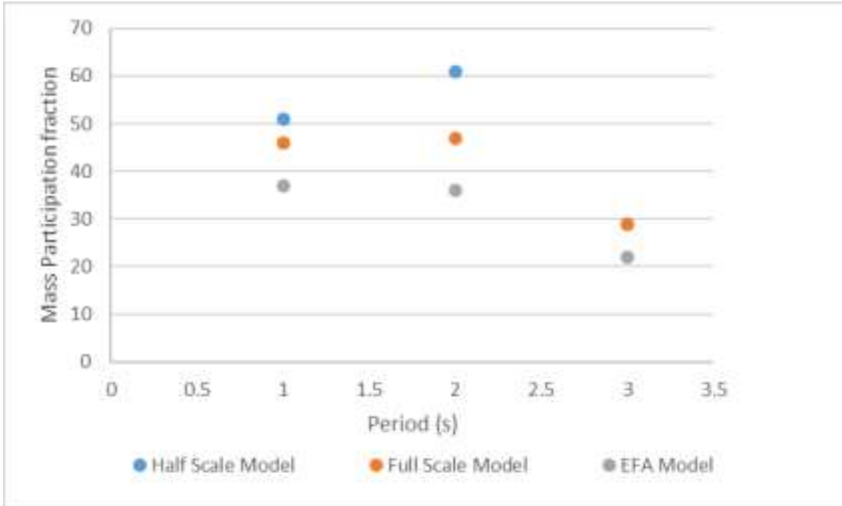

Figure 3.27. Comparison of Period/Mass Participation Fraction for the Modes with the Highest Mass Participation, in the X, in the Y and about the Z (Rotational). (Here the Modulus of Elasticity was Changed to the Values Listed in Table 3.23 for each Respective Model)

3.13.3 Comparative Analysis of Modulus of Elasticity Results

The sensitivity of frame elements to changes in stiffness, especially when the Modulus of Elasticity is significantly increased, results in drastic changes in mode shapes. On the other hand, the inherent properties of shell elements, including their stress distribution and damping characteristics, can lead to more stable mode shapes even when the material stiffness is altered. These inherent differences in behavior between frame and shell elements explain why the modes in the frame model changed significantly while those in the shell model remained relatively stable. Taking into account all modes incorporated within the analysis, it is noteworthy that the cumulative effect of these 20 modes yields mass participation exceeding 80% for the structural parameters UX, UY, and RZ, as stipulated by relevant code standards. (According to tables in the appendix).

Table 3.27. Comparative Analysis of Modulus of Elasticity Results

Modulus of Elasticity (*E*): 840			Modulus of Elasticity (*E*): According to Experimental Test		
Frame Model (Half Scale) Modulus of Elasticity (*E*) = 840			Frame Model (Half Scale) After changing (E) Modulus of Elasticity (*E*) = 6450		
Mode	Displacement	Highest Mass Participation (%)	Mode	Displacement	Highest Mass Participation (%)
2	UX	52	1	UX	37
3	UY	29	10	UY	36
5	RZ	45	8	RZ	22

Modulus of Elasticity (*E*): 840			Modulus of Elasticity (*E*): According to Experimental Test		
Shell Model (Half Scale) Modulus of Elasticity (*E*) = 840			Shell Model (Half Scale) After changing (E) Modulus of Elasticity (*E*) = 1800		
Mode	Displacement	Highest Mass Participation (%)	Mode	Displacement	Highest Mass Participation (%)
1	UX	57	1	UX	51
2	UY	67	2	UY	61
7	RZ	34	7	RZ	29
Shell Model (Full Scale) Modulus of Elasticity (*E*) = 840			Shell Model (Full Scale) Modulus of Elasticity (*E*) = 1900		
Mode	Displacement	Highest Mass Participation (%)	Mode	Displacement	Highest Mass Participation (%)
1	UX	50	1	UX	46
2	UY	60	2	UY	47
7	RZ	40	7	RZ	29

When *E* (Modulus of Elasticity) was increased from 840 MPa to 6450 MPa, the equivalent frame analysis model become significantly stiffer. This increased stiffness affected the mode shapes and how the structure responded to applied loads while reducing the mass participation ratios associated with the X and Y translational modes. In contrast, the shell model remained relatively insensitive to the value of the Modulus of Elasticity (*E*).

3.14 Conclusion

In the comparison between full-scale and half-scale models, the focus has been on understanding the impact of scaling on structural behavior, especially in terms of modal characteristics and mass distribution. This comparison is deemed vital because it sheds light on how geometric scaling affects the dynamic properties of a structure, such as changes in vibration periods and mass distribution. In dynamic simulations like those used for seismic analysis, understanding these differences is crucial, as they directly influence the inertia forces during dynamic loading. The analysis of modal characteristics, including periods of vibration and mass participation ratios, reveals how each different modelling approach influences the obtained response for the same building, highlighting the potential discrepancies and similarities between scaled and full-scale models.

4 Chapter 4: Nonlinear Modelling of the Two-Storey URM Building

4.1 Introduction

In this chapter we pursue nonlinear modelling so as to interpret the patterns of damage that occurred in the building model during the several runs of simulated seismic testing. In the context of an unreinforced masonry building in SAP2000, nonlinear analysis refers to an advanced computational approach to simulate the behavior of the building using realistic material models. Unlike linear analysis, which assumes that material properties to remain constant and linear under various loads, nonlinear analysis considers the complex nonlinear behavior exhibited by masonry materials under significant stresses, including large deformations, material yielding, and potential structural failure. In the case of unreinforced masonry structures, which are prone to exhibiting nonlinear behavior under loading, this type of analysis becomes particularly important for seismic evaluation procedures. By applying nonlinear analysis techniques, the objective is to estimate the building response under gravity and lateral forces (such as seismic loads), as well as other dynamic loads. Nonlinear material models account for the stiffness loss due to cracking, strength, and deformation characteristics of masonry elements with increasing magnitude of deformation. Using this analysis, it is sought to identify stress concentrations and failure mechanisms. In the previous chapter the linear elastic models of the building were developed using the equivalent frame and shell-element type of idealization of the structural layout. The relevance of the idealization with the true structural model was judged by the correlation of the fundamental period of the structure with what was reported in the experiments; in this manner each of these types of modelling were tested against the experiment, and their success was also evaluated by comparison of their respective results.

In the present chapter these models are taken one step further, into nonlinear analysis, by implementing nonlinear stress strain material models for the masonry wall idealizations. Increasing values of lateral loads were applied in an attempt to reproduce the observed patterns of damage seen in the tests.

4.2 Methodology

Masonry, like concrete, is not a linear elastic material. However, all the solutions presented in Chapter 3 only focused on Modal analysis of the linear elastic response, aiming to capture successfully the elastic dynamic characteristics of the structure through comparison with the free vibration tests that were done between successive earthquake excitations. Classical Modal analysis is implicitly an elastic method – as it is based on the principle of superposition. The nonlinear analysis presented here focusses into extracting the pushover resistance curve of the building to also correlate the maximum displacement response attained by the building model during the tests. To project the seismic response of a nonlinear structure, it is essential to conduct a nonlinear analysis and laterally push the structure to determine its maximum displacement.

4.3 Geometry and Modeling

4.3.1 Model Creation

As in Chapter 3, nonlinear analysis is conducted for the frame model, and the scaled and full-scale shell-element models. So nonlinear modeling was done by modification of the input files in order to specifically account for material inelasticity. No other nonlinearities (e.g. geometric) were considered.

4.3.2 Material Properties

Figure 4.1 represents the typical uniaxial response of masonry walls under compression. For the structure here the peak stress was calculated in Chapter 3 as f'_{mc}=7.3 MPa, considering the composite action of masonry blocks and mortar whereas the experimental report based on wallete tests conducted by the experimental team had reported a much higher value of f'_{mc}; the general response is described by a nonlinear model of the type:

$$\sigma_c(\varepsilon_c) = f'_{cm} \cdot \left(\frac{\varepsilon_c}{\varepsilon_o} - \left(\frac{\varepsilon_c}{\varepsilon_o}\right)^2\right) \tag{4.1}$$

The polynomial given in Eq. (4.1) is known as the Hognestad parabola and it is used extensively in the literature to model the uniaxial response of concrete in compression; in the present as well as in several background studies it is also used to model the uniaxial response of masonry in compression. In the above, σ_c is the axial compressive stress at compressive strain ε_c; the latter represents the amount of shortening, ΔH, that occurs under compression over a member with initial height H, whereas, ε_o is the axial strain at peak compressive stress – this value for masonry is taken equal to 0.0025-0.0035. For strains that exceed the value of ε_o the material resistance decays to zero at collapse.

The effective modulus of elasticity, which is calculated according with the Canadian Code as E_m =850f'_{cm} and according to Vanin et al. (2017) as 1250f'_{cm}, is the slope of the tangent in the ascending branch at zero strain; after differentiation of Eq. (4.1) @$\varepsilon_c \dashrightarrow 0$, it may be shown that $E_m = 2f'_{cm}/\varepsilon_o = af'_{cm}$ where a represents the coefficient by which compressive strength is multiplied to estimate the initial stiffness according to the preceding references.

The response in tension is negligible, characterized by an initial, linear elastic envelope $\sigma_t(\varepsilon_t) = E_m \cdot \varepsilon_t = af'_{cm} \cdot \varepsilon_t$ up to the tensile cracking stress, $f_{t,cr}$. For tensile strains ε_t higher than the cracking limit $\varepsilon_{t,cr} = f_{t,cr}/E_m$, the stress decays to zero.

In the analysis conducted in the present study, the reported, experimental values, have been considered to establish the properties of the materials; for example the reported value for compressive strength of a masonry prism was f'_{cm} =16.2 MPa; here it is noted that period matching of the linear model with the experimental structure had yielded an uncracked value of E=1900 MPa, whereas the wallette experiments conducted by the investigators under compression yielded a value of 6100 MPa. Subsequently, by applying these values in the so-called Hognestad's parabola described in the preceding, the compression and tension values were calculated.

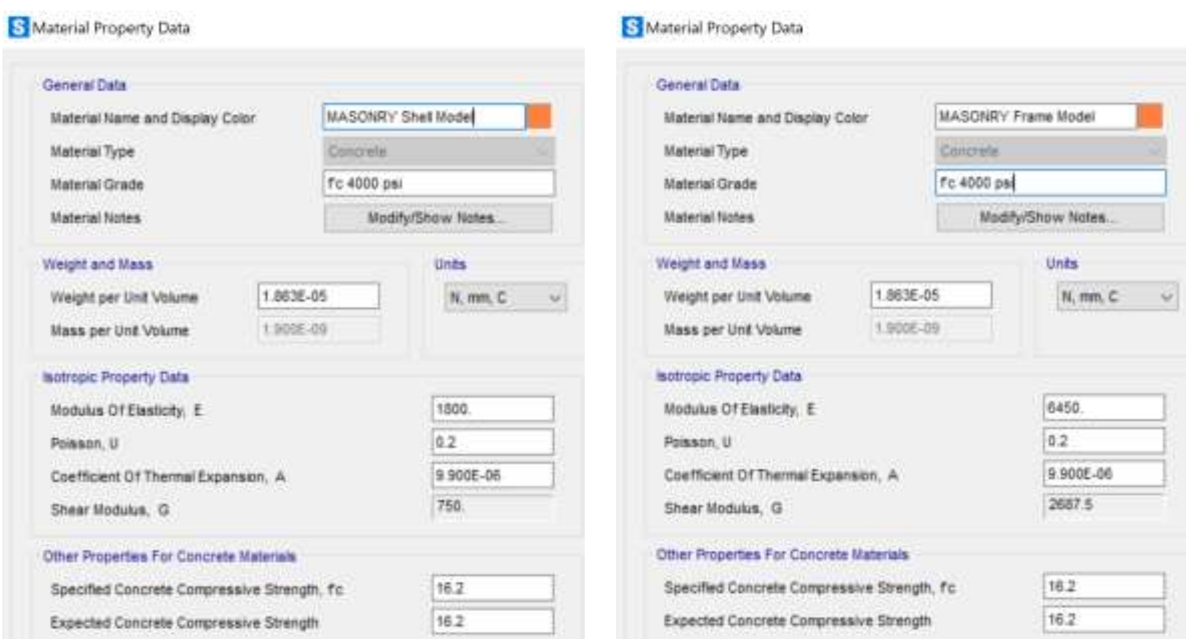

Figure 4.1. Shell and Frame Model General Data

In our analysis of material properties, we specifically focused on masonry, and opting for an initially isotropic directional symmetry type. The Uniaxial Nonlinear material model of shell discretization and input was used. In defining the stress-strain curve, we selected the user-defined option and determined the number of points according to the Hognestad parabola, ensuring a detailed and accurate representation of the material's behavior. The data points used to describe the stress-strain curve of the masonry composite in compression and tension are listed in Table 4.1. They were obtained after application of Eq. 4.1 for $f_{mc}{}' = 16.2$ and ε_o=0.0035 and are plotted in Fig. 4.3 using a compression-negative sign convention consistent with the program's sign convention (SAP2000).

Table 4.1. Uniaxial Nonlinear Stress-Strain

Points	(Epsilon)	(Sigma MPa)
1	0.001	0
2	0.000223798	1.9
3	0	0
4	-0.0005	-4.244897959
5	-0.001	-7.836734694
6	-0.0015	-10.7755102
7	-0.002	-13.06122449
8	-0.0025	-14.69387755
9	-0.003	-15.67346939
10	-0.0035	-16
11	-0.004	-15.67346939
12	-0.005	-13.06122449
13	-0.006	-7.836734694
14	-0.007	0

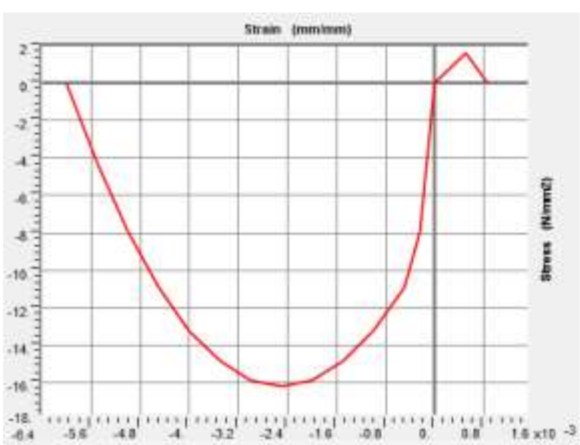

points	strain	stress
1	0.001	0
2	0.000223798	1.9
3	0	0
4	-0.0005	-4.244897959
5	-0.001	-7.836734694
6	-0.0015	-10.7755102
7	-0.002	-13.06122449
8	-0.0025	-14.69387755
9	-0.003	-15.67346939
10	-0.0035	-16
11	-0.004	-15.67346939
12	-0.005	-13.06122449
13	-0.006	-7.836734694
14	-0.007	0

Figure 4.2. Uniaxial Nonlinear Stress-Strain (stress is in MPa)

Cracking and Crushing in Post-peak behavior often involves the occurrence of cracks within the masonry elements. These cracks signify localized failures and can lead to a reduction in the load-bearing capacity of the structure. Additionally, masonry materials can experience crushing, where portions of the material disintegrate due to extreme stress, further compromising structural integrity. Masonry materials may also exhibit strain softening, a phenomenon where the material becomes softer and less resistant to compressive deformation after reaching its peak strength. This behavior can lead to increased deformations under sustained loads, influencing the structural response significantly.

4.4 Shell Elements in Layers

Shell elements in SAP2000 are used to model surfaces that can support loads both in-plane and out-of-plane, such as walls, floors, or complex curved structures. To conduct nonlinear analysis with shell elements, layered discretization is adopted, to allow the calculation of the layered stresses pointwise as a function of the corresponding layer strain, considering the material laws described in the preceding. Summation of forces on the shell cross section through its thickness is obtained from the contribution of the individual layers.

In modelling, the shell Layer/Nonlinear is selected in the Area Section Definition (Figure 4.3). For example, for the full scale shell model, having a wall thickness of 222mm, 6 layers are defined in Figure 4.2 where the distances listed in the table insert to the figure represent distances of the layer centroid to the centroid of the layered cross section. The 'Type' distinguishes between shells that can resist bending and membrane elements that only resist in-plane forces. The 'Num Int. Points' indicates the number of points used to integrate the stress across the thickness, impacting the precision of the analysis.

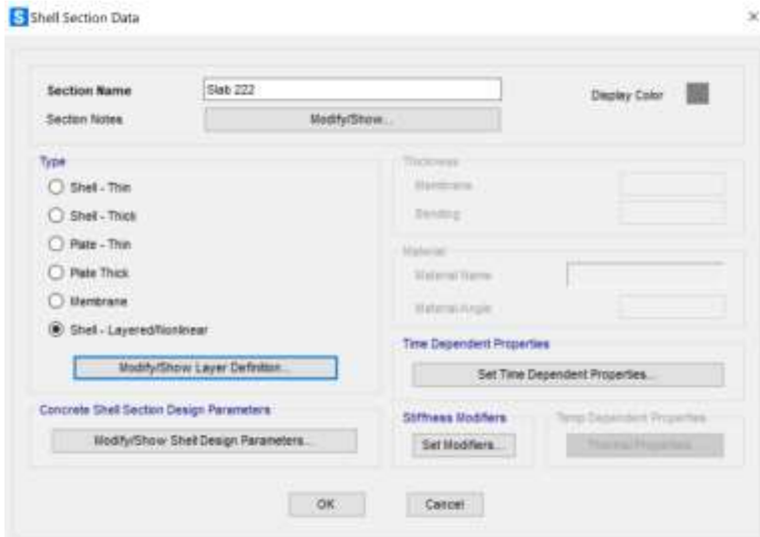

Figure 4.3. Selection of Layered Shell Approach

Material properties, along with the angle at which the material is laid, define the directional strength and stiffness. Lastly, the behavior setting allows for the selection of linear or nonlinear material responses, crucial for modeling the real-life performance of structures under various loads.

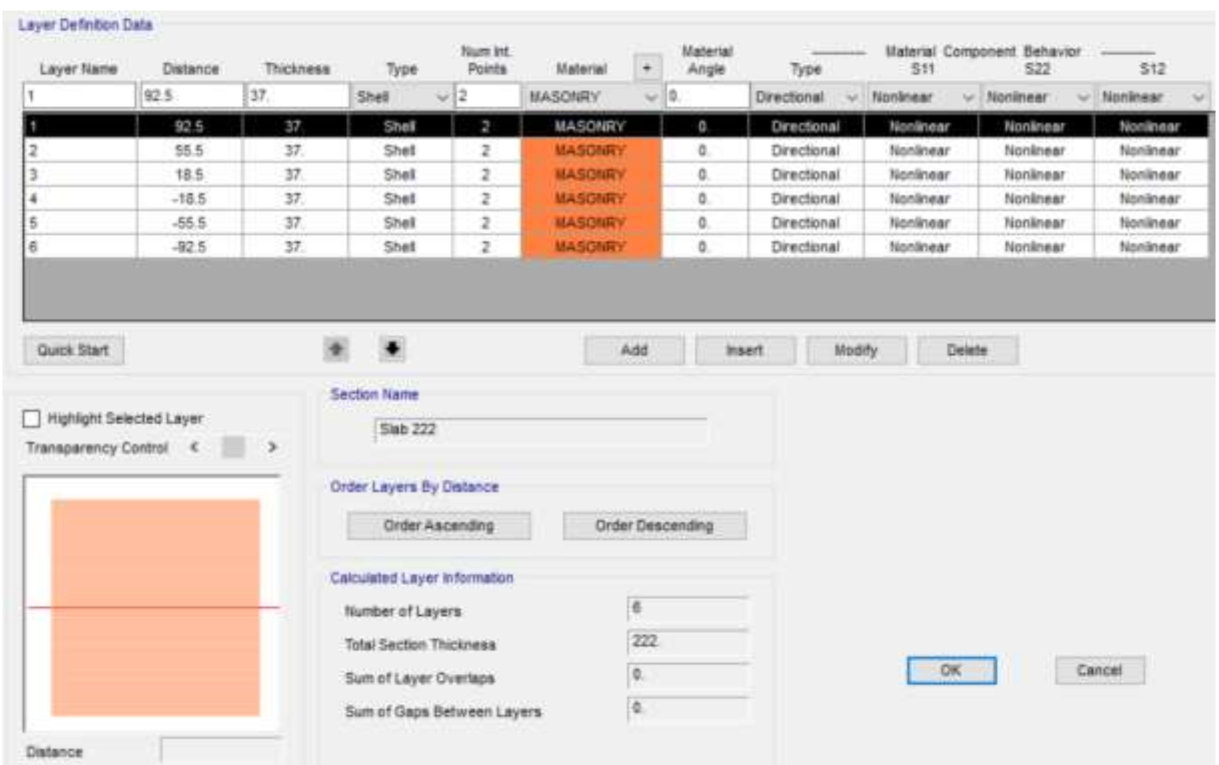

Figure 4.4. Shell Element Layer Definition Data

4.5 Loading Conditions

A comprehensive analysis of both gravity and lateral loads is necessary in the study of unreinforced building models studied here. The building's self-weight, resulting from the mass of all structural components including walls, slabs, columns, and roofs, creates a permanent vertical load. Live Load is neglected in this project because it was not used in the experiment. Nonlinear analysis solution is conducted for the self-weight being applied first – lateral loads applied either as an acceleration response spectrum, or as a uniform field of acceleration, act upon the masses resulting from self-weight; lumped masses, where they occur; if they are defined as masses and not as weights, they must be applied to act in each separate direction of action (in the joints/mass specification option). It is noted that it is opted that P-Delta effects be accounted for in the nonlinear analysis.

4.6 Pushover Analysis

The primary goal of Pushover Analysis is to obtain the lateral load resistance curve of the building modelling the inertia forces under the lateral motion induced during earthquakes. To be able to capture the nonlinear resistance curve, the Pushover Analysis considers the nonlinear behavior of materials and connections. To perform Pushover Nonlinear Analysis in SAP2000, several specific steps have been followed. The load case type for pushover is static; initial conditions are set to 'continue from state at the end of the nonlinear case to gravity.'

Depending on the idealization method nonlinearity may be considered either in the definition of the material properties using layered shell elements (presented in the preceding sections) or, alternatively in the form of plastic hinges for frame components. Pushover analysis is conducted incrementally by applying lateral loads of increasing intensity, typically following a specific force pattern. Starting with a small lateral load, the force gradually increases until a predetermined target displacement or resistance capacity is attained. Plastic hinges, indicative of yielding and potential failure locations, form at points in the structure where plastic deformations occur. By identifying these plastic hinges and their locations, pushover analysis helps pinpoint potential failure points within the structure. The outcome of pushover analysis is represented by a resistance or capacity curve, delineating the relationship between lateral load (or base shear) and the top displacement of the structure. This curve offers valuable insights into the structure's overall lateral load resistance and deformation capacity. Pushover analysis is instrumental in comparing seismic demand (earthquake-induced forces) with the structure's capacity (derived from the capacity curve). This comparison is needed in order to estimate the condition of damage the structure will undergo at different levels of ground motion intensity.

It was stated that the nonlinearity in the equivalent frame analysis model is accounted for by lumped plastic hinges in the ends of all linear beam-column elements. The idealized model is shown in Figure 4.8; the input in this case is the Moment – Plastic rotation envelope of the end cross sections of all the elements. In the present case of equivalent frame analysis, the values recommended by ASCE/SEI 41 (2017) were used as a starting input.

4.6.1 Input Definition of Hinge Properties

The typical input property of a plastic hinge is a nonlinear Moment – Plastic Rotation Envelope. The hinges are located in the ends of the member and are activated only when end rotations exceed the rotation (or drift ratio) at the onset of yielding. With reference to Figure 4.5, the input values include the properties E_m, I, for the entire member which will remain elastic throughout the response, and the M-θ_{pl} values shown.

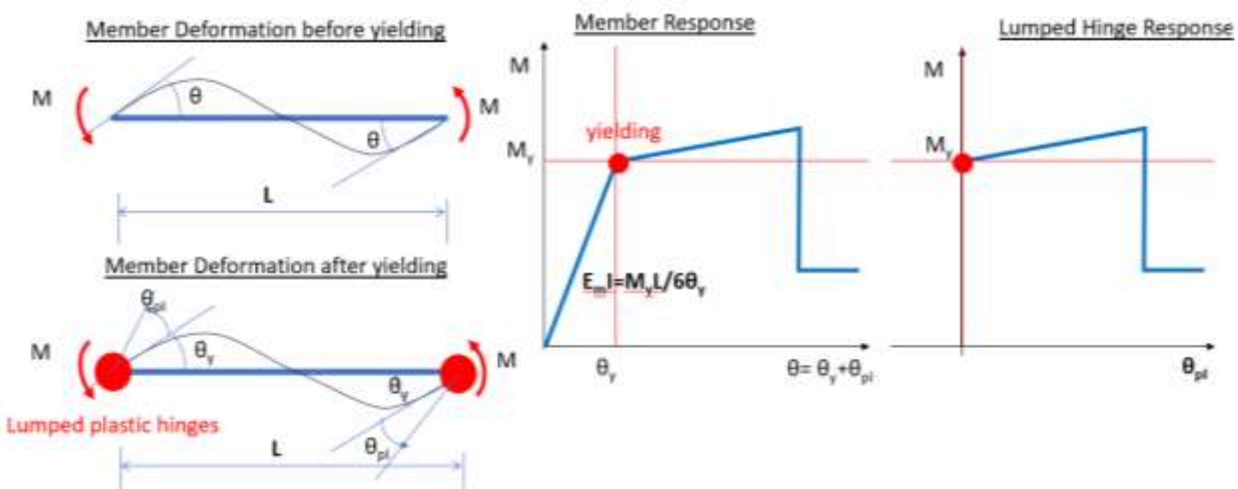

Figure 4.5. Hinge properties for Nonlinear Modeling of frame members for Pushover Analysis

Input includes values identifying various stages of behavior: initial elasticity, yielding, post-yield stiffness degradation, and ultimate capacity. The graph serves as the envelope of the hysteresis behavior under cyclic loading. Load behavior beyond ultimate capacity, scaling factors for force and deformation, and acceptance criteria for different performance levels—like immediate occupancy and collapse prevention—are also specified, ensuring the structure meets seismic performance objectives. Hysteresis type selection allows for the modeling of energy dissipation, for realistic simulation of structural response during earthquakes. Hysteresis refers to the behavior of a material or system that depends on its past history as well as its current condition. In the context of structural engineering, it describes the loop formed on a force-displacement (or stress-strain) diagram during cyclic loading, such as that experienced during an earthquake. This loop indicates that the energy is being dissipated by the structure as it undergoes loading and unloading cycles. The shape and size of the hysteresis loop provide information on the energy dissipation characteristics and the ductility of the material or structure. Structures with larger and more pliable hysteresis loops generally have better energy dissipation capabilities and are more ductile, which is desirable in seismic design to prevent sudden failure.

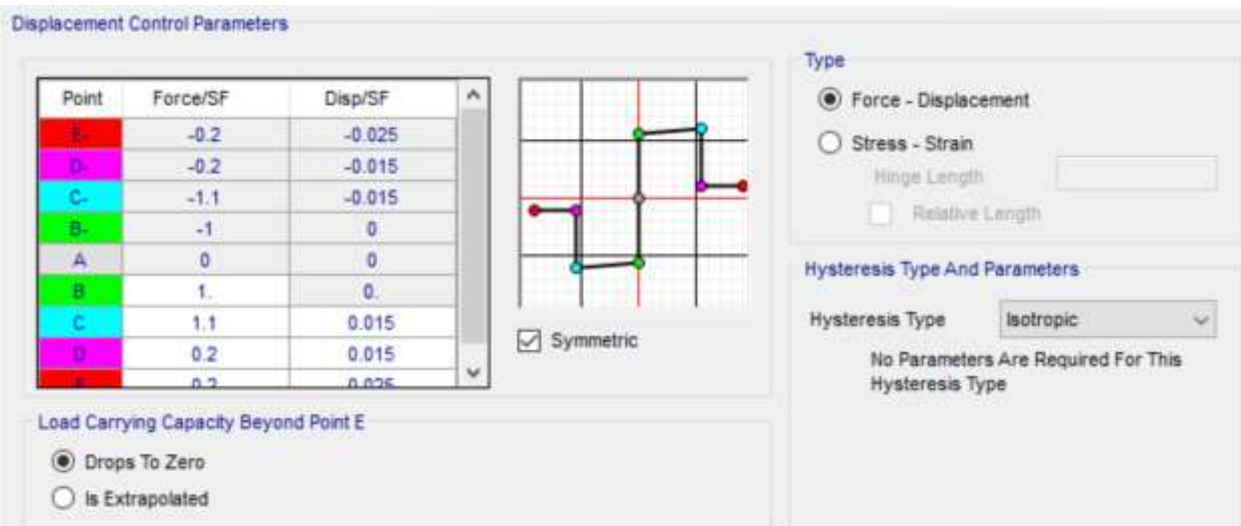

Figure 4.6. Nonlinear Hinge Properties for Pushover Analysis in SAP2000

Figure 4.7. Nonlinear Hinge Properties for Pushover Analysis using the Equivalent Frame Model of the Test Structure, in SAP2000

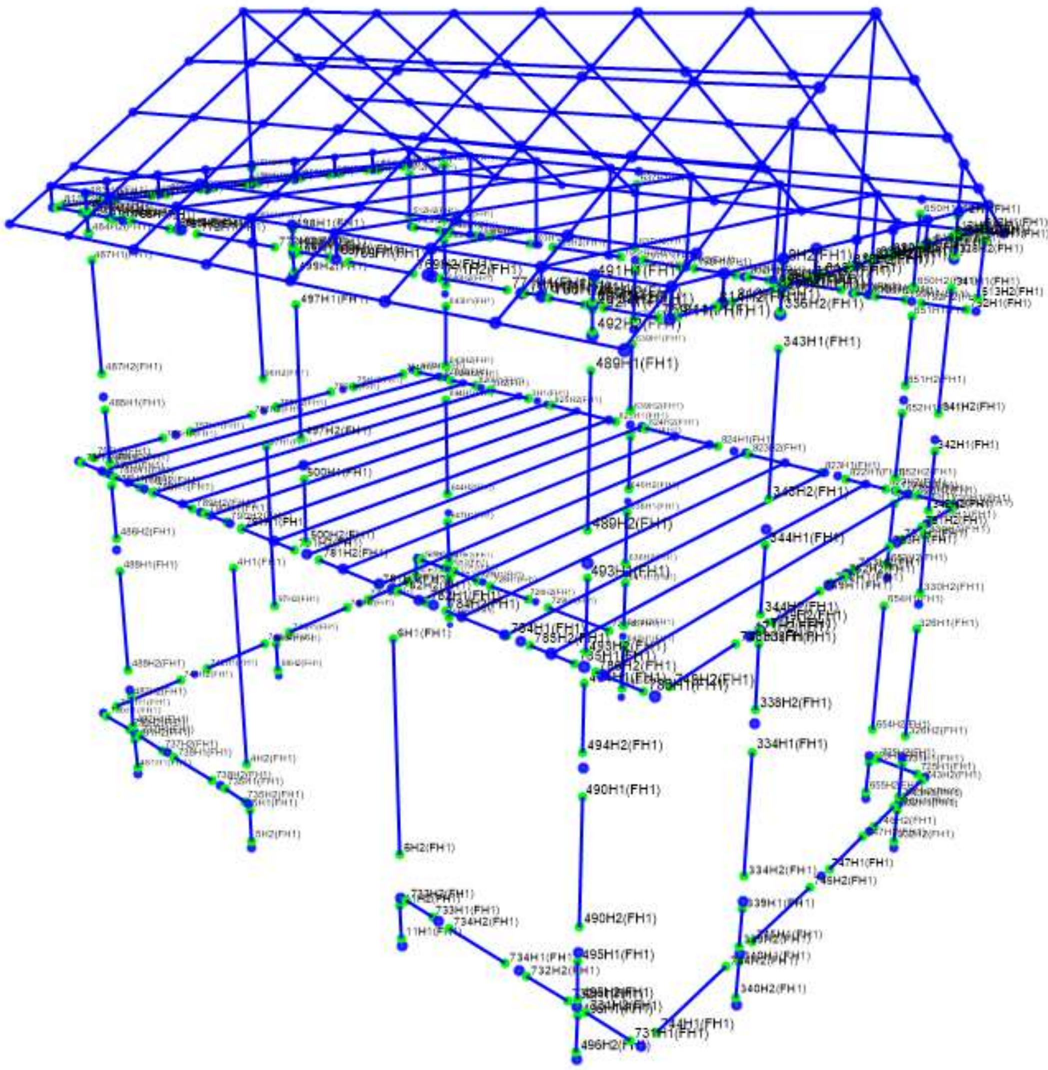

Figure 4.8. Frame Hinges for the Equivalent Frame Model

4.6.2 Application of Earthquake Loads in Longitudinal and Transverse Directions

Earthquake loads are modeled as lateral forces that act horizontally on the structure. The accelerations generated attract inertia forces wherever the building has mass. To simulate this lateral force, loads are applied in both the X and Y directions, which are typically parallel to the ground surface. When subjected to earthquake loading in the longitudinal direction, the portable pitched roof, gable walls, and corners experience the highest pressure, leading to increased risk of collapse and damage. Under earthquake loading in the transverse direction, the central section of the building's long façade exhibits the greatest out of plane displacement or curvature compared to the corners. Additionally, significant damage is observed around windows and doors.

Table 4.2. Shell Model Lateral Load of Earthquake

Mode	Period/ Sec	Displacement	Highest Mass Participation	Deformed Shape shell model	
1	0.104	UX	40 %	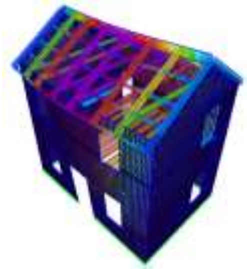	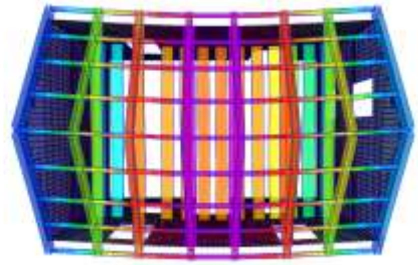
2	0.073	UY	31 %	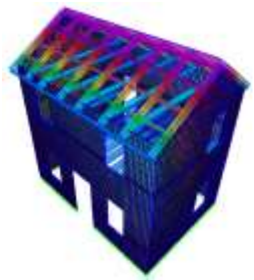 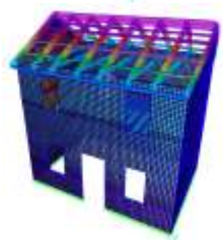	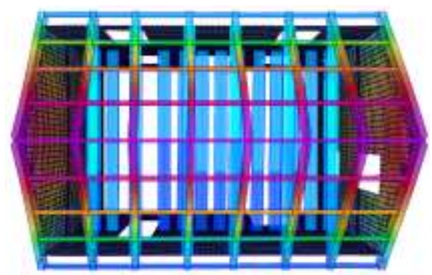

4.6.3 Building Corners and Gables in Lateral Forces: (COMB1: DEAD + Gravity X)

The load combination, e.g. "COMB1: DEAD + Gravity X," typically represents a combination of dead load and a gravitational acceleration field applied in the X direction. Combining these loads in the X direction implies a lateral load component, potentially representing an earthquake force. Results are evaluated from the relative displacement magnitudes between corners and mid-side of the long direction of the building, as well as the out of plane deflection of the gables, because these are locations that are particularly vulnerable to the effects of lateral forces during the earthquake action.

Lateral loads may induce torsional effects on a building due to the irregular arrangement of the openings. The diaphragm of a structure plays a crucial role in distributing lateral loads. If the diaphragm is flexible (as in the present case) or it has discontinuities, especially near corners or gables, it can compromise the overall stability of those parts of the structural walls that are particularly flexible, and can cause stress concentrations and eventual failure. Insufficient shear resistance in the walls or structural elements near the corners and gables can result in localized failure under lateral loads. The dynamic response of the structure to lateral loads may result in higher displacements and forces at the corners and gables, making them more susceptible to damage or collapse.

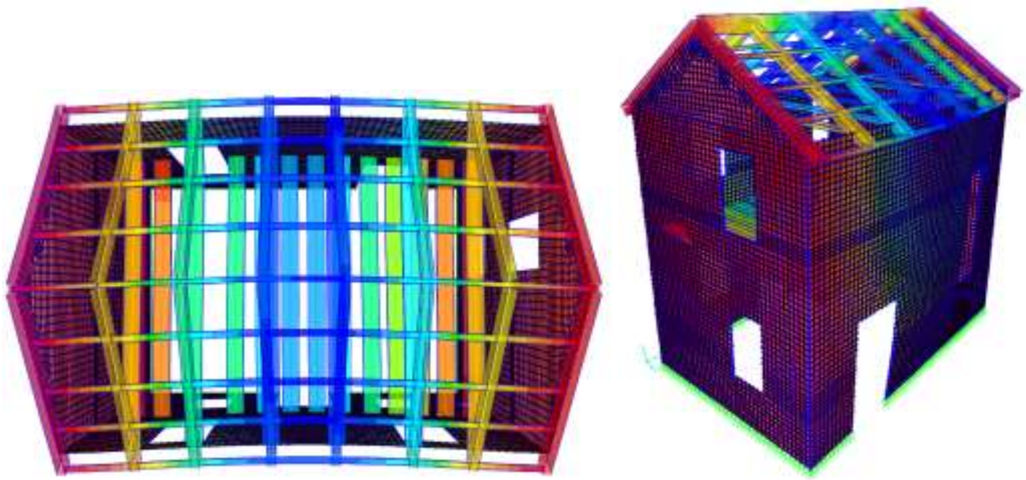

Figure 4.9. COMB2: DEAD + Gravity Y

Table 4.3. Nonlinear Analysis Frame Model Lateral Load of Earthquake (E=840)

Mode	Period/ Sec	Displacement	Highest Mass Participation	Deformed Shape frame model E=840	
1	0.22	UX	52 %	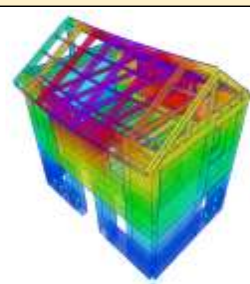	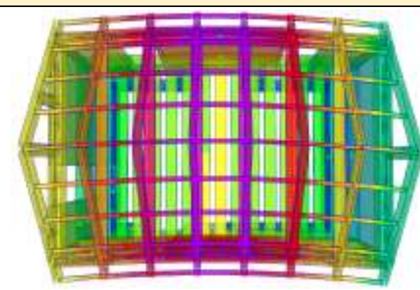
3	0.13	UY	28 %	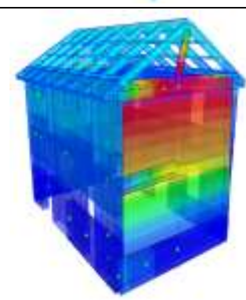	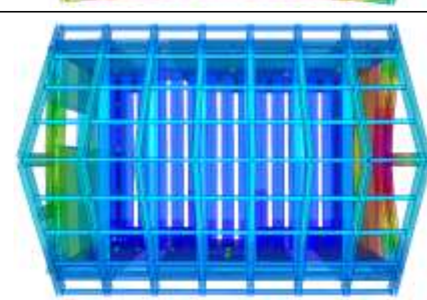

4.6.4 The Influence of Hinges in Nonlinear Analysis

When performing nonlinear analysis with nonlinear hinges, local flexibility occurs in the ends of yielding structural components, by allowing rotations or deformations at those locations where plastic rotation has been exceeded. As a result, the structure becomes more flexible, especially at the hinged locations. The introduction of hinges alters the distribution of mass participation in different modes of vibration. The locations of hinges become critical points where mass is more likely to participate in the dynamic response of the structure. Hinges also significantly modify the stiffness distribution within the structure. This change in stiffness affects the natural frequencies and mode shapes, leading to a reconfiguration of mass participation among different modes. Hinges concentrate flexibility and deformation at specific points, influencing the local response of the structure. This localization can impact the distribution of mass participation in modes associated with the hinged regions. The changes in mass participation can have implications for the dynamic behavior and seismic response of the structure during nonlinear analyses.

Table 4.4. Lateral load of earthquake Frame model with Hinges, (E= 6450)

Mode	Period/ Sec	Displacement	Highest Mass Participation	Deformed Shape frame model E=840	
1	0.112	UX	35 %	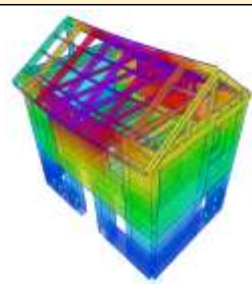	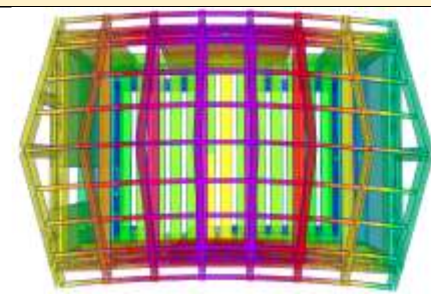
3	0.0623	UY	20 %	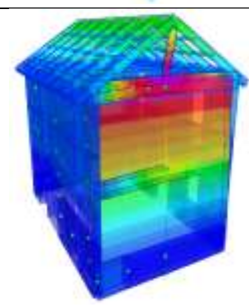	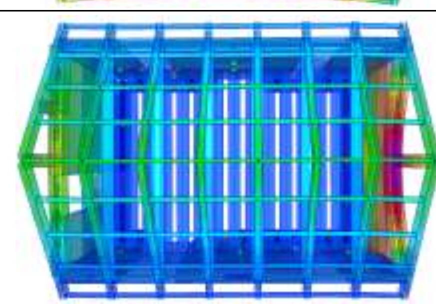

4.6.5 Period of the Building in Nonlinear and Linear Analysis

After yielding, the plastic hinges are activated, leading to increased flexibility and change in stiffness distribution, as they enable plastic rotations or deformations.

Table 4.5. Period of the Shell and Frame Building in Nonlinear Analysis

Model	Modulus of Elasticity (E)	Period and Frequency
Frame model half scale (Linear)	6450	Mode 1, T=0.1153 s.
Frame model half scale (Nonlinear)	6450	Mode 1, T=0.1125 s.
Shell model half scale (Nonlinear)	1800	Mode 1, T=0.1154 s.
Shell model full scale (Linear)	1900	Mode 1, T=0.1590 s.
Shell model full scale (Nonlinear)	1900	Mode 1, T=0.1047 s.

4.7 Response Spectrum Analysis

The Response Spectrum is a graphical representation of the maximum acceleration response of all possible single degree of freedom structures subjected to dynamic loads (e.g. ground motion) as a function of the respective natural periods of these single degree of freedom systems. Response Spectrum analysis is used in the present analysis using the function defined by the National Building Code of Canada 2015 – using the load type ACCEL. Modal combination is implemented using CQC, and directional combination is applied through SRSS.

4.7.1 3D Frame Model of Unreinforced Masonry Building Earthquake is Acting in X Direction, E=6450, EQX-X Direction

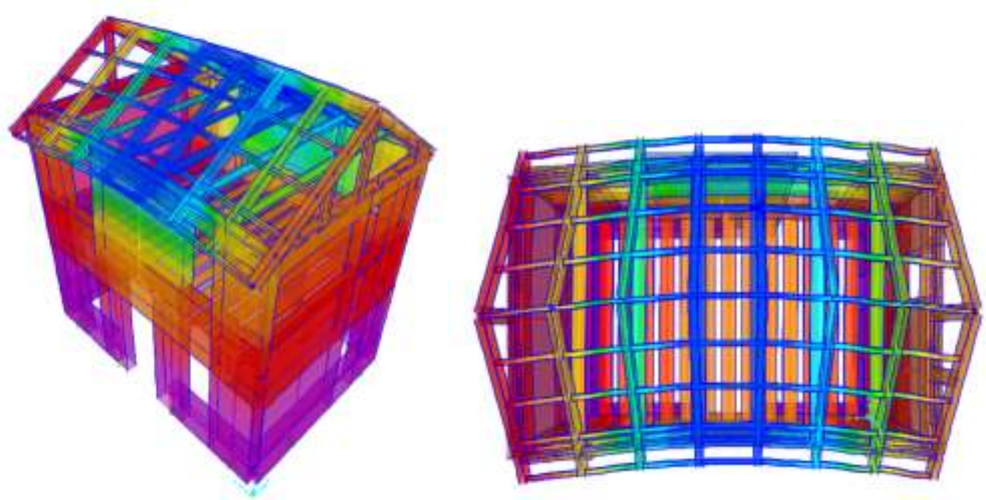

Figure 4.10. 3D Frame Model of Unreinforced Masonry Building Earthquake is Acting in X Direction

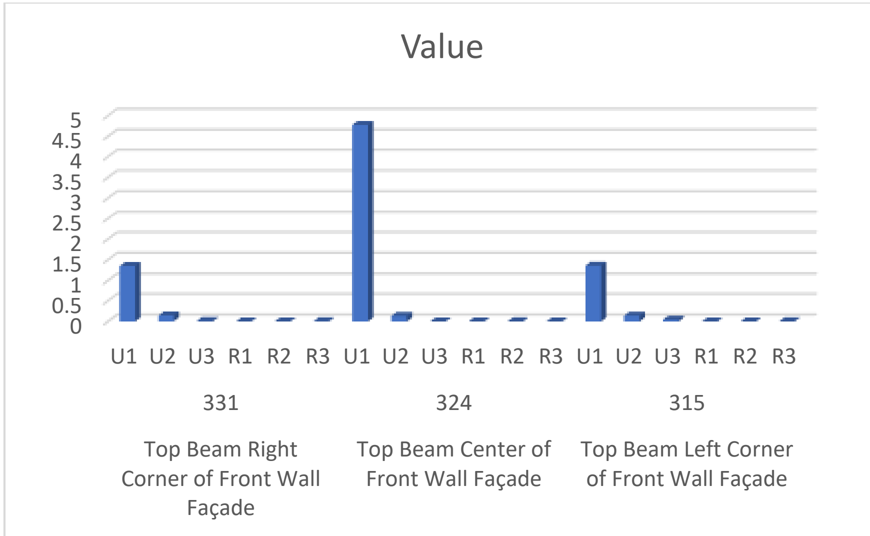

Figure 4.11. Comparison of Out of Plane Motion at the Top of Unreinforced Masonry Long Wall, E=6450

Table 4.6. Categories of Out of Plane Motion at the Top of Unreinforced Masonry Building

Category	Point Objects (Pt Obj) / Point Elements (Pt Elm)	Description	Value	Out of Plane Motion
Top Beam Right Corner of Front Wall Façade	331	U1	1.3492	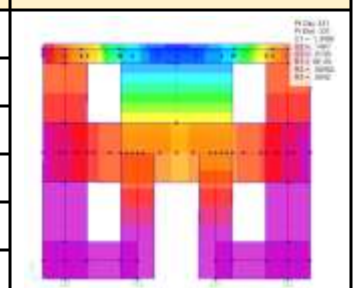
		U2	0.1467	
		U3	0.0139	
		R1	8E-05	
		R2	0.00082	
		R3	0.0042	
Top Beam Center of Front Wall Façade	324	U1	4.7759	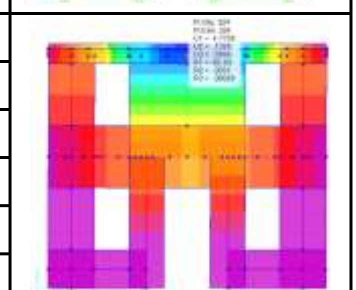
		U2	0.1328	
		U3	0.0026	
		R1	6E-05	
		R2	0.0031	
		R3	0.00029	
Top Beam Left Corner of Front Wall Façade	315	U1	1.3582	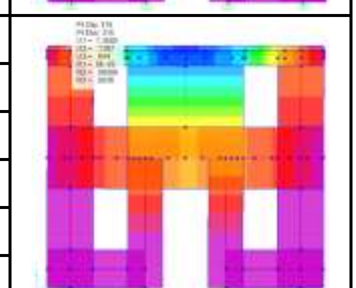
		U2	0.1387	
		U3	0.044	
		R1	8E-05	
		R2	0.00088	
		R3	0.0036	

Table 4.7. Categories of Out of Plane Motion at the Middle of Unreinforced Masonry Building

Category	Point Objects (Pt Obj) / Point Elements (Pt Elm)	Description	Value	Out of Plane Motion
Middle Beam Right Corner of Front Wall Façade	363	U1	0.5542	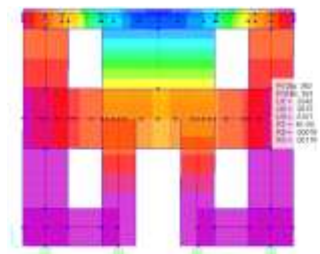
		U2	0.0675	
		U3	0.0107	
		R1	4E-05	
		R2	0.00078	
		R3	0.00179	
Middle Beam Center of Front Wall Façade	2	U1	1.767	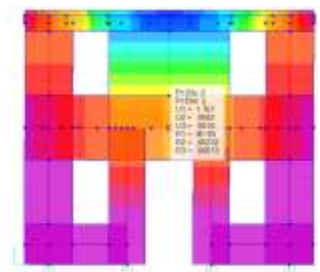
		U2	0.0682	
		U3	0.0019	
		R1	4E-05	
		R2	0.00232	
		R3	0.00013	
Middle Beam Left Corner of Front Wall Façade	326	U1	0.5555	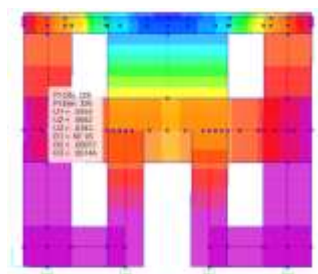
		U2	0.0682	
		U3	0.0383	
		R1	6E-05	
		R2	0.00057	
		R3	0.00146	

Table 4.8. Categories of Out of Plane Motion at the Bottom of Unreinforced Masonry Building

Category	Point Objects (Pt Obj) / Point Elements (Pt Elm)	Description	Value	Out of Plane Motion
Bottom Beam Right Corner of Front Wall Façade	365	U1	0.0173	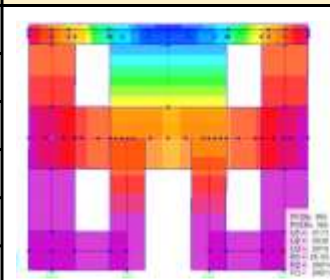
		U2	0.0038	
		U3	0.0019	
		R1	2E-05	
		R2	0.00014	
		R3	0.00013	
Bottom Beam Center of Front Wall Façade	369	U1	0.0497	
		U2	0.0035	
		U3	0.0004	
		R1	2E-05	

Category	Point Objects (Pt Obj) / Point Elements (Pt Elm)	Description	Value	Out of Plane Motion
		R2	0.00047	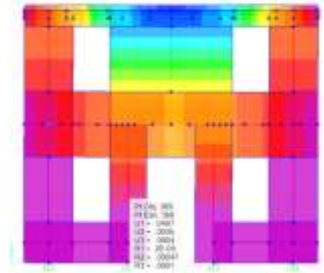
		R3	0.0001	
Bottom Beam Left Corner of Front Wall Façade	366	U1	0.021	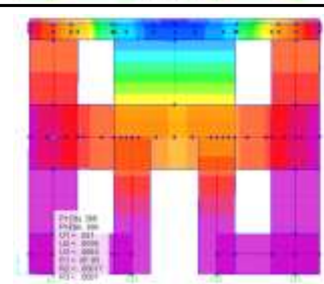
		U2	0.0036	
		U3	0.0063	
		R1	2E-05	
		R2	0.00017	
		R3	0.0001	

4.7.1.1 Frame Model Half Scale Horizontal Drift (Front Wall)

Table 4.9. Frame Model Half Scale Horizontal Drift (Front Wall), E=6450, EQX-X Direction

Horizontal Drift	Value
The Out of Plane Drift Ratio, in the Horizontal Direction	$\frac{4.7759-1.3492}{1500\ mm} =$ 0.002284=0.23%
The Drift Ratio of the Upper Floor	$\frac{4.7759-1.767}{1120\ mm} = 0.002686 = 0.27\%$
The Drift Ratio of the First Floor	$\frac{1.767}{1360\ mm} =$ 0.001299=0.13%

4.7.2 3D Frame Model of Unreinforced Masonry Building Earthquake is Acting in X Direction, E=6450, COMB-Dead&X-NL

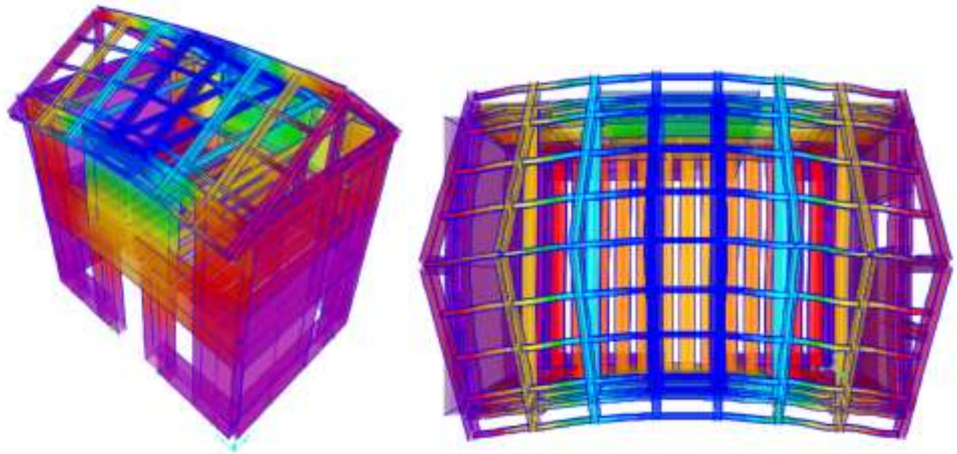

Figure 4.12. 3D Frame Model of Unreinforced Masonry Building Earthquake is Acting in X Direction

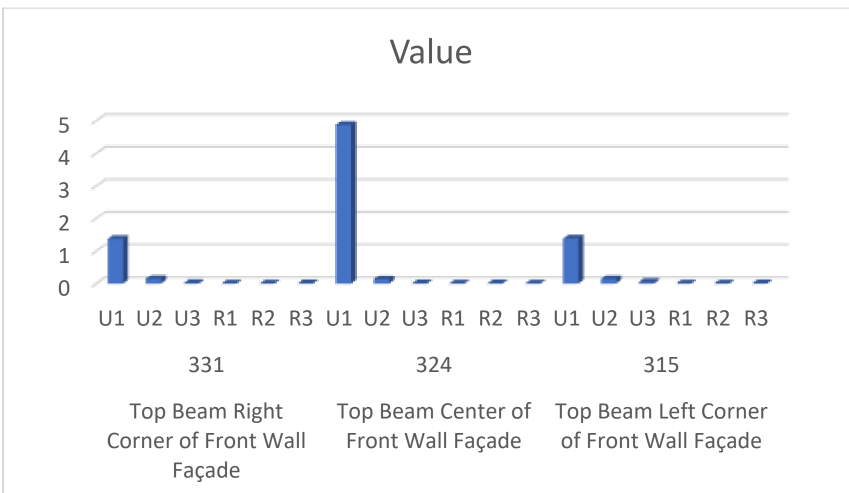

Figure 4.13. Comparison of Out of Plane Motion at the Top of Unreinforced Masonry Long Wall, E=6450

Table 4.10. Categories of Out of Plane Motion at the Top of Unreinforced Masonry Building

Category	Point Objects (Pt Obj) / Point Elements (Pt Elm)	Description	Value	Out of Plane Motion
Top Beam Right Corner of Front Wall Façade	331	U1	1.3754	
		U2	0.1495	
		U3	0.0142	
		R1	8E-05	
		R2	0.00084	

Category	Point Objects (Pt Obj) / Point Elements (Pt Elm)	Description	Value	Out of Plane Motion
		R3	0.00428	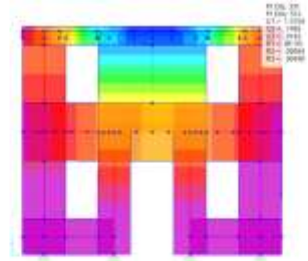
Top Beam Center of Front Wall Façade	324	U1	4.8684	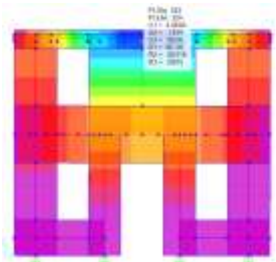
		U2	0.1354	
		U3	0.0026	
		R1	6E-05	
		R2	0.00316	
		R3	0.0003	
Top Beam Left Corner of Front Wall Façade	315	U1	1.3854	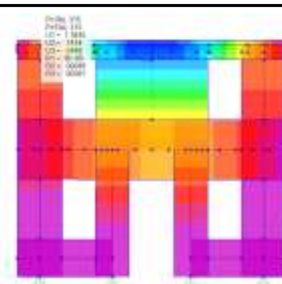
		U2	0.1414	
		U3	0.0448	
		R1	8E-05	
		R2	0.00089	
		R3	0.00367	

Table 4.11. Categories of Out of Plane Motion at the Middle of Unreinforced Masonry Building

Category	Point Objects (Pt Obj) / Point Elements (Pt Elm)	Description	Value	Out of Plane Motion
Middle Beam Right Corner of Front Wall Façade	363	U1	0.565	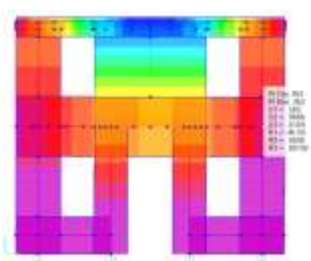
		U2	0.0688	
		U3	0.0109	
		R1	4E-05	
		R2	0.0008	
		R3	0.00182	
Middle Beam Center of Front Wall Façade	2	U1	1.8013	
		U2	0.0695	
		U3	0.002	
		R1	4E-05	
		R2	0.00237	

Category	Point Objects (Pt Obj) / Point Elements (Pt Elm)	Description	Value	Out of Plane Motion
		R3	0.00014	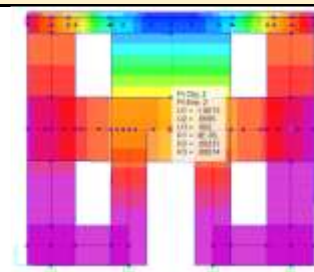
Middle Beam Left Corner of Front Wall Façade	326	U1	0.5663	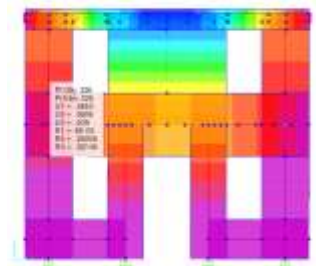
		U2	0.0695	
		U3	0.039	
		R1	6E-05	
		R2	0.00058	
		R3	0.00149	

Table 4.12. Categories of Out of Plane Motion at the Bottom of Unreinforced Masonry Building

Category	Point Objects (Pt Obj) / Point Elements (Pt Elm)	Description	Value	Out of Plane Motion
Bottom Beam Right Corner of Front Wall Façade	365	U1	0.0176	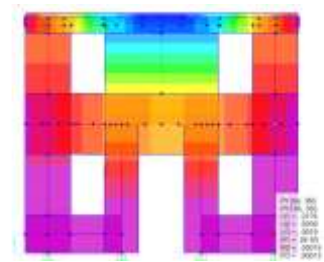
		U2	0.0039	
		U3	0.0019	
		R1	2E-05	
		R2	0.00015	
		R3	0.00013	
Bottom Beam Center of Front Wall Façade	369	U1	0.0506	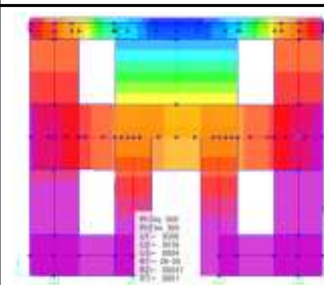
		U2	0.0036	
		U3	0.0004	
		R1	2E-05	
		R2	0.00047	
		R3	0.0001	
Bottom Beam Left Corner of Front Wall Façade	366	U1	0.0214	
		U2	0.0101	
		U3	0.0037	
		R1	2E-05	
		R2	0.00018	

Category	Point Objects (Pt Obj) / Point Elements (Pt Elm)	Description	Value	Out of Plane Motion
		R3	0.0001	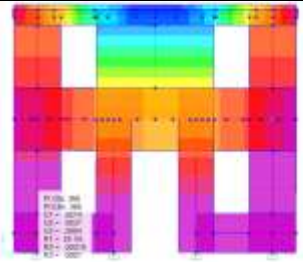

4.7.2.1 Frame Model Half Scale Horizontal Drift (Front Wall)

Table 4.13. Frame Model Half Scale Horizontal Drift (Front Wall), E=6450, COMB-Dead&X-NL

Horizontal Drift	Value
The Out of Plane Drift Ratio, in the Horizontal Direction	$\frac{4.8684 - 1.3754}{1500\ mm} = 0.0023286 = 0.23\%$
The Drift Ratio of the Upper Floor	$\frac{4.8684 - 1.8013}{1120\ mm} = 0.0027384 = 0.27\%$
The Drift Ratio of the First Floor	$\frac{1.8013}{1360\ mm} = 0.0013244 = 0.13\%$

The analysis at hand delves into the seismic response of a frame model with a particular focus on out-of-plane displacements induced by earthquake forces. Such analysis is pivotal in predicting structural performance in the face of seismic events. The data encapsulated in the tables list displacement values in three directions (U1, U2, U3) and rotational values (R1, R2, R3) for various points of the structure. Adjacent to the displacement data, graphical representations chart the out-of-plane motion profiles for different structural components. These graphs are instrumental in pinpointing displacement patterns and identifying the loci of maximal deflection. Peaks within these visual depictions suggest potential zones of weakness or sections that may exhibit inelastic behavior if subjected to seismic forces. Additionally, the document sheds light on drift ratios—quantitative measures of inter-story displacement in relation to the overall height of the building. These ratios are of essence in gauging the building's seismic performance, offering insights into its lateral deformation capabilities. Evaluating whether the structure can maintain its structural integrity during severe seismic occurrences hinges on these ratios. To affirm the building's adequacy in lateral deformation, these ratios must conform to the thresholds prescribed by the applicable building codes. The directional impact of seismic forces is also underscored within the analysis. It is observed that the seismic load predominantly acts parallel to the short (X) axis, exerting a more pronounced effect on the long walls. This directional influence is crucial for understanding the structure's anisotropic response. The drift ratio is a key indicator of a building's seismic performance. It measures the relative displacement of one level compared to another, providing insight into the building's overall flexibility and ductility. Factors such as the distribution of stiffness and mass, coupled with the directional orientation of seismic forces, significantly influence the demands placed upon various structural elements.

4.7.3 The Earthquake is Acting Parallel to the Long (i.e., Y) Direction, Affecting Mainly the Short Walls.

When an earthquake acts parallel to the long direction (Y-axis) of a building, the primary impact is on the short walls of the structure. The out-of-plane forces can lead to significant bending stresses, especially at the connections with the roof. This situation presents specific challenges in seismic analysis:

1. Direction of Seismic Forces: In this scenario, the seismic forces act along the Y-axis, which is parallel to the long walls. Consequently, the short walls, oriented perpendicular to this direction, bear the brunt of the seismic forces.

2. Impact on Short Walls: The short walls face significant seismic loading in two main ways:

   - In-Plane Shear Forces: The short walls experience shear forces within their plane, as the earthquake forces push them back and forth along their length.

   - Out-of-Plane Bending: While in-plane forces are significant, the out-of-plane forces can be more critical for short walls. These forces tend to push the walls out of their plane, potentially leading to bending and buckling.

4.7.3.1 3D Frame Model of Unreinforced Masonry Building Earthquake is Acting in Y Direction, Direction, E=6450, EQX-Y Direction

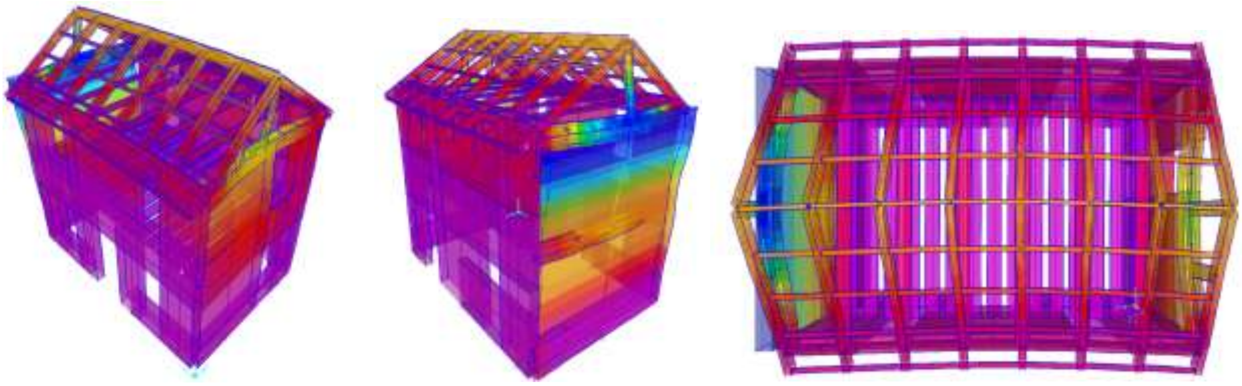

Figure 4.14. 3D Frame Model of Unreinforced Masonry Building Earthquake is Acting in Y Direction

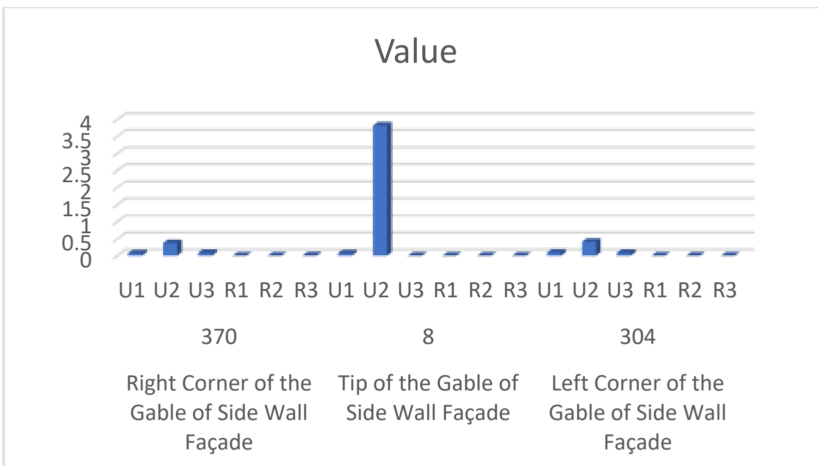

Figure 4.15. Comparison of Out of Plane Motion at the Top of Unreinforced Masonry Short Wall, E=6450, EQX-Y Direction

Table 4.14. Categories of Out of Plane Motion at the Top of Unreinforced Masonry Short Wall

Category	Point Objects (Pt Obj) / Point Elements (Pt Elm)	Description	Value	Out of Plane Motion
Right Corner of the Gable of Side Wall Façade	370	U1	0.0691	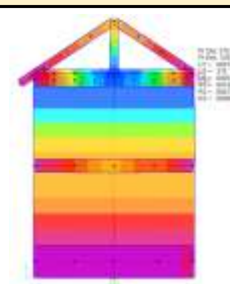
		U2	0.375	
		U3	0.0805	
		R1	0.00159	
		R2	0.0001	
		R3	0.00589	
	8	U1	0.0684	

Category	Point Objects (Pt Obj) / Point Elements (Pt Elm)	Description	Value	Out of Plane Motion
Tip of the Gable of Side Wall Façade		U2	3.8098	
		U3	0.0025	
		R1	0.00239	
		R2	3E-05	
		R3	0.0004	
Left Corner of the Gable of Side Wall Façade	304	U1	0.0901	
		U2	0.4159	
		U3	0.0817	
		R1	0.0003	
		R2	8E-05	
		R3	0.00259	

Table 4.15. Categories of Out of Plane Motion at the Middle of Unreinforced Masonry Short Wall

Category	Point Objects (Pt Obj) / Point Elements (Pt Elm)	Description	Value	Out of Plane Motion
Middle Beam Right Corner of Side Wall Façade	12	U1	0.0403	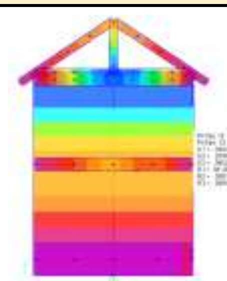
		U2	0.2049	
		U3	0.0652	
		R1	9E-05	
		R2	0.00019	
		R3	0.00059	
Middle Beam Center of Side Wall Façade	338	U1	0.034	
		U2	1.5261	
		U3	0.0016	
		R1	0.0019	
		R2	2E-05	
		R3	0.00021	
Middle Beam Left Corner of Side Wall Façade	115	U1	0.0537	
		U2	0.2097	
		U3	0.0575	
		R1	0.00011	
		R2	0.00012	
		R3	0.00044	

Table 4.16. Categories of Out of Plane Motion at the Bottom of Unreinforced Masonry Short Wall

Category	Point Objects (Pt Obj) / Point Elements (Pt Elm)	Description	Value	Out of Plane Motion
Bottom Beam Right Corner of Side Wall Façade	1	U1	0.0028	
		U2	0.3515	
		U3	0.0115	
		R1	0.00041	
		R2	2E-05	
		R3	0.00049	
Bottom Beam Center of Side Wall Façade	387	U1	0.0028	
		U2	0.0432	
		U3	0.0003	
		R1	0.00041	
		R2	4.796E-06	
		R3	4E-05	
Bottom Beam Left Corner of Side Wall Façade	274	U1	0.0026	
		U2	0.0117	
		U3	0.0186	
		R1	6E-05	
		R2	2E-05	
		R3	2E-05	

4.7.3.2 Frame Model Half Scale Horizontal Drift (Side Wall)

Table 4.17. Frame Model Half Scale Horizontal Drift (Side Wall), E=6450, EQX-Y Direction

Horizontal Drift	Value
The Out of Plane Drift Ratio, in the Horizontal Direction	$\frac{3.8098 - 0.375}{960\ mm} = 0.003577 = 0.36\%$
The Drift Ratio of the Upper Floor	$\frac{3.8098 - 1.5261}{1760\ mm} = 0.001297 = 0.13\%$
The Drift Ratio of the First Floor	$\frac{1.5261}{1360\ mm} = 0.001122 = 0.11\%$

4.7.4 3D Frame Model of Unreinforced Masonry Building Earthquake is Acting in Y Direction, Direction, E=6450, COMB-Dead&Y-NL

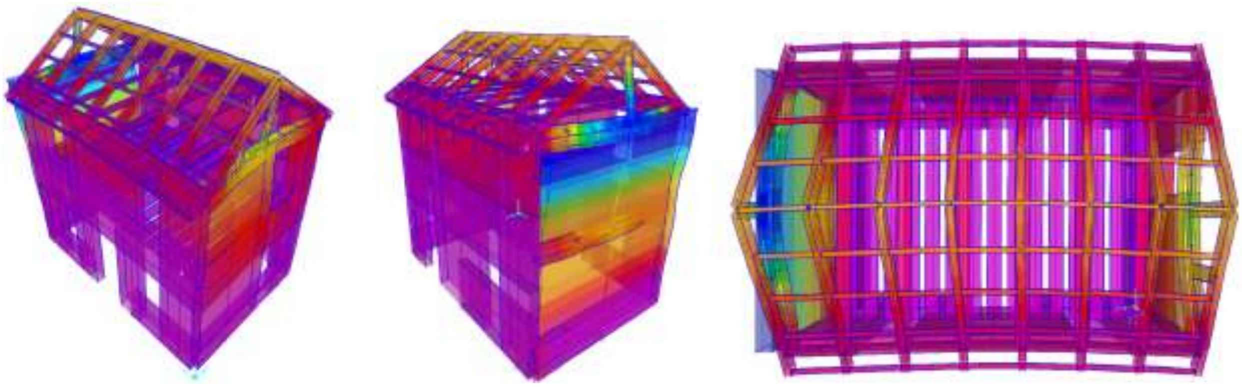

Figure 4.16. 3D Frame Model of Unreinforced Masonry Building Earthquake is Acting in Y Direction

Table 4.18. Categories of Out of Plane Motion at the Top of Unreinforced Masonry Short Wall

Category	Point Objects (Pt Obj) / Point Elements (Pt Elm)	Description	Value	Out of Plane Motion
Right Corner of the Gable of Side Wall Façade	370	U1	0.0705	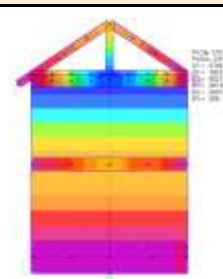
		U2	0.3823	
		U3	0.0821	
		R1	0.00159	
		R2	0.0001	
		R3	0.006	
Tip of the Gable of Side Wall Façade	8	U1	0.0697	
		U2	3.8836	
		U3	0.0025	
		R1	0.00243	
		R2	3E-05	
		R3	0.00041	
Left Corner of the Gable of Side Wall Façade	304	U1	0.0918	
		U2	0.424	
		U3	0.0833	
		R1	0.0003	
		R2	9E-05	
		R3	0.00264	

Table 4.19. Categories of Out of Plane Motion at the Middle of Unreinforced Masonry Short Wall

Category	Point Objects (Pt Obj) / Point Elements (Pt Elm)	Description	Value	Out of Plane Motion
Middle Beam Right Corner of Side Wall Façade	12	U1	0.0411	
		U2	0.2089	
		U3	0.0664	
		R1	9E-05	
		R2	0.00019	
		R3	0.0006	
Middle Beam Center of Side Wall Façade	338	U1	0.0346	
		U2	1.5557	
		U3	0.0016	
		R1	0.00193	
		R2	2E-05	
		R3	0.00021	
Middle Beam Left Corner of Side Wall Façade	115	U1	0.2463	
		U2	0.6571	
		U3	0.3083	
		R1	0.00061	
		R2	0.00034	
		R3	0.00251	

Table 4.20. Categories of Out of Plane Motion at the Bottom of Unreinforced Masonry Short Wall

Category	Point Objects (Pt Obj) / Point Elements (Pt Elm)	Description	Value	Out of Plane Motion
Bottom Beam Right Corner of Side Wall Façade	1	U1	0.0028	
		U2	0.3583	
		U3	0.0118	
		R1	0.00042	
		R2	2E-05	
		R3	0.0005	
Bottom Beam Center of Side Wall Façade	387	U1	0.0028	
		U2	0.044	
		U3	0.0003	
		R1	0.00042	
		R2	4.889E-06	

Category	Point Objects (Pt Obj) / Point Elements (Pt Elm)	Description	Value	Out of Plane Motion
		R3	4E-05	
Bottom Beam Left Corner of Side Wall Façade	274	U1	0.0026	
		U2	0.0119	
		U3	0.0189	
		R1	6E-05	
		R2	2E-05	
		R3	2E-05	

4.7.4.1 Frame Model Half Scale Horizontal Drift (Side Wall)

Table 4.21. Frame Model Half Scale Horizontal Drift (Side Wall), E=6450, COMB-Dead&Y-NL

Horizontal Drift	Value
The Out of Plane Drift Ratio, in the Horizontal Direction	$\frac{3.8836-0.3823}{960\ mm} =$ 0.003647=0.365%
The Drift Ratio of the Upper Floor	$\frac{3.8836-1.5557}{1760\ mm} =$ 0.001322=0.13%
The Drift Ratio of the First Floor	$\frac{1.5557}{1360\ mm} = 0.001143 = 0.115\%$

4.7.5 Values of the Displacements in Terms of Out of Plane Motion for Spectral Analysis, (Shell Model)

4.7.5.1 The Earthquake is Acting Parallel to the Short (i.e., X) Direction, Affecting Mainly the Long Walls, E=1800, EQX-X Direction

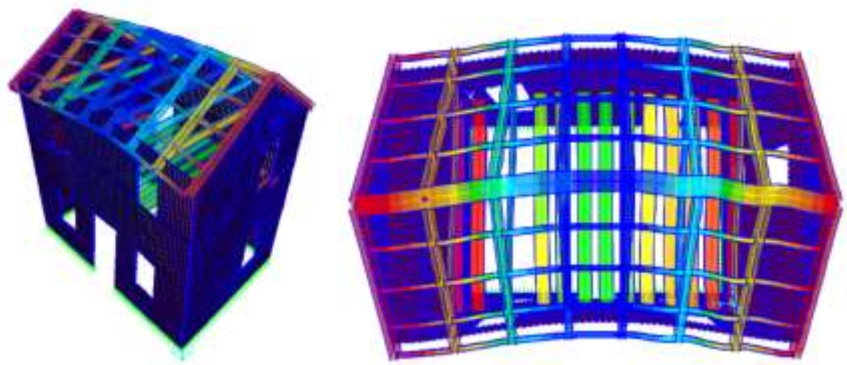

Figure 4.17. 3D Shell Model of Unreinforced Masonry Building Earthquake is Acting in X Direction

Table 4.22. Categories of Out of Plane Motion at the Top of Unreinforced Masonry Building

Category	Point Objects (Pt Obj) / Point Elements (Pt Elm)	Description	Value	Out of Plane Motion
Top, Right Corner of Front Wall Façade	15346	U1	0.6995	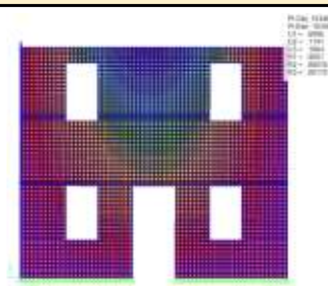
		U2	0.1141	
		U3	0.1864	
		R1	0.0001	
		R2	0.00016	
		R3	0.00172	
Top Center of Front Wall Façade	16403	U1	5.7754	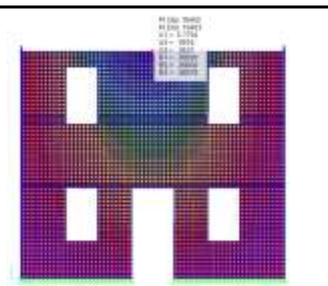
		U2	0.0916	
		U3	0.0537	
		R1	0.00029	
		R2	0.00202	
		R3	0.00078	
Top, Left Corner of Front Wall Façade	14607	U1	1.0273	
		U2	0.1446	
		U3	0.197	
		R1	5E-05	
		R2	0.00027	

Category	Point Objects (Pt Obj) / Point Elements (Pt Elm)	Description	Value	Out of Plane Motion
		R3	0.003	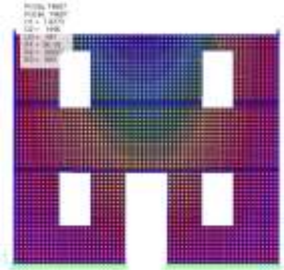

Table 4.23. Categories of Out of Plane Motion at the Middle of Unreinforced Masonry Building

Category	Point Objects (Pt Obj) / Point Elements (Pt Elm)	Description	Value	Out of Plane Motion
Middle of Front Wall Façade Right Corner	15271	U1	0.437	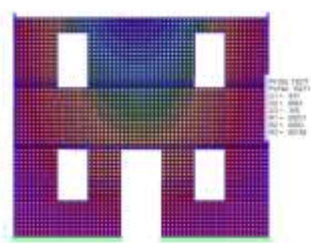
		U2	0.0661	
		U3	0.155	
		R1	0.00011	
		R2	0.0003	
		R3	0.00182	
Middle of Front Wall Façade Center	16214	U1	3.7643	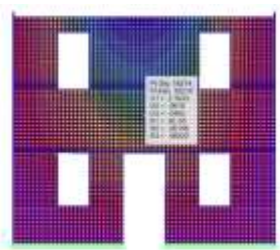
		U2	0.0676	
		U3	0.0465	
		R1	3E-05	
		R2	0.00196	
		R3	0.00022	
Middle of Front Wall Façade Left Corner	14780	U1	0.6426	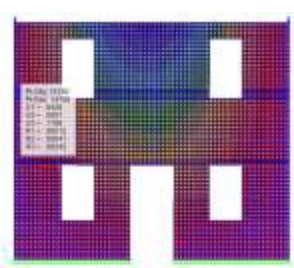
		U2	0.0897	
		U3	0.1788	
		R1	0.00012	
		R2	0.00041	
		R3	0.00242	

Table 4.24. Categories of Out of Plane Motion at the Bottom of Unreinforced Masonry Building

Category	Point Objects (Pt Obj) / Point Elements (Pt Elm)	Description	Value	Out of Plane Motion
Bottom Right	15122	U1	0.0146	
		U2	0.0009	

Category	Point Objects (Pt Obj) / Point Elements (Pt Elm)	Description	Value	Out of Plane Motion
Corner of Front Wall Façade		U3	0.0092	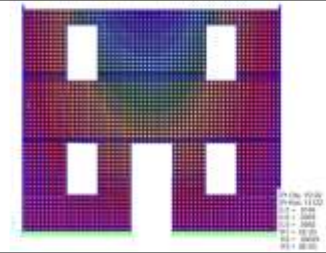
		R1	5E-05	
		R2	0.00029	
		R3	8E-05	
Bottom Center of Front Wall Façade	15663	U1	0.148	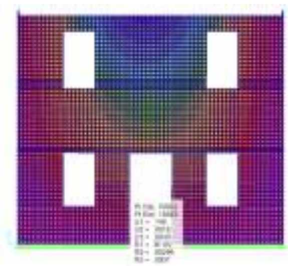
		U2	0.0018	
		U3	0.0039	
		R1	3E-05	
		R2	0.00296	
		R3	0.0001	
Bottom Left Corner of Front Wall Façade	15006	U1	0.0181	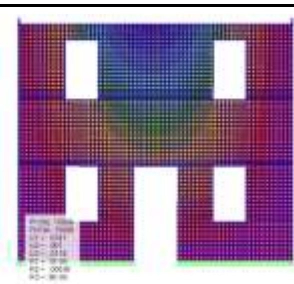
		U2	0.001	
		U3	0.0118	
		R1	7E-05	
		R2	0.00036	
		R3	9E-05	

4.7.5.2 Shell Model Half Scale Horizontal Drift (Front Wall)

Table 4.25. Shell Model Half Scale Horizontal Drift (Front Wall), E=1800, EQX-X Direction

Horizontal Drift	Value
The Out of Plane Drift Ratio, in the Horizontal Direction	$\frac{5.7754 - 0.6995}{1500\ mm} = 0.003383 = 0.34\%$
The Drift Ratio of the Upper Floor	$\frac{5.7754 - 3.7643}{1120\ mm} = 0.001795 = 0.18\%$
The Drift Ratio of the First Floor	$\frac{3.7643}{1360\ mm} = 0.002767 = 0.28\%$

4.7.6 Shell Model Half Scale Horizontal Drift (Front Wall)

4.7.6.1 The Earthquake is Acting Parallel to the Short (i.e., X) Direction, Affecting Mainly the Long Walls, E=1800, COMB-Dead&X-NL

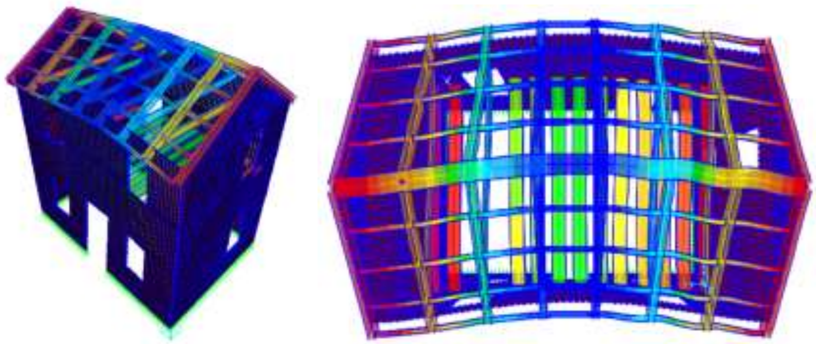

Figure 4.18. 3D Shell Model of Unreinforced Masonry Building Earthquake is Acting in X Direction, COMB-Dead&X-NL

Table 4.26. Categories of Out of Plane Motion at the Top of Unreinforced Masonry Building

Category	Point Objects (Pt Obj) / Point Elements (Pt Elm)	Description	Value	Out of Plane Motion
Top, Right Corner of Front Wall Façade	15346	U1	0.713	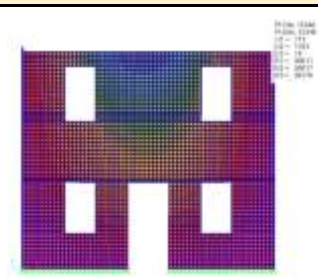
		U2	0.1163	
		U3	0.19	
		R1	0.00011	
		R2	0.00017	
		R3	0.00176	
Top Center of Front Wall Façade	16403	U1	5.8872	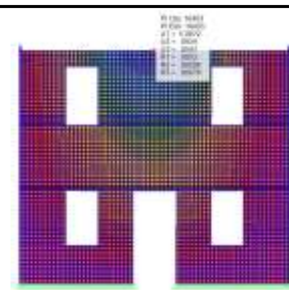
		U2	0.0934	
		U3	0.0547	
		R1	0.0003	
		R2	0.00206	
		R3	0.00079	
Top, Left Corner of Front Wall Façade	14607	U1	1.0472	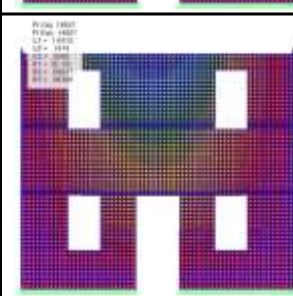
		U2	0.1474	
		U3	0.2008	
		R1	5E-05	
		R2	0.00027	
		R3	0.00306	

Table 4.27. Categories of Out of Plane Motion at the Middle of Unreinforced Masonry Building

Category	Point Objects (Pt Obj) / Point Elements (Pt Elm)	Description	Value	Out of Plane Motion
Middle of Front Wall Façade Right Corner	15271	U1	0.4455	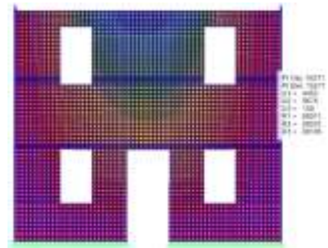
		U2	0.0674	
		U3	0.158	
		R1	0.00011	
		R2	0.00031	
		R3	0.00158	
Middle of Front Wall Façade Center	16214	U1	3.8372	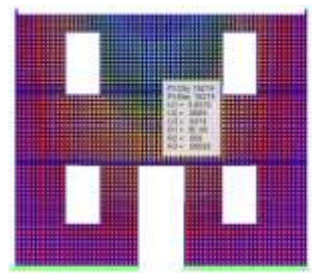
		U2	0.0689	
		U3	0.0474	
		R1	3E-05	
		R2	0.002	
		R3	0.00022	
Middle of Front Wall Façade Left Corner	14780	U1	0.655	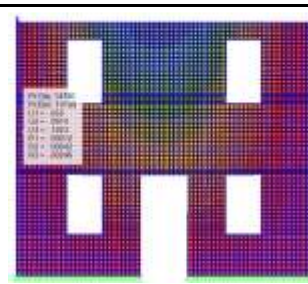
		U2	0.0914	
		U3	0.1823	
		R1	0.00012	
		R2	0.00042	
		R3	0.00246	

Table 4.28. Categories of Out of Plane Motion at the Bottom of Unreinforced Masonry Building

Category	Point Objects (Pt Obj) / Point Elements (Pt Elm)	Description	Value	Out of Plane Motion
Bottom Right Corner of Front Wall Façade	15122	U1	0.0149	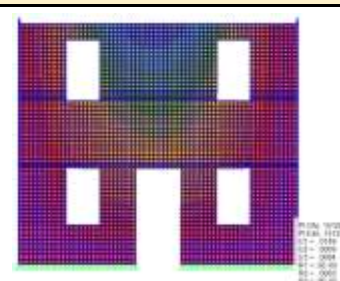
		U2	0.0009	
		U3	0.0094	
		R1	5E-05	
		R2	0.0003	
		R3	9E-05	
Bottom Center of Front Wall Façade	15663	U1	0.1509	
		U2	0.0018	
		U3	0.004	
		R1	3E-05	
		R2	0.00302	

Category	Point Objects (Pt Obj) / Point Elements (Pt Elm)	Description	Value	Out of Plane Motion
		R3	0.00011	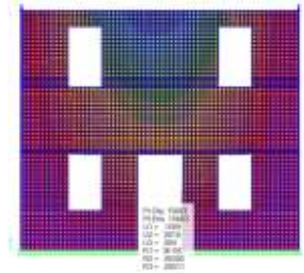
Bottom Left Corner of Front Wall Façade	15006	U1	0.0184	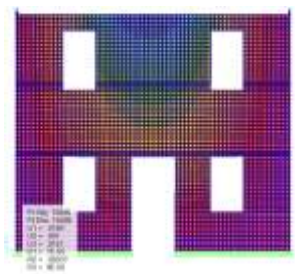
		U2	0.001	
		U3	0.0121	
		R1	7E-05	
		R2	0.00037	
		R3	9E-05	

4.7.6.2 Shell Model Half Scale Horizontal Drift (Front Wall)

Table 4.29. Shell Model Half Scale Horizontal Drift (Front Wall), E=1800, COMB-Dead&X-NL

Horizontal Drift	Value
The Out of Plane Drift Ratio, in the Horizontal Direction	$\frac{5.8872-0.713}{1500\ mm} = 0.0034494 = 0.34\%$
The Drift Ratio of the Upper Floor	$\frac{5.8872-3.8372}{1120\ mm} = 0.0018303 = 0.18\%$
The Drift Ratio of the First Floor	$\frac{3.8372}{1360\ mm} = 0.0028214 = 0.28\%$

4.7.7 Shell Model Half Scale Horizontal Drift (Side Wall)

4.7.7.1 The Earthquake is Acting Parallel to the Long (i.e., Y) Direction, Affecting Mainly the Short Walls, E=1800, EQX-Y Direction

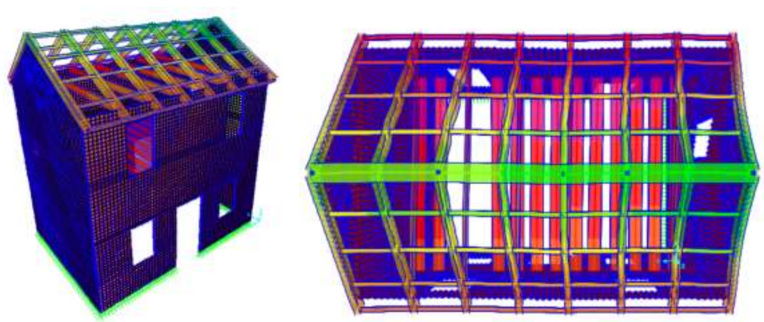

Figure 4.19. 3D Shell Model of Unreinforced Masonry Building Earthquake is Acting in Y Direction

Table 4.30. Categories of Out of Plane Motion at the Top of Unreinforced Masonry Short Wall

Category	Point Objects (Pt Obj) / Point Elements (Pt Elm)	Description	Value	Out of Plane Motion
Right Corner of the Gable of Side Wall Façade	20661	U1	0.1212	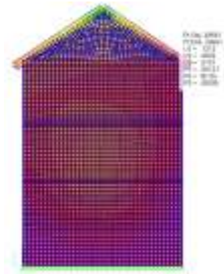
		U2	0.6822	
		U3	0.0737	
		R1	0.00121	
		R2	3E-05	
		R3	0.00035	
Tip of the Gable of Side Wall Façade	37	U1	0.1538	
		U2	1.9557	
		U3	0.1014	
		R1	0.00164	
		R2	5E-05	
		R3	0.00026	
Left Corner of the Gable of Side Wall Façade	20529	U1	0.1213	
		U2	1.1072	
		U3	0.1409	
		R1	0.0013	
		R2	8E-05	
		R3	0.00016	

Table 4.31. Categories of Out of Plane Motion at the Middle of Unreinforced Masonry Short Wall

Category	Point Objects (Pt Obj) / Point Elements (Pt Elm)	Description	Value	Out of Plane Motion
Middle Right Corner of Side Wall Façade	22150	U1	0.059	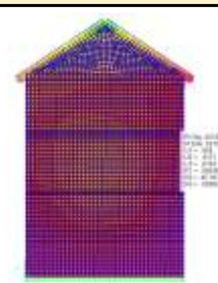
		U2	0.4137	
		U3	0.0744	
		R1	0.00036	
		R2	4E-05	
		R3	0.00082	
Middle Center of Side Wall Façade	21945	U1	0.0623	
		U2	1.2084	
		U3	0.0701	
		R1	0.00029	
		R2	5E-05	

Category	Point Objects (Pt Obj) / Point Elements (Pt Elm)	Description	Value	Out of Plane Motion
		R3	0.00023	
Middle Left Corner of Side Wall Façade	21754	U1	0.777	
		U2	0.6887	
		U3	0.1201	
		R1	0.00027	
		R2	4E-05	
		R3	0.00084	

Table 4.32. Categories of Out of Plane Motion at the Bottom of Unreinforced Masonry Short Wall

Category	Point Objects (Pt Obj) / Point Elements (Pt Elm)	Description	Value	Out of Plane Motion
Bottom Right Corner of Side Wall Façade	21265	U1	0.0012	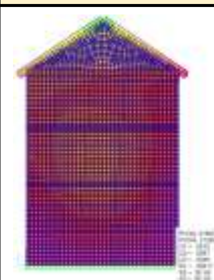
		U2	0.0087	
		U3	0.0046	
		R1	0.00017	
		R2	2E-05	
		R3	6E-05	
Bottom Center of Side Wall Façade	21135	U1	0.001	
		U2	0.059	
		U3	0.003	
		R1	0.00118	
		R2	1E-05	
		R3	7.9E-06	
Bottom Left Corner of Side Wall Façade	21018	U1	0.0011	
		U2	0.0141	
		U3	0.0113	
		R1	0.00029	
		R2	6E-05	
		R3	7E-05	

4.7.7.2 Shell Model Half Scale Horizontal Drift (Side Wall)

Table 4.33. Shell Model Half Scale Horizontal Drift (Side Wall), E=1800, EQX-Y Direction, According to NBCC

Horizontal Drift	Value
The Out of Plane Drift Ratio, in the Horizontal Direction	$\frac{1.9557 - 0.6822}{960\ mm} = 0.001326 = 0.13\%$
The Drift Ratio of the Upper Floor	$\frac{1.9557 - 1.2084}{1760\ mm} = 0.00042460 = 0.05\%$
The Drift Ratio of the First Floor	$\frac{1.2084}{1360\ mm} = 0.00088852 = 0.08\%$

4.7.7.3 The Earthquake is Acting Parallel to the Long (i.e., Y) Direction, Affecting Mainly the Short Walls, E=1800, COMB-Dead&Y-NL

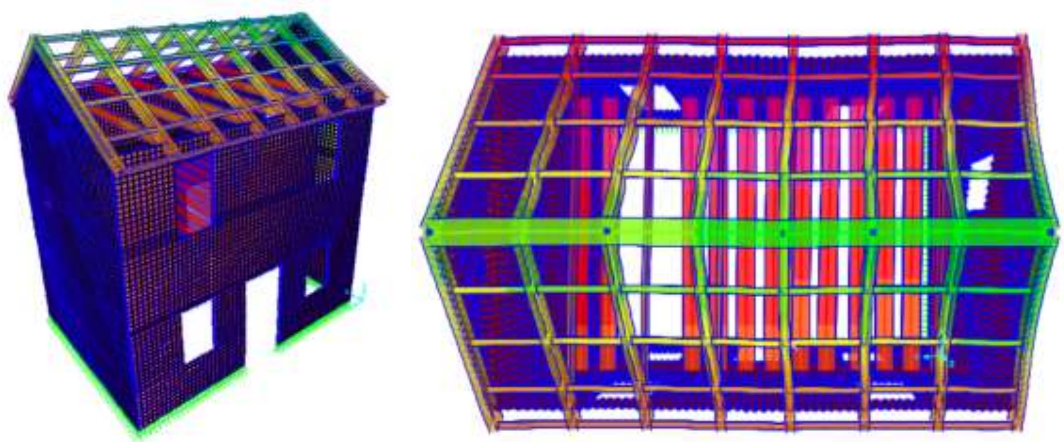

Figure 4.20. 3D Shell Model of Unreinforced Masonry Building Earthquake is Acting in Y Direction

Table 4.34. Categories of Out of Plane Motion at the Top of Unreinforced Masonry Short Wall

Category	Point Objects (Pt Obj) / Point Elements (Pt Elm)	Description	Value	Out of Plane Motion
Right Corner of the Gable of Side Wall Façade	20661	U1	0.1235	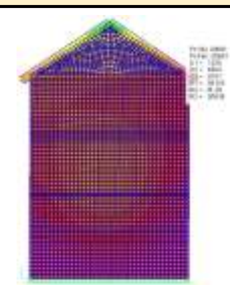
		U2	0.6954	
		U3	0.0751	
		R1	0.00123	
		R2	3E-05	
		R3	0.00036	
Tip of the Gable of	37	U1	0.1568	
		U2	1.9936	

Category	Point Objects (Pt Obj) / Point Elements (Pt Elm)	Description	Value	Out of Plane Motion
Side Wall Façade		U3	0.1033	
		R1	0.00168	
		R2	5E-05	
		R3	0.00026	
Left Corner of the Gable of Side Wall Façade	20529	U1	0.1236	
		U2	1.1286	
		U3	0.1436	
		R1	0.00133	
		R2	8E-05	
		R3	0.00018	

Table 4.35. Categories of Out of Plane Motion at the Middle of Unreinforced Masonry Short Wall

Category	Point Objects (Pt Obj) / Point Elements (Pt Elm)	Description	Value	Out of Plane Motion
Middle Right Corner of Side Wall Façade	22150	U1	0.0601	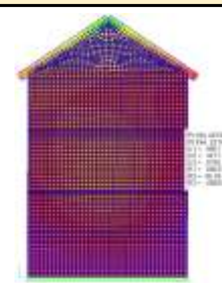
		U2	0.4217	
		U3	0.0758	
		R1	0.00037	
		R2	4E-05	
		R3	0.00083	
Middle Center of Side Wall Façade	21945	U1	0.0635	
		U2	1.2318	
		U3	0.0715	
		R1	0.0003	
		R2	5E-05	
		R3	0.00023	
Middle Left Corner of Side Wall Façade	21754	U1	0.0792	
		U2	0.702	
		U3	0.1224	
		R1	0.00027	
		R2	4E-05	
		R3	0.00086	

Table 4.36. Categories of Out of Plane Motion at the Bottom of Unreinforced Masonry Short Wall

Category	Point Objects (Pt Obj) / Point Elements (Pt Elm)	Description	Value	Out of Plane Motion
Bottom Right Corner of Side Wall Façade	21265	U1	0.0012	
		U2	0.0089	
		U3	0.0047	
		R1	0.00018	
		R2	2E-05	
		R3	6E-05	
Bottom Center of Side Wall Façade	21135	U1	0.001	
		U2	0.0601	
		U3	0.003	
		R1	0.0012	
		R2	1E-05	
		R3	8.048E-06	
Bottom Left Corner of Side Wall Façade	21018	U1	0.0011	
		U2	0.0144	
		U3	0.0115	
		R1	0.00029	
		R2	6E-05	
		R3	7E-05	

4.7.7.4 Shell Model Half Scale Horizontal Drift (Side Wall)

Table 4.37. Shell Model Half Scale Horizontal Drift (Side Wall), E=1800, COMB-Dead&Y-NL, UNIFRS

Horizontal Drift	Value
The Out of Plane Drift Ratio, in the Horizontal Direction	$\frac{1.9936-0.6954}{960\ mm} = 0.0013522 = 0.13\%$
The Drift Ratio of the Upper Floor	$\frac{1.9936-1.2318}{1760\ mm} = 0.0004328 = 0.04\%$
The Drift Ratio of the First Floor	$\frac{1.2318}{1360\ mm} = 0.000905735 = 0.09\%$

4.8 Seismic Dynamics and Structural Response

The seismic response of a building is significantly influenced by its height. Taller structures typically experience amplified sway or lateral displacement during seismic events, primarily due to the increased flexibility and longer natural periods associated with height. This phenomenon results in the upper floors and roof areas undergoing relatively greater seismic movements compared to the lower levels, such as the base or first floor. Furthermore, the orientation of structural elements relative to the direction of seismic waves plays a critical role in their behavior. Walls that are perpendicular to the earthquake's direction often endure compressive forces, which can lead to differential displacement patterns across the structure. As a result, the mid-sections of buildings, particularly those not directly supported by stiffening elements like shear walls or cores, may exhibit more pronounced displacement compared to the more rigidly constrained corners.

Unreinforced masonry (URM) structures exhibit a dichotomy in their response to seismic forces, characterized by rigidity in their diaphragms and wall elements for in-plane actions, while displaying flexibility in out-of-plane resistance. In-plane, URM walls are notably stiff and prone to cracking or failure without significant deformation due to their inherent shear resistance, a function of the masonry units and mortar in compression. Conversely, these walls demonstrate a degree of flexibility when subjected to out-of-plane seismic forces, attributable to the absence of tensile reinforcement necessary to counteract bending and shear in this direction. This lack of reinforcement leads to a behavior akin to cantilevers under out-of-plane forces, rendering them especially susceptible to such seismic impacts.

In URM structures, diaphragms are often flexible, leading to a less uniform distribution of forces. The out-of-plane behavior of walls in URM structures is significantly affected by diaphragm flexibility. When diaphragms are flexible, walls orthogonal to the earthquake's direction act as cantilevers, bearing the brunt of the out-of-plane forces, which can lead to failure due to their limited tensile and bending capacity. In the absence of stiff diaphragms, inertial forces tend to transfer from the walls orthogonal to the earthquake direction to those that are parallel. This transfer is dependent on the quality of connections between walls. If the connections are weak, the effective transfer of forces is compromised, leading to increased vulnerability of the orthogonal walls to out-of-plane failure. The masonry's brittle nature means that once its tensile strength is exceeded, cracks develop rapidly, leading to a sudden loss of out-of-plane resistance. Guidelines provided by NIST for the stress-strain model of masonry components are crucial in defining the material properties in the computational model. These include the specification of deformations and capacities at various performance limit states, essential for assessing the structure's ability to withstand and respond to seismic demands.

Nonlinear Static Analysis (pushover) can identify the potential failure modes and the capacity of the structure to resist seismic forces before global or local collapse occurs. The Nonlinear Static Procedure (NSP), also known as pushover analysis, is an analytical approach used to estimate the seismic capacity of a building structure. It involves creating a simplified model of the structure with components that exhibit nonlinear behavior, capturing the relationship between forces and deformations. Lateral loads, intended to represent seismic inertia forces and proportional to the structure's mass distribution and fundamental vibration mode, are applied incrementally until a predefined target displacement is exceeded by 50% at a control node, usually located at the center of mass of the roof level. Simultaneously, gravity loads are factored into the seismic load combination. To facilitate analysis, the actual nonlinear resistance curve of the structure is linearized into a bilinear or trilinear curve, ensuring that the area under the curve—representing energy dissipation—remains consistent. This linearized curve captures the initial stiffness, yield point, and post-yield behavior up to the point of peak resistance and subsequent softening, allowing for a tractable yet representative depiction of the structure's anticipated seismic performance. (Pantazopoulou, S.J., 2022. Submitted to NRC)

4.9 Pushover Analysis

Pushover analysis is a nonlinear technique used to evaluate the seismic performance of buildings. It involves applying gradually increasing lateral forces to a structure, simulating earthquake conditions, to identify its weaknesses and potential failure points. This method is critical for designing earthquake-resistant structures, as it helps engineers understand how a building will deform and at what points it may fail under seismic stress. The analysis generates a capacity curve, showing the relationship between applied forces and the building's displacements, offering insights for design improvements or retrofitting.

4.9.1 Pushover Analysis Acting in X Direction

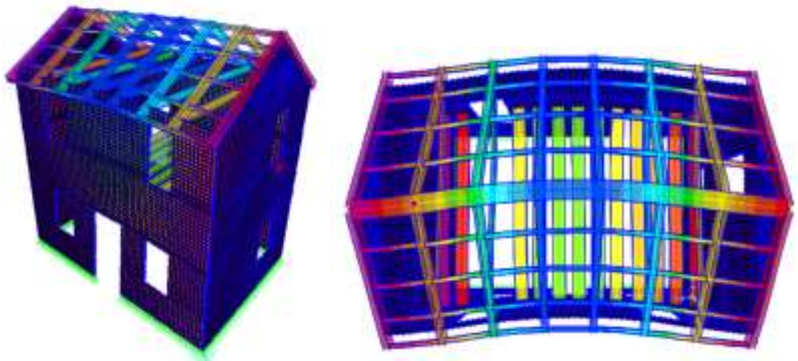

4.21. 3D Shell Model of Unreinforced Masonry Building Pushover is Acting in X Direction

4.9.1.1 Pushover Analysis Acting in X Direction to Front Wall Façade

Table 4.38. Categories of Out of Plane Motion at the Top of Unreinforced Masonry Building

Category	Point Objects (Pt Obj) / Point Elements (Pt Elm)	Description	Value	Out of Plane Motion
Top, Right Corner of Front Wall Façade	15346	U1	7.6308	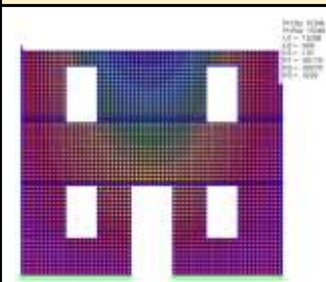
		U2	-0.606	
		U3	1.97	
		R1	-0.00119	
		R2	-0.00079	
		R3	0.222	
Top Center of Front Wall Façade	16403	U1	75.6737	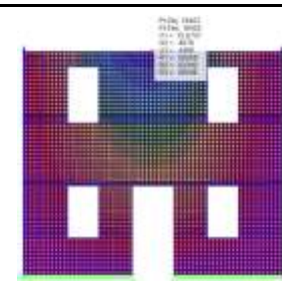
		U2	0.4678	
		U3	0.4498	
		R1	0.00267	
		R2	0.02392	
		R3	0.00598	
Top, Left Corner of Front Wall Façade	14607	U1	12.2389	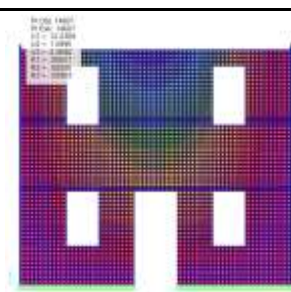
		U2	1.5995	
		U3	2.2688	
		R1	0.00027	
		R2	0.00256	
		R3	-0.03903	

Table 4.39. Categories of Out of Plane Motion at the Middle of Unreinforced Masonry Building

Category	Point Objects (Pt Obj) / Point Elements (Pt Elm)	Description	Value	Out of Plane Motion
Middle of Front Wall Façade Right Corner	15271	U1	4.9448	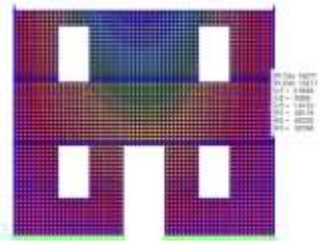
		U2	-0.0886	
		U3	1.6153	
		R1	0.00119	
		R2	0.00335	
		R3	0.02358	
Middle of Front Wall Façade Center	16214	U1	49.235	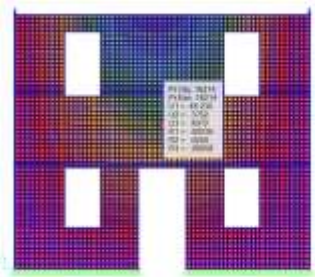
		U2	0.3752	
		U3	0.4072	
		R1	-0.00036	
		R2	0.0258	
		R3	-0.00058	
Middle of Front Wall Façade Left Corner	14780	U1	7.7649	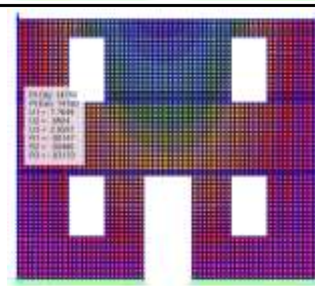
		U2	0.8924	
		U3	2.0597	
		R1	-0.00147	
		R2	0.00486	
		R3	-0.03133	

Table 4.40. Categories of Out of Plane Motion at the Bottom of Unreinforced Masonry Building

Category	Point Objects (Pt Obj) / Point Elements (Pt Elm)	Description	Value	Out of Plane Motion
Bottom Right Corner of Front Wall Façade	15122	U1	0.1684	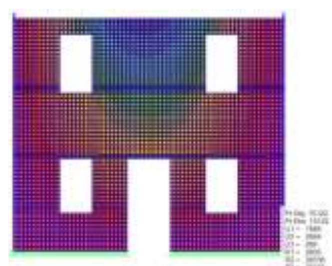
		U2	0.0054	
		U3	0.094	
		R1	0.0005	
		R2	0.00336	
		R3	0.00103	
Bottom Center of Front Wall Façade	15663	U1	1.8704	
		U2	-0.0118	
		U3	0.0249	
		R1	0.00015	
		R2	0.03742	

Category	Point Objects (Pt Obj) / Point Elements (Pt Elm)	Description	Value	Out of Plane Motion
		R3	-0.00131	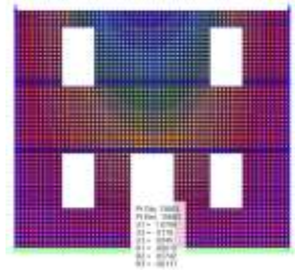
Bottom Left Corner of Front Wall Façade	15006	U1	0.2168	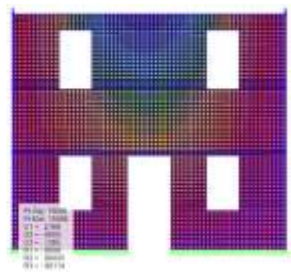
		U2	-0.0005	
		U3	0.1385	
		R1	-0.0008	
		R2	0.00434	
		R3	-0.00114	

4.9.1.2 Shell Model Half Scale Pushover Horizontal Drift (Front Wall)

Table 4.41. Shell Model Half Scale Horizontal Drift (Front Wall), E=1800, Pushover Acting in X Direction

Horizontal Drift	Value
The Out of Plane Drift Ratio, in the Horizontal Direction	$\frac{75.6737-7.6308}{1500\ mm} = 0.0453619 = 4.5\%$
The Drift Ratio of the Upper Floor	$\frac{75.6737-49.235}{1120\ mm} = 0.0236059 = 2.3\%$
The Drift Ratio of the First Floor	$\frac{49.235}{1360\ mm} = 0.036202 = 3.6\%$

4.9.1.3 Pushover Analysis Acting in X Direction to Building Back Wall Façade

Table 4.42. Categories of Out of Plane Motion at the Top of Unreinforced Masonry Building

Category	Point Objects (Pt Obj) / Point Elements (Pt Elm)	Description	Value	Out of Plane Motion
Top, Right Corner of Back Wall Façade	16646	U1	7.6675	
		U2	0.2357	
		U3	-1.929	
		R1	0.00062	
		R2	-0.00126	

Category	Point Objects (Pt Obj) / Point Elements (Pt Elm)	Description	Value	Out of Plane Motion
		R3	0.2303	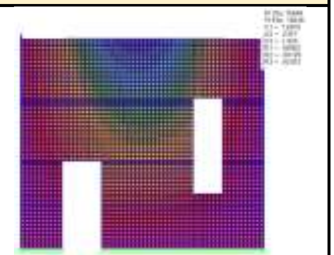
Top Center of Back Wall Façade	17596	U1	75.8736	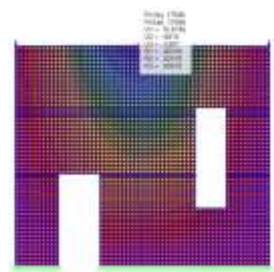
		U2	-0.6815	
		U3	-0.5307	
		R1	0.00378	
		R2	0.02576	
		R3	0.00072	
Top, Left Corner of Back Wall Façade	16851	U1	12.6437	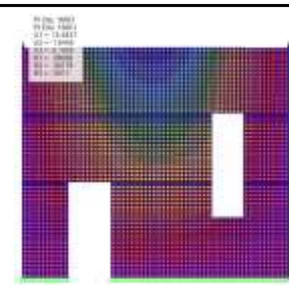
		U2	-1.6445	
		U3	-2.1425	
		R1	0.00056	
		R2	0.00179	
		R3	-0.0411	

Table 4.43. Categories of Out of Plane Motion at the Middle of Unreinforced Masonry Building

Category	Point Objects (Pt Obj) / Point Elements (Pt Elm)	Description	Value	Out of Plane Motion
Middle of Back Wall Façade Right Corner	18395	U1	4.7365	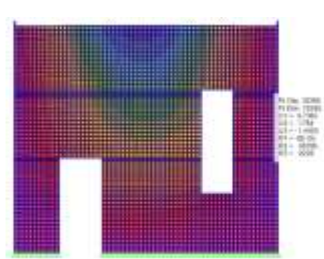
		U2	0.1764	
		U3	-1.4403	
		R1	-8E-05	
		R2	0.00395	
		R3	0.0226	
Middle of Back Wall Façade Center	18165	U1	47.828	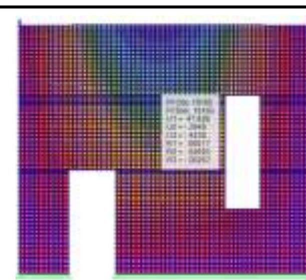
		U2	-0.3948	
		U3	-0.4228	
		R1	0.00017	
		R2	0.2693	
		R3	-0.00257	

Category	Point Objects (Pt Obj) / Point Elements (Pt Elm)	Description	Value	Out of Plane Motion
Middle of Back Wall Façade Left Corner	17024	U1	7.7522	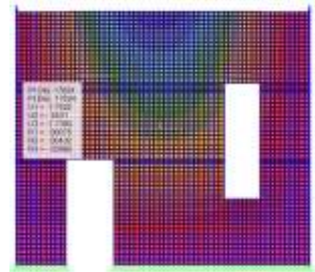
		U2	-0.5531	
		U3	-1.7305	
		R1	0.00075	
		R2	0.00432	
		R3	-0.03065	

Table 4.44. Categories of Out of Plane Motion at the Bottom of Unreinforced Masonry Building

Category	Point Objects (Pt Obj) / Point Elements (Pt Elm)	Description	Value	Out of Plane Motion
Bottom Right Corner of Back Wall Façade	18870	U1	0.1717	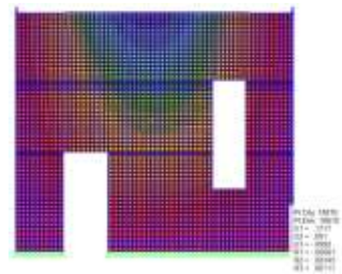
		U2	0.001	
		U3	-0.0992	
		R1	-0.00061	
		R2	0.00343	
		R3	0.00111	
Bottom Center of Back Wall Façade	18590	U1	1.9392	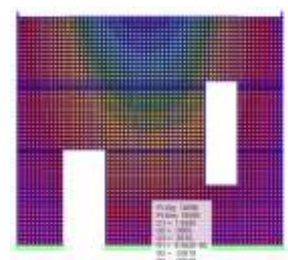
		U2	0.0005	
		U3	-0.0115	
		R1	6.952E-06	
		R2	0.03878	
		R3	0.00039	
Bottom Left Corner of Back Wall Façade	18468	U1	0.1579	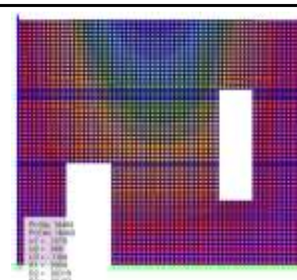
		U2	0.008	
		U3	-0.1164	
		R1	0.0004	
		R2	0.00319	
		R3	-0.00103	

4.9.1.4 Shell Model Half Scale Horizontal Drift (Front Wall)

Table 4.45. Shell Model Half Scale Horizontal Drift (Back Wall), E=1800, Pushover Acting in X Direction

Horizontal Drift	Value
The Out of Plane Drift Ratio, in the Horizontal Direction	$\frac{75.8736-7.6675}{1500\ mm} = 0.0454707 = 4.5\%$
The Drift Ratio of the Upper Floor	$\frac{75.8736-47.828}{1120\ mm} = 0.0250407 = 2.5\%$
The Drift Ratio of the First Floor	$\frac{47.828}{1360\ mm} = 0.035167 = 3.5\%$

4.9.2 Pushover Analysis Acting in Y Direction

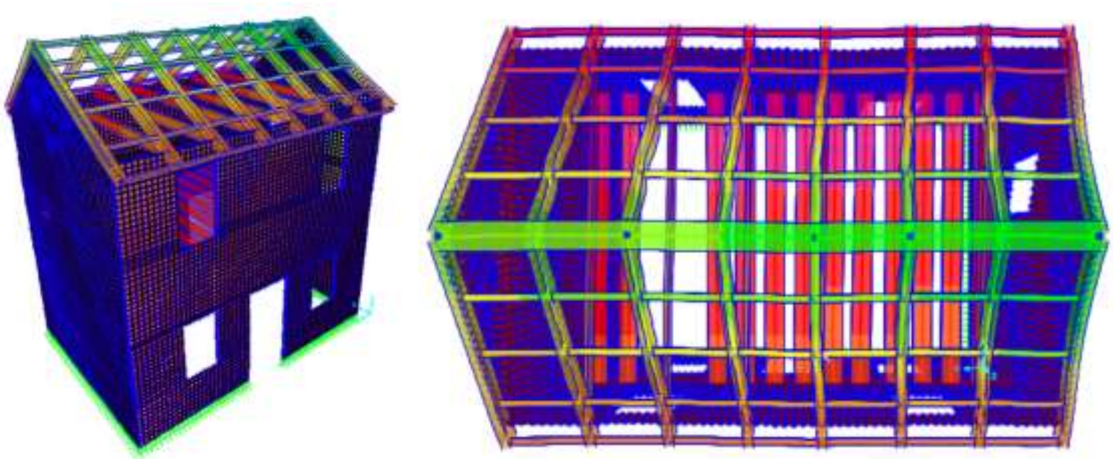

Figure 4.22. 3D Shell Model of Unreinforced Masonry Building Pushover is Acting in Y Direction

4.9.2.1 Pushover Analysis Acting in Y Direction to Short Wall Without Opening

Table 4.46. Categories of Out of Plane Motion at the Top of Unreinforced Masonry Short Wall

Category	Point Objects (Pt Obj) / Point Elements (Pt Elm)	Description	Value	Out of Plane Motion
Right Corner of the Gable of Side Wall Façade	20661	U1	-10.1511	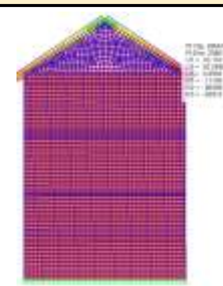
		U2	52.5488	
		U3	-4.8962	
		R1	-0.11104	
		R2	-0.00086	
		R3	-0.02914	
	37	U1	-12.9281	

Category	Point Objects (Pt Obj) / Point Elements (Pt Elm)	Description	Value	Out of Plane Motion
Tip of the Gable of Side Wall Façade		U2	177.6271	
		U3	-8.4308	
		R1	-0.15177	
		R2	-0.00405	
		R3	-0.0217	
Left Corner of the Gable of Side Wall Façade	20529	U1	-10.1817	
		U2	91.8936	
		U3	-12.3551	
		R1	-0.11941	
		R2	-0.00714	
		R3	-0.0135	

Table 4.47. Categories of Out of Plane Motion at the Middle of Unreinforced Masonry Short Wall

Category	Point Objects (Pt Obj) / Point Elements (Pt Elm)	Description	Value	Out of Plane Motion
Middle Right Corner of Side Wall Façade	22150	U1	-4.0357	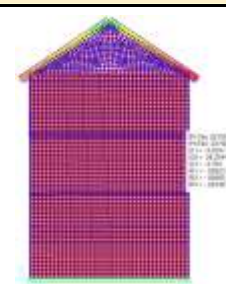
		U2	28.2544	
		U3	-4.704	
		R1	-0.02623	
		R2	-0.00065	
		R3	-0.02348	
Middle Center of Side Wall Façade	21945	U1	-5.1608	
		U2	55.0635	
		U3	-5.7707	
		R1	0.0003	
		R2	-0.00384	
		R3	-0.019	
Middle Left Corner of Side Wall Façade	21754	U1	-6.6303	
		U2	54.4434	
		U3	-10.2968	
		R1	-0.02112	
		R2	-0.00265	
		R3	0.00854	

Table 4.48. Categories of Out of Plane Motion at the Bottom of Unreinforced Masonry Short Wall

Category	Point Objects (Pt Obj) / Point Elements (Pt Elm)	Description	Value	Out of Plane Motion
Bottom Right Corner of Side Wall Façade	21265	U1	-0.0849	
		U2	0.5854	
		U3	-0.2767	
		R1	-0.01176	
		R2	0.00085	
		R3	-0.00249	
Bottom Center of Side Wall Façade	21135	U1	-0.0669	
		U2	2.7342	
		U3	-0.2439	
		R1	-0.05468	
		R2	-0.00087	
		R3	-0.0003	
Bottom Left Corner of Side Wall Façade	21018	U1	-0.0565	
		U2	1.0422	
		U3	-0.9408	
		R1	-0.02119	
		R2	-0.00518	
		R3	0.00277	

4.9.2.2 Shell Model Half Scale Pushover Horizontal Drift (Side Wall)

Table 4.49. Shell Model Half Scale Horizontal Drift (Side Wall), E=1800, Pushover Acting in Y Direction

Horizontal Drift	Value
The Out of Plane Drift Ratio, in the Horizontal Direction	$\frac{177.6271-52.5488}{960\ mm} = 0.1302898 = 13\%$
The Drift Ratio of the Upper Floor	$\frac{177.6271-55.0635}{1760\ mm} = 0.0696384 = 7\%$
The Drift Ratio of the First Floor	$\frac{55.0635}{1360\ mm} = 0.04048786 = 4\%$

4.9.2.3 Pushover Analysis Acting in Y Direction to Short Wall With Opening

Table 4.50. Categories of Out of Plane Motion at the Top of Unreinforced Masonry Short Wall

Category	Point Objects (Pt Obj) / Point Elements (Pt Elm)	Description	Value	Out of Plane Motion
Right Corner of the Gable of Side Wall Façade	18995	U1	8.4353	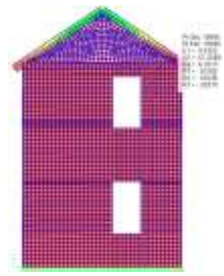
		U2	51.2589	
		U3	6.1613	
		R1	0.1292	
		R2	0.01036	
		R3	-0.22272	
Tip of the Gable of Side Wall Façade	31	U1	11.5412	
		U2	271.9575	
		U3	9.1055	
		R1	0.09794	
		R2	0.00078	
		R3	0	
Left Corner of the Gable of Side Wall Façade	19459	U1	13.4079	
		U2	92.3358	
		U3	10.9607	
		R1	-0.00516	
		R2	-0.00064	
		R3	0.19092	

Table 4.51. Categories of Out of Plane Motion at the Middle of Unreinforced Masonry Short Wall

Category	Point Objects (Pt Obj) / Point Elements (Pt Elm)	Description	Value	Out of Plane Motion
Middle Right Corner of Side Wall Façade	19216	U1	2.2346	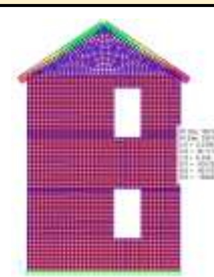
		U2	40.1112	
		U3	6.256	
		R1	-0.01678	
		R2	0.00175	
		R3	-0.16086	
Middle Center of Side Wall Façade	19995	U1	6.0211	
		U2	212.6084	
		U3	5.2983	

Category	Point Objects (Pt Obj) / Point Elements (Pt Elm)	Description	Value	Out of Plane Motion
		R1	-0.1338	
		R2	0.00218	
		R3	-0.00213	
Middle Left Corner of Side Wall Façade	19804	U1	10.3359	
		U2	61.8542	
		U3	11.0831	
		R1	-0.03034	
		R2	0.00516	
		R3	0.12601	

Table 4.52. Categories of Out of Plane Motion at the Bottom of Unreinforced Masonry Short Wall

Category	Point Objects (Pt Obj) / Point Elements (Pt Elm)	Description	Value	Out of Plane Motion
Bottom Right Corner of Side Wall Façade	19279	U1	0.0998	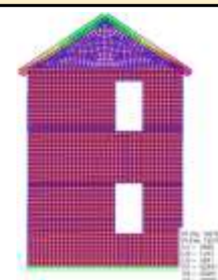
		U2	1.233	
		U3	0.5891	
		R1	-0.02497	
		R2	-0.00261	
		R3	-0.00785	
Bottom Center of Side Wall Façade	20138	U1	0.0298	
		U2	7.1048	
		U3	0.1081	
		R1	-0.14226	
		R2	0.00028	
		R3	0.00034	
Bottom Left Corner of Side Wall Façade	20019	U1	0.0801	
		U2	1.3291	
		U3	1.0008	
		R1	-0.02693	
		R2	0.00571	
		R3	0.00698	

4.9.2.4 Shell Model Half Scale c (Side Wall)

Table 4.53. Shell Model Half Scale Horizontal Drift (Side Wall), E=1800, Pushover Acting in Y Direction

Horizontal Drift	Value
The Out of Plane Drift Ratio, in the Horizontal Direction	$\frac{271.9575-51.2589}{960\ mm} = 0.229894375$ = 23%
The Drift Ratio of the Upper Floor	$\frac{271.9575-212.6084}{1760\ mm} = 0.033721$ = 3.4%
The Drift Ratio of the First Floor	$\frac{212.6084}{1360\ mm} = 0.1563297$ = 15.6%

The difference in horizontal drift values between the front and back walls in long walls is minor, as both have openings. However, the difference in horizontal drift values between the side walls at the short walls is major because one of the walls does not have an opening and is a solid wall.

4.10 Conclusion

The notional yielding or wall cracking drift limits for walls according to KADET (2018), that for out of plane Shear Yielding: γ_y=0.20% and, Failure: γ_u=0.40% (for secondary elements, γ_u =0.60%). The values for drift Capacity of Unreinforced Masonry walls according with ASCE/SEI - 41 (2017) Chapter 11, and accordingly with the EC8-III (2005) are in the same order as the values mentioned above. The immediate occupancy is 0.1% and for the modelling, the sliding failure occurs at 0.4%. Also (Vanin *et al.*, 2017) says in the Drift at Cracking of the wall $\delta_{cr} = 0.20\%$, and depending on the wall type the drift at shear failure ranges from 0.60 to 1.50% and for flexural failure ranges between 0.90 and 2.25%. So, the numbers obtained in the present study are close to failure and anything that is above 0.2% means that the wall has yielded. The excessive values obtained from the Pushover analysis underlines the topling tendency of the gables in the short walls.

5 Chapter 5: Strengthening Methods to Improve the Seismic Performance of the Building

5.1 Introduction

In Canada, around 5,000 earthquakes are documented annually, predominantly minor tremors. The highest seismic risk is at the British Columbia region due to its proximity to the so-called Pacific Ring of Fire; significance seismicity also occurs in the St. Lawrence and Ottawa River valleys, and north of the Hudson Bay in the northern territories. Over the past century, at least nine earthquakes with a magnitude surpassing 7 have been recorded in or near Canada. Some of these instances led to extensive destruction. Even a quake measuring 6 on the magnitude scale could cause substantial damage in densely populated areas where older, URM buildings survive as heritage structures from the previous centuries (e.g. Quebec city, Montreal, Toronto). In fact, a powerful earthquake near one of Canada's major urban centers would likely constitute the most devastating natural disaster the country could endure. (Public Safety Canada, Canadian Red Cross, Natural Resources Canada, & St. John Ambulance. (2011). Earthquakes. https://www.getprepared.gc.ca/cnt/rsrcs/pblctns/rthqks-wtd/index-en.aspx). Even what is known as stable Canada in the prairies is facing increased risk on account of the extensive fracking for oil extraction which is known to cause earthquakes of moderate magnitude (<5 R). However, these magnitudes of earthquakes generated by fracking are sufficiently large to cause extensive damage in the extremely vulnerable URM structures or lightly reinforced masonry structures built in the past in those regions on account of the low natural seismicity – such damages have already been reported in the Netherlands (Groningen) where similar fracking activity is taking place.

The objective of the present chapter is to explore the effectiveness of a variety of alternative interventions that may be used to strengthen the building and mitigate its seismic vulnerability. Generalized application of some of these methods may be used in heritage structures – but some are limited by the Unesco Convention regarding reversibility and non-invasiveness referred to in Chapter 2, so this class of strengthening schemes would only to masnry structures that are declassified or are common dwellings.

It was seen in the previous chapters that some of the particular characteristics of URM that increase their seismic vulnerability are:

(a) The mass distribution of the walls, which attracts inertia forces that act normal to the walls in the form of outwards of pressure. The magnitude of the pressure is $p = \gamma_w \cdot t \cdot S_a(T)$ where γ_w is the mass density of the masonry walls (here, in the example considered, this is 1.8 tn/m3), t is the wall thickness, and $S_a(T)$ is the spectral acceleration value (obtained from the design spectrum) for T being the fundamental period. As an example, for the period of the full scale building in the short direction being 0.2 s, and a double-wythe wall of 0.22m thickness, for a spectral acceleration equal to approximately 0.4g (for the Kern County earthquake – referred to as "Taft Earthquake" in the experimental study) – the lateral pressure is $p = 0.22m \times \frac{1.8tn}{m^3} \times 0.4 \times \frac{10m}{s^2} = 1.6\ kN/m^2$, which would cause a flexural moment heightwise in the top storey of the wall equal to 1.6 kN/m^2×1m×2.282m2/2 = 4.15 kN-m per meter of the wall, whereas actoss the breath of the wall the moment is equal to $1.6\frac{kN}{m^2} \times 1m \times \frac{5.4^2}{8} = 5.8\ kNm/m$, where 50% of which may be taken at the supports therefore opening the corners, and the other 50% bending the midspan. It is noted that the flexural strength of the wall based on the tensile strength of masonry (about 0.1MPa) is only $100\frac{kN}{m^2} \times 1m \times \frac{0.22^2}{6} = 0.8\ kN/m$. It is therefore evident that the structure is very vulnerable to out-of-plane failure owing to the very low tensile strength of masonry.

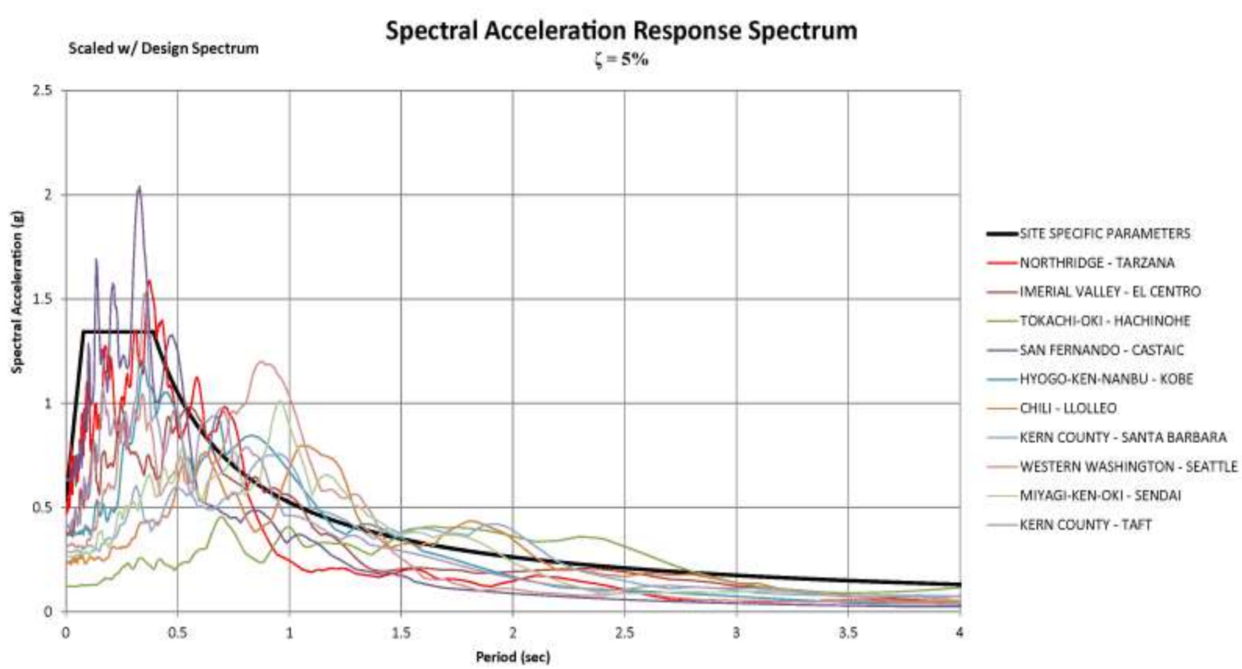

Figure 5.1. Collection of Spectra from Several Strong Gound Motions (from https://www.structuremag.org/wp-content/uploads/C-PracSolutions-Harris-March131.pdf)

(b) The diaphragms of the structure are flexible, and therefore cannot provide restraint against differential movement of the walls in the out of plane direction. Similarly, the gables are unconnected with the roof and therefore are vulnerable to tipping over – a mode of failure that was clearly observed in the tests.

To mitigate these contingencies several alternative options were considered as follows:

I. Stiffening and strengthening the masonry walls using either of:

(a) Deep repointing

(b) Jacketing

(c) Shotcreting

II. Stiffening the horizontal Diaphragms

(a) By addition of a timber ceiling to the underside of roof joists therefore creating box cross sections

(b) By addition of Diagonal Steel Rods

(c) By addition of a concrete slab

In the present study, the success of the strengthening is gauged by the shift in the fundamental period of vibration in X and Y, the reduction in the rotational mass participation of the twisting modes of vibration, and the reduction in the relative magnitude of differential displacement within any floor of the system.

5.2 Strengthening Unreinforced Masonry Structures: A Comprehensive Structural Analysis Using SAP2000

The primary deficiency in URM construction lies in the insufficient connection of diaphragms to walls, that can lead to collapse of parts of the building (FEMA 547). A viable solution involves integrating a network of small ties that firmly link the walls to the floor and roof diaphragms, significantly enhancing the building's strength. These ties must withstand two crucial forces: shear, caused by diaphragms attempting to slide along the walls, and tension, generated by the diaphragm and wall attempting to separate. The absence of these ties leaves the walls unsupported under lateral loads, causing them to act as cantilevers from ground level. Consequently, floors and roofs become highly susceptible to dislodgment from their supports, a prevalent mode of failure in URM buildings during earthquakes. (Robinson and Bowman, 2000)

Moreover, walls receive lateral support not only from floors and roofs but also from cross walls, columns, and buttresses, all of which must be considered. The performance of walls is influenced by their thickness and length; lower-level walls in URM buildings are typically several layers thick and exhibit significant resistance against out-of-plane forces. The shear resistance of these walls can be substantial, especially if they have few or no openings (Robinson & Bowman 2000). Horizontal diaphragms formed by floors or roofs play a crucial role in distributing loads to other load-resisting elements and binding the building components together. However, these diaphragm systems often have insufficient or nonexistent connections that require upgrading to effectively contribute to the building's stability. If the building's resistance remains below the level demanded by the design earthquake, even after reinforcing these connections, further strengthening measures become necessary. (Turnbull et al., 2004)

5.2.1 The Installation Process of Securing the Transverse Flanges of the Timber Ceiling

The first proposed retrofitting method involves installing timber ceilings on the first floor, securely fastened to the joists (timber beams). This approach enhances the cross-sectional rigidity of the structure significantly. In contrast, scenario #2 focuses solely on retrofitting the top beams while leaving the bottom beams untouched. The third retrofitting scheme, denoted as scenario #3, replicates the aforementioned method by applying it to the top horizontal beams of the roof as well as installing timber ceilings on the first floor. By evaluating the impact of each approach, we aim to discern the differences and assess the effectiveness of these retrofitting strategies.

Installing timber ceilings on the first floor, securely attached to joists, enhances the building's rigidity. SAP2000 will be employed to model this intervention, analyzing the cross-sectional stiffness augmentation. Modal analysis will reveal the impact on structural modes, demonstrating how the added rigidity influences the building's dynamic behavior. The primary goal of this method is to enhance the structural stability of unreinforced masonry buildings, which might be vulnerable to seismic activity or other structural stresses. By adding timber ceilings, the overall structural integrity of the building can be significantly improved. The addition of timber ceilings effectively increases the cross-sectional rigidity of the structure. By reinforcing the existing timber framework, the building becomes more resistant to lateral movement and other structural stresses.

The installed timber ceilings help distribute loads more evenly, reducing the strain on the masonry walls and foundation. This load distribution is crucial for preventing localized stress points and potential structural failures. The timber ceilings add stiffness to the overall structure, making it more resistant to deformation and movement. By distributing loads effectively, the building gains stability, reducing the risk of collapse during seismic events or other stress-inducing situations. This method is often employed in historic buildings, allowing for structural reinforcement without altering the building's original appearance significantly.

5.2.1.1 Section Design

Considering the load distribution across the transverse flanges, taking into account factors such as beam spacing, joist spans, and the expected load-bearing capacity of the timber, including the width, depth, and thickness of the flanges.

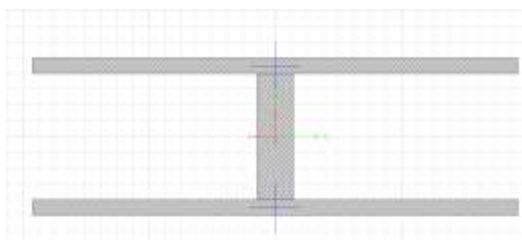

Figure 5.2. Section Design of Joist and Timber Transverse Flanges for the First Floor

Table 5.1. Shape Properties of Joist Section Design

Property	Value
Name	joist section (Middle Rectangle)
Material	Timber
X Center	0
Y Center	0
Height	250
Width	70
Rotation	0

Table 5.2. Shape Properties of Timber Ceiling Top Section Design

Property	Value
Name	top section (Rectangle2)
Material	Timber
X Center	6.104E-05
Y Center	140
Height	30
Width	960
Rotation	0

Table 5.3. Shape Properties of Timber Ceiling Bottom Section Design

Property	Value
Name	bottom section (Rectangle3)
Material	Timber
X Center	-6.104E-05
Y Center	-140
Height	30
Width	960
Rotation	0

5.2.1.2 Modal Period Before and After Adding the Transverse Flanges

In the full-scale Shell Model with a modulus of elasticity (E) of 1800, the period in mode 1 is 0.159017. After adding a timber ceiling on the first floor, securely nailed to the joists (timber beams) to increase cross-sectional rigidity, the period decreased in the modified full-scale Shell Model. In SAP2000, the period of a structure's vibration mode represents the time it takes for the structure to complete one full cycle of oscillation in that mode. The period is a crucial parameter in structural dynamics as it indicates how quickly a structure responds to dynamic loads, such as seismic or wind forces. The decrease in the period after adding the timber ceiling indicates that the structure responds more rapidly to dynamic loads. This change is likely due to the increased stiffness and rigidity introduced by the timber ceiling. The additional mass and enhanced structural integrity provided by the timber ceiling led to a shorter period, meaning that the structure vibrates more quickly in this particular mode. This modification is significant, especially in the context of seismic design or any situation where reducing the period of vibration is desirable. It signifies that the structure has become more responsive and can better withstand dynamic forces, enhancing its overall stability and safety.

- MODAL before adding the transverse flanges:

  Mode: 1

  Period: 0.159017 seconds

  Frequency: 6.288626553 cycles per second

  This represents the initial state of the structure without any modifications to the transverse flanges.

- MODAL After adding the transverse flanges to the floor (scenario #1):

Mode: 1

Period: 0.14314 seconds

Frequency: 6.986157139 cycles per second

In this scenario, transverse flanges were added to the floor, resulting in a decreased period and an increased frequency compared to the initial state. This modification indicates that the structure responds more quickly to dynamic loads in mode 1 after adding these floor flanges.

- MODAL After adding the transverse flanges to the roof (scenario #2):

  Mode: 1

  Period: 0.148508 seconds

  Frequency: 6.733660131 cycles per second

  Here, transverse flanges were added to the roof. While the period is shorter compared to the initial state, it is slightly longer than the scenario with floor flanges. The frequency also decreased, indicating a slightly slower response to dynamic loads in mode 1 compared to scenario #1.

- MODAL After adding the Timber transverse flanges in floor and roof (scenario #3):

  Mode: 1

  Period: 0.138819 seconds

  Frequency: 7.203621958 cycles per second

  In this scenario, timber transverse flanges were added to both the floor and the roof. This modification further reduced the period and increased the frequency, showing that the structure now responds even more rapidly to dynamic loads in mode 1 compared to the other scenarios.

Table 5.4. Modal Periods and Frequencies regarding adding the transverse flanges

Output Case	Step Type	Step Num	Period	Frequency	Circ Freq	Eigenvalue
Text	Text	Unitless	Sec	Cyc/sec	rad/sec	rad2/sec2
MODAL before adding the transverse flanges.	Mode	1	0.159017	6.288626553	39.51260596	1561.24603
MODAL After adding the transverse flanges to the floor. (scenario #1)	Mode	1	0.14314	6.986157139	43.89531989	1926.799108
MODAL After adding the transverse flanges to the roof. (scenario #2)	Mode	1	0.148508	6.733660131	42.3088344	1790.037468
MODAL After adding the Timber transverse flanges in floor and roof. (scenario #3)	Mode	1	0.138819	7.203621958	45.26169165	2048.620731

5.2.1.2.1 Mass Participation (X & Y) Before and After Adding the Transverse Flanges

presented here are the results of comparison between Mass participation (X & Y) of Full-Scale Shell Model with joists and without Timber Ceiling and Full-Scale Shell Model with joists and Timber Ceiling in the Floor.

Table 5.5. Mass participation (X & Y) after adding the transverse flanges

Mass participation (X & Y)	Charts
Mass participation (X & Y), Full-Scale Shell Model with joists and without Timber Ceiling, Period is 0.159	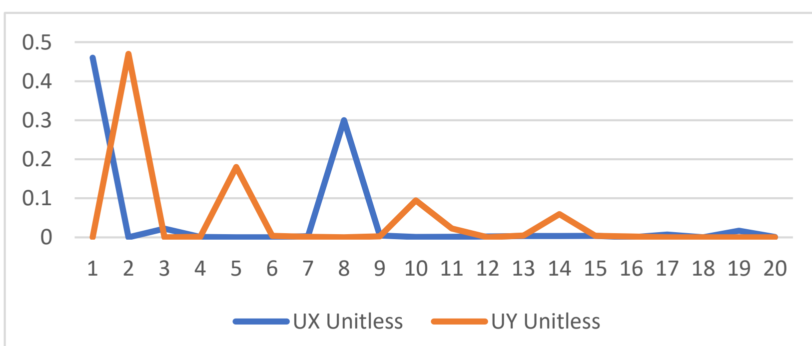

<table>
<tr><th>Mass participation (X & Y)</th><th>Charts</th></tr>
<tr><td>Mass participation (X & Y), Full-Scale Shell Model After adding the transverse flanges to the floor, Period is 0.14314 (scenario #1)</td><td>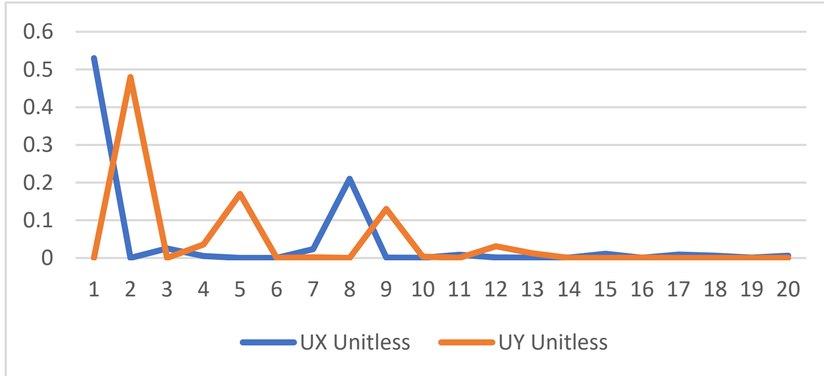
</td></tr>
<tr><td>Mass participation (X & Y), Full-Scale Shell Model After adding the transverse flanges to the roof, Period is 0.148 (scenario #2)</td><td>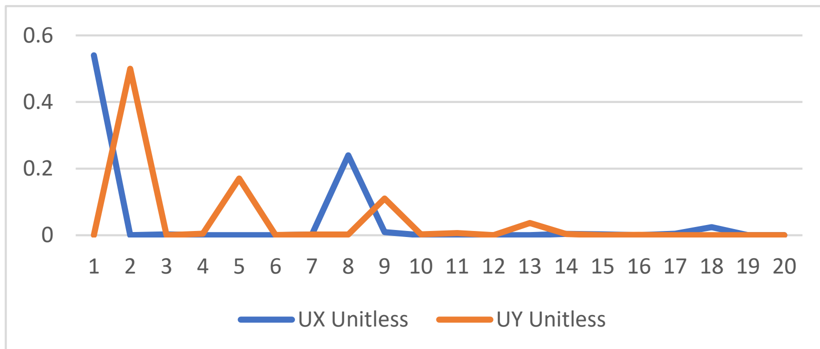
</td></tr>
<tr><td>Mass participation (X & Y), Full-Scale Shell Model after Installing timber cross beams in both the floor and roof structures, Period is 0.138 (scenario #3)</td><td>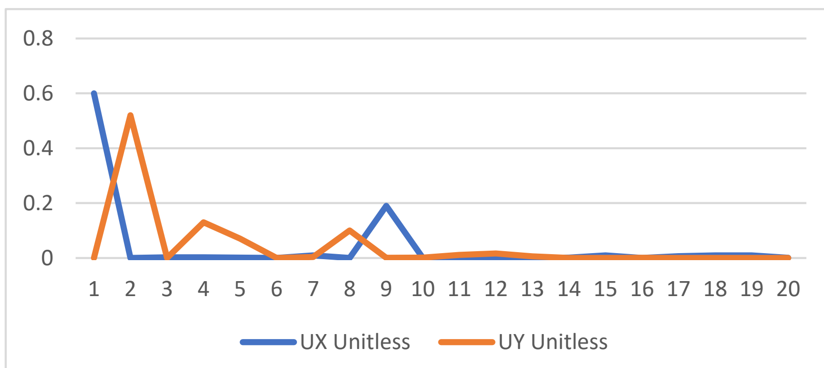
</td></tr>
</table>

In the full-scale Shell Model with a modulus of elasticity (E) of 1800, the highest mass participation occurs in modes 1, 2, and 7. After installing timber cross beams individually to the ceiling of the first floor and then to the roof, securely nailed to the joists (timber beams) to increase cross-sectional rigidity, the mass participation increased, and the higher mass participation modes remained unchanged. However, in the Full-Scale Shell Model, after installing timber cross beams in both the floor and roof structures (scenario #3) in the UZ direction, the higher mass participation changed from 7 to 10. This comparison is made to analyze the effects of the modification.

Table 5.6. Full-Scale Shell Model with Joists and without Timber Ceiling

Mode	Displacement	Highest Mass Participation	Deformed Shape
1	UX	46 %	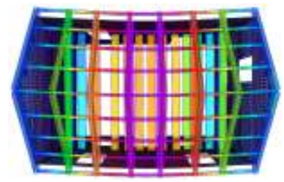
2	UY	47 %	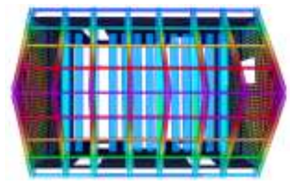
7	RZ	29 %	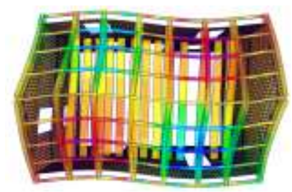

Table 5.7. Full-Scale Shell Model after Installing Timber Cross Beams in the Ceiling of the First Floor. (Scenario #1)

Mode	Displacement	Highest Mass Participation	Deformed Shape
1	UX	53 %	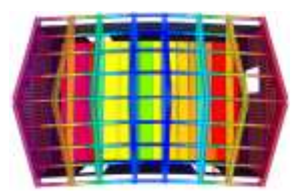
2	UY	48 %	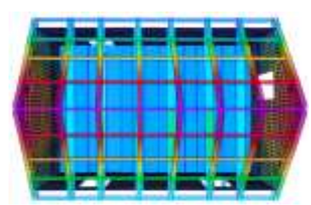
7	RZ	39 %	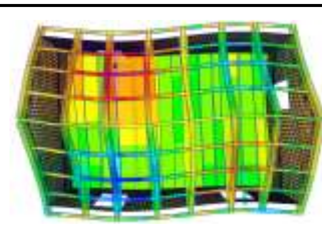

Table 5.8. Full-Scale Shell Model After Installing Timber Cross Beams in the Roof. (Scenario #2)

Mode	Displacement	Highest Mass Participation	Deformed Shape
1	UX	54 %	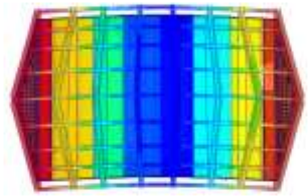
2	UY	50 %	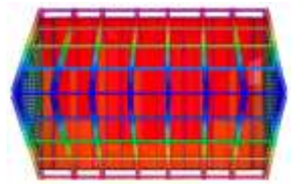
7	RZ	41 %	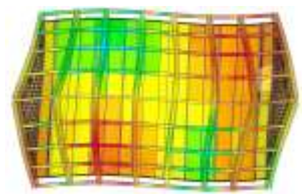

Table 5.9. Full-Scale Shell Model After Installing Timber Cross Beams in the Floor and Roof of the Structure. (Scenario #3)

Mode	**Displacement**	**Highest Mass Participation**	**Deformed Shape**
1	UX	60 %	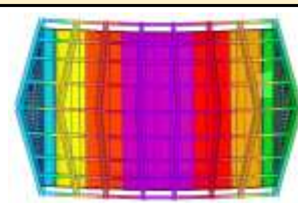
2	UY	52 %	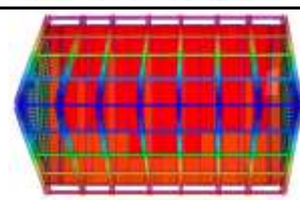
10	RZ	48 %	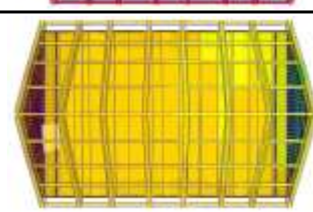

5.2.1.2.2 Properties Before and After Adding the Transverse Flanges

In the Full-Scale Shell Model without a timber ceiling and with a modulus of elasticity (E) of 1800, the moment of inertia is 9×10^7. After adding a timber ceiling, the moment of inertia increased to 1.2×10^9. In SAP2000, the moment of inertia for a structural element is a fundamental property that defines its resistance to bending deformation. It is a measure of how the mass of a section is distributed about a particular axis. The moment of inertia is calculated based on the geometry and material properties of the section.

The model is modified by adding a timber ceiling on the first floor, securely attached to the existing structural elements (possibly joists or beams). The addition of the timber ceiling changes the overall geometry and distribution of mass in the structure. Recalculation of the moment of inertia with the modified geometry and added timber ceiling results in an increased moment of inertia, specifically to 1.2×10^9. The increase in the moment of inertia after adding the timber ceiling indicates that the modified structure has a higher resistance to bending deformations. This is because the additional mass and geometry introduced by the timber ceiling contribute to a more substantial distribution of material away from the bending axis, making the structure more rigid and better able to withstand bending forces.

Table 5.10. Property Data of Full-Scale Shell Model with Joists and without Timber Ceiling

Properties	Measurements
Axial Cross-Section Area	17500
Inertia of Cross-Section, Axis 3	91145833.0
Inertia of Cross-Section, Axis 2	7145833.0
Cross-Product of Inertia, Axis 2-3	0.0
Constant of Torsion	23576195.0
Shear Surface, Axis 2	14583.405
Shear Surface, Axis 3	14583.405
Center of Gravity Displacement, Axis 3	0.0
Center of Gravity Displacement, Axis 2	0.0
Displacement of Shear Center, Axis 3*	Not Computed (N/C)
Displacement of Shear Center, Axis 2*	Not Computed (N/C)
Modulus of Section, Axis 3 Top	729166.7
Modulus of Section, Axis 3 Bottom	729166.7
Modulus of Section, Axis 2 Left	204166.67
Modulus of Section, Axis 2 Right	204166.67
Constant of Warping (Cw)	Not Computed (N/C)
Plastic Section Modulus, Axis 3	1093750.0
Plastic Section Modulus, Axis 2	306250.0
Gyration Radius, Axis 3	72.1688

Properties	Measurements
Gyration Radius, Axis 2	20.2073

Table 5.11. Property Data of Full-Scale Shell Model with Joists and Timber Ceiling

Properties	Measurements
Area, Axial Cross-Section	75100
Moment of Inertia, Axis 3	1.224E+09
Moment of Inertia, Axis 2	4.431E+09
Inertia Product, Axes 2-3	-492.2266
Constant for Torsion	47766975.0
Shear Area, Direction 2	21683.713
Shear Area, Direction 3	54322.84
CG Displacement, Direction 3	0.0
CG Displacement, Direction 2	0.0
Offset of Shear Center, Axis 3*	Not Applicable (N/C)
Offset of Shear Center, Axis 2*	Not Applicable (N/C)
Section Modulus, Axis 3 Top	7899522.0
Section Modulus, Axis 3 Bottom	7899522.0
Section Modulus, Axis 2 Left	9230886.0
Section Modulus, Axis 2 Right	9230886.0
Warping Constant (Cw)	Not Applicable (N/C)
Plastic Modulus, Axis 3	9157750.0
Plastic Modulus, Axis 2	14130250.0
Gyration Radius, Axis 3	127.6869
Gyration Radius, Axis 2	242.8971

5.2.1.2.3 Adding Diagonal Braces to Secure the Transverse Flanges of the Timber Ceiling

In the context of strengthening unreinforced masonry structures, "adding diagonal braces to secure the transverse flanges of the timber ceiling" is a structural reinforcement technique. Unreinforced masonry structures are vulnerable to various forces, such as earthquakes, due to their lack of internal supporting elements like steel or concrete reinforcements. To enhance the stability and structural integrity of such buildings, diagonal braces are used, which are diagonal members installed within the structure. These braces provide lateral support and help distribute loads more evenly, reducing the risk of collapse during seismic events or other dynamic forces. In the specific case mentioned, the diagonal braces are used to secure the transverse flanges of a timber ceiling. Transverse flanges are horizontal beams that run perpendicular to the main structure. By adding diagonal braces to these flanges, the entire timber ceiling structure becomes more resistant to lateral movements and deformations. This reinforcement method prevents the timber ceiling from collapsing or shifting during seismic activity, thereby strengthening the overall stability of the unreinforced masonry structure.

5.2.1.3 The Impact of Securing Transverse Flanges with Diagonal Braces

Securing transverse flanges with diagonal braces is an effective strategy for strengthening unreinforced masonry structures. This retrofitting technique improves the dynamic response of such buildings to seismic forces. The initial modal period of the structure was 0.159 seconds. After the retrofitting process, the period decreased across scenarios: to 0.14314 seconds when transverse flanges were added to the floor (scenario #1), and even further to 0.138819 seconds when both the floor and roof were retrofitted (scenario #3). These changes indicate an enhanced stiffness, as a shorter modal period correlates with a more rapid response to dynamic loads.

Also, the moment of inertia saw a significant increase from 9×10^7 to 1.2×10^9 with the installation of the timber ceiling, highlighting an improved resistance to bending forces. The mass participation rates also shifted, with increases observed after the addition of timber cross beams in the ceiling and roof. For example, in scenario #1, the mass participation increased to 53% for UX displacement, indicating a more substantial and balanced distribution of seismic forces across the structure. The installation of timber ceilings and the addition of diagonal braces to secure the transverse flanges together contribute to a more resilient structural system capable of resisting lateral seismic loads more effectively. This comprehensive retrofitting approach not only provides immediate structural benefits but also contributes to the long-term durability and safety of the building.

5.2.2 MODAL Period Before and After Adding Diagonal Braces

Table 5.12. Modal Periods and Frequencies after Adding Diagonal Braces

Output Case	Step Type	Step Num	Period	Frequency	Circ Freq	Eigenvalue
Text	Text	Unitless	Sec	Cyc/sec	rad/sec	rad2/sec2
MODAL before adding diagonal braces.	Mode	1	0.159017	6.288626553	39.51260596	1561.24603
MODAL After adding diagonal braces to the floor. (scenario #1)	Mode	1	0.153855	6.499615929	40.83829131	1667.766037
MODAL After adding the diagonal braces to the roof. (scenario #2)	Mode	1	0.154666	6.465531089	40.62412994	1650.319934

Output Case	Step Type	Step Num	Period	Frequency	Circ Freq	Eigenvalue
Text	Text	Unitless	Sec	Cyc/sec	rad/sec	rad2/sec2
MODAL After adding diagonal braces to the floor and roof. (scenario #3)	Mode	1	0.152454	6.559334945	41.21351695	1698.55398

5.2.2.1 Mass Participation (X & Y) Before and After Adding Diagonal Braces

Applying diagonal braces to the building enhanced the distribution of mass among various parts, yet the change in mass participation was not significant compared to that of the full-scale shell model without the addition of diagonal braces.

Table 5.13. Mass Participation (X & Y) Before and After Adding Diagonal Braces

Mass participation (X & Y)	Charts
Mass participation (X & Y), Full-Scale Shell Model with joists and without adding diagonal braces, Period is 0.159	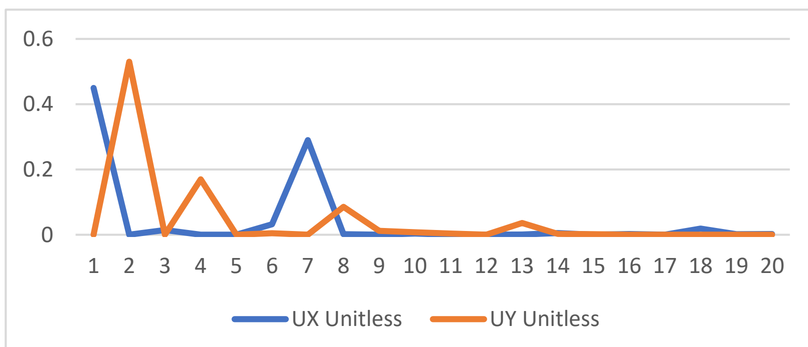
Mass participation (X & Y), Full-Scale Shell Model After adding diagonal braces to the floor, Period is 0.153 (scenario #1)	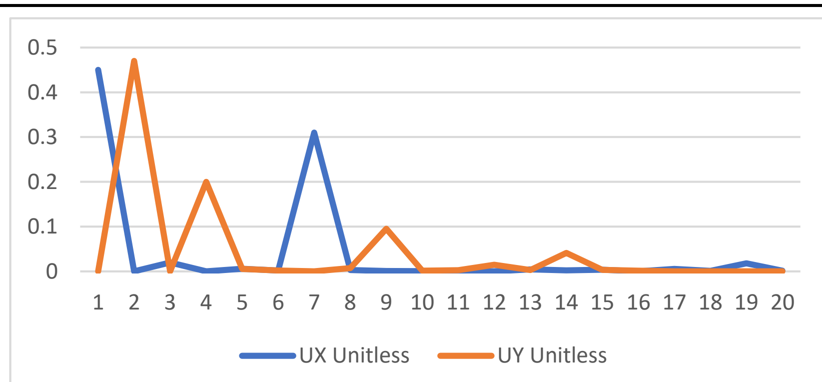

Mass participation (X & Y)	Charts
Mass participation (X & Y), Full-Scale Shell Model After adding diagonal braces to the roof, Period is 0.154 (scenario #2)	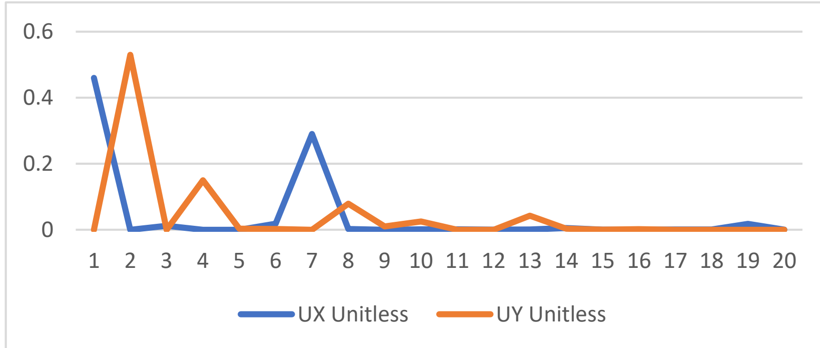
Mass participation (X & Y), Full-Scale Shell Model after adding diagonal braces to the floor and roof, Period is 0.152 (scenario #3)	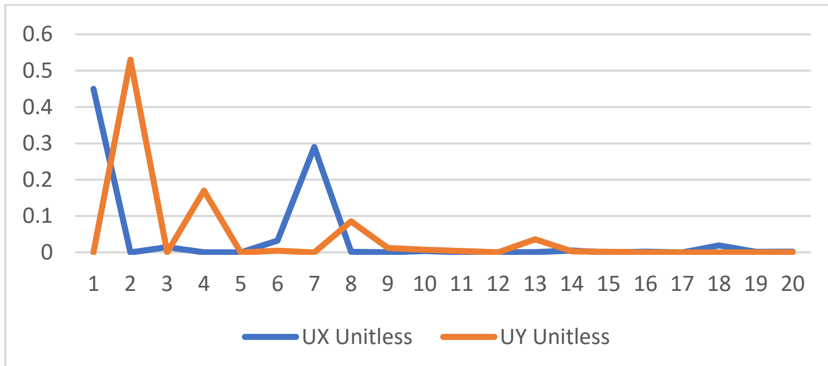

Table 5.14. Full-Scale Shell Model with Joists and without Installing Diagonal Braces

Mode	Displacement	Highest Mass Participation	Deformed Shape
1	UX	46 %	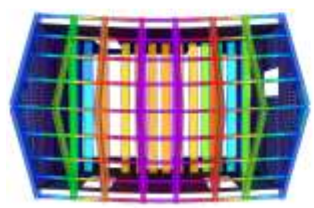
2	UY	47 %	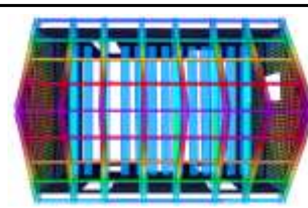
7	RZ	29 %	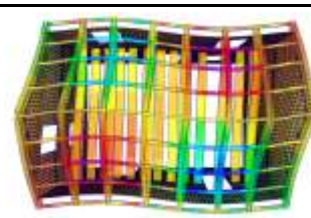

Table 5.15. Full-Scale Shell Model after Installing Diagonal Braces to the Ceiling of the First Floor. (Scenario #1)

Mode	Displacement	Highest Mass Participation	Deformed Shape
1	UX	45 %	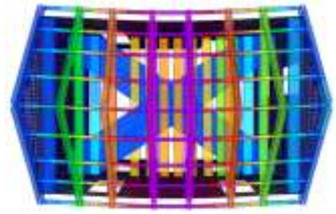
2	UY	47 %	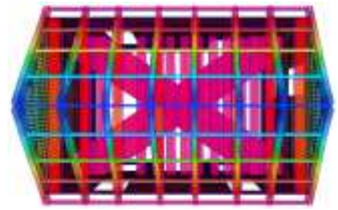
8	RZ	26 %	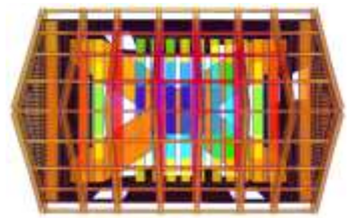

Table 5.16. Full-Scale Shell Model After Installing Diagonal Braces to the Roof. (Scenario #2)

Mode	Displacement	Highest Mass Participation	Deformed Shape
1	UX	46 %	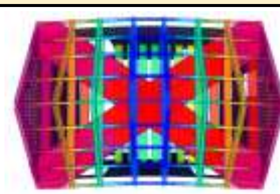
2	UY	53 %	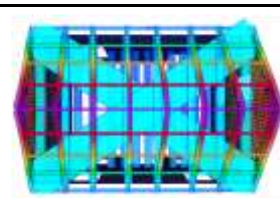
9	RZ	41 %	

Table 5.17. Full-Scale Shell Model after Installing Diagonal Braces to the Floor and Roof. (Scenario #3)

Mode	Displacement	Highest Mass Participation	Deformed Shape
1	UX	45 %	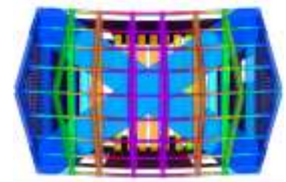
2	UY	53 %	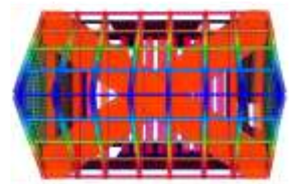
9	RZ	43 %	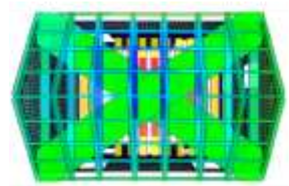

5.2.2.2 The Impact of Adding Diagonal Braces

Adding diagonal braces to unreinforced masonry structures was effective in enhancing stiffness and seismic performance. Installing diagonal braces decreases the modal periods, which suggests an increase in the structure's natural frequency and thus its stiffness. Before adding braces, the modal period was 0.159 seconds, and after installation, it decreased across all scenarios: to 0.153855 seconds when braces were added to the floor (scenario #1), to 0.154666 seconds when added to the roof (scenario #2), and to 0.152454 seconds when added to both the floor and roof (scenario #3). These decreases in modal periods demonstrate an improved dynamic response of the structure, which is a desirable characteristic in seismic design. These changes in mass participation rates after the installation of braces in different scenarios indicate a more balanced load distribution across the structure. This is particularly evident in scenario #3, where braces were added to both the floor and the roof, resulting in an increase in the highest mass participation for the Y-axis to 53%. These changes suggest that the braces not only enhance the stiffness of the masonry structure but also contribute to a more even distribution of seismic forces throughout the structure, potentially reducing the likelihood of damage during an earthquake.

It is crucial to highlight that, considering the results and in comparison to other strengthening methods, installing diagonal braces on the ceiling had the least impact on enhancing structural resistance. Although these braces are made of timber and are compatible with the Venice Charter and structural conservation, the use of this method is not recommended.

5.2.3 Strengthening Unreinforced Masonry Structures with Steel Rods

Strengthening Unreinforced Masonry Structures with Steel Rods involves a structural enhancement technique wherein steel rods are strategically installed horizontally and parallel to the ceiling and roof of a building constructed with unreinforced masonry. Unreinforced masonry structures, commonly found in older buildings, lack the necessary reinforcements to withstand seismic forces or other loads effectively. To address this vulnerability, steel rods are added as a strengthening measure. The steel rods are placed in a carefully planned pattern, typically running horizontally and parallel to the existing surfaces, which in this case include both the ceiling of the first floor and the roof. Installing these steel rods in this manner reinforces the structure, improving its overall stability and load-bearing capacity. The horizontal and parallel installation of steel rods distributes and absorbs forces evenly, thereby preventing potential collapse or damage to the masonry structure.

5.2.3.1 Section Design

This section provides an outline for designing a steel rod with a 25mm diameter to install horizontally and parallel to the ceiling of the first floor and the roof.

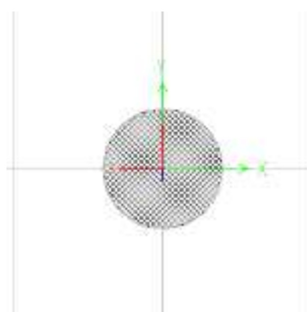

Figure 5.3. Section Design of Steel Rods

Table 5.18. Section Design Properties of Steel Rods

Shape Properties - solid	
Property	**Value**
Name	Circle1
Material	STEEL-G40-300W
X Center	0
Y Center	0
Diameter	25

5.2.3.2 Properties After Installing the Steel Rods

The significant change in the moment of inertia from 9×10^7 to 18929.7 after adding and installing steel rods with a diameter of 25mm and a modulus of elasticity of 200,000 MPa, several significant changes occur in the structural properties of the Full-Scale Shell Model. Compared to the original material of the full-scale shell model building, E=1800 MPa. The steel rods are significantly stiffer than the surrounding material. When these stiff steel rods are added, they enhance the overall stiffness of the structure.

The addition of steel rods to the full-scale shell model enhances its overall stiffness, reducing deformations, improving resistance against external loads, and maintaining shape and stability. These rods, stiffer than the surrounding material, efficiently distribute loads, allowing the structure to support heavier loads without excessive deflection or failure. The steel rods resist bending moments, crucial for stability under various loads, preventing excessive bending and ensuring stability. Reinforcing critical sections like corners and edges, the rods prevent buckling and enable the structure to withstand vertical and lateral loads effectively. Against dynamic forces like seismic loads, steel rods dissipate and redistribute forces, minimizing the risk of damage or failure. They also enhance crack resistance, reducing the likelihood of cracks in masonry or concrete and improving overall durability. With proper corrosion protection, steel rods resist environmental factors, preserving structural integrity over the long term. The moment of inertia, crucial for stiffness and geometry, increases with larger E values and the 25mm diameter of the steel rods, enhancing mass distribution around the axis. Linked at the center, these rods create a reinforced framework, significantly improving the structure's ability to resist bending moments by concentrating mass at the centerline and affecting mass distribution around the axis.

Table 5.19. Property Data of Full-Scale Shell Model with Steel Rods

Properties	Measurements
Area of Cross-Section	487.7258
Inertial Moment of Axis 3	18929.764
Inertial Moment of Axis 2	18929.764
Inertia Product about Axes 2-3	0.0
Torsion Constant	37856.89
Shear Area, Axis 2	440.3016
Shear Area, Axis 3	440.3016
Offset of CG, Axis 3	0.0
Offset of CG, Axis 2	0.0
Offset of Shear Center (x3)	Not Calculated (N/C)
Offset of Shear Center (x2)	Not Calculated (N/C)

Properties	Measurements
Modulus of Section, Top Edge about Axis 3	1514.3811
Modulus of Section, Bottom Edge about Axis 3	1514.3811
Modulus of Section, Left Edge about Axis 2	1514.3811
Modulus of Section, Right Edge about Axis 2	1514.3811
Warping Constant (Cw)	Not Calculated (N/C)
Plastic Modulus about Axis 3	2579.1475
Plastic Modulus about Axis 2	2579.1475
Radius of Gyration about Axis 3	6.23
Radius of Gyration about Axis 2	6.23

5.2.3.3 Modal Period Before and After Installing Steel Rods.

Table 5.20. Modal Periods and Frequencies after Installing Steel Rods

Output Case	Step Type	Step Num	Period	Frequency	Circ Freq	Eigenvalue
Text	Text	Unitless	Sec	Cyc/sec	rad/sec	rad2/sec2
MODAL before installing Steel rods	Mode	1	0.159017	6.288626	39.51260	1561.2460
MODAL After installing Steel rods to the floor. (scenario #1)	Mode	1	0.488955	2.045179	12.85024	165.128739
MODAL After installing Steel rods to the roof. (scenario #2)	Mode	1	0.488955	2.045176	12.85022	165.128272
MODAL After installing Steel rods to the floor and roof. (scenario #3)	Mode	1	0.488955	2.045176	12.85022	165.128271

5.2.3.4 Modal Before Installing Steel Rods

Table 5.21. Full-Scale Shell Model with Joists and without Installing Diagonal Braces

Mode	Period/ Sec	Displacement	Highest Mass Participation	Deformed Shape
1	0.159017	UX	46 %	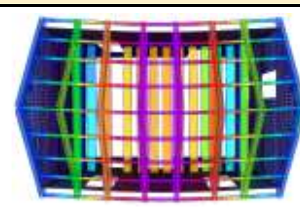
2	0.110722	UY	47 %	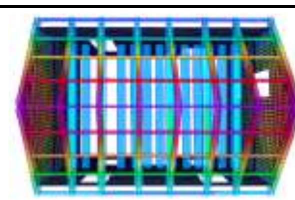

7	0.061816	RZ	29 %	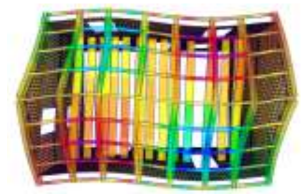

5.2.3.5 Full-Scale Shell Model After Installing Steel Rods to the Floor (Scenario #1)

In this scenario, steel rods are installed horizontally and parallel to the ceiling of the first floor. This method aims to reinforce the first-floor ceiling, providing additional support to prevent ceiling collapse. By reinforcing the horizontal plane, this approach can help distribute loads more effectively across the ceiling. Steel rods provide enhanced support for the first-floor ceiling, reducing the risk of collapse and improving the distribution of loads, potentially reducing stress concentrations in specific areas. Steel rods have limited improvement in vertical load-bearing capacity for the entire structure and insufficient lateral stability, especially under horizontal forces like seismic activity.

Table 5.22. Table. Full-Scale Shell Model after Installing Steel Rods to the Floor. (Scenario #1)

Mode	Period/ Sec	Displacement	Highest Mass Participation	Deformed Shape
2	0.15623	UX	46 %	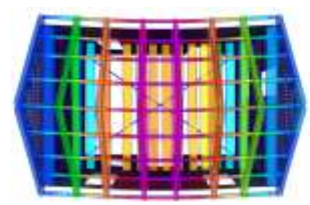
3	0.10986	UY	47 %	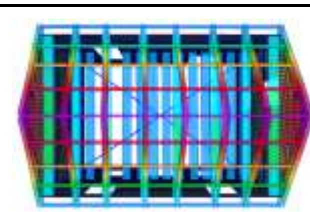
8	0.057474	RZ	21 %	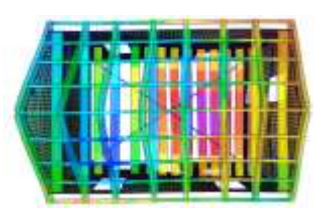

5.2.3.6 Full-Scale Shell Model After Installing Steel Rods to the Roof (Scenario #2)

In this scenario, steel rods are installed at the top of the walls, connecting the masonry walls and reinforcing the roof. This method strengthens the upper part of the building, providing improved resistance against vertical loads and potential roof collapses. However, lateral stability may still be a concern without additional reinforcement on the lower floor. Installing Steel rods at the top of the walls Improved vertical load-bearing capacity, reducing the risk of roof collapses and enhancing resistance against gravity loads and roof-related stresses. But still limited improvement in lateral stability, especially under horizontal forces like seismic activity and Insufficient protection against potential first-floor ceiling failures.

Table 5.23. Table. Full-Scale Shell Model after Installing Steel Rods to the Roof. (Scenario #2)

Mode	Period/ Sec	Displacement	Highest Mass Participation	Deformed Shape
2	0.156175	UX	46 %	
3	0.109765	UY	47 %	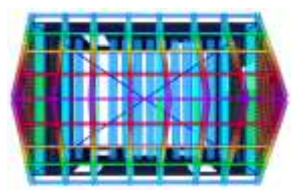
7	0.069766	RZ	31 %	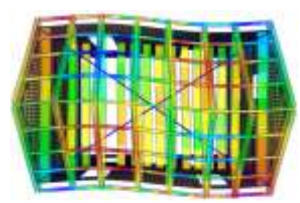

5.2.3.7 Full-Scale Shell Model Installing Steel Rods to the Floor and Roof (Scenario #3)

In this scenario, steel rods are installed horizontally and parallel to the surfaces, providing comprehensive reinforcement to both the ceiling of the first floor and the roof. This approach effectively addresses vertical and lateral stability concerns for both levels of the building. The rods in the first-floor ceiling and roof offer essential horizontal support to their respective levels, thereby increasing overall structural integrity and minimizing the risk of failure under various loading scenarios.

Table 5.24. Full-Scale Shell Model after Installing Steel Rods to the Floor and Roof. (Scenario #3)

Mode	Period/ Sec	Displacement	Highest Mass Participation	Deformed Shape
3	0.156137	UX	46 %	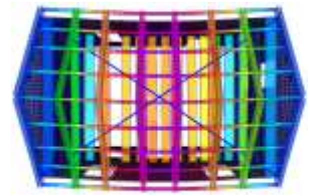
4	0.109728	UY	47 %	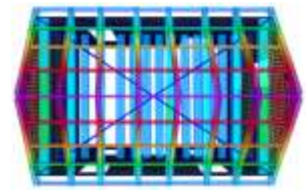
8	0.06915	RZ	34 %	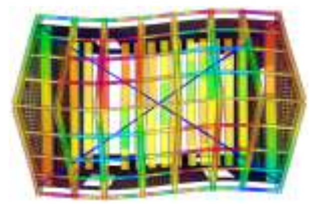

5.2.3.8 The Impact of Installing the Steel Rods in URM

The introduction of steel rods as a strengthening measure in unreinforced masonry structures results in a significant improvement in structural stability and resistance to loads, including seismic forces. This technique involves the horizontal installation of steel rods parallel to the ceiling and roof, which reinforces the masonry and increases its load-bearing capacity.

The data provided shows a substantial increase in the moment of inertia, indicating enhanced stiffness and better distribution of forces throughout the structure. For instance, after the installation of steel rods, the Full-Scale Shell Model showed an increase in stiffness, as evidenced by the change in moment of inertia from 9×10^7 to 18929.7. This change is attributed to the properties of the steel rods, which have a higher modulus of elasticity (200,000 MPa) compared to the original building material (1800 MPa).

However, the modal analysis reveals an increase in modal periods after installing steel rods, from 0.159017 seconds before installation to 0.488955 seconds in three different scenarios, which could indicate a reduction in structural stiffness contrary to the expected outcome. This requires careful interpretation, as it might suggest that while the steel rods improve certain aspects of the structure's performance, they could potentially introduce flexibility in other modes or directions.

In terms of specific scenarios, installing steel rods on the floor (Scenario #1) or the roof (Scenario #2) alone provided limited improvement in vertical load-bearing capacity and lateral stability. It was only with the installation of steel rods to both the floor and the roof (Scenario #3) that a comprehensive enhancement in structural stability was observed.

5.2.4 Strengthening Unreinforced Masonry Structures with Repointing

Repointing is a meticulous process integral to the restoration and reinforcement of masonry structures, particularly those constructed with bricks. Over time, mortar joints between masonry units deteriorate due to weathering, moisture, and natural aging, compromising the structure's integrity and making it vulnerable to instability and potential collapse, especially during seismic events. Restoring structural integrity, repointing replaces degraded mortar with fresh, high-quality material, reinforcing bonding between masonry units. Proper repointing ensures uniform load distribution, preventing localized stress concentrations, thereby reducing the risk of structural failure. Additionally, repointing plays a pivotal role in preserving historic and heritage buildings, maintaining their original aesthetics while ensuring long-term stability and safety. By stabilizing mortar joints, repointing mitigates structural movements caused by settling, ground vibrations, or external factors, maintaining alignment and stability. In earthquake-prone areas, repointing is vital for enhancing seismic performance. Well-reinforced mortar joints resist lateral forces during seismic events, minimizing structural damage or collapse. Moreover, repointed joints act as a barrier against water infiltration, preventing moisture-induced deterioration, including freeze-thaw cycles and erosion, safeguarding the structure against weather-related damage.

5.2.4.1 Masonry Mortar Type S

The CSA A179-14 standard, which focuses on mortar and grout for unit masonry, covers various mortar types and their mixing techniques. Mortar Type S, a specific blend, is widely used in construction and masonry projects due to its high compressive strength, making it ideal for applications requiring durability and strength. It consists of Portland cement, lime, sand, and occasionally other additives, with a minimum compressive strength of 1,800 psi, allowing it to withstand substantial pressure without breaking. Mortar Type S is commonly employed in building walls, chimneys, and other structural elements, offering excellent workability and durability. It adheres well to different surfaces, ensuring a strong bond between masonry units, making it crucial for load-bearing walls and other structural components of buildings.

This type of mortar is vital in structural masonry due to its balanced strength and bonding, crucial for effective seismic performance. Its strong bond is achieved through properties like workability, adhesion, cohesion, and water retention, rather than just compressive strength. Mortar mixes typically include Portland cement for strength and durability, while mortar cement, masonry cement, or lime contribute essential properties for a solid bond. Mixing mortar on-site is common, following the material proportions outlined in CSA A179-14. Properly filled and tooled mortar joints are essential for optimal performance. In structural stability and weather resistance, concave tooled joints are recommended, accommodating slight dimensional variations in masonry units. Mortar joints influence the architectural appeal of the masonry assembly through their color and modularity. In load-bearing masonry, mortar bed joints should not exceed a thickness of 0.5 inch (12mm). However, for the starting course, the bed joint must be at least 1/4 inch (6mm) thick and no more than 3/4 inch (20mm) thick, allowing adjustments to meet the required dimensions.

Material Properties for Brick Masonry for the Period of Interest, Compressive strength, fm', for brick masonry (numbers in bold are in MPa; Note that 1 ksi = 6.9 MPa; and $1.0\sqrt{fm}(psi)$=(1/12)$\sqrt{fm}(MPa)$), according to table5.25. (Voula (S. J.) Pantazopoulou, 2022)

Table 5.26. Brick Masonry's Strength (MPa) with Conversion from ksi (Pantazopoulou, 2022)

Block Compressive Strength (ksi / MPa)	Compressive Yield with Type M Mortar (ksi / MPa)	Compressive Yield with Type S Mortar (ksi / MPa)	Compressive Yield with Type N Mortar (ksi / MPa)
Above 14/over 90	4.0/30	3.9/25	3.2/21
12/80	4.0/27	3.4/23	2.8/19
10/70	3.4/24	2.9/20	2.4/17
8.0/55	2.8/19	2.4/16	2.0/14
6.0/40	2.2/15	1.9/13	1.6/11
4.0/25	1.6/10	1.4/8.8	1.2/7.5
2.0/15	1.0/7.5	0.9/6.8	0.8/6.0

5.2.4.2 Strength Variability in Masonry Design

The knowledge factor κ, representing the minimum knowledge level, is typically set between 0.75 and 0.9 based on default values and design drawings. However, these values are not applicable to nonlinear analysis methods, as per ASCE/SEI-41, 2017, Section 6.2.4.3. These advanced analysis methods require a high level of usual or comprehensive knowledge, denoted by κ=1, along with expected material properties derived from mean test values. Lower bound values are calculated by subtracting one Standard Deviation from the mean test values. Alternatively, if lower bound values are provided, the expected strengths can be obtained by multiplying these values by a factor of 1.3 (refer to Table 11-1, ASCE/SEI 41, 2017). It's important to note that values in older drawings might indicate working stress limits rather than true lower-bound strengths. A κ value of 0.75 can be used if the coefficient of variation of test results exceeds 0.25 (Section 11.2.4, ASCE/SEI-41).

Masonry, a composite material comprising masonry units, mortar joints, and grouting, exhibits a wide range of mechanical strengths due to various combinations of block unit and mortar properties. The volume fraction of the block phase dominates because of the larger unit dimensions compared to the relatively thin joints. The compressive strength of the masonry wall, treated as a homogenized medium, depends on both the compressive strength of the mortar joints (fjc) and the masonry unit (fbc). The homogenized compressive strength of masonry as a composite, denoted as $f'mc$, is determined by a function k, which varies based on the mortar joint thickness, ranging from 0.55 for 6mm joints to 0.35 for 15mm joints. According to the CSA Report from Design of masonry structures the tensile strength of masonry is minimal, falling within a negligible range, ($0.03 \cdot fmc \leq fmt \leq 0.09 \cdot fmc$).

In the CSA-S304-2014 standard in section 10.2.4, addressing the Tensile Strength of Masonry. According to this section, the calculation of the factored bending resistance of reinforced walls and columns should neglect the Tensile Strength of Masonry. Section 5.2.3 specifies that axial tensile strength is considered zero for unreinforced masonry under direct (axial) tension normal to the bed joint. However, section 5.2.1 outlines that the specified flexural strength, denoted as ft, must adhere to the provided Table.

Table 5.27. Specified Type S Mortar Compressive Strength for Masonry (CSA S304-14)

Specified compressive strength of unit (average net area), MPa	Type S mortar Ungrouted hollow units	Type S mortar Solid units or grouted hollow units
30 or more	17.5	13.5
20	13	10
15	10	7.5
10	6.5	5

5.2.4.3 Material Property Data

The section focuses on investigating the impact of modifying mortar strengths and simulating masonry specimens. This study delves into the intricate relationship between the strengths of individual mortar components and the resulting overall strength of masonry structures. By systematically altering the strengths of each material, a comprehensive analysis will be conducted to discern the nuanced contributions of specific mortar components to the structural integrity of masonry assemblies.

Figure 5.4. Material Property Data

5.2.4.4 Modal Period Before and After Repointing with Mortar Type S

Modal periods represent the time taken for a structure to complete one full cycle of vibration, measured in seconds. In Mode 1, before repointing, the modal period is 0.159 seconds. After repointing with mortar type S, Mode 1 experienced a decrease in modal period to 0.092 seconds, resulting in an increase in frequency to 10.90 Hz. This data suggests that after repointing with mortar type S, Mode 1 of the structure exhibited a higher natural frequency, indicating a stiffer and potentially more stable response to vibrations. The decrease in modal period and increase in frequency are positive outcomes, demonstrating the effectiveness of the repointing process in enhancing the structural performance of the analyzed system.

Table 5.28. Modal Periods and Frequencies After Repointing Mortar Type S

Output Case	Step Type	Step Num	Period	Frequency	Circ Freq	Eigenvalue
Text	Text	Unitless	Sec	Cyc/sec	rad/sec	rad2/sec2
MODAL before repointing	Mode	1	0.159017	6.288626	39.512605	1561.24603
MODAL After Repointing mortar type S	Mode	1	0.091713	10.90362	68.509513	4693.553439

5.2.4.5 Highest Mass Participation and Deformed Shape

Table 5.29. Full-Scale Shell Model with Joists and without Installing Diagonal Braces.

Mode	**Period/ Sec**	**Displacement**	**Highest Mass Participation**	**Deformed Shape**
1	0.159017	UX	46 %	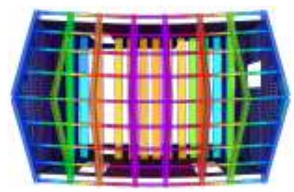
2	0.110722	UY	47 %	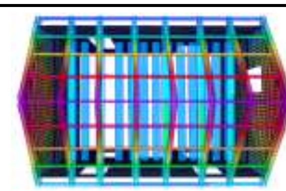
7	0.061816	RZ	29 %	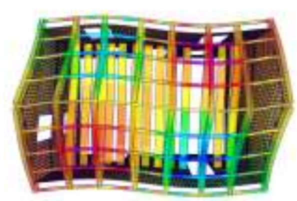

Table 5.30. Full-Scale Shell Model after Repointing with Mortar Type S

Mode	**Period/ Sec**	**Displacement**	**Highest Mass Participation**	**Deformed Shape**	
1	0.0917	UX	41 %	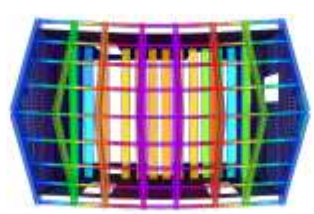	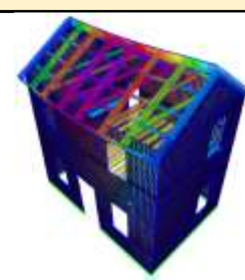

2	0.0649	UY	31 %	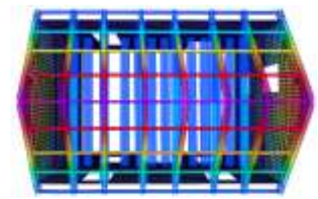	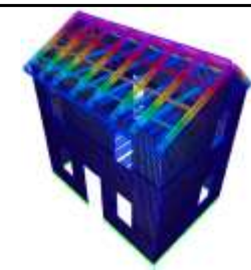
14	0.0233	RZ	14 %	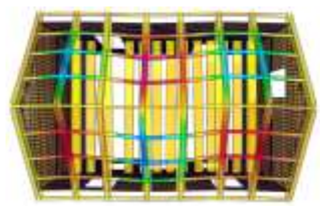	

5.2.4.6 The Impact of Concrete Repointing Using Mortar Type S

Strengthening unreinforced masonry structures with repointing using mortar type S significantly enhances structural integrity and seismic resilience. Repointing is a critical maintenance process that not only restores the aesthetic appeal of masonry but also reinforces its structural performance by replacing deteriorated mortar with new, high-quality mortar. Mortar type S, in particular, with its high compressive strength and good bonding properties, is well-suited for structural applications, effectively improving the load-bearing capacity and stiffness of masonry structures.

The positive changes in modal periods and frequencies post-repointing indicate an increased stiffness, a crucial factor for seismic resistance. The decrease in the modal period from 0.159 seconds to 0.0917 seconds and the increase in frequency from 6.29 Hz to 10.90 Hz post-repointing demonstrate the improved dynamic performance of the masonry. These changes suggest a structure's better ability to resist dynamic loads, such as those induced by earthquakes.

Furthermore, the data on mass participation and deformed shape show a reduction in displacement and highest mass participation rates after repointing, implying a more balanced distribution of mass and stiffness. This indicates that the structure is less likely to experience extreme deformation under load, reducing the likelihood of damage or failure during seismic events.

The technical specifications and standards such as CSA A179-14 and ASCE/SEI-41 provide a framework for assessing and applying the correct properties of materials. The empirical formulas and guidelines ensure that the repointing process is carried out to maximize the structural benefits while adhering to safety and durability requirements.

5.2.5 Strengthening Unreinforced Masonry Structures with Shotcreting

The construction method known as shotcrete, pioneered by Carl Akeley in 1910 through the invention of a specialized double-chambered cement gun for dry mixing and spraying sand-cement products, was officially named gunite in 1912 (ACI 2005). This technique gained widespread adoption in North America by the early 1920s, finding applications in the construction, repair, and safeguarding of various structures such as buildings, bridges, dams, tunnels, water storage tanks, and reservoirs, (Yoggy, 2005).

The American Concrete Institute officially embraced the term "shotcrete" in 1951, encompassing both dry-mix and wet-mix processes. Shotcrete, when reinforced with fibers, has been utilized as shear reinforcement for reinforced concrete beams. In the context of strengthening unreinforced masonry (URM) buildings, conventional shotcrete, often mixed in a ratio of one part cement to three parts sand, has been a traditional approach (Fillitsa and Michael 1992). Typically, conventional shotcrete necessitates a minimum thickness of 50 mm, incorporating steel mesh within the shotcrete layer to enhance tensile strength and limit crack widths. Seismic strengthening designs often require thicker shotcrete layers (above 100 mm), occasionally leading to the removal of a single leaf from masonry walls to mitigate the additional thickness effects. Establishing additional connections and employing formwork between the shotcrete and the masonry wall are essential, (Kahn, 1984).

Unreinforced masonry buildings lack crucial tensile-resisting elements, rendering them susceptible to seismic forces and resulting in their classification as "earthquake-prone buildings." Several techniques, including steel moment-resisting frames and conventional shotcrete, have been utilized to reinforce URM buildings. However, when selecting strengthening methods, it is imperative to consider the preservation of the building's architectural character and cultural significance. This necessitates minimal alteration of the original appearance and the preservation of its initial function (Lin 2013).

Figure 5.5. Strengthening Structure with the Shotcreting Method (Lin, 2013)

5.2.5.1 Material Property Data of Concrete Shotcrete

The unreinforced masonry wall's original material properties are relatively lower in compressive strength and modulus of elasticity compared to the shotcrete layer. By applying a shotcrete layer with significantly higher compressive strength and modulus of elasticity, the structural integrity of the entire system is improved. The shotcrete layer effectively reinforces the masonry, providing the necessary strength and stability to the weakened structure, making it more resistant to various loads and potential damages. The shotcrete layer is made of concrete according to CSA A23.3 and it's grade is fc 25 MPa.

Table 5.31. Material Property for Concrete Shotcrete

Property	Value
Weight	23.5 kN/m³
Modulus of Elasticity	24942 MPa
Compressive Strength	25 MPa
Poisson's Ratio	0.2
Shear Modulus	10392 MPa

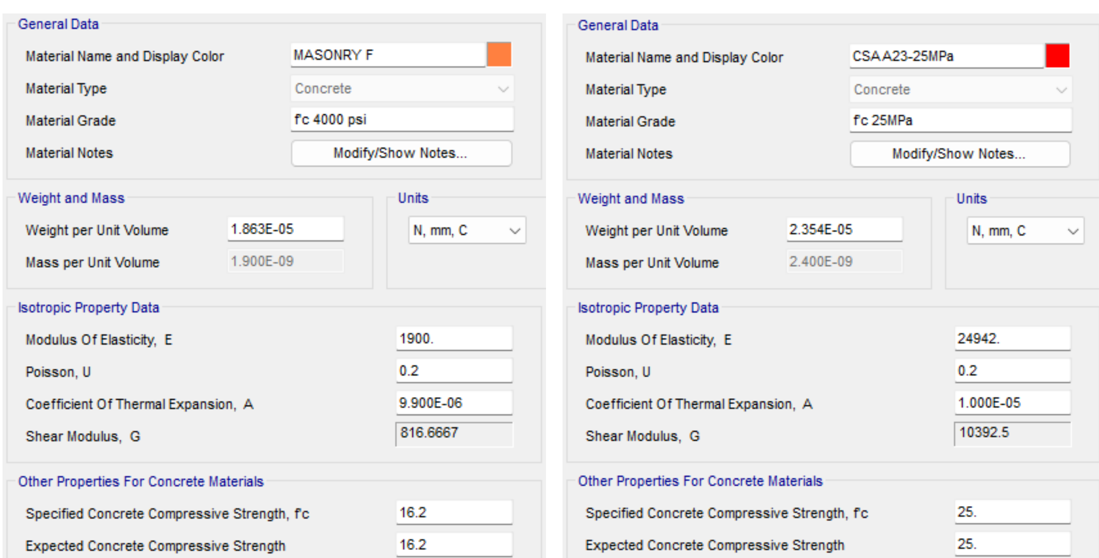

Figure 5.6. Material Property Data of Strengthening with Concrete Shotcrete.

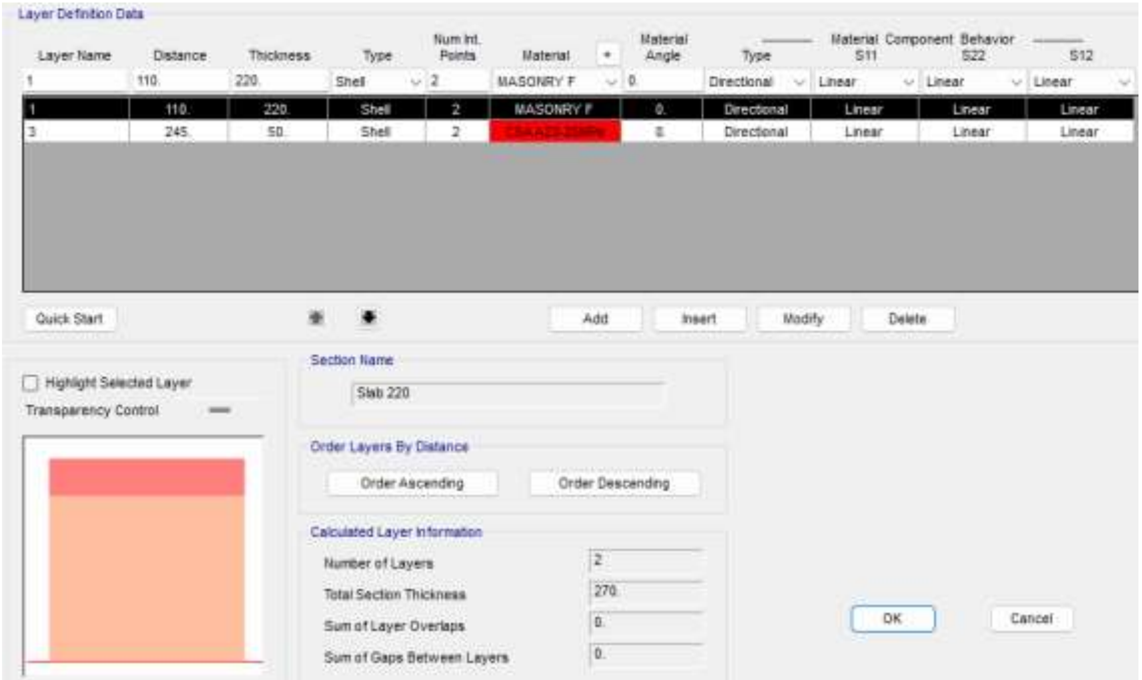

Figure 5.7. Shell Section Layer Definition Data for 50mm Thickness of Concrete and 220mm Thickness of Masonry Wall

Table 5.32. Modal Periods and Frequencies After Concrete Shotcrete to Exterior Side of the Wall

Output Case	**Step Type**	**Step Num**	**Period**	**Frequency**	**Circ Freq**	**Eigenvalue**
Text	Text	Unitless	Sec	Cyc/sec	rad/sec	rad2/sec2
MODAL before shotcrete	Mode	1	0.159017	6.288626	39.512605	1561.2460
MODAL after concrete shotcrete	Mode	1	0.098394	10.16318	63.857188	4077.7405

Table 5.33. Full-Scale Shell Model with Concrete Shotcrete to Exterior Side of the Wall

Mode	**Period/ Sec**	**Displacement**	**Highest Mass Participation**	**Deformed Shape**	
1	0.09839	UX	48 %	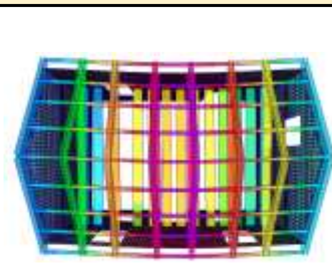	

2	0.06494	UY	57 %	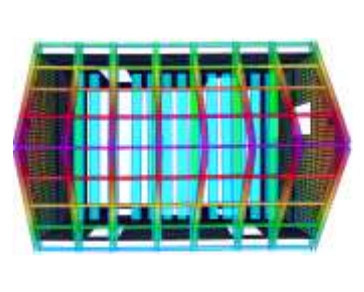	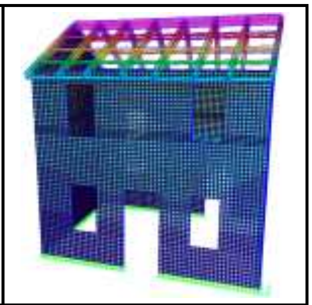
8	0.03668	RZ	33 %		

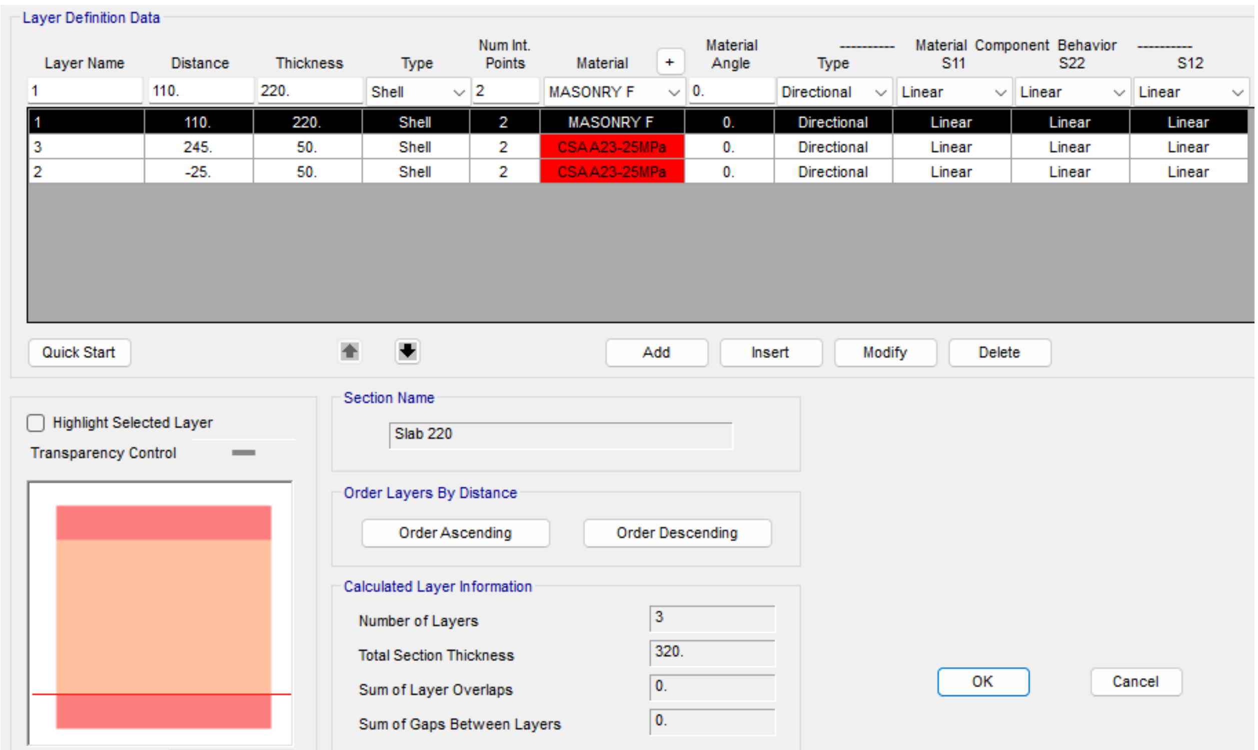

Figure 5.8. Shell Section Layer Definition Data for 50mm Thickness of Concrete in Both Sides of the Wall (Totally 10mm) and 220mm Thickness of Masonry Wall

5.2.5.2 MODAL Period Before and After Concrete Shotcrete Both Side of the Wall

Table 5.34. Modal Periods and Frequencies of Concrete Shotcrete Both Side of the Wall

Output Case	**Step Type**	**Step Num**	**Period**	**Frequency**	**Circ Freq**	**Eigenvalue**
Text	Text	Unitless	Sec	Cyc/sec	rad/sec	rad2/sec2
MODAL before shotcrete	Mode	1	0.159017	6.288626553	39.51260596	1561.24603
MODAL after concrete shotcrete both side of the wall	Mode	1	0.055142	18.13485787	113.9446725	12983.38839

Table 5.35. Full-Scale Shell Model with Concrete Shotcrete Both Side of the Wall

Mode	**Period/ Sec**	**Displacement**	**Highest Mass Participation**	**Deformed Shape**	
1	0.055142	UX	54 %	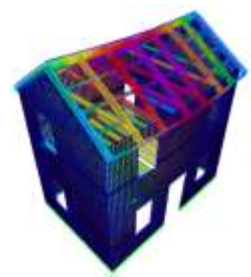	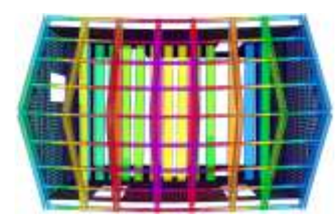
2	0.045	UY	59 %	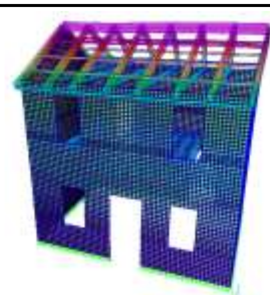	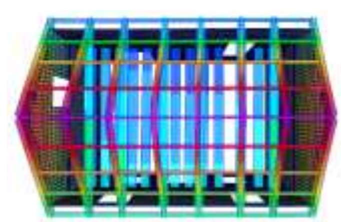
6	0.02542	RZ	34 %		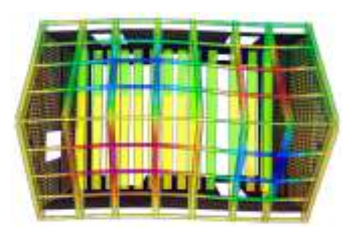

5.2.5.3 The Impact of Concrete Shotcrete

Based on the provided data, the application of concrete shotcrete has significantly enhanced the structural properties of an unreinforced masonry wall. The original material properties of the wall, with lower compressive strength and modulus of elasticity, are substantially improved by adding a shotcrete layer. This layer, which adheres to CSA A23.3 standards with a grade of fc 25 MPa, not only increases the wall's resistance to loads but also its stability and resilience to potential damage. The concrete shotcrete's material properties, including its weight, modulus of elasticity, compressive strength, Poisson’s ratio, and shear modulus, contribute to this reinforcement. The modal analysis before and after shotcrete application shows a considerable improvement in the wall's dynamic response. The periods and frequencies after shotcrete application indicate a stiffer system, with higher frequencies and lower periods, suggesting an increase in the wall's ability to resist dynamic actions such as seismic events. The application of shotcrete on both sides of the wall significantly reduces the modal periods, increases frequencies, and enhances the mass participation in the structural response. This implies that the structure has become more rigid and thus more capable of withstanding dynamic loads. The data demonstrates that the addition of a concrete shotcrete layer, especially on both sides of an unreinforced masonry wall, provides a pronounced improvement in both the static and dynamic material properties of the structure. The shotcrete layer effectively acts as a reinforcing and strengthening agent, ensuring the masonry wall can better resist and perform under various load conditions.

5.3 Conclusion

In addressing the seismic vulnerabilities of unreinforced masonry (URM) structures in Canada, a region with a notable history of seismic activity, this chapter has meticulously evaluated a range of structural strengthening techniques. The focus has been particularly on the seismic reinforcement of heritage buildings and older structures that are integral to Canada's urban architectural landscape.

The exploration of seismic strengthening methods commenced with a detailed understanding of the challenges inherent in URM structures, including the risk of out-of-plane failures and diaphragm flexibility. Our analysis highlighted the critical need for interventions that could effectively alter the fundamental periods of vibration, reduce rotational mass participation in twisting modes, and limit differential displacements within building floors. Techniques such as the integration of timber ceilings and the inclusion of diagonal steel rods were scrutinized for their efficacy in enhancing the rigidity of horizontal diaphragms.

A portion was dedicated to the innovative use of steel rods, strategically installed to reinforce structural planes parallel to the ceilings and roofs. This method, while improving vertical load-bearing capacity, also brought to light the intricacies and challenges of ensuring adequate lateral stability in seismic retrofitting. The practice of repointing with Mortar Type S emerged as not only a preservation technique but also a means to augment the structural resilience of masonry buildings. The observed decrease in modal periods provided a clear indication of increased structural stiffness and dynamic response capabilities.

The chapter then advanced to the application of concrete shotcrete, conforming to the CSA A23.3 standards, as a transformative method for bolstering the seismic resilience of URM walls. The shotcrete layer's enhanced compressive strength and modulus of elasticity were found to significantly increase the structural stiffness of the walls. The application of shotcrete on both sides of the walls was particularly effective, evidenced by the substantial reductions in modal periods and heightened frequencies, signifying a more robust response to seismic forces. According to restoration standards and the principles of the Venice Charter, retrofitting interventions ought to be reversible and non-detrimental to the structure's integrity. However, concrete shotcrete, by its very nature, is not reversible, thereby rendering it unsuitable for use in the retrofitting of historical heritages.

The provided information in the Appendix evaluates retrofitting measures on the Bothara experimental building and highlights a range of seismic strengthening methods that aim to enhance safety while preserving architectural integrity. Key approaches include upgrading to meet minimum code requirements, using techniques like crack repair, bonding agents, and metal inserts for structural stabilization, and introducing advanced methods such as moment frames and braced frames. Out-of-plane and in-plane wall strengthening are emphasized, employing vertical steel sections and additional material layers, respectively. Reduction of seismic forces through mass reduction, base isolation, and dampers is also discussed. Overall, the focus is on selecting retrofitting strategies that balance structural needs with the preservation of the building's heritage character, emphasizing minimal visual impact, and respecting historical value.

In conclusion, this chapter provides a detailed understanding of the challenges and potential solutions for strengthening URM structures in seismic zones. While it underscores the effectiveness of various retrofitting techniques, it also emphasizes the need to balance structural reinforcement with heritage conservation principles. The insights and findings from this study are invaluable for developing strategies that ensure the safety and longevity of historical structures in seismic regions.

6 Chapter 6: Conclusion and Future Work

6.1 Summary and Conclusions

The research in this thesis yields conclusions regarding the mechanical behavior of masonry and the applicable numerical modeling techniques for masonry and unreinforced masonry (URM) structures with a special focus on the seismic assessment and retrofitting of unreinforced masonry (URM) structures, particularly those of heritage importance. The research provides significant insights into the dynamic response of URM buildings to seismic loads, including the investigation of natural frequencies, damping ratios, deformation patterns, and their correlation with actual damage patterns.

To investigate the effectiveness of the modelling methods used for seismic evaluation of masonry structures, a two-storey clay-brick masonry building that had been previously tested to a series of ground motions of increasing intensity using a shake table was used as benchmark. The experimental structure demonstrated a gradual progression of damage which was reflected by the gradual increase of its fundamental period.

Two different modelling approaches were tested and correlated against the experimental results: a) the equivalent frame analysis method, which is the established method of analysis recommended by the current evaluation codes (ASCE/SEI-41 (2017); the Eurocode 8-III 2005 and 2022, and the Italian Code (MIT 2009). b) Detailed finite element analysis using shell-elements to model the continuous walls of the structure. The latter approach follows the detailed geometry of the structure, whereas the former involves a substantial degree of idealization where surface elements such as walls and piers are modelled as equivalent linear elements (columns, beams and rigid zones at the regions of intersection of the horizontal spandrels and the vertical wall surfaces). The equivalent frame analysis was the only method available about a decade ago, in order to perform also nonlinear analysis through the addition of plastic hinges in the member ends. With the development of software capabilities in recent years, shell element analysis can be used in practical applications such as the one considered with relatively straightforward effort, and because it may be used to model the structural details more faithfully, in this study it was considered the preferred approach.

The two models were calibrated to match the structural frequencies, according with the experimental evidence; from this effort it was found that the Elastic modulus that correlated the experimental results was vastly different in the two modelling approaches. Next the similar full-scale structure which served as a prototype for designing the experimental half-scale test-structure was modelled using identical shell-element based analysis. When using the same material properties with the half-scale finite element model the frequencies of the full and half scale idealization followed closely the similitude law requirements according to which, $T_{1:1} = \sqrt{2}T_{1:2}$- where $T_{1:1}$ is the fundamental period of the full-scale model and $T_{1:2}$ is the fundamental period of the half-scale model. Nevertheless, the participating mass was different – underscoring the effects of similitude modeling in the dynamic response of the system: it is noted that due to the scaling laws, and because mass was scalled down by the cubic power of the geometric scale ratio, λ, whereas the weight, which is proportional to mass and has units of force, should be scaling down with the square power of λ, it follows that mass addition was in order in the scaled specimen. Because it would be practically impossible to distribute the mass heightwise throughout the masonry walls, which however are responsible for the mass of the building, the added masses were placed at the floor and roof levels, effectively modifying the dynamic properties of the building ½ scaled model from that of the full-scale structure.

After calibration of the fundamental properties of the building, spectral analysis was conducted in order to identify the deformations and stress demands in the structure and examine the relevance of these results with the experimental evidence. One of the key contributions of this thesis was the pioneering analysis of various retrofitting techniques in order to examine alternative strategies to upgrade the structure’s seismic resistance. The techniques considered in the retrofitting campaign, would be categorized into two broad areas – invasive methods which are very effective in substantially strengthening the structure, and non-invasive, moderate interventions that aim to balance resilience and heritage conservation, ensuring compatibility with international standards. The advancements in nonlinear modeling, addressing the challenges in material behavior representation and simulation convergence, have been validated through practical applications using SAP2000, incorporating sensitivity analyses. It is shown that the deformations are critically moderated when stiff diaphragms are added in the URM structure. This property highlights enhancement of diaphragm action as an important retrofitting strategy for unreinforced masonry structures with timber floors, which abound in heritage construction.

The study showcases the effectiveness of three-dimensional finite element modeling with shell-type elements for evaluating the dynamic response of URM structures and in capturing the prevalent tendency of out of plane failures in the absence of stiff diaphragms. Critical for the replication of fundamental periods and mode shapes of the computational models with the experimental structure was achieved through proper consideration of boundary conditions and contact modeling. Additionally, the application of three-dimensional finite element modeling utilizing shell-type elements furnishes a robust means of simulating the dynamic response of URM structures, facilitating seismic performance assessment while also providing a platform for the development of pertinent retrofit schemes which are studied through parametric investigations

This thesis not only integrates theoretical analysis with practical application but also makes significant strides in developing seismic risk mitigation strategies by providing a balanced approach between enhancing seismic resilience and maintaining historical integrity and the preservation of heritage structures. The research findings have far-reaching implications proof testing new models for assessing mechanical properties and retrofit strategies. The study on the influence of retrofitting techniques, including the use of high-strength mortar and shotcrete, demonstrates their impact on enhancing structural integrity and seismic resistance. The importance of nonlinear analysis in SAP2000 is highlighted, showing its critical role in capturing the complex behavior of masonry materials under seismic stress.

6.2 Findings

This project focuses on several critical areas in the field of structural engineering, particularly concerning unreinforced masonry (URM) structures. Firstly, it aims to establish dependable and comprehensive seismic assessment methods specifically tailored for URM structures. This involves calibrating and validating computer models with experimental data and field evidence to enhance the accuracy and reliability of these assessment techniques. In terms of retrofit solutions, the study is dedicated to uncovering realistic and effective methods for URM buildings, specifically addressing critical failure modes like out-of-plane differential translation and axial stress transfer, which are essential for developing methods to improve seismic resilience.

A pivotal contribution of this project is the development of a nonlinear modeling approach for masonry structures. This approach focuses on calibrating stiffness and lateral strength calculations to accurately represent the dynamic attributes of URM constructions. This concept has the potential to be extended to other masonry buildings, thereby enhancing seismic evaluation methodologies.

Throughout this thesis, the following key findings have been identified, focusing on the seismic behavior, assessment, and retrofitting of unreinforced masonry (URM) structures, particularly those with heritage value. The major conclusions are summarized as follows:

➢ Drift Capacity of clay masonry walls was determined from the reported results of codes and database studies. It was determined that URM components crack at very low drift ratios in the order of 0.15-0.2%, whereas their ultimate drift capacity depends on the typology of construction, but seldom will it exceed the limit of 0.5%. For context, it is noted that reinforced masonry components yield at 0.5% and beyond that point they can develop lateral drifts in the order of 1.5-2.5% without loss of strength. It is therefore evident that URM components are particularly brittle and cannot provide significant seismic protection.

➢ New and enhanced models for assessing the mechanical properties of masonry were evaluated and implemented in the computational study. These advancements include new calculations for effective stiffness of the walls (Effective Elastic modulus).

➢ Implications for Retrofit Interventions: The research delved into the effects of various retrofit interventions, like mortar injections, deep-repointing, addition of diaphragm rigidity, cross bracings, and other more invasive interventions on the stiffness, strength, and drift capacity of unreinforced masonry structures. This analysis provided crucial insights into the effectiveness of these interventions in conservation and strengthening solutions of existing URM structures.

➢ Enhancement of Structural Assessment Procedures: The findings contribute significantly to the enhancement of assessment procedures for masonry structures, offering updated values, models, and expressions for various limit states. This aids in developing more precise and reliable methods for assessing the seismic performance of masonry structures.

➢ Importance of Nonlinear Analysis in SAP2000: The study emphasizes the critical role of nonlinear analysis in SAP2000 for accurately predicting the seismic response of unreinforced masonry buildings. This analysis captures complex behaviors of masonry materials under stress, such as cracking, crushing, and sliding, which linear models fail to address.

➢ Detailed 3D Modeling using alternative methods of analysis: Comparative evaluation of the equivalent frame analysis and shell element modeling for seismic evaluation illustrated significant points of systematic difference between these methods, a finding that has important implications for the Code-recommended methods of seismic evaluation of URM structures to be used by practitioners. It was also illustrated that the use of detailed 3D models in SAP2000, coupled with accurately defined material properties in the form of stress-strain relationships rather than nonlinear hinges with predetermined plastic rotation capacities, - which, as discussed in the preceding, may not be available for a structural component comprising URM materials, is fundamental. This approach allows for more realistic simulation of the building's behavior under various seismic conditions.

6.3 Next Steps

Upon the completion of this thesis, several promising directions for future research in the field of heritage URM structures have emerged. One critical area is the expanded modeling of URM structures, particularly those featuring complex architectural elements such as pitched roofs, arched ceilings, domes, and sloping tile. By extending the modeling efforts to include a broader range of specimens with unique characteristics, the developed methodologies can be further calibrated, refined and made more comprehensive, allowing for their application to a diverse array of structures.

Further development is also needed in the realm of three-dimensional finite element models. These models are essential for further calibrating empirical equations that define the mechanical properties of URM structures. Achieving more accurate and realistic estimates of material properties is crucial for reliable seismic assessment.

This thesis has significantly advanced our understanding of the capabilities of numerical modeling in analyzing and assessing URM structures. Continuing to explore and apply the methodologies discussed will be instrumental in ensuring the safe, non-invasive restoration and preservation of heritage URM structures. It will also contribute to their enhanced resilience against future seismic events, thereby minimizing potential damage and loss. The path forward involves not just technical advancements but also a deep appreciation of the cultural and historical significance of these structures, ensuring that they continue to stand as testaments to our architectural heritage.

References

American Society of Civil Engineers (2017) , December. ASCE/SEI 41-17: Seismic Evaluation and Retrofit of Existing Buildings. American Society of Civil Engineers.

American Society of Civil Engineers, 2014, May. Seismic evaluation and retrofit of existing buildings. American Society of Civil Engineers.

American Society of Civil Engineers, 2014, May. Seismic evaluation and retrofit of existing buildings. American Society of Civil Engineers.

American Society of Civil Engineers, 2017, December. Seismic evaluation and retrofit of existing buildings. American Society of Civil Engineers.

ASCE/SEI 41. 2017. Seismic evaluation and retrofit of existing buildings. American Society of Civil Engineers (ASCE). Reston, VA: USA.

Aşıkoğlu, A. and Avşar, Ö. (2022) 'Investigation of drift-based damage limit states for historical masonry structures', International Journal of Architectural Heritage, pp. 1–19.

Bothara, J.K., Dhakal, R.P. and Mander, J.B. (2010) 'Seismic performance of an unreinforced masonry building: An experimental investigation', Earthquake Engineering & Structural Dynamics, 39(1), pp. 45–68. Available at: https://doi.org/10.1002/EQE.932.

Calvi, G.M. and Magenes, G., 1997, March. Seismic evaluation and rehabilitation of masonry buildings. In Proceedings of the US-Italian workshop on seismic evaluation and retrofit (pp. 123-142). National Center for Earthquake Engineering Research (Technical Report NCEER, 97-0003), Buffalo, New York, US.

CEN (2005a) EN 1998-3: 2005 Eurocode 8: design of structures for earthquake resistance—part 3: assessment and retrofitting of buildings. Comite´ Europe´en de Normalisation, Brussels, Belgium

CEN (2005b) EN 1996-1-1:2005 Eurocode 6: design of masonry structures—part 1-1: common rules for reinforced and unreinforced masonry structures. Comite´ Europe´en de Normalisation, Brussels, Belgium

Costa, A., Guedes, J. M. and Varum, H. (2014) Structural Rehabilitation of Old Buildings, Building Pathology and Rehabilitation. doi: 10.1007/978-3-642-39686-1.

European Commission (2009-2012) 'NIKER: New Integrated Knowledge Based Approaches to the Protection of Cultural Heritage from Earthquake-Induced Risk', 7th Framework Programme, co-operation, Environment theme, EC contract no. 244123. (www.niker.eu)

Grünthal, G. and Levret, A., 1998. Conseil de l'Europe. European Macroseismic Scale (EMS).

Grünthal, G., 1998. European macroseismic scale 1998 (EMS-98).

Harris, K.D. and Robinson, N.D., 2013. PRACTICAL SOLUTIONS. STRUCTURE, 18. Available at: https://www.structuremag.org/wp-content/uploads/C-PracSolutions-Harris-March131.pdf

Harun, G. B. (2021) 'Heritage Considerations in Fire Safety Engineering'.

Hendry, A.W., Sinha, B.P. and Davies, S.R. eds., 2017. Design of masonry structures. CRC Press.

Howell, R.W., 2008. Auger processes in the 21st century. International journal of radiation biology, 84(12), pp.959-975.

ICOMOS, V.C., 1964. International Charter for the Conservation and Restoration of Monuments and Sites-Developed at the 2nd International Congress of Architects and Technicians of Historic Monuments. Venice, Italy.

IInd International Congress of Architects and Technicians of Historic Monuments Committee. (1964). Decisions and Resolutions. Venice. (1964). Available at: http://www.international.icomos.org/publications/hommedecin.pdf (Accessed: 22 December 2022).

ISCARSAH GUIDELINES 2005.pdf (no date). Available at: https://documentcloud.adobe.com/spodintegration/index.html?locale=en-us (Accessed: 25 January 2023).

ISCARSAH Principles. 2003. ICOMOC chapter – Principles for the analysis, conservation and structural restoration of architectural heritage. Int. Scientific Committee on the Analysis and Restoration of Structures of Architectural Heritage.

Karantoni, F.V., Papadopoulos, M.L. and Pantazopoulou, S.J., 2016. Simple seismic assessment of traditional unreinforced masonry buildings. International Journal of Architectural Heritage, 10(8), pp.1055-1077.

Kraiem, M., Gendron, A., Nollet, M.J. and Chouinard, L., 2019. Characterization of the lateral capacity of unreinforced masonry residential buildings in Montreal for seismic risk study.

Lin, Y.W., 2013. Strengthening of Unreinforced Masonry Walls using ECC Shotcrete (Doctoral dissertation, ResearchSpace@ Auckland).

Magenes, G. and Calvi, G.M., 1997. In-plane seismic response of brick masonry walls. Earthquake engineering & structural dynamics, 26(11), pp.1091-1112.

Minh, H. Le et al. (2022) 'Structural damage identification in thin-shell structures using a new technique combining finite element model updating and improved Cuckoo search algorithm', Advances in Engineering Software, 173(July), p. 103206. doi: 10.1016/j.advengsoft.2022.103206.

MIT (2009) Ministry of Infrastructures and Transportation, Circ. N. 617 of 2/2/2009: Istruzioni per l'applicazione delle nuove norme tecniche per le costruzioni di cui al Decreto Ministeriale 14 Gennaio 2008. Italy

Ngu, B.H., Mit, E., Shahbodin, F. and Tuovinen, J., 2009. Chemistry problem solving instruction: a comparison of three computer-based formats for learning from hierarchical network problem representations. Instructional Science, 37, pp.21-42.

Oscier, C., Bosley, N. and Milner, Q. (2008) 'Scholar (13)', Update in Anaesthesia, pp. 112–114.

Pantazopoulou, S. J. (2013) 'State of the Art Report for the Analysis Methods for Unreinforced Masonry Heritage Structures and Monuments', (October).

Pantazopoulou, S.J., 2022. Recommending Modelling Parameters and Acceptance Criteria for Nonlinear Analysis for Seismic Evaluation and Retrofit of Existing Buildings in Canada: Masonry Structures. Revised July 2022. Submitted to the National Research Council of Canada (NRC).

Public Safety Canada, Canadian Red Cross, Natural Resources Canada, & St. John Ambulance. (2011). Earthquakes. Available at:

https://www.getprepared.gc.ca/cnt/rsrcs/pblctns/rthqks-wtd/index-en.aspx (Accessed: 5 December 2023).

Reconstruction: changing attitudes (no date). Available at: https://en.unesco.org/courier/july-september-2017/reconstruction-changing-attitudes (Accessed: 22 December 2022).

Roca, P., Pelà, L. and Molins, C. (2021) ‘The iscarsah guidelines on the analysis, conservation and structural restoration of architectural heritage’, in 12th International Conference on Structural Analysis of Historical Constructions (SAHC).

Salmanpour, A. H., Mojsilović, N. and Schwartz, J. (2015) ‘Displacement capacity of contemporary unreinforced masonry walls: An experimental study’, Engineering Structures, 89, pp. 1–16. doi: 10.1016/j.engstruct.2015.01.052.

Sim, J., Saunders, B., Waterfield, J. and Kingstone, T., 2018. Can sample size in qualitative research be determined a priori?. International journal of social research methodology, 21(5), pp.619-634.

Tomazevic, M., 1999. Earthquake-resistant design of masonry buildings (Vol. 1). World Scientific.

Turnšek, V. and Čačovič, F., 1971, April. Some experimental results on the strength of brick masonry walls. In Proceedings of the 2nd international brick masonry conference (pp. 149-156). Stoke-on-Trent, UK: British Ceramic Research Association.

United Nations Educational Scientific and Cultural Organization (UNESCO). Intergovernmental Committee for the Protection of the World Cultural and Natural Heritage (ICPWCNH), 1983. Operational guidelines for the implementation of the World Heritage Convention. UNESCO, World Heritage Committee.

Valadao, R. M. (2021). 'Seismic Analysis and Assessment of Historic Unreinforced Masonry Structures: A Thesis Submitted to the Faculty of Graduate Studies in Partial Fulfillment of the Degree Requirements for the Degree of Master of Applied Science, Graduate Program in Civil Engineering', (October).

Vamvatsikos, D. and Pantazopoulou, S.J., 2016. Simplified mechanical model to estimate the seismic vulnerability of heritage unreinforced masonry buildings. Journal of Earthquake Engineering, 20(2), pp.298-325.

Vanin, F. et al. (2017) 'Estimates for the stiffness, strength and drift capacity of stone masonry walls based on 123 quasi-static cyclic tests reported in the literature', Bulletin of Earthquake Engineering, 15(12), pp. 5435–5479. Available at: https://doi.org/10.1007/s10518-017-0188-5.

Vintzileou, E. et al. (2015) 'Seismic behavior of three-leaf stone masonry buildings before and after interventions: Shaking table tests on a two-storey masonry model', Bulletin of Earthquake Engineering, 13(10), pp. 3107–3133. Available at: https://doi.org/10.1007/s10518-015-9746-x.

Voula (S. J.) Pantazopoulou, 2022, "Recommending Modelling Parameters and Acceptance Criteria for Nonlinear Analysis for Seismic Evaluation and Retrofit of Existing Buildings in Canada: Masonry Structures", Report to the NRC, September 2022.

http://parkscanadahistory.com/series/chs/10/chs10-1j.htm

https://altonmill.ca/

https://en.wikipedia.org/wiki/Acropolis_of_Athens

https://en.wikipedia.org/wiki/Alhambra

https://en.wikipedia.org/wiki/Angkor_Wat

https://en.wikipedia.org/wiki/Centre_Block

https://en.wikipedia.org/wiki/Colosseum

https://en.wikipedia.org/wiki/Distillery_District

https://en.wikipedia.org/wiki/Gastown

https://en.wikipedia.org/wiki/Great_Pyramid_of_Giza

https://en.wikipedia.org/wiki/Great_Wall_of_China

https://en.wikipedia.org/wiki/Hagia_Sophia

https://en.wikipedia.org/wiki/Notre-Dame_Basilica_(Montreal) https://en.wikipedia.org/wiki/Ontario_Legislative_Building

https://en.wikipedia.org/wiki/Parliament_Hill#/media/File:Ottawa_-_ON_-_Stadtansicht.jpg

https://en.wikipedia.org/wiki/Saskatchewan_Legislative_Building

https://en.wikipedia.org/wiki/Western_Wall

https://fr.wikipedia.org/wiki/Place_Royale_(Qu%C3%A9bec)

https://nrc.canada.ca/en/certifications-evaluations-standards/codes-canada/codes-canada-publications/historical-editions-codes-canada-publications-1941-1998

https://whc.unesco.org/en/list/1208/

https://www.toronto.ca/city-government/planning-development/planning-studies-initiatives/university-of-toronto-st-george-campus-secondary-plan/

https://www.zrs.berlin/en/project/niker-europe-wide-research-project/

Charter of Venice - Origin and significance - Romoe Conservators Network (no date). Available at: https://www.romoe.com/en/conservation/chartervenice/ (Accessed: 24 December 2022). https://issuu.com/patillakme/docs/venice_charter

(Canadian Historic Sites: Occasional Papers in Archaeology and History), http://parkscanadahistory.com/series/chs/index.htm

Venice Charter. (2023, July 7). In Wikipedia. https://en.wikipedia.org/wiki/Venice_Charter

Appendices

Appendix A: Various Methods for Strengthening the Structure

A.1 Requirements for Strengthening

Many codes mandate upgrades for buildings that fall below 33% of current code requirements. A minimum target for upgrading is compliance to 67% of the load. Buildings with strength between 33% and 67% are considered earthquake-prone, while those above 67% are deemed satisfactory, albeit still at risk for significant earthquake damage. Many URM buildings, both un-strengthened and previously strengthened, fall short of the 67% threshold, particularly in seismically active areas of the world (e.g., see Russell & Ingham 2010).

Heritage conservation controlled by International Guidelines (e.g. the Venice Charter and ICOMOS) requires that seismic retrofitting should respect and preserve the building's historical and architectural integrity (Robinson & Bowman 2000). The approach should involve minimal intrusion, maintaining the building's character and allowing for future reversibility as was reviewed in Chapter 2. Retrofitting solutions for this class of structures should aim at strengthening them structurally but also preserving their inherent heritage value.

A.2 Preliminary Assessments and Structural Stabilization

The primary challenge with URM buildings is that they were not originally designed to withstand earthquake loads. Although they can be modified to perform adequately during earthquakes, they inherently lack essential connections that enable the building to function as a unified structure under seismic stress. Regarding URM Material Stabilization, environmental exposure leads to the deterioration of URM over time, causing failures and cracks that diminish the building's effectiveness. External factors like dampness, subsidence, earthquakes, and impacts also contribute to damage. Techniques for repairing cracks, securing lintels, and reinstating damage include the injection of bonding agents like grout or epoxy into the mortar, and the use of various metal-based inserts.

In addressing seismic vulnerabilities in heritage URM buildings specific reinforcement techniques are essential (Croci 1998). Acceptable techniques will ensure minimal visual impact, while enhancing the facade's structural integrity compared to its previously cracked state. However, such interventions are often irreversible, requiring attention to color matching and discreetly concealing any drill holes used for rod insertion. Lintels and arches, typically URM components, benefit from drilled, inserted, and grouted or epoxied rods, offering necessary tensile strength with minimal visual disturbance. Addressing the use of lime mortars, it's crucial to use new lime mortars for repointing to avoid compatibility issues with Portland cement mortars.

For mitigating falling hazards, especially in URM buildings adorned with architectural elements like parapets and chimneys, targeted strengthening like attaching steel sections along parapets and securing chimneys to building diaphragms, offers robust solutions with minimal aesthetic impact and potential for reversibility. Similarly, decorative plaster elements can be secured using bolted connections, with more intricate features like plaster finials or balusters stabilized using epoxied bolts and stainless-steel wires. These approaches ensure safety while respecting the building's heritage character.

In seismic retrofitting of Unreinforced Masonry (URM) buildings, one crucial aspect is the enhancement of floor and roof connections, as identified by FEMA 547 and Robinson & Bowman (2000). These buildings often lack adequate connections between diaphragms and walls, a deficiency that can lead to catastrophic collapse during earthquakes. Strengthening these connections involves adding a network of ties and securing walls to floor and roof diaphragms to counter shear forces and prevent separation under lateral loads. Horizontal diaphragms like floors or roofs play a vital role in load distribution and building integrity, but their connections are often weak or absent and require upgrading. Without ties, walls behave like unsupported cantilevers, increasing the risk of dislodgement of floors and roofs, a common failure mode in earthquakes. The effectiveness of tied walls is also influenced by various factors, including the presence of cross walls, columns, buttresses, and their thickness and length. For instance, lower-level walls in URM buildings, being multi-leaf in construction, offer considerable out-of-plane resistance and shear response.

According to Russell (2010), timber is a common flooring material in URM buildings, though concrete is also used. The connection strategies vary depending on the direction of the floor joists, often involving additional timber components and steel fasteners to ensure firm attachment to the URM walls. This method can be visually unobtrusive if executed with care, considering the available new hardware and materials.

A.3 Improving Existing Walls

In seismic retrofitting, it is crucial to enhance existing walls with a focus on preserving architectural integrity, particularly in prominent areas like façades and public spaces. The challenge lies in reinforcing Unreinforced Masonry (URM) walls without altering their thickness or compromising their aesthetic appeal.

A.3.1 Out-of-Plane Strengthening

In seismic retrofitting, enhancing the out-of-plane strength of URM walls is essential due to their inherent weakness against non-compressive forces, as Rutherford & Chekene (1990) observed. For walls lacking sufficient thickness or additional structural support like cross-walls or buttresses, various strengthening techniques are required. One method is to install vertical steel sections inside the wall at appropriate intervals, transforming a large wall into effectively buttressed segments. This method is adaptable to various building types, depending on whether visible steel aligns with the building's character or can be architecturally integrated. This approach is reversible if it involves bolting to existing structures without significant loss of historic material.

Previously, these systems were designed to support floors in case of wall failure. Another strategy includes horizontal steel members mid-wall height, braced with diagonal struts to the floor or ceiling, which may be more appropriate for conserving features like cornices. These methods, along with substitutes like concrete or timber, require careful consideration for visual impact and material loss, especially when recessed into the wall.

Post-tensioning, as Ismail et al. (2010) describe, is another effective method for out-of-plane strengthening. It involves drilling cores through URM walls and inserting tensioned steel rods, modifying the wall's stress behavior under bending forces, and enhancing shear strength. While visually unobtrusive, this technique requires careful consideration regarding access, wall thickness, and potential loss of historic material.

Other core reinforcement methods include non-stressed bars set in grout, offering similar visual and reversibility impacts as post-tensioning but with less structural effectiveness. Additionally, techniques like near-surface mounting (NSM) of fiber-reinforced polymer (FRP) strips in vertical saw cuts within URM, as Dizhur et al. (2011) discuss, provide an effective yet minimally invasive strengthening solution, particularly in plastered or repainted walls. Each method has its pros and cons, requiring careful evaluation to balance structural needs with preservation of historic integrity.

Figure A. 1. Struts Extending from the Upper Floor Enhance the Out-of-Plane Stability.
Dizhur et al. (2011)

A.3.2 In-Plane Strengthening

In-plane strengthening of Unreinforced Masonry (URM) walls, essential for transferring shear loads, can often be achieved by enhancing the capacity of existing walls rather than adding new structures. This reinforcement usually involves applying an additional layer of material to the URM surface, thereby increasing its strength. While some methods like post-tensioning alter the wall structure itself, most strategies involve adding an independent structural layer over the URM, creating new shear walls.

One critical aspect of in-plane strengthening is addressing the reduced stiffness in wall sections with openings, as these are more prone to failure during earthquakes. Historically, filling these openings has been suggested to make the wall continuous, enhancing its uniformity and strength. However, this method should be considered cautiously due to potential alterations to the building's character and the challenge of matching brick and mortar colors. The reversibility of this method varies; using brick for infilling offers some level of reversibility, whereas concrete infilling is less so and can also impact the wall's ductile behavior due to stiffness mismatches. Localized steel cross bracing near openings is another viable solution, although its visibility and potential impact on the building's character must be carefully evaluated before implementation.

Figure A. 2. In-Plane Strengthening. Dizhur et al. (2011)

A.4 Advanced Building Strengthening Methods

In seismic retrofitting, especially for taller buildings with Unreinforced Masonry (URM) walls, new strengthening systems are often required. These URM walls, typically featuring a series of piers with openings, lack adequate planar surfaces to form effective shear walls, making them prone to earthquake damage. To address this, various strengthening techniques are employed.

One such method is the use of moment frames, which are highly adaptable in providing additional horizontal resistance. They may also be customized to fit the specific architectural character of the building offering minimal spatial disruption. The frames comprise beams and columns and can be fitted to masonry piers either inside or outside, depending on their impact on the building's aesthetic. While steel moment frames are ductile and need to be compatible with the existing URM structure's stiffness, concrete frames present a different set of challenges and opportunities. These frames can be integrated into the existing structure or constructed separately, emphasizing the preservation of architectural character and historic material. Steel moment frames offer higher reversibility due to their mechanical connections, whereas concrete frames, though less reversible, can sometimes be better concealed.

Another technique involves braced frames, which come in configurations like concentric, tension-only concentric, eccentric, and ‘K’ bracing. Unlike moment frames, braced frames include diagonal braces that prevent continuity between spaces on either side of the frame and are typically more rigid, being constructed from steel. While efficient in transferring horizontal forces, braced frames pose design challenges, especially in façades with windows, as diagonal braces crossing openings can disrupt the design. Nonetheless, they can be effectively used in secondary spaces and, with careful design consideration, can fit into the building's architectural context. Steel braced frames generally offer good reversibility and can provide robust strengthening when appropriately applied.

Figure A. 3. Braced Frame. (Dunning Thornton Consultants)

In the context of strengthening Unreinforced Masonry (URM) buildings, shear walls play a pivotal role. They are either integrated into existing URM structures or added as new elements to enhance strength. Common materials for shear walls include gypsum plasterboard, particle board, plywood, or plate steel, as indicated by Robinson & Bowman (2000). These materials are usually bolted to the URM via a supplementary structure. However, this approach can cover the surface of URM, potentially impacting decorative elements and increasing wall thickness, which may affect the interior space and aesthetics. While stand-alone shear walls offer an alternative, they present similar challenges in terms of visual impact.

During the 1980s, Shotcrete shear walls were prevalent, involving the application of concrete onto URM walls to create a new wall layer. Although this technique provides substantial strength, it is now often considered unacceptable due to its intrusive nature, significant increase in wall thickness, and difficulty in removal. Furthermore, the installation of Shotcrete typically requires extensive interior alterations, leading to the loss of heritage material. An alternative approach uses fiber-reinforced polymer (FRP) sheets, which, while permanent, offer a less invasive option compared to Shotcrete. However, FRP sheets are impermeable, potentially leading to moisture-related issues such as damp and mold.

Diaphragms distribute lateral forces and help unify the building structure at each level, making a building more resistant to earthquake damage. Floor diaphragms typically consist of chords, sheathing material, and supplementary structure, requiring mechanical fastenings for shear and tensile loads. The visual impact of these diaphragms varies; new sheathing may affect the character of historic flooring, although innovative designs can mitigate this. Ties to external walls may require visible metal load spreaders, but many New Zealand buildings have accepted these as part of the strengthening process. Roof diaphragms can be more easily integrated, especially in areas with suspended ceilings or where roofing is being replaced.

Finally, foundation upgrades are often necessary in URM buildings to support the additional loads from new strengthening elements. Techniques include enlarging existing foundations and introducing ground beams for increased stiffness. While foundations themselves may not hold significant heritage value, the ground level floor often does, necessitating careful consideration during strengthening to minimize damage to above-ground heritage elements.

A.5 Reduction of Forces

In seismic retrofitting of Unreinforced Masonry (URM) buildings, reducing the building's mass is a strategy to lessen seismic forces, as seismic actions are proportionate to the building's mass. However, past experiences, as noted by Robinson & Bowman (2000), show that indiscriminate removal of mass, especially decorative elements like parapets and chimneys, can detrimentally affect heritage value. More minor approaches, such as removing internal URM partitions, are preferable to preserve architectural integrity.

Base isolation, a newer method, involves introducing a damping layer between the building and the ground, effectively isolating the building's mass from ground movement-induced lateral loads. This technique, while minimizing the need for strengthening above ground level, is not without its challenges, including extensive foundation strengthening and being generally irreversible and costly. Another less commonly used approach is the installation of energy dissipaters or dampers, acting like hydraulic cylinders to provide resistance during seismic activity. These are most effective in flexible buildings but are expensive and challenging to integrate aesthetically. Torsion, caused by asymmetry in the building's mass and structural stiffness, can significantly contribute to seismic forces. Aligning the building's center of mass with its center of stiffness can mitigate torsional effects. Strategies to address torsion involve uniformly distributing the building's stiffness, either by reinforcing weaker walls or reducing stiffness in stronger walls through methods like vertical saw cuts. However, the architectural impact of these interventions must be carefully considered. (Goodwin, C., Tonks, G., and Ingham, J. 2011)

A.6 Approaches to Seismic Improvement

In the seismic improvement of heritage buildings, the architecture and layout significantly influence the selection of strengthening methods. While considering the most efficient structural systems, it is crucial to evaluate their overall impact on the building, particularly in terms of visual, functional, and heritage aspects. The reversibility of these improvements and the extent of historic material removal are also key considerations. For instance, walls with multiple openings might not be suitable for shear walls or diagonal bracing but could be apt for moment frames. Conversely, an ornate brick wall might not accommodate moment frames well, but post-tensioning bars could be more fitting. In industrial buildings with existing exposed steel structures, additional steel, distinct from the original structure, can be an effective solution. The placement of new structures should ideally be close to the load sources to minimize the need for extensive modifications. It's generally advised against subdividing significant interior spaces, as intrusive bracing in walkways or central areas can disrupt the building's spatial harmony.

Regarding visibility, concealing new structures is not always necessary. Sometimes, it's preferable to integrate these elements as part of the building's evolving history, especially if done with architectural sensitivity. (Goodwin, C., Tonks, G., and Ingham, J. 2011)

A.7 Practical Application Methods to Strengthen URM Buildings

The following sections present some examples covering key aspects:

A.7.1 Adding Steel Bracings

Installing steel braces or frames can significantly enhance the lateral stability of the structure. These braces are anchored to the building's walls and provide additional support.

Figure A. 4. Strengthening the Buildings with Steel Bracings, (SSG Urban Outfitters)

A.7.2 Diaphragm Reinforcement

Diaphragm reinforcement involving the addition of timber slabs to the floor diaphragm is designed to enhance a building's ability to withstand seismic forces. In this method, timber slabs are integrated into the existing floor structure, strengthening the diaphragm and improving the overall seismic resilience of the building. Assessment and Planning outlines the placement, size, and integration of timber slabs to reinforce the floor diaphragm effectively. Timber slabs are strategically placed within the floor structure, usually perpendicular to the existing floor joists or trusses. This strategic orientation ensures optimal load distribution. Timber slabs are securely attached to the existing structure using appropriate fasteners, ensuring a stable and reliable connection. Bolts, screws, or other fastening methods compatible with both timber and existing materials are utilized. Timber slabs add flexibility to the floor diaphragm, allowing it to absorb seismic forces and distribute loads effectively. The integration of timber slabs significantly enhances the diaphragm's resistance to lateral movements during seismic events, minimizing structural damage. Timber slabs must be compatible with existing building materials to ensure seamless integration. Proper compatibility ensures structural cohesion and effectiveness in reinforcing the diaphragm. Timber slabs must have the necessary load-bearing capacity to support additional loads. (Goodwin, C., Tonks, G., and Ingham, J. 2011)

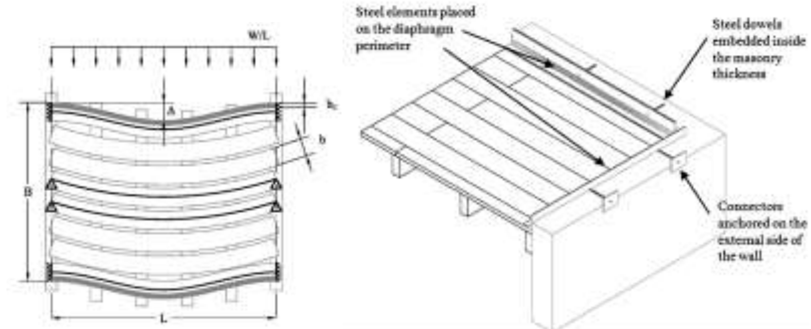

Figure A. 5. The Mathematical Model (Brignola, Pampanin and Podestà, 2012)

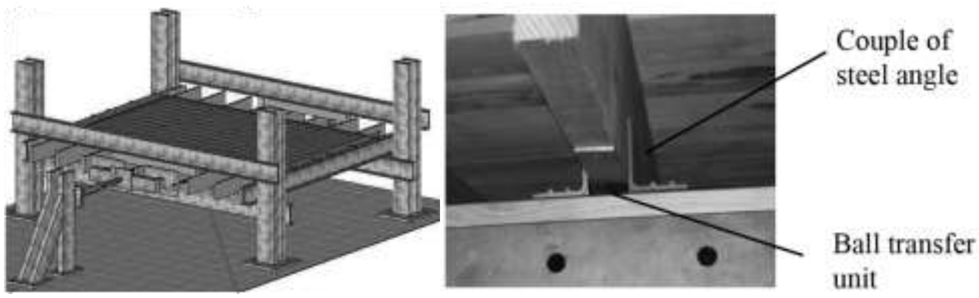

Figure A. 6. Detail of Diaphragm Specimen, (Brignola, Pampanin and Podestà, 2012)

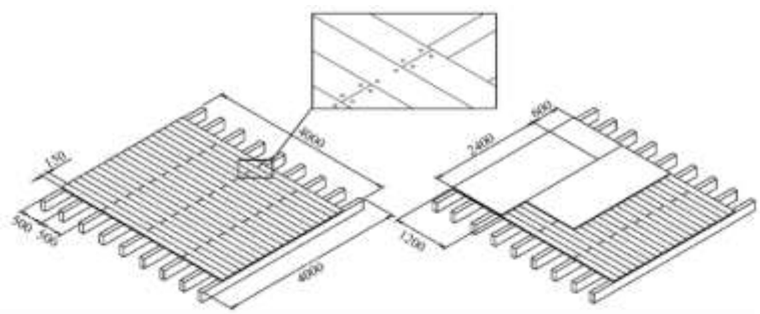

Figure A. 7. Diaphragm Reinforcement Details, (Brignola, Pampanin and Podestà, 2012)

A.7.3 Timber Diaphragm Specimen Preparation

Braces are placed diagonally between structural elements like roof trusses or floor joists, forming an 'X' shape. This arrangement offers maximum stability. Braces are securely fastened to structural components using appropriate connectors, ensuring a strong and stable connection. Timber braces provide flexibility, allowing controlled movement during seismic events without compromising structural integrity. Timber bracing can be seamlessly integrated into historic structures, preserving their original appearance while enhancing stability. (Giongo *et al.*, 2015)

Figure A. 8. Timber Cross Bracing (Giongo *et al.*, 2015)

A.7.4 Fiber Reinforced Polymers

Fiber-reinforced polymers (FRP) fall within the category of materials known as composites. Composites are created by combining two or more original materials to produce a superior compound with enhanced properties compared to its individual components. Typically, FRP materials consist of robust continuous fibers embedded within a polymer matrix, or resin. These fibers serve as the primary reinforcement, while the polymer matrix acts as a binder, safeguarding the fibers and facilitating the transfer of loads between them. In the construction sector, there are three primary types of fibers utilized: E-, S-, and Z-glass fibers, aramid fibers, and carbon fibers (including ultra-high modulus and high-strength variants). Thermosetting matrices are formed through the application of heat and once set, do not melt or soften upon reheating or exposure to solvents. Thermosetting resins, widely preferred for their superior mechanical performance, exhibit excellent impregnation and adhesion properties with fibers. Generally, resins can be composed of polymers, metals, or ceramics. Among these, polymers are the most used material due to their straightforward manufacturing process and relatively low production costs. (Oliveira, D.V., Basilio, I. and Lourenço, P.B., 2010)

Figure A. 9. Strengthening the Structure with Fiber Reinforced Polymer, (Oliveira, D.V., Basilio, I. and Lourenço, P.B., 2010)

A.7.5 Reinforcement with Steel Shear Walls

A shear wall is a wall designed to resist lateral loads, such as those caused by earthquakes, in a building. In fact, reinforcing with shear walls increases the structural rigidity and shear resistance of the building, reducing the impact of external forces on the structure and thereby preventing deformations in its components. By reinforcing walls with steel elements, the structure gains increased strength and structural integrity, making it more resilient and capable of withstanding seismic activities. Shear walls are used in building reinforcement when structural elements (such as beams and columns) are vulnerable to seismic forces and lateral loads. In addition, due to the greater rigidity of shear walls compared to braces, the number of openings required for accommodating them is fewer than the openings needed for braces. As a result, it creates fewer architectural challenges. These steel shear walls are strategically placed within the building, providing stability and reducing its vulnerability to horizontal movement.

The use of shear walls significantly enhances the resistance, stiffness, and ductility of a structure. It improves the seismic behavior of the building and reduces deformations and damage to other concrete elements. When the beams and columns of a reinforced concrete structure can withstand gravity loads but are vulnerable to seismic forces, adding shear walls absorbs lateral seismic forces, preventing these forces and seismic deformations from affecting the beams and columns. Consequently, incorporating just two or four shear walls reduces the vulnerability of all beams and columns. However, it is crucial to note that due to the high rigidity of shear walls, substantial forces are typically exerted on the foundation beneath them. Addressing this requires reinforcing the existing foundation significantly or adding piles at the base of shear walls. The connection between shear walls and the structure must be designed to transfer lateral loads to the walls effectively. Proper connections, usually made using bolts between the shear wall and the slab, are essential. Additionally, utilizing bolts in beams, columns, and embedding them in the concrete of shear walls ensures a strong bond between the walls and the existing structure. Continuous reinforcement bars in shear walls across the floors allow seismic forces to be uniformly transmitted from top to bottom, ultimately reaching the foundation. (A.Charleson, 2008), (Blagojević, Brzev and Cvetković, 2023)

Figure A. 10. Strengthening the Structure with Jacketing in an Older Brick Masonry Building in California, USA (Photo: J. Shestorbitoff). (A.Charleson, 2008)

A.7.6 Strengthening Structural Buildings Using Shotcrete Method

Strengthening structural buildings using the shotcrete method involves applying a layer of high-strength concrete mixed with fibers or mortar mix onto existing surfaces. This technique is commonly used to reinforce and enhance the structural integrity of buildings and other structures. The shotcrete method utilizes a high-pressure hose to spray the concrete mixture onto surfaces, forming a durable and tightly adhering layer. This process helps improve the strength, durability, and overall stability of the structure, making it more resistant to various external forces and extending its lifespan. Adding fibers, such as glass or polymeric fibers, to the mortar or grout mix can enhance the tensile strength of the masonry. Fiber reinforcement helps prevent cracking and improves the masonry's ability to withstand seismic forces.

Figure A. 11. Strengthening Structural Masonry of Building with Shotcreting Method, (Çakıroğlu et al., 2021)

A.7.7 Adding Reinforcement Bars (Rebars)

Inserting steel reinforcement bars into the masonry walls and securing them with grout or mortar improves the overall structural integrity. This method is often used in combination with shotcreting.

A.7.8 Retrofitted URM Wall with RC Jacketing

The RC jacketing method involves creating one- or two-sided RC jackets that are affixed to the exterior and/or interior surfaces of walls. These jackets consist of a 3 to 5 cm thick concrete overlay reinforced with a steel mesh (typically small-size bars, 4 to 8 mm in diameter). Attaching RC jackets to existing masonry walls is done using steel anchors placed in pre-drilled holes, which are later filled with cement- or epoxy-based grout. The size and spacing of these anchors depend on seismic requirements and the desired jacket thickness. The RC jackets can be made using either cast-in-place concrete or sprayed concrete (shotcrete). The figure below illustrates a retrofitted URM wall with RC jacketing, including components like the existing masonry wall, layers of concrete, steel wire mesh, steel anchors, grouted holes, and cement-based plaster. (Blagojević, Brzev and Cvetković, 2023)

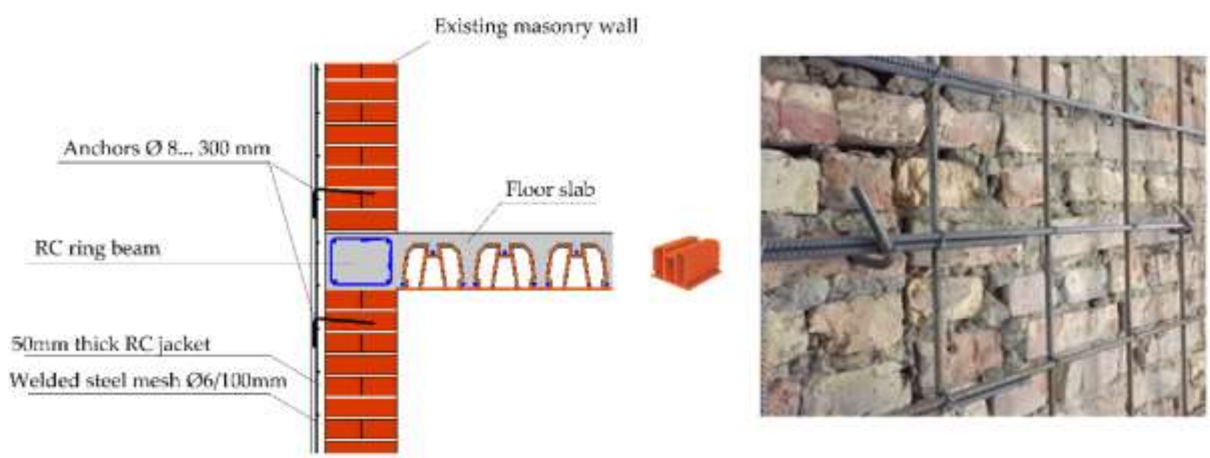

Figure A. 12. Retrofitted URM Wall with RC Jacketing, (Blagojević, Brzev and Cvetković, 2023)

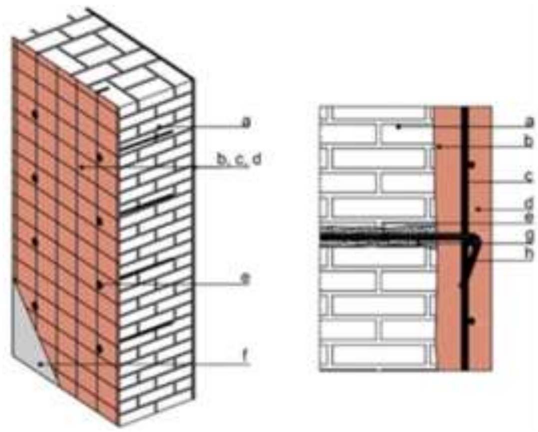

s

Figure A. 13. A Schematic Diagram of a Retrofitted URM Wall with RC Jacketing (Legend: (a) Existing Masonry Wall; (b) First Layer of Concrete; (c) Steel Wire Mesh; (d) Second Layer of Concrete; (e) Steel Anchors; (g) A Grouted Hole; (f) Cement-Based Plaster; and (h) A Steel Anchor with a 90-Degree Hook. (Blagojević, Brzev and Cvetković, 2023)

A.7.9 Repointing with Cement Mortar for Brick Walls

Re-rendering brick walls with high-quality mortar involves applying a new layer of cement mortar over existing brick surfaces. This process serves to improve the mechanical strength and durability of the wall. By using a superior mortar mix, the structural integrity of the wall is enhanced, making it more resistant to wear and environmental factors. Pointing stone buildings with cement mortar is another technique used to enhance the structure's stability and appearance. In this process, the gaps or joints between individual stones are filled with cement mortar. This not only provides a neater and more uniform look but also significantly enhances the adhesion between the existing stones. Proper pointing ensures a secure bond, especially for loose or irregularly shaped stones, creating a more unified and stable structure. (Khan, Akhtar and Hussain, 2019)

Figure A. 14. Strengthening Structure of Building with Repointing Method, (Khan, Akhtar and Hussain, 2019)

A.7.10 Closing Openings

Sections of a structure where doors and windows are located are most susceptible to collapse during pressure or seismic events. Several strategies are employed to address this issue. One approach is to close non-essential windows or doors. By eliminating unnecessary openings and replacing them with columns or walls, the resistance of the walls can be increased significantly. The fundamentals of historic masonry restoration, and brick repair, Infinity Design Solutions, Available at: https://www.ids-dmv.com/ids-resources/.

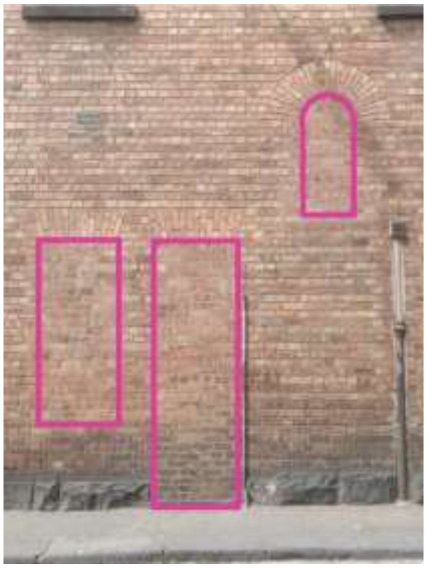

Figure A. 15. Strengthening Structure of Building with Closing the Opening, https://www.ids-dmv.com/masonry/brick-infills-in-historic-masonry-walls/

The brick infill technique involves adding new brick walls within existing buildings, often done during interior layout changes. While not always structurally necessary, this method aims for aesthetic consistency. Historic bricks are sometimes salvaged for this purpose, although perfect matches are challenging due to variations in fabrication methods and brick age. Special bricks and mortar might be sourced for closer matches, especially in spot repairs. Spot repair focuses on critical areas but isn't always recommended, especially when the existing mortar is older than its expected lifespan. In the process, differences in mortar consistency and placement depth are noticeable between old and new sections. Mortar joints in infill areas are often installed closer to the outer brick surface for aesthetic reasons, matching the original appearance during wholesale pointing efforts. While recess depth choices are subjective, aligning infill mortar with the newer pointing mortar is a common practice during maintenance tuckpointing, ensuring visual harmony across the entire wall. (https://www.ids-dmv.com/masonry/brick-infills-in-historic-masonry-walls/)

A.7.11 URM Parapet Bracing

URM parapet bracing refers to the reinforcement and support structures added to the upper edges of unreinforced masonry (URM) walls, known as parapets. These bracing elements are implemented to enhance the stability and seismic resistance of URM buildings. By reinforcing the parapets, which are vulnerable areas in URM structures, the risk of collapse during seismic events is significantly reduced. URM parapet bracing involves adding materials such as steel bars, concrete, or other strengthening elements to fortify these architectural features, ensuring the building's overall structural integrity.

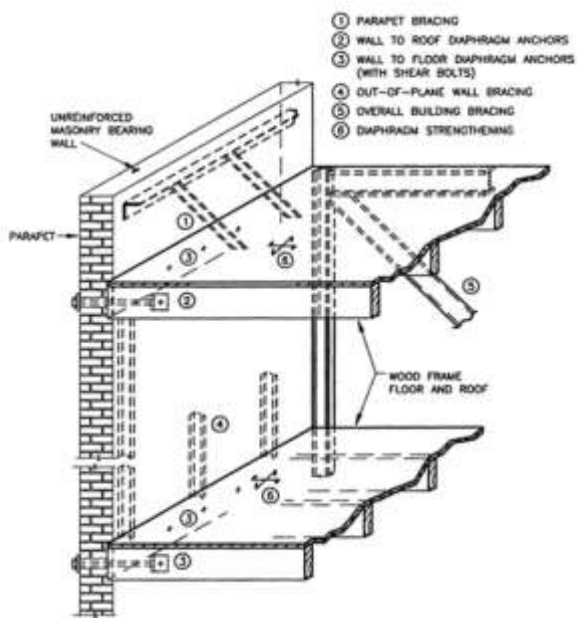

Figure A. 16. URM Bracing, *ASCE 31-03*

A.7.12 URM Wall Anchorage

URM wall anchorage is a critical aspect of reinforcing unreinforced masonry (URM) buildings to enhance their seismic resistance. To prevent out-of-plane loading and potential catastrophic failures during seismic events, URM walls need to be securely tied to the horizontal diaphragms, including the roof and floors. Various methods can be employed for this purpose. One common technique involves through-bolting the walls to the diaphragms using large bearing plates on the exterior. However, this method presents visual challenges and restrictions in terms of egress.

Another widely used approach is the use of epoxy anchor adhesives installed at an angle through multiple layers of URM wall (referred to as wythes). These adhesives provide both tensile and shear resistance, creating a robust connection between the URM wall and the roof or floor. Grouted anchors are another option, although they have undergone less rigorous testing compared to epoxy anchor adhesives. Choosing the optimal location for these anchors can be challenging, especially in URM buildings that utilize beam pockets to support joists. An effective strategy involves installing the wall anchor at a distance from the beam pocket, as this configuration enhances its performance. Ideally, selecting an anchor location at the midpoint between framing members is more favorable. However, this may require additional framing elements to attach the anchor to the joist effectively. Careful consideration of these factors is essential to ensure the URM wall anchorage is both structurally sound and effective in enhancing the building's seismic resilience.

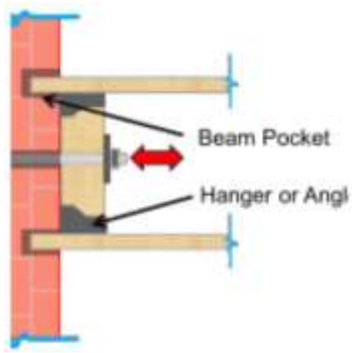

Figure A. 17. Image Credit: Sam Hensen, Simpson Strong-Tie. Structural engineering Blog. (https://seblog.strongtie.com/2013/04/seismic-retrofit-of-unreinforced-masonry-urm-buildings)

A.7.13 Implementation of Bracing

To enhance the structural integrity of unreinforced masonry buildings, steel bracing elements, like plates and profiles, are directly affixed to the walls or structural diaphragms. This method is vital when dealing with buildings showing considerable deflection. Calculations must consider the relative stiffness of both the original structure and the added steel bracing. This approach is especially useful when the URM walls exceed the specified height-to-thickness ratios in the International Existing Building Code (IEBC). Bracing elements, such as steel or wood columns (strong-backs), are attached between diaphragms to prevent out-of-plane movement and bolster the URM wall assembly's lateral strength, particularly during seismic events. These braces absorb and dissipate seismic energy during an earthquake, reducing the lateral movement of the building.

Steel braces absorb these forces, preventing excessive movement and reducing stress on the masonry walls. The braces deform and absorb seismic energy through elastic and inelastic behavior, safeguarding the building from severe damage. Braces provide stiffness, ensuring the building doesn't sway excessively. Additionally, they offer ductility, allowing controlled deformation to prevent sudden failure. CBFs significantly enhance the building's lateral strength, enabling it to withstand seismic forces. (Paxton, B., 2014). Romanian Seismic Code (P100-1/2006).

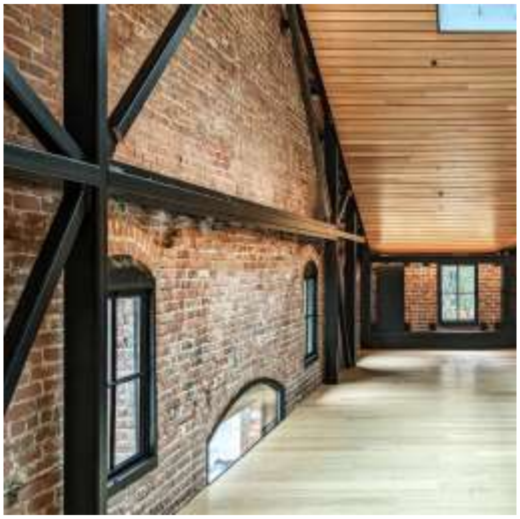

Figure A. 18. Reinforcement of Masonry Wall with Steel Columns and Cross Bracing.
(American Institute of Steel Construction)

A.7.14 Use of Vertical Tie Columns

During earthquakes, partial collapse and detachment of walls in corners and T-shaped connections made of masonry materials are often observed. When these failures occur but the walls remain standing, the use of vertical tie columns is required. This involves carefully removing adjacent sections. It's important to note that the execution of tie columns must be symmetrical in plan, and these columns should be connected to each other at the level of the floors. The dimensions of tie columns are determined based on the dimensions of the walls connected to them and should not be less than 20 centimeters in any case. The distance between these tie columns should not exceed 5 meters. In cases where brick materials in corners remain undamaged or are impossible to remove, separate steel bars are used inside the walls instead of constructing tie columns. In this scenario, the steel bars are placed within vertical channels cut inside the brickwork and are supported and anchored to the walls using lateral hooks known as "rack pins. (Schacher, T., 2009)

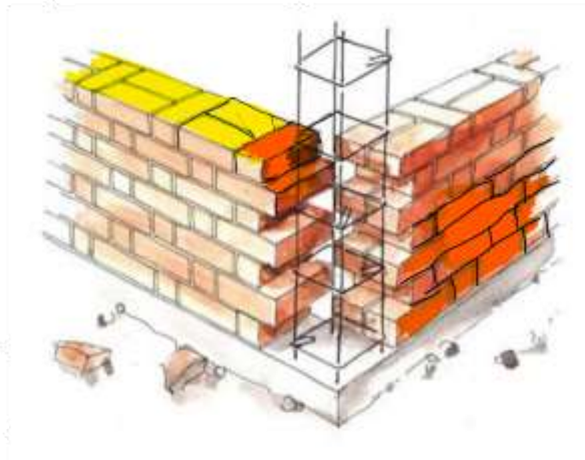

Figure A. 19. Strengthening the Structure of the Building with Vertical Tie Columns, (Schacher, T., 2009)

A.7.15 Adding Buckling Restrained Braces (BRB)

Using buckling restrained braces (BRB) is one of the methods employed for strengthening buildings, especially in multi-story structures. BRBs are a relatively modern technique in structural reinforcement and find applications in strengthening masonry buildings.

Figure A. 20. Strengthening the Structure of Building with Adding Buckling Restrained Braces, (Zhou *et al.*, 2021)

A.7.16 Adding Shear Walls

Constructing new reinforced shear walls inside the building or on the exterior can enhance lateral stability. Shear walls are designed to resist horizontal forces and prevent the building from swaying excessively during seismic events. In structural construction, building shear walls is a common and cost-effective practice, executed either vertically or diagonally. These walls are typically constructed in a staggered pattern to create a connection, known as "lock and key," within the building's framework. Shear walls are often built at the intersection of walls, forming an additional structural element that reinforces the building from all sides, increasing its resistance to lateral forces and earthquakes. When the building's layout allows for spaces to be interconnected, combining thick walls with shear walls enhances the structure's seismic performance. This method contributes to the improved seismic behavior of masonry buildings.

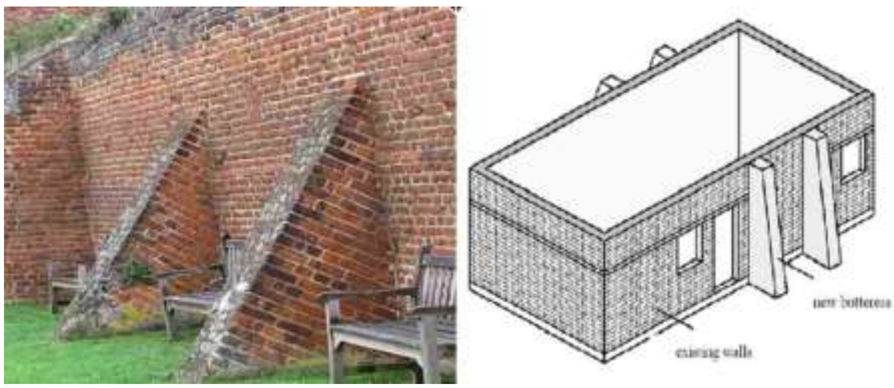

Figure A. 21. Strengthening the Structure of the Building with Shear Walls, (Khan, Akhtar and Hussain, 2019)

A.7.17 Adding Central Cores

Adding central cores refers to the process of enhancing the stability of a masonry building wall by inserting a core, which is filled with grout, into the center of the wall. This technique transforms the behavior of the wall, making it similar to a reinforced wall. For this transformation to be effective, the grout used must establish a strong bond between the strengthening elements (such as the core) and the existing materials of the building. This bond is crucial for transferring seismic forces effectively. Additionally, the properties of the grout, including its strength and elasticity, must be compatible with the existing building materials to ensure the structural integrity and stability of the wall.

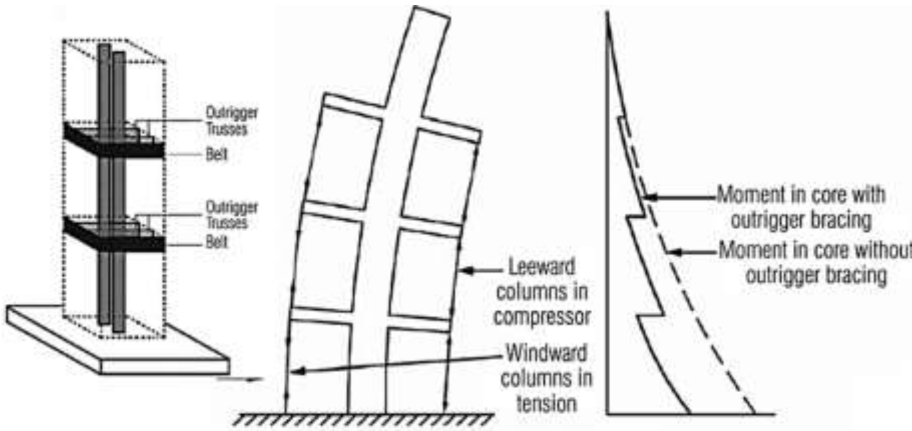

Figure A. 22. Strengthening the Structure of the Building with Adding Central Cores, (Memon *et al.*, 2020)

A.7.18 Construction of New Structural Walls

Aligning the center of mass and stiffness can prevent torsional movement during an earthquake. To achieve this, constructing new walls (while adhering to architectural principles) can create symmetry in the building. Even the addition of intersecting walls on long walls can increase their load-bearing capacity. Proper connection between new and existing walls should be ensured by using steel and concrete keys embedded in the walls, creating a strong bond between the old and new walls.

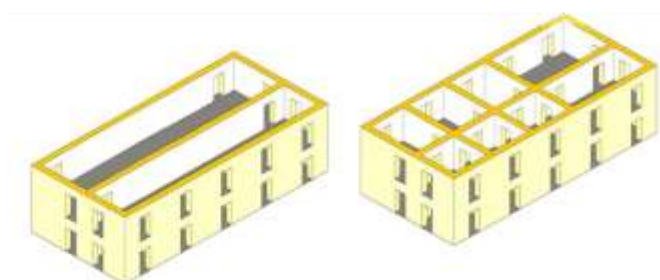

Figure A. 23. Strengthening the Structure of the Building with Construction of New Structural Walls. (https://dogoharani.com)

A.7.19 Column Strengthening Using Steel Jackets

Column strengthening using steel jackets involves encasing existing columns in high-strength steel casings. This process enhances load-bearing capacity, structural integrity, and seismic resistance. Steel jackets are precisely fitted and anchored to the column, improving overall stability and ensuring the column can support heavier loads. This method is cost-effective and widely used in retrofitting existing structures.(Latifi *et al.*, 2023)

Figure A. 24. Strengthening the Structure of the Building with Steel Jackets, (Latifi *et al.*, 2023) https://www.mdpi.com/1996-1944/16/5/1882

A.7.20 Crack Stitching

Stitching cracked walls is a repair technique used to fix cracks in walls, especially those caused by structural issues or settlement. In this method, metal staples or stitches are inserted across the crack and secured with epoxy or other bonding agents. These stitches bridge the crack, preventing it from widening and reinforcing the wall's stability. Stitching cracked walls is a reliable way to strengthen and restore the integrity of damaged structures.

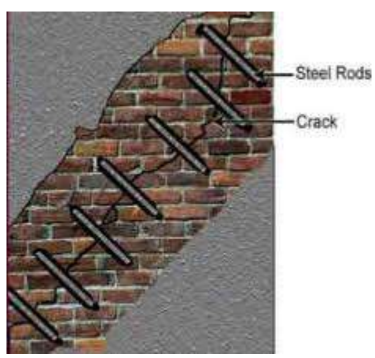

Figure A. 25. Strengthening the Structure of the Building with Crack Stitching, (Khan, Akhtar and Hussain, 2019)

Inserting bars in strengthening structures involves placing helical steel bars into existing masonry, concrete, or brickwork to enhance their structural integrity. Bars are designed with a twisted, helical shape that allows them to be securely embedded in building materials. Once inserted, these bars are bonded with a high-strength grout or adhesive, creating a strong connection that reinforces the structure. Bars are commonly used for repairing cracks, reinforcing walls, and stabilizing buildings, making them an effective method for strengthening and restoring the integrity of various structures. (Khan, Akhtar and Hussain, 2019)

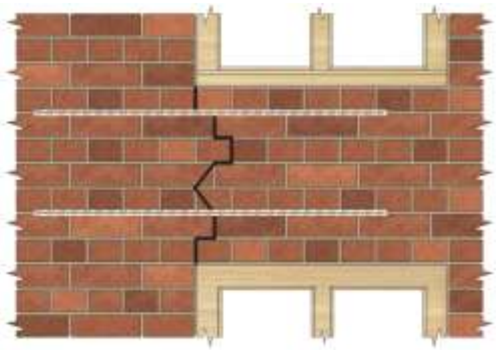

Figure A. 26. Strengthening the Structure of the Building with Crack Stitching (Helifix, 2014)

A.7.21 External Steel Retrofitting with Plate Anchor Connection

In order to strengthen the masonry structure, engineers install steel plates outside the building and anchor it with steel rods. This is done to prevent the masonry bricks from being pushed outwards by the force of the floor timber during an earthquake. External Steel Retrofitting is a method of reinforcing buildings by adding steel elements to the exterior. During an earthquake, buildings are subjected to horizontal movements, which can cause structural damage or collapse. These elements enhance the building's ability to withstand seismic forces, improving overall stability during earthquakes. This method is flexible in design, preserves interior space. These linkages, referred to as wall-to-diaphragm connections, are pivotal in minimizing the vertical height impact on unreinforced masonry (URM) walls when subjected to out-of-plane (OOP) loading. In URM buildings, plate anchors typically comprise two essential elements. The initial component is the wall anchorage, often a through-bolt inserted through a drilled hole with an external bearing plate affixed to the masonry wall. The second part involves the diaphragm connection, which forms a bolted attachment to a section of the timber diaphragm. (Dizhur *et al.*, 2021)

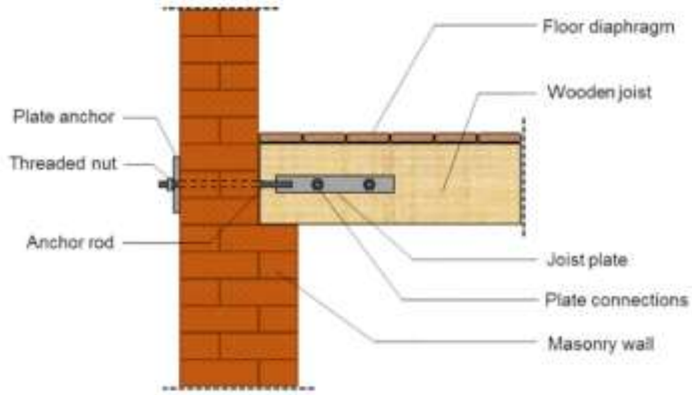

Figure A. 27. A Typical Wall-to-Diaphragm Plate Anchor Connection Configuration. (Dizhur *et al.*, 2021)

Figure A. 28. External Steel Retrofitting with Plate Anchor Connection. (Dizhur *et al.*, 2021)

A.7.22 Cavity Wall Retrofitting

Creating a cavity between the existing masonry wall and a new reinforced concrete or steel frame wall can significantly improve the structure's resistance to seismic forces. The gap acts as a buffer, allowing the masonry to move independently during an earthquake.

Figure A. 29. Cavity Wall Retrofitting. https://www.checkatrade.com/blog/cost-guides/cavity-wall-insulation-cost/

Figure A. 30. A Top View of the Cavity-Wall Section. (Miglietta *et al.*, 2021)

A.7.23 Foundation Strengthening

Strengthening the foundation by underpinning or adding additional foundation elements can improve the overall stability of the structure. This is particularly important in regions prone to liquefaction or soil settlement during earthquakes.

Figure A. 31. Foundation Strengthening, https://engineeringdiscoveries.com/what-is-underpinning-uses-in-foundation-strengthening-and-methods/

Figure A. 32. Foundation Strengthening of masonry building, https://www.horseen.com/index/solution/content/id/1464?page=1

A.7.24 Masonry Jacketing

Applying reinforced masonry jackets involves adding a new layer of reinforced masonry, concrete, or shotcrete on the existing walls. This method enhances both the structural integrity and seismic performance of the building.

Figure A. 33. Masonry Jacketing. (Churilov and Dumova-Jovanoska, 2013)

A.7.25 Masonry Pier and Spandrel Retrofit

The Masonry Pier and Spandrel Retrofit method involves reinforcing specific vertical columns (known as piers) and horizontal members (known as spandrels) within an unreinforced masonry building. Piers support the weight of the structure vertically, while spandrels connect and support the piers horizontally. During the retrofitting process, engineers focus on these vulnerable areas. They add materials like steel beams or concrete to strengthen the piers vertically and use techniques such as steel braces or additional concrete elements to reinforce the spandrels horizontally. This targeted reinforcement enhances the building's ability to withstand seismic forces. Reinforcing piers and spandrels significantly improves the building's stability during earthquakes, preventing collapse and ensuring the safety of occupants. This method exemplifies a precise and efficient approach to enhancing the seismic resilience of unreinforced masonry structures. (Baker, 2007)

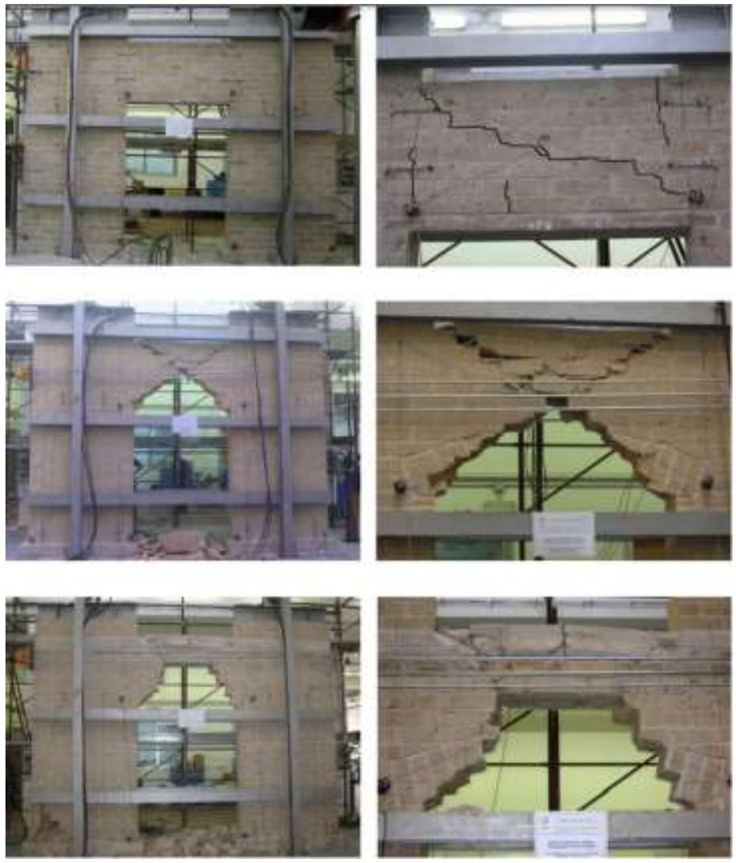

Figure A. 34. Strengthening the Structure of the Building with Masonry Pier and Spandrel, (Baker, 2007)

A.7.26 Retrofitting with Reinforced Concrete

Constructing reinforced concrete elements, such as beams and columns, around or within the existing masonry structure. These concrete elements provide additional strength and ductility, making the building more resistant to seismic forces.

Figure A. 35. Strengthening the Structure of the Building with Reinforced Concrete, https://constrofacilitator.com/retrofitting-of-structures-design-and-techniques/

A.7.27 Adding Mass

Increasing the mass of the structure by adding dense materials, such as concrete or steel, can help improve its seismic performance. The added mass reduces the building's response to ground motion, making it more stable during earthquakes.

A.7.28 Pre-Stressed Rock Bolting

pre-stressed rock bolting involves securing steel rods deeply into the ground to lend crucial lateral support to masonry walls. This technique enhances stability, fortifies against seismic forces, and safeguards the structure during earthquakes. Pre-stressed Bolts are sturdy steel rods inserted deep into the ground behind or within existing masonry walls. The term "pre-stressed" means these bolts are tightened with significant force, creating tension within them, ensuring stability. Existing masonry walls often lack the strength to withstand sideways forces during earthquakes. Pre-stressed rock bolts provide crucial lateral support. By anchoring deep into the ground, they resist horizontal pressures, preventing the walls from collapsing or shifting. The bolts create a stable foundation for the masonry. By anchoring securely into stable soil or rock layers, they essentially anchor the wall, preventing tilting or shifting during seismic events. During earthquakes, buildings experience lateral forces. Pre-stressed rock bolting reinforces masonry, making it resistant to these forces. This reinforcement prevents structural damage, ensuring the safety of the building and its occupants. (Čajka, R., Kozielova, M., Burkovič, K. and Mynarzová, L., 2014)

A.7.29 Brick Infills in Historic Masonry Walls

The infill wall technique involves reinforcing historic masonry walls by constructing new walls within them. This method enhances the structural integrity of unreinforced historic masonry buildings. The new walls, often made of materials like reinforced concrete, are strategically placed inside the existing walls, providing additional support and stability. This technique helps distribute loads effectively, strengthening the building and safeguarding it against various forces, including seismic activity. In essence, it fortifies the original masonry walls, ensuring the historical structure's longevity and resilience. (M. Memari and Aliaari, 2018). When dealing with historic buildings, it is crucial to use preservation-friendly materials and techniques. Lime-based mortars and plasters, for example, are often preferred over modern Portland cement-based materials because they allow the masonry to breathe and flex, reducing the risk of future damage. (M. Memari and Aliaari, 2018)

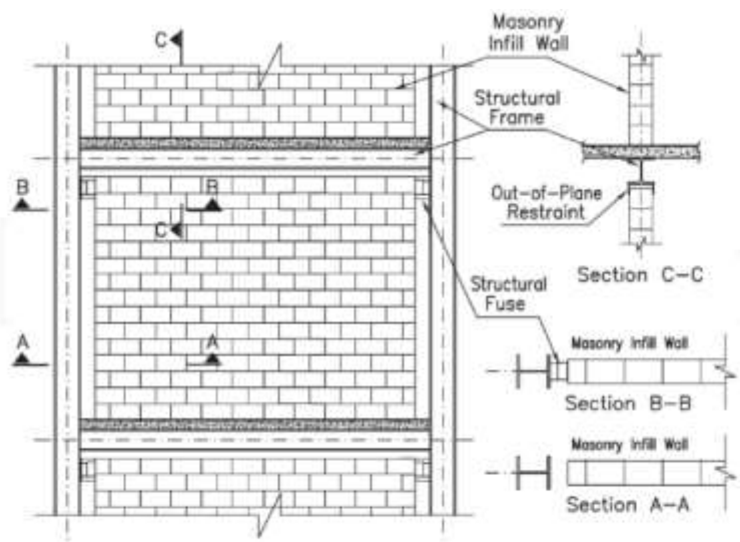

Figure A. 36. Schematic Representation of Fuse Elements in a Masonry Infill Wall (M. Memari and Aliaari, 2018)

A.7.30 Adhesive Anchor Connections

Adhesive anchors are designed to provide additional support and stability to masonry structures, especially during seismic events. By properly installing adhesive anchors, masonry walls can be reinforced to resist lateral forces, prevent out-of-plane failures, and enhance the overall structural integrity of the building. These anchors are particularly valuable for strengthening URM buildings without significantly altering their historical or architectural features, making them a practical choice in preservation efforts. (Dizhur, Schultz and Ingham, 2016a)

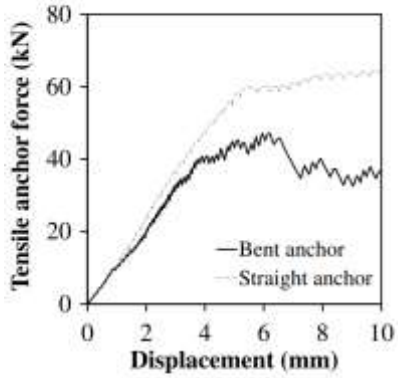

Figure A. 37. Test Results Analysis for Typical Force-Displacement Response for Anchors, (Dizhur, Schultz and Ingham, 2016b).

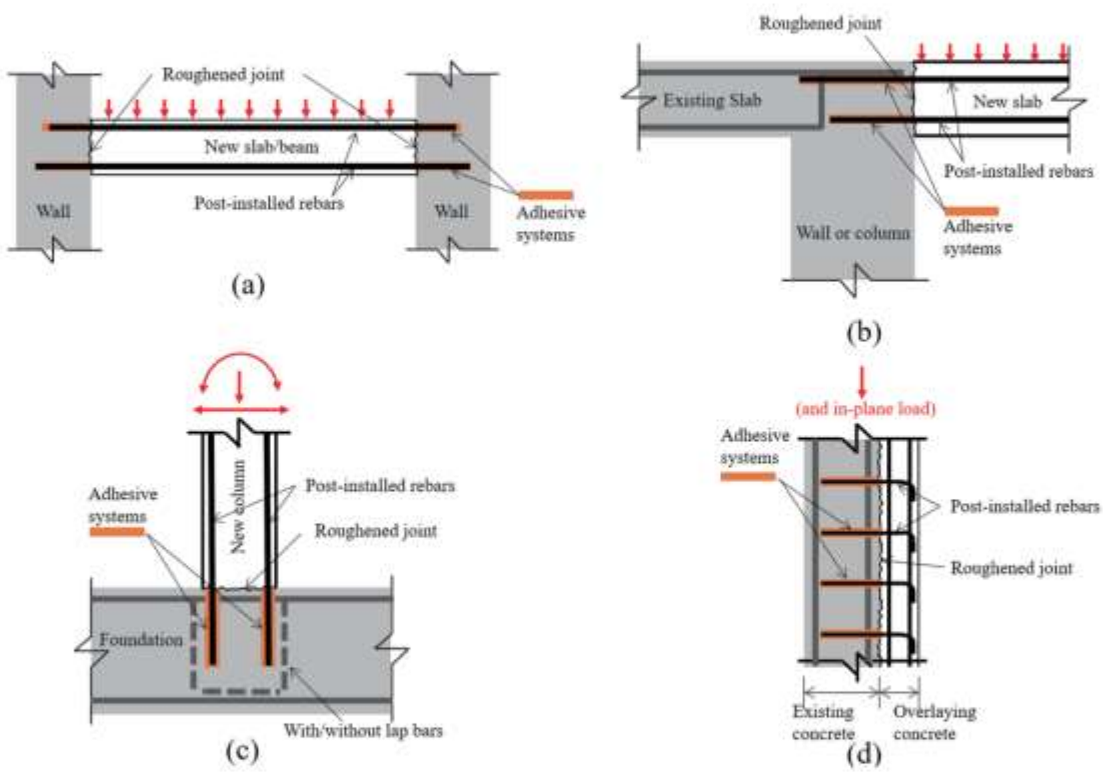

Figure A. 38. Demonstrates Common Uses of Post-Installed Reinforcements: (a) Attaching new Slabs or Beams to Walls (Shear or Diaphragm Walls) using end Anchors. (b) Creating Lap Splices Between new and Existing Slabs. (c) Employing end Anchors, with or without Lap Splices, for Moment-Resisting Connections. (d) Applying new Concrete Overlays for Tasks like Wall Strengthening, Column Jacketing, and Slab Thickening. (Su, Looi and Zhang, 2021)

A.7.31 Base Isolation

Base isolation in seismic retrofitting is a technique used to protect buildings and structures from the damaging effects of earthquakes. It involves placing flexible bearings or isolators between the building's foundation and superstructure. These isolators allow the building to move independently of the ground motion during an earthquake, effectively decoupling the structure from the shaking of the earth. The primary purpose of base isolation is to absorb and dissipate seismic energy, reducing the forces transmitted to the building. By allowing controlled movement, base isolation prevents or minimizes structural damage, ensuring the safety of occupants and preserving the integrity of the building. This technique is commonly applied in critical infrastructure such as heritage buildings, and other vulnerable masonry structures, where maintaining functionality during and after an earthquake is crucial. (Olariu, Olariu and Sarbu, 2022), (Habieb, Valente and Milani, 2019)

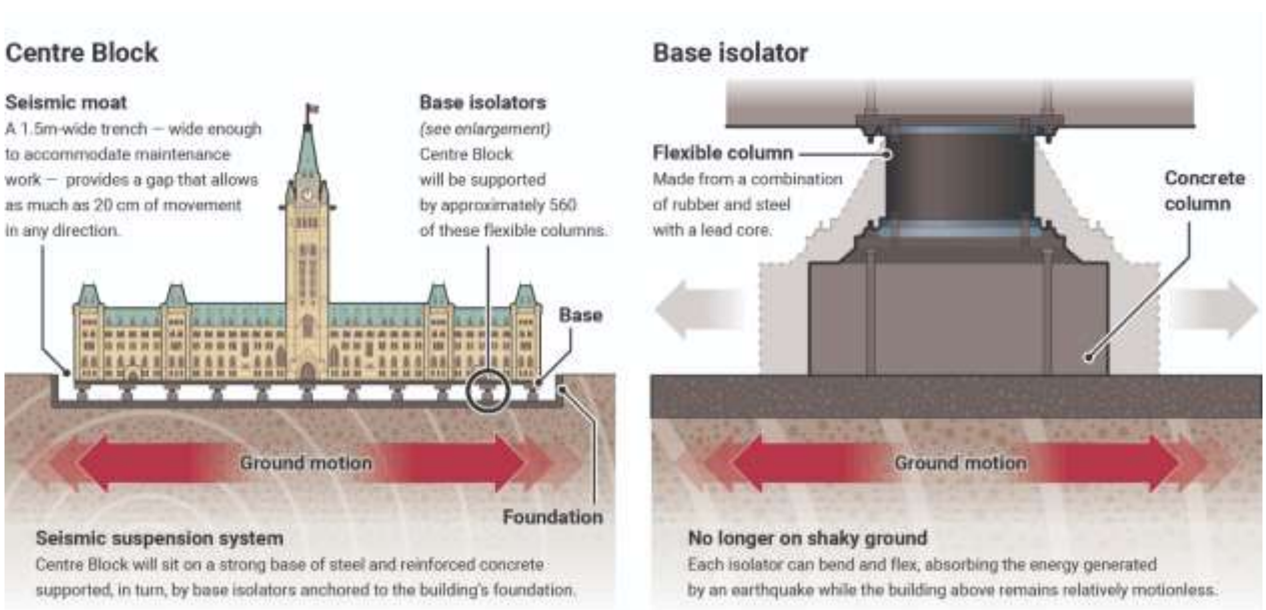

Figure A. 39. Base Isolation's Operational Mechanism. (Public services and procurement Canada, Teratec Inc)

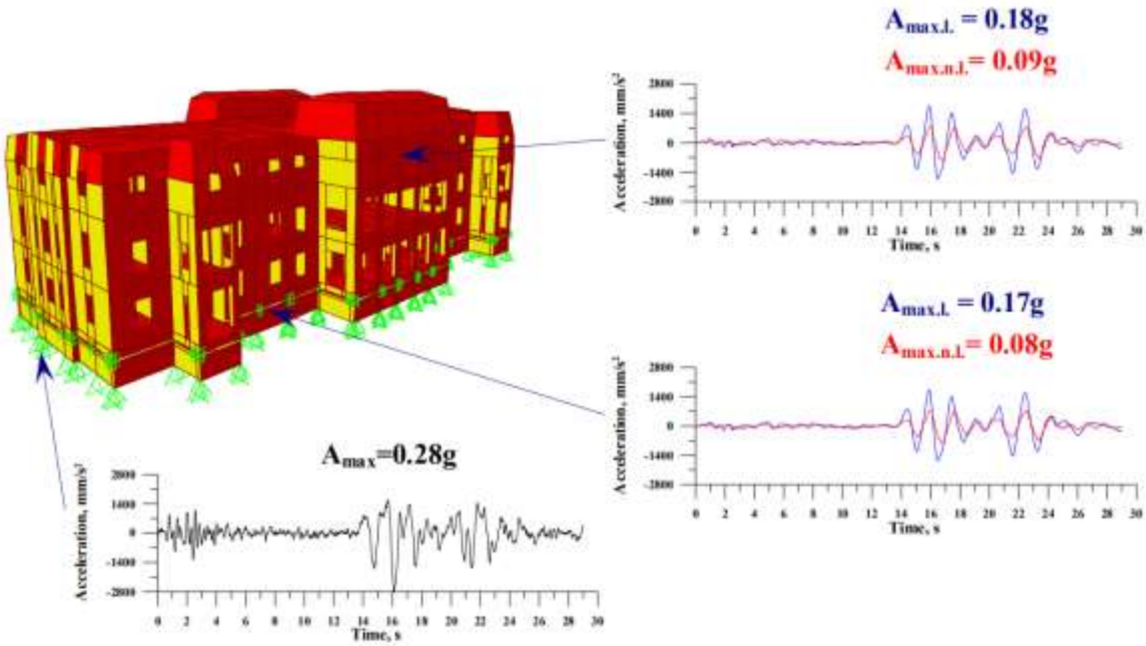

Figure A. 40. A Comparison of Response Accelerations on the Top Levels of Isolators and the Conference Hall Slab Using Linear and Nonlinear Analyses in the Longitudinal Direction. The analysis was Performed with the NS Muntele Rosu Accelerogram Dated August 30, 1986, with a Natural Period (Tc) of 0.7 Seconds. (Melkumyan, Mihul and Gevorgyan, 2011)

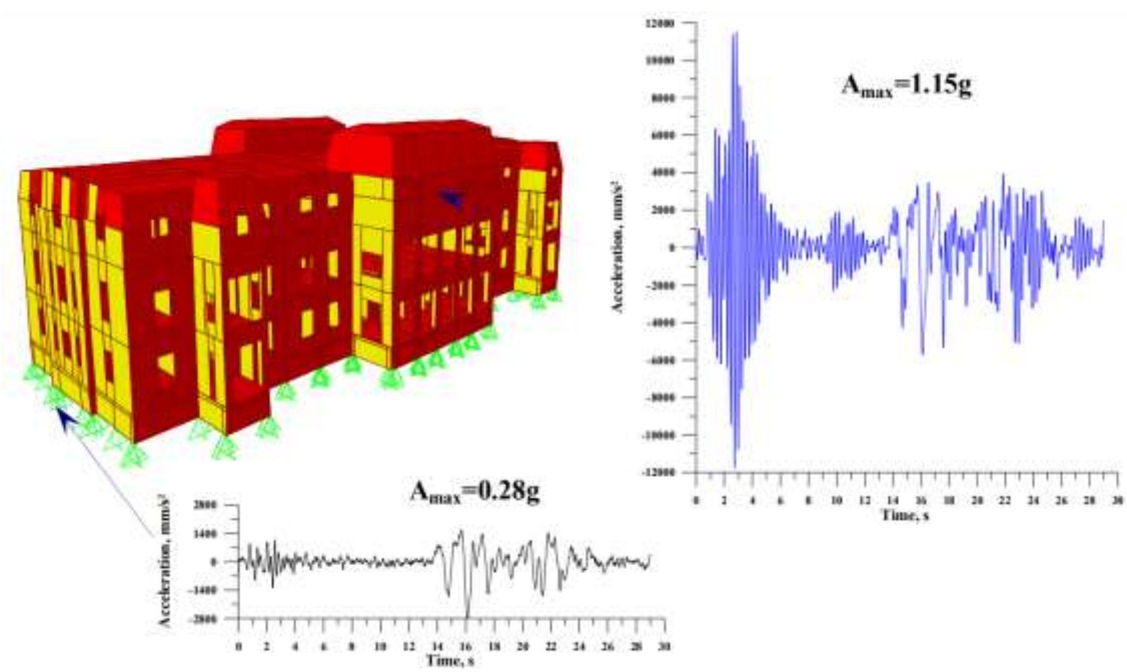

Figure A. 41. Response Acceleration at the Top (the Slab of Conference Hall) of Fixed Base Building in Longitudinal Direction using 30.08.1986, NS Muntele Rosu Accelerogram with T_c=0.7 sec. (Melkumyan, Mihul and Gevorgyan, 2011)

Base isolation protection systems are typically installed at the foundation or underground level, requiring minimal intervention in adding a foundation insulation layer. This approach helps preserve the historical appearance of the structures. Base isolation security improvements will considerably improve disaster management for such historical buildings during earthquakes and reduce post-earthquake repair costs. (Usta, 2021)

A.7.32 Enhancing the Earthquake Resilience of Gable Roofs

In seismic zones, gable-ended roofs made of brick can be vulnerable to damage. To address this, it is recommended to retrofit such roofs with diagonal bracing to prevent lateral movement during earthquakes and maintain the building's habitability. Observations from seismic activity in New Zealand reveal that buildings with light timber framing are more resistant to quakes. Nevertheless, brick gable-ended roofs often require additional measures to protect against seismic damage due to their inherent fragility. This is particularly true for older buildings with timber framing and unfortified masonry where bracing is not present. To improve the earthquake resistance of these structures, it is imperative to install diagonal braces at angles between 45 and 60 degrees. These braces should be evenly spaced between 0.9 to 2 meters and securely attached from the roof to the ceiling joists.

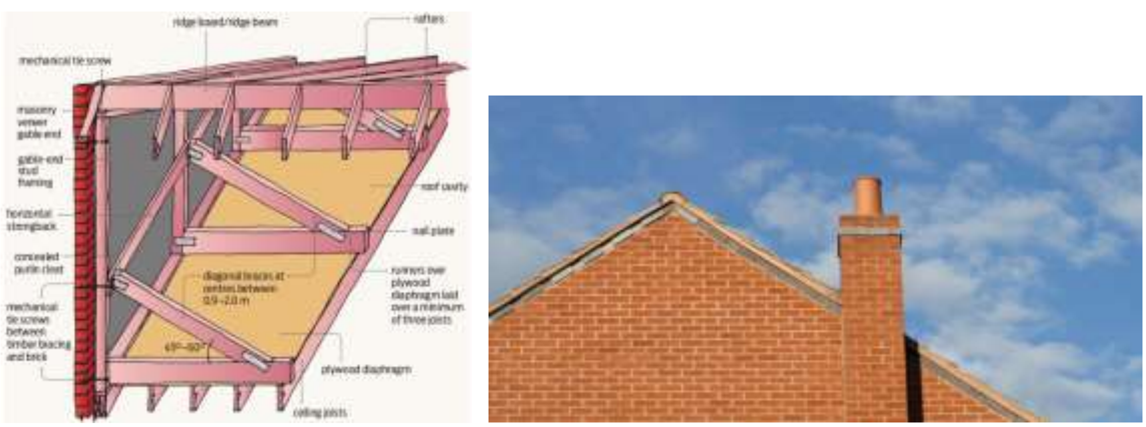

Figure A. 42. Retrofitting Brick Gable-End Roofs with Diagonal Bracing,
https://underconstruction.placemakers.co.nz/remove-brick-gable-end-vulnerabilities/

References

American institute of steel construction, https://www.aisc.org/awards-and-competitions/ideas2-awards/ideas2-awards-archives/maclac-building-d-rebirth-of-an-historic-paint-factory/

American institute of steel construction, https://www.aisc.org/awards-and-competitions/ideas2-awards/ideas2-awards-archives/maclac-building-d-rebirth-of-an-historic-paint-factory/

Blagojević, P., Brzev, S. and Cvetković, R., 2023. Seismic retrofitting of mid-rise unreinforced masonry residential buildings after the 2010 Kraljevo, Serbia earthquake: A case study. Buildings, 13(3), p.597.

Brignola, A., Pampanin, S. and Podestà, S., 2012. Experimental evaluation of the in-plane stiffness of timber diaphragms. Earthquake Spectra, 28(4), pp.1687-1709.

Çakıroğlu, M.A., İnce, G., Kabas, H.T. and Süzen, A.A., 2021. Experimental examination of the behavior of shotcrete-reinforced masonry walls and XgBoost neural network prediction model. Arabian Journal for Science and Engineering, 46(11), pp.10613-10630.

Cattanach, A.G., G.W. Alley, and A.W. Thornton. (2006) 'Appropriateness of Seismic Strengthening Interventions in Heritage Buildings: A framework for Appraisal' Paper 30 Presented at the 2008 New Zealand Society for Earthquake Engineering Conference: Napier, NZ.

Charleson, A., 2008. LONG-SPAN TIMBER BUILDINGS–A REVIEW OF RECENT INTERNATIONAL PROJECTS.

Croci, G. (1998) 'The Conservation and Structural Restoration of Architectural Heritage.' Southampton, U.K.: Computational Mechanics Publications/WIT Press.

Čajka, R., Kozielova, M., Burkovič, K. and Mynarzová, L., 2014. Strengthening of Masonry Structures on the Undermined Area by Prestressing. *Acta Montanistica Slovaca*, *19*(2).

Dizhur, D., Derakhshan, H., Grifith, M. C., Ingham, J.

Dizhur, D., Schultz, A. and Ingham, J., 2016. Pull-out behavior of adhesive connections in unreinforced masonry walls. Earthquake Spectra, 32(4), pp.2357-2375. https://doi.org/10.1193/011115EQS006M

Dizhur, D., Wei, S., Giaretton, M., Schultz, A.E., Ingham, J.M. and Giongo, I., 2021. Testing of URM wall-to-diaphragm through-bolt plate anchor connections. Earthquake Spectra, 37(1), pp.304-323. https://journals.sagepub.com/doi/epub/10.1177/8755293020944187

FEMA, (2006) 'FEMA 547 Techniques for the Seismic Rehabilitation of Existing Buildings.' Washington D.C.: FEMA.

FEMA. (2003), 'FEMA 397 Incremental Seismic Rehabilitation of Office Buildings.' Washington D.C.: FEMA.

FEMA. (2004) 'FEMA 398 Incremental Seismic Rehabilitation of Multifamily Apartment Buildings'. Washington D.C.: FEMA.

FEMA. (2004) 'FEMA 399 Incremental Seismic Rehabilitation of Retail Buildings.' Washington D.C.: FEMA.

Gibson, J. et al. (2014) 'SEATTLE UNREINFORCED MASONRY RETROFIT POLICY: Benefit Cost Analysis'.

Giongo, I. et al. (2015) 'Field Testing of Flexible Timber Diaphragms in an Existing Vintage URM Building', Journal of Structural Engineering, 141(1), pp. 1–11. Available at: https://doi.org/10.1061/(asce)st.1943-541x.0001045.

Giongo, I., Dizhur, D., Tomasi, R. and Ingham, J.M., 2015. Field testing of flexible timber diaphragms in an existing vintage URM building. Journal of Structural Engineering, 141(1), p.D4014009.

GooDWin, C., Tonks, G. and Ingham, J., 2011. Retrofit techniques for seismic improvement of URM buildings. SESOC Journal, 24(1), pp.30-45.
GooDWin, C., Tonks, G. and Ingham, J., 2011. Retrofit techniques for seismic improvement of URM buildings. SESOC Journal, 24(1), pp.30-45.
Grünthal, G., 1998. European macroseismic scale 1998 (EMS-98).

Habieb, A.B., Valente, M. and Milani, G., 2019. Effectiveness of different base isolation systems for seismic protection: Numerical insights into an existing masonry bell tower. Soil Dynamics and Earthquake Engineering, 125, p.105752.

Helifix, 2014, CS01-Crack-Stitching, PDF (helifix.com.au)

ICOMOS NZ. (1993) ‘Charter for the Conservation of Places of Cultural Heritage Value’ International Council on Monuments and Sites New Zealand.

Infinity Design Solutions, Available at: https://www.ids-dmv.com/ids-resources/

Ismail, N., Laursen, P. T., Ingham, J. M. (2010) ‘Seismic performance of face loaded unreinforced masonry walls retrofitted using post-tensioning.’ AJSE.

Khan, W., Akhtar, S. and Hussain, A., 2019, September. Rehabilitation of concrete and masonry structures. In AIP Conference Proceedings (Vol. 2158, No. 1, p. 020028). AIP Publishing LLC.

Latifi, R., Hadzima-Nyarko, M., Radu, D. and Rouhi, R., 2023. A brief overview on crack patterns, repair and strengthening of historical masonry structures. Materials, 16(5), p.1882.

Latifi, R., Hadzima-Nyarko, M., Radu, D. and Rouhi, R., 2023. A brief overview on crack patterns, repair and strengthening of historical masonry structures. Materials, 16(5), p.1882.

M. (2011) ‘In-Situ Testing of a Low Intervention NSM Seismic Strengthening Technique for Historical URM Buildings’, International Journal of Materials and Structural Integrity (IJMSI) (submitted May 2010).

Melkumyan, M., Mihul, V. and Gevorgyan, E., 2011, May. Retrofitting by base isolation of existing buildings in Armenia and in Romania and comparative analysis of innovative vs. conventional retrofitting. In 3rd International Conf. on Computational Methods in Structural Dynamics and Earthquake Engineering.

Memari, A.M. and Aliaari, M., 2018. Finite element modeling of masonry infill walls equipped with structural fuse. In New Trends in Structural Engineering. IntechOpen.

Memon, S.A., Zain, M., Zhang, D., Rehman, S.K.U., Usman, M. and Lee, D., 2020. Emerging trends in the growth of structural systems for tall buildings. Journal of Structural Integrity and Maintenance, 5(3), pp.155-170.

Memon, S.A., Zain, M., Zhang, D., Rehman, S.K.U., Usman, M. and Lee, D., 2020. Emerging trends in the growth of structural systems for tall buildings. Journal of Structural Integrity and Maintenance, 5(3), pp.155-170.

Miglietta, M., Damiani, N., Guerrini, G. and Graziotti, F., 2021. Full-scale shake-table tests on two unreinforced masonry cavity-wall buildings: effect of an innovative timber retrofit. Bulletin of Earthquake Engineering, 19, pp.2561-2596.

Olariu, I., Olariu, F. and Sarbu, D., 2022. Base isolation for seismic retrofitting of existing structures. In Seismic Design and Practice into the Next Century (pp. 417-424). Routledge.

Oliveira, D.V., Basilio, I. and Lourenço, P.B., 2010. Experimental behavior of FRP strengthened masonry arches. Journal of Composites for Construction, 14(3), pp.312-322.

Paxton, B., 2014. Quantifying unreinforced masonry seismic risk and mitigation options in Victoria, BC (Doctoral dissertation, University of British Columbia).

Paxton, B., 2014. Quantifying unreinforced masonry seismic risk and mitigation options in Victoria, BC (Doctoral dissertation, University of British Columbia).

Public services and procurement Canada, Teratec Inc

Robinson, L. and I. Bowman. (2000) ‘Guidelines for Earthquake Strengthening.’ Wellington, NZ: New Zealand Historic Places Trust.

Romanian Seismic Code (P100-1/2006), https://graitec.com/uk/resources/technical-support/documentation/advance-design-technical-articles/bracing-members-design-advance-design/

Romanian Seismic Code (P100-1/2006), https://graitec.com/uk/resources/technical-support/documentation/advance-design-technical-articles/bracing-members-design-advance-design/

Russell, A. P., Ingham, J. M. (2010) ’Prevalence of New Zealand’s Unreinforced Masonry Buildings’. Bulletin of the New Zealand Society for Earthquake Engineering (submitted January 2010).

Russell, A.P. (2010), ‘Seismic Assessment of In- Plane Unreinforced Masonry Walls in New Zealand,’ PhD Thesis, University of Auckland: Auckland, NZ.

Rutherford & Chekene. (1990). ‘Seismic Retrofit Alternatives for San Francisco’s Unreinforced Masonry Buildings: Estimates of Construction Cost & Seismic Damage.’ San Francisco, CA. City and County of San Francisco Department of City Planning (prepared by Rutherford & Chekene, Consulting Engineers).

Schacher, T., 2009. Confined Masonry. India: National Information Centre of Earthquake Engineering.

Schacher, T., 2009. Confined Masonry. India: National Information Centre of Earthquake Engineering.

Su, K.L., Looi, D.T. and Zhang, Y., 2021. Guide for Design, Installation, and Assessment of Post-installed Reinforcements. Hong Kong University Press.

Usta, P. (2021) ‘Investigation of a base-isolator system’s effects on the seismic behavior of a historical structure’, Buildings, 11(5). Available at: https://doi.org/10.3390/buildings11050217.

Zhou, Y., Shao, H., Cao, Y. and Lui, E.M., 2021. Application of buckling-restrained braces to earthquake-resistant design of buildings: A review. Engineering Structures, 246, p.112991.

Zhou, Y., Shao, H., Cao, Y. and Lui, E.M., 2021. Application of buckling-restrained braces to earthquake-resistant design of buildings: A review. Engineering Structures, 246, p.112991.

(SSG Urban Outfitters) https://ssgse.com/urbanoutfitters/

Baker, J.W. (2007) ‘Measuring bias in structural response caused by ground motion scaling’, Pacific Conference on Earthquake Engineering, (056), pp. 1–6. Available at: https://doi.org/10.1002/eqe.

https://ascelibrary.org/toc/jsendh/141/1

https://graitec.com/uk/resources/technical-support/documentation/advance-design-technical-articles/bracing-members-design-advance-design/

https://hkupress.hku.hk/image/catalog/pdf-preview/9789888528608.pdf

https://seblog.strongtie.com/2013/04/seismic-retrofit-of-unreinforced-masonry-urm-buildings

https://underconstruction.placemakers.co.nz/remove-brick-gable-end-vulnerabilities/

https://www.ids-dmv.com/blog

https://www.ids-dmv.com/masonry/brick-infills-in-historic-masonry-walls/

https://www.mdpi.com/2075-5309/13/3/597

https://www.nicee.org/.

https://www.nicee.org/.

https://www.pseau.org/outils/ouvrages/nicee_confined_masonry_1_2_storey_buildings_schacher.pdf

https://www.pseau.org/outils/ouvrages/nicee_confined_masonry_1_2_storey_buildings_schacher.pdf

https://www.seattle.gov/documents/Departments/SDCI/Codes/ChangesToCodes/UnreinforcedMasonry/URMBenefitsCostStudy.pdf

Appendix B: Model Analysis Deformed Shape in SAP2000

Figure B. 1. Half scale Frame model, X Direction

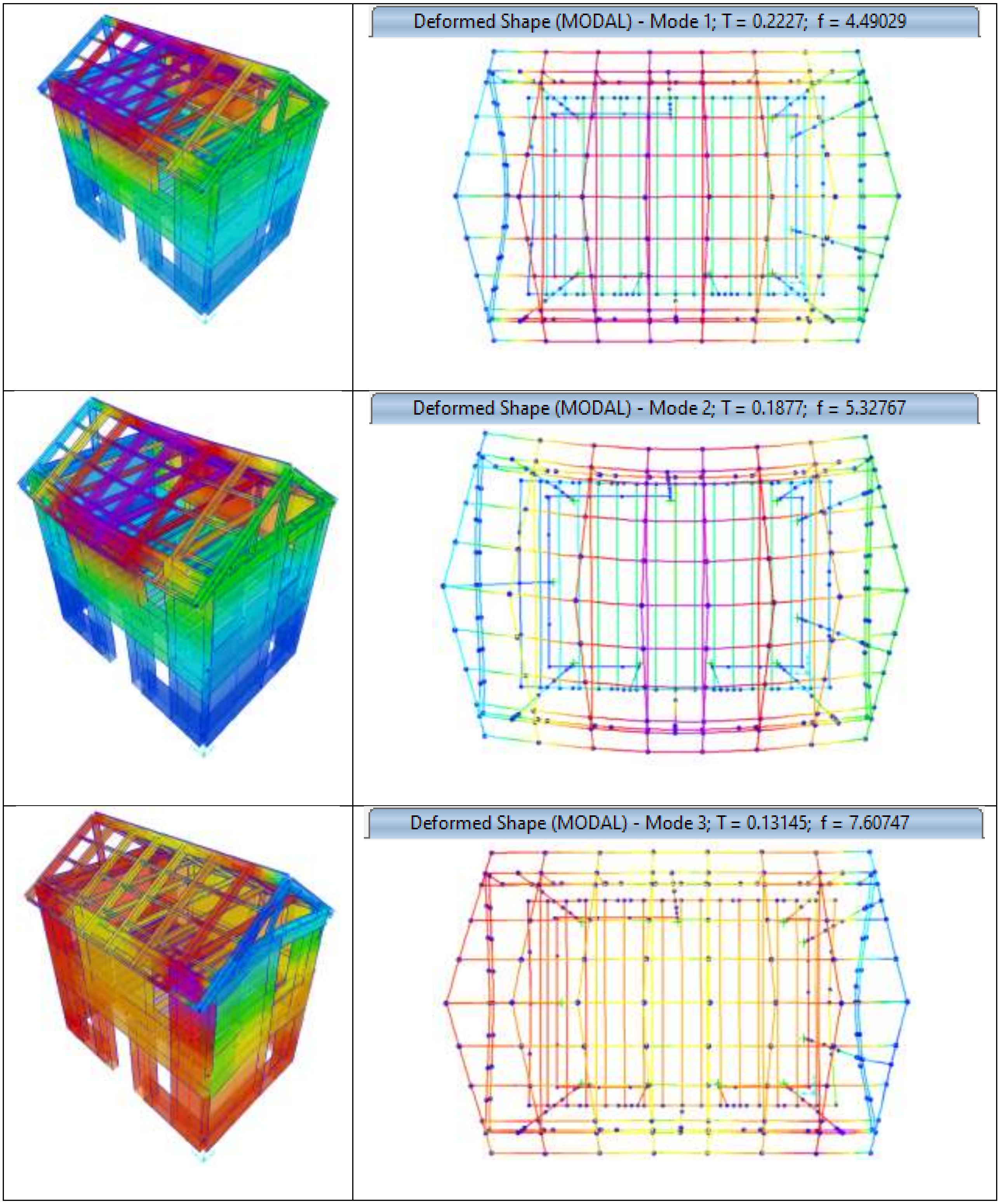

Half scale Frame model, X Direction

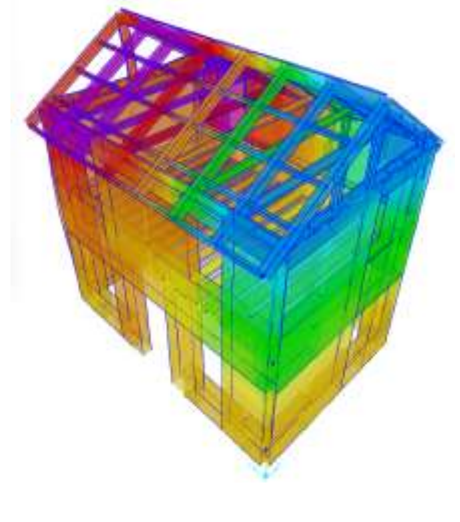

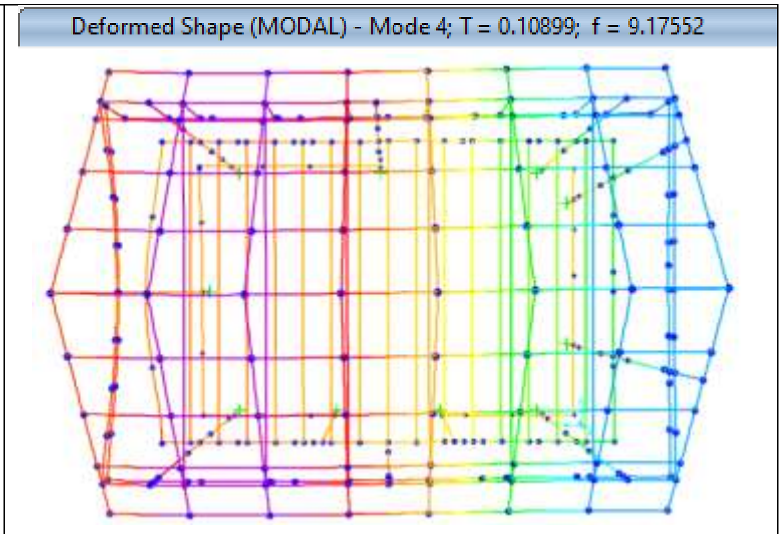

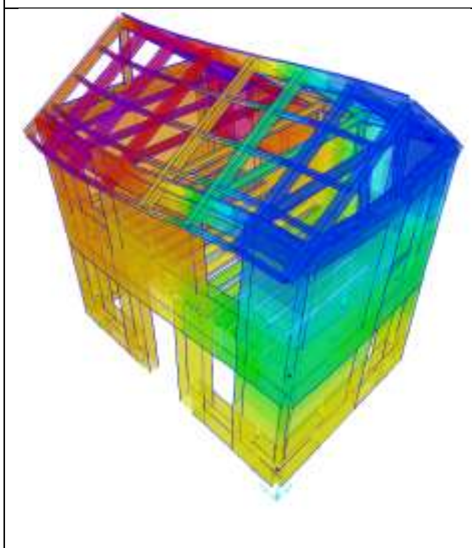

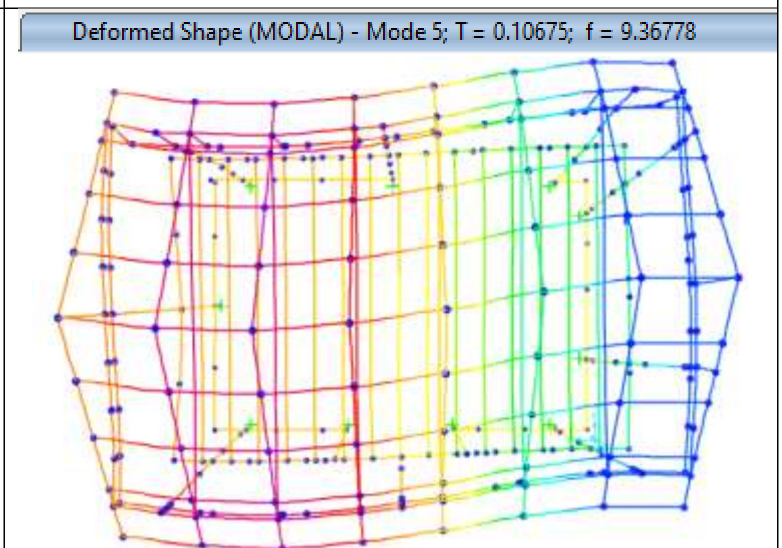

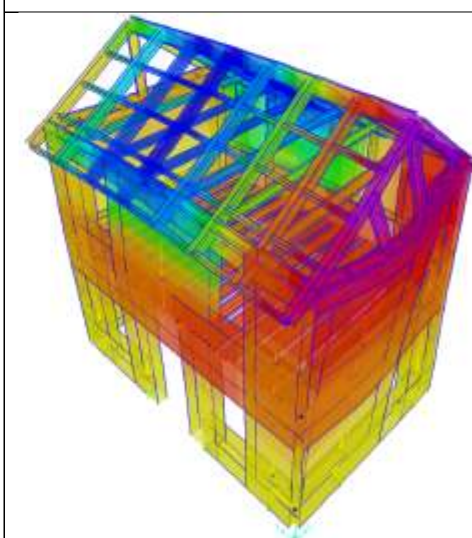

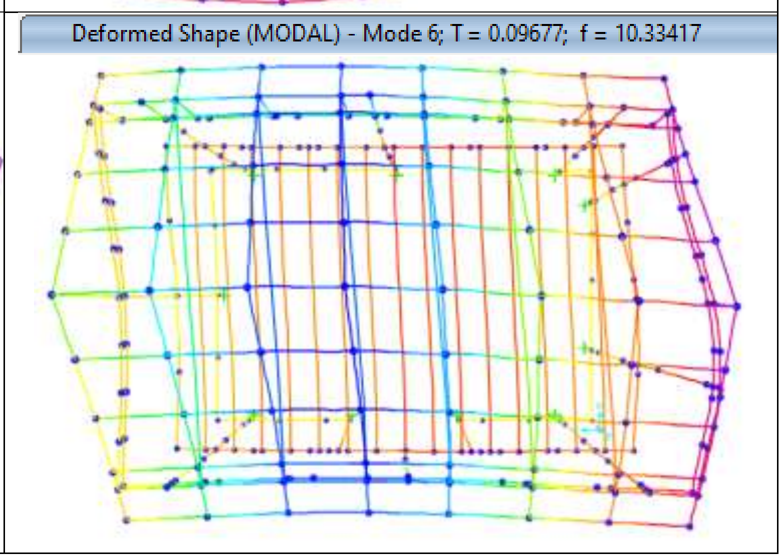

Half scale Frame model, X Direction

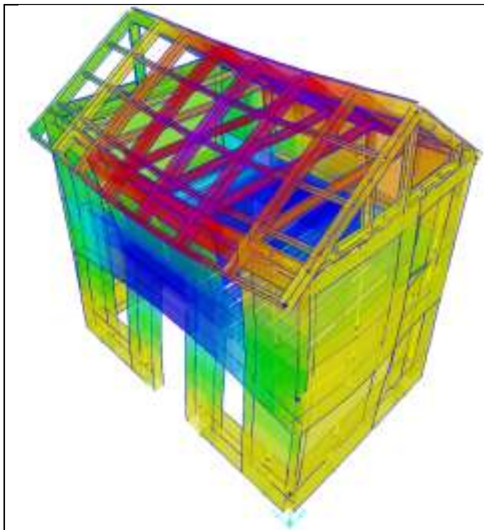

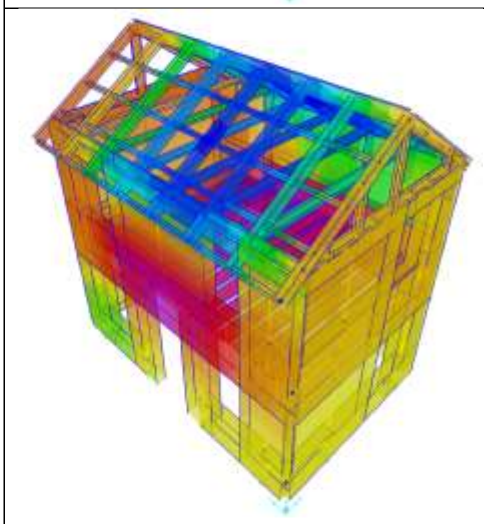

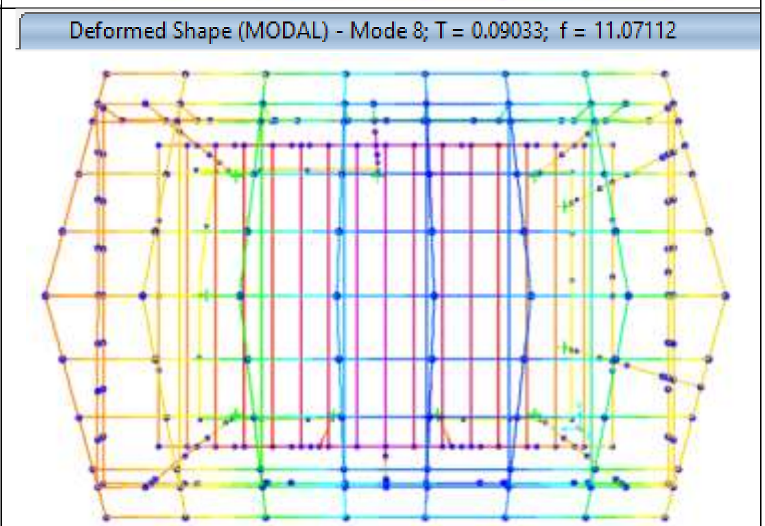

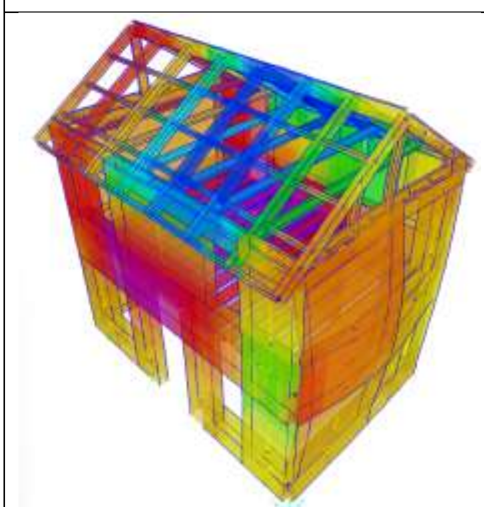

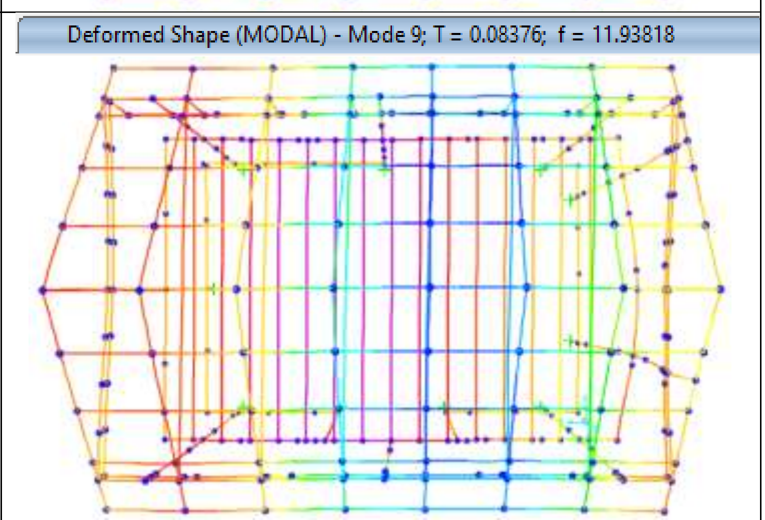

Half scale Frame model, X Direction

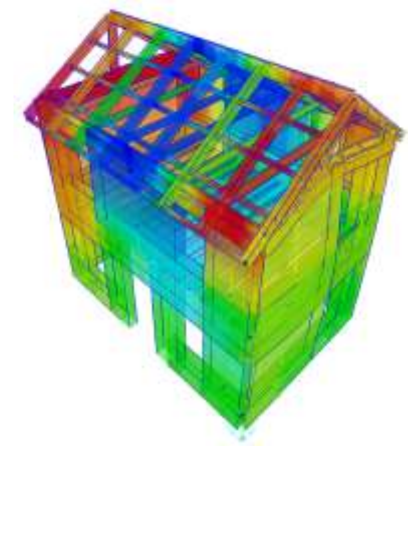

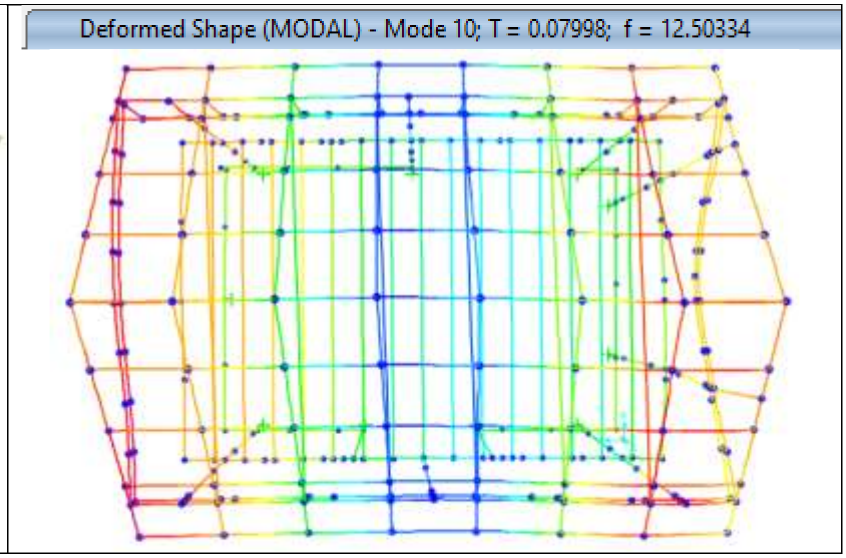

Figure B. 2. Half scale Frame model, Y Direction

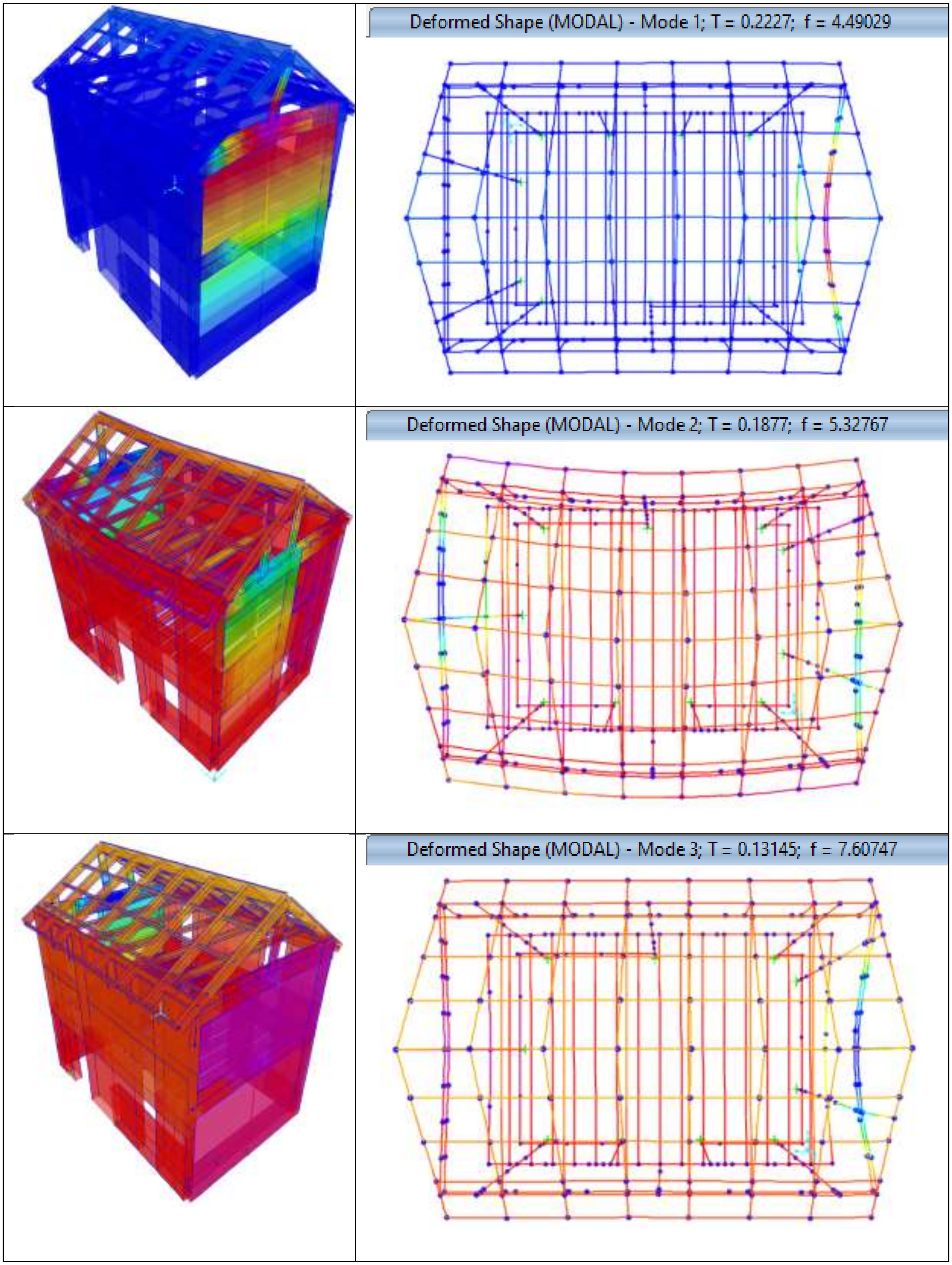

Half scale Frame model, Y Direction

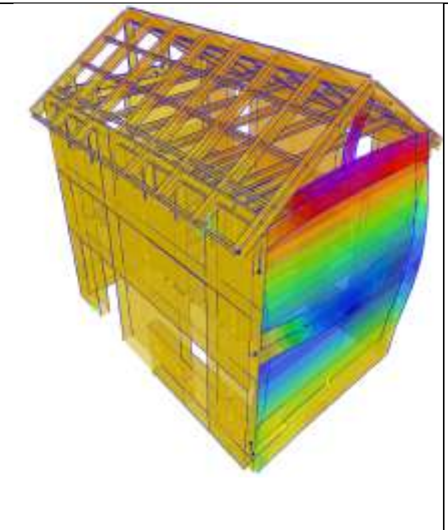

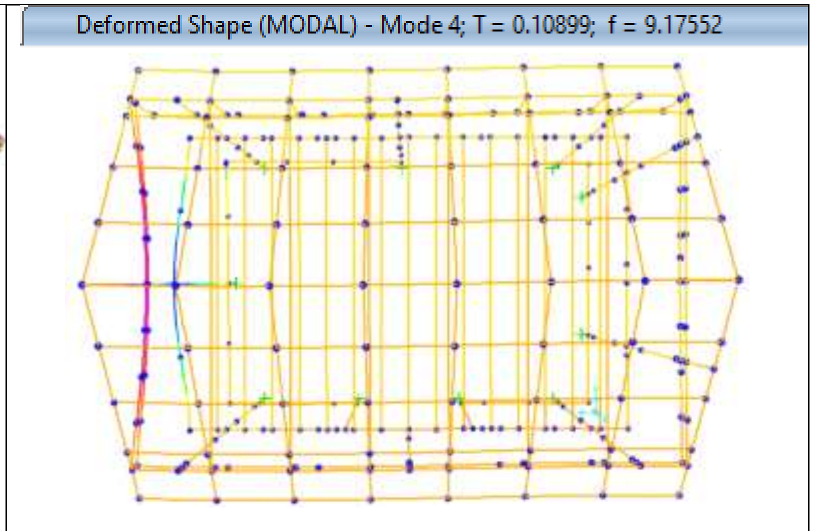

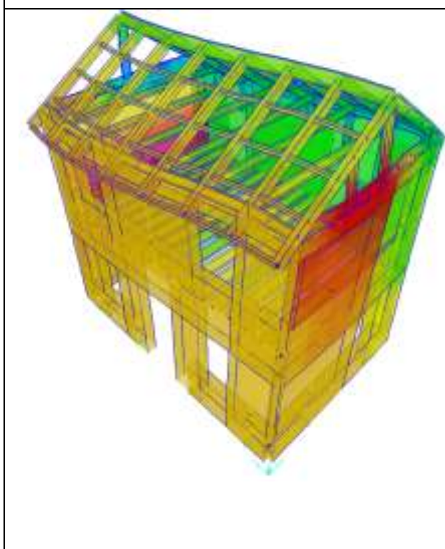

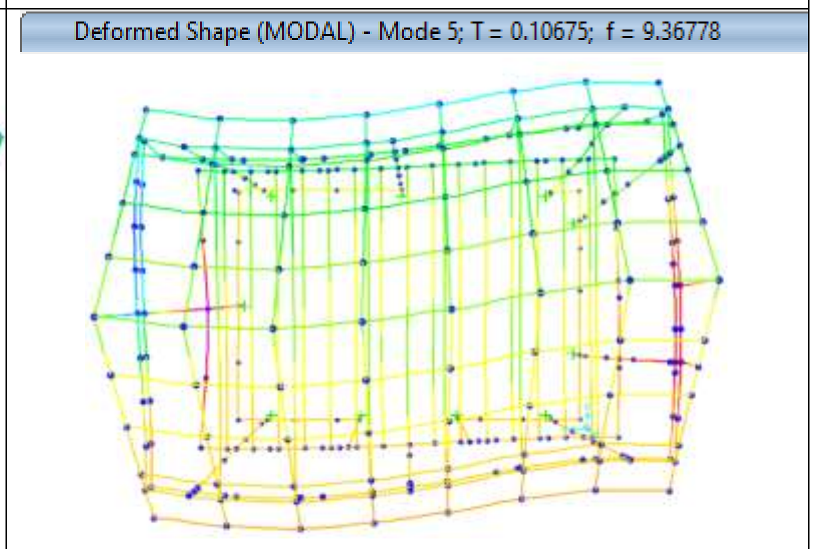

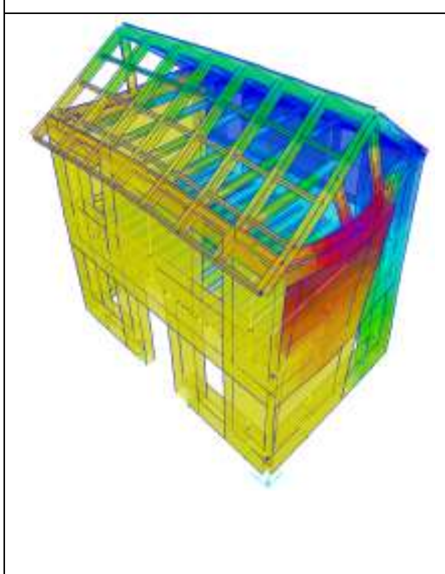

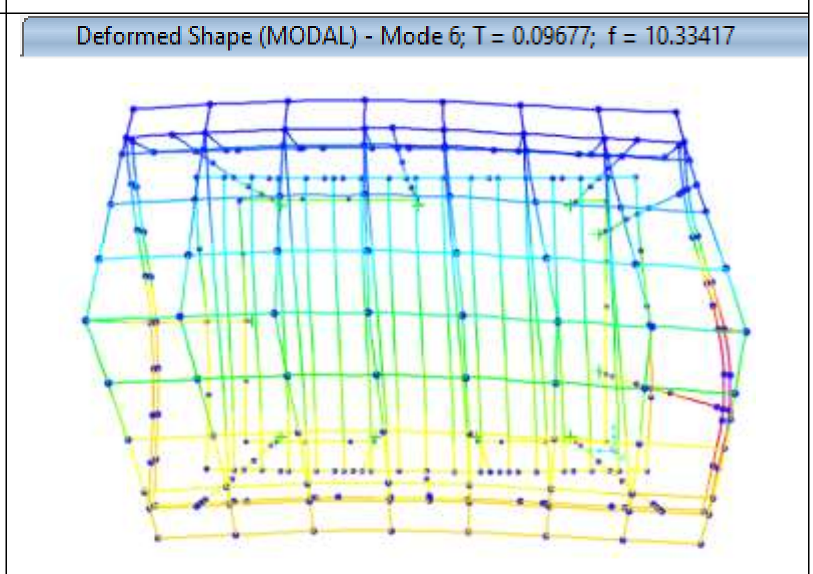

Half scale Frame model, Y Direction

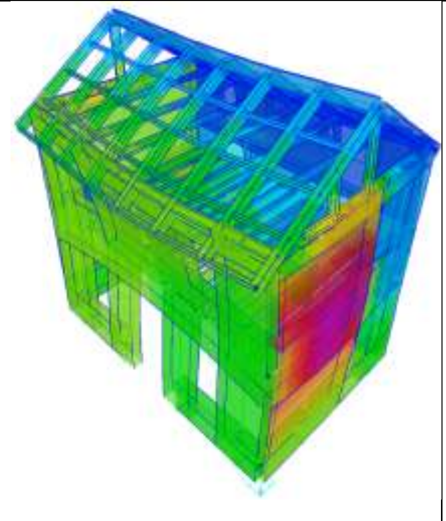

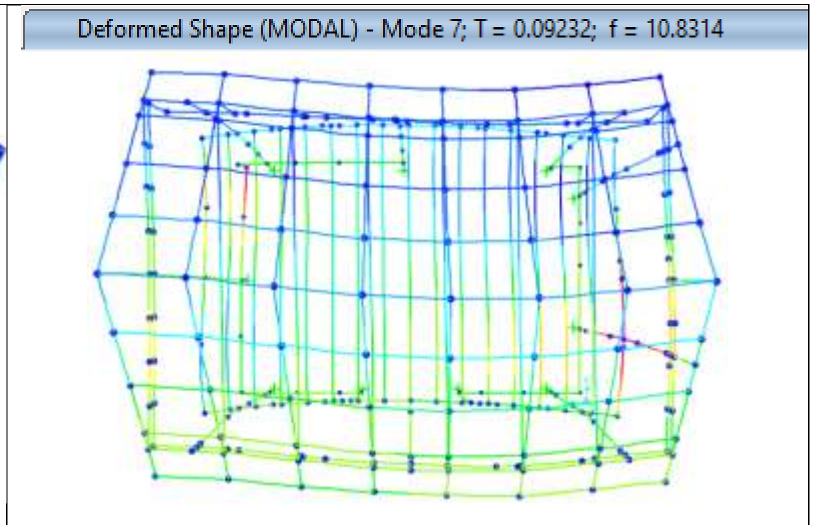

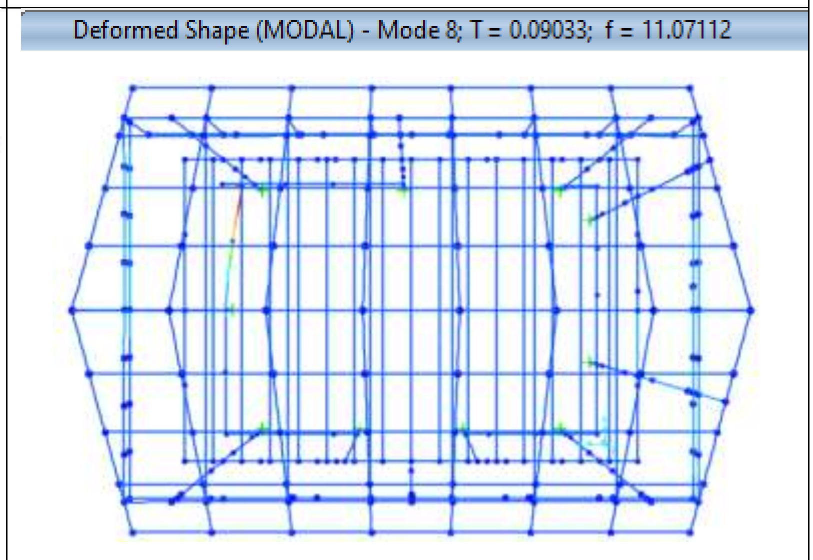

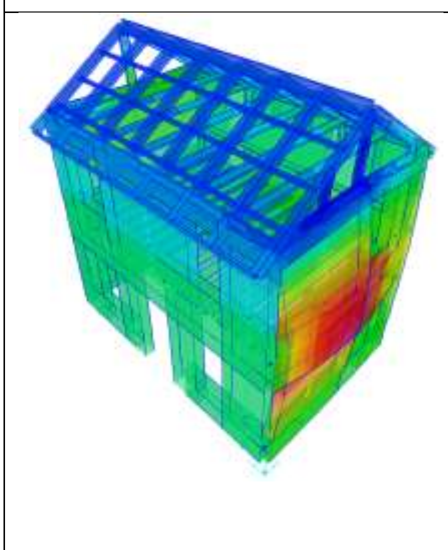

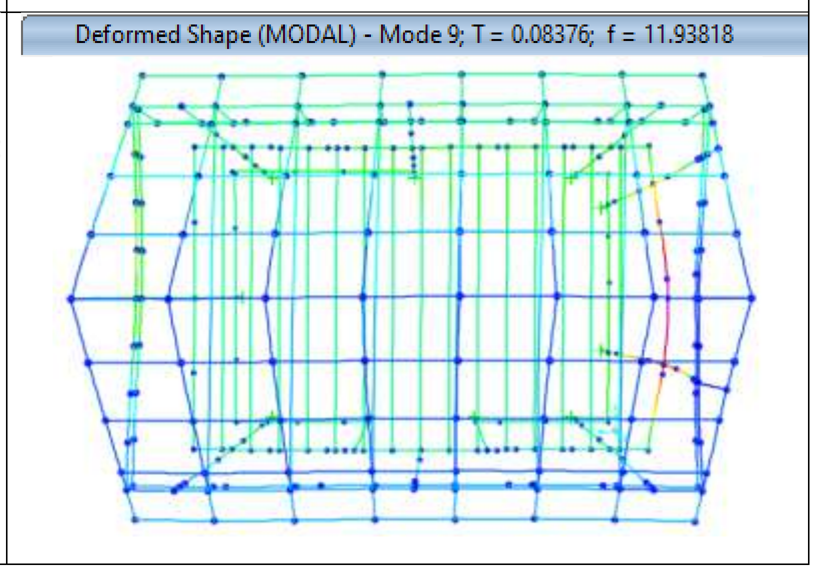

Half scale Frame model, Y Direction

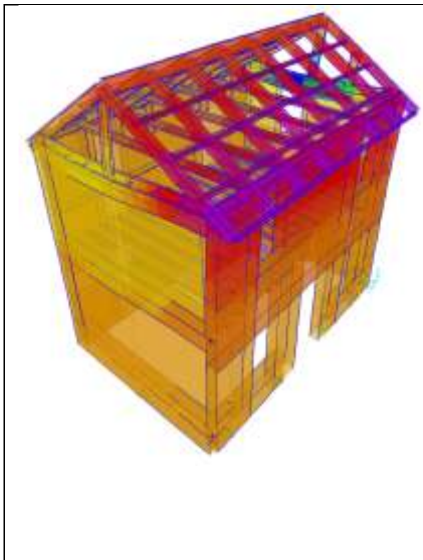

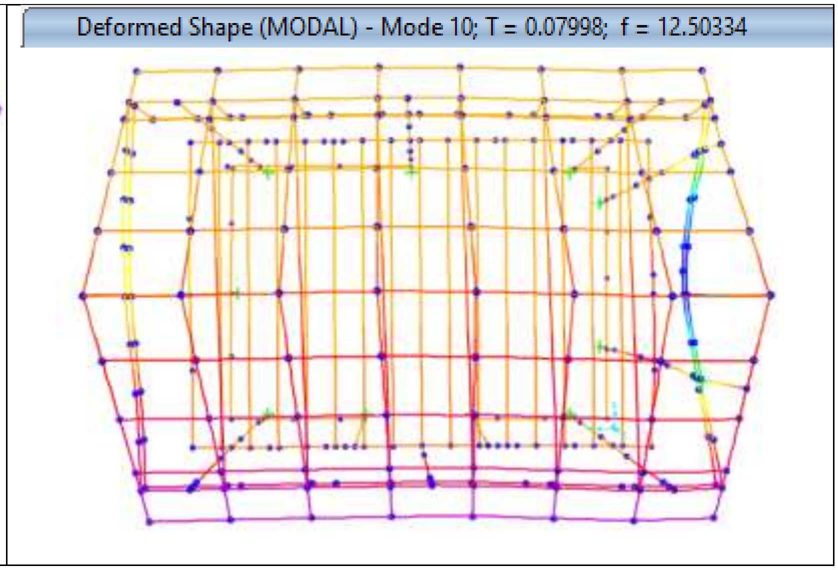

Figure B. 3. Half scale Shell model, X Direction

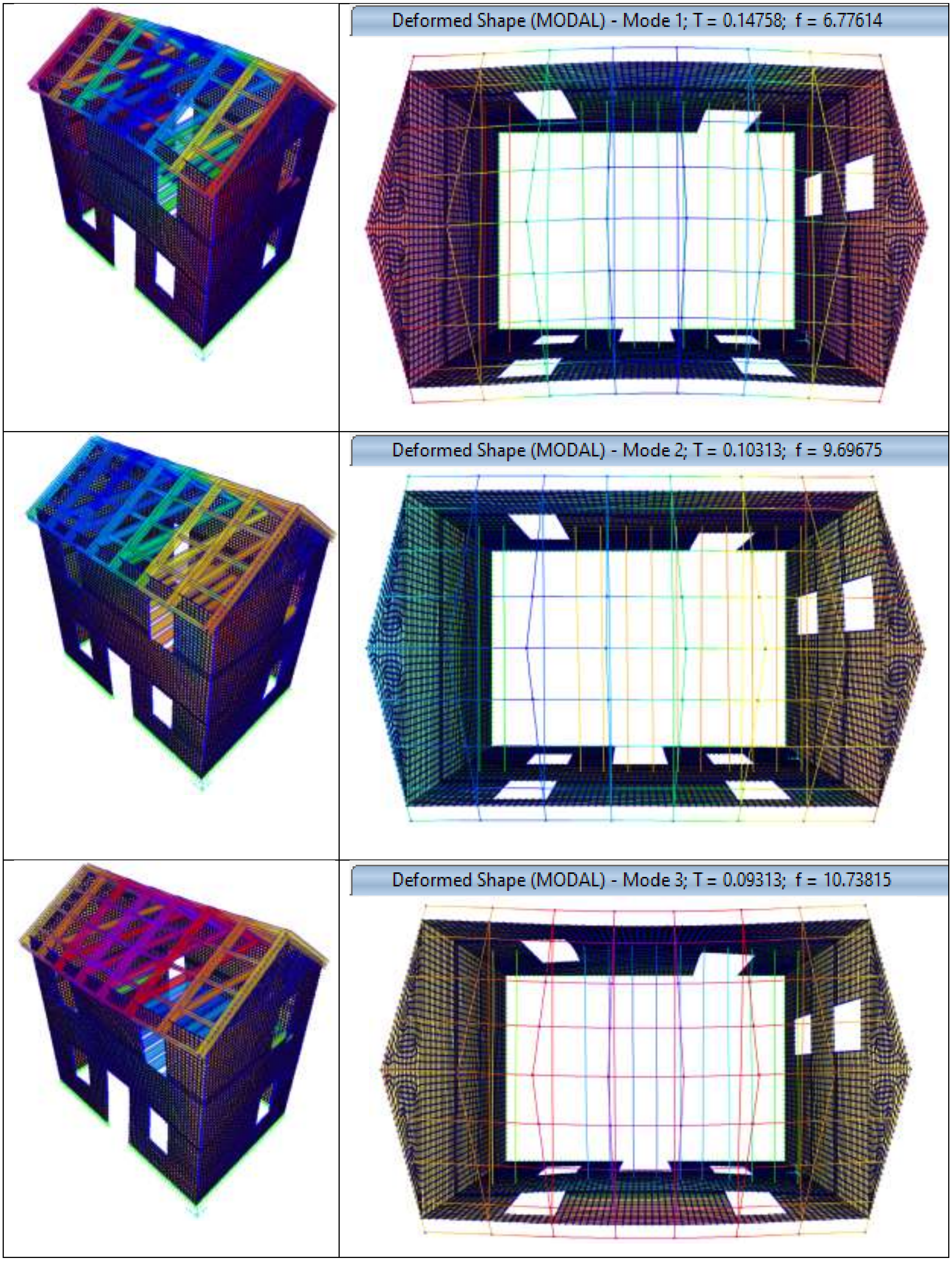

Half scale Shell model, X Direction

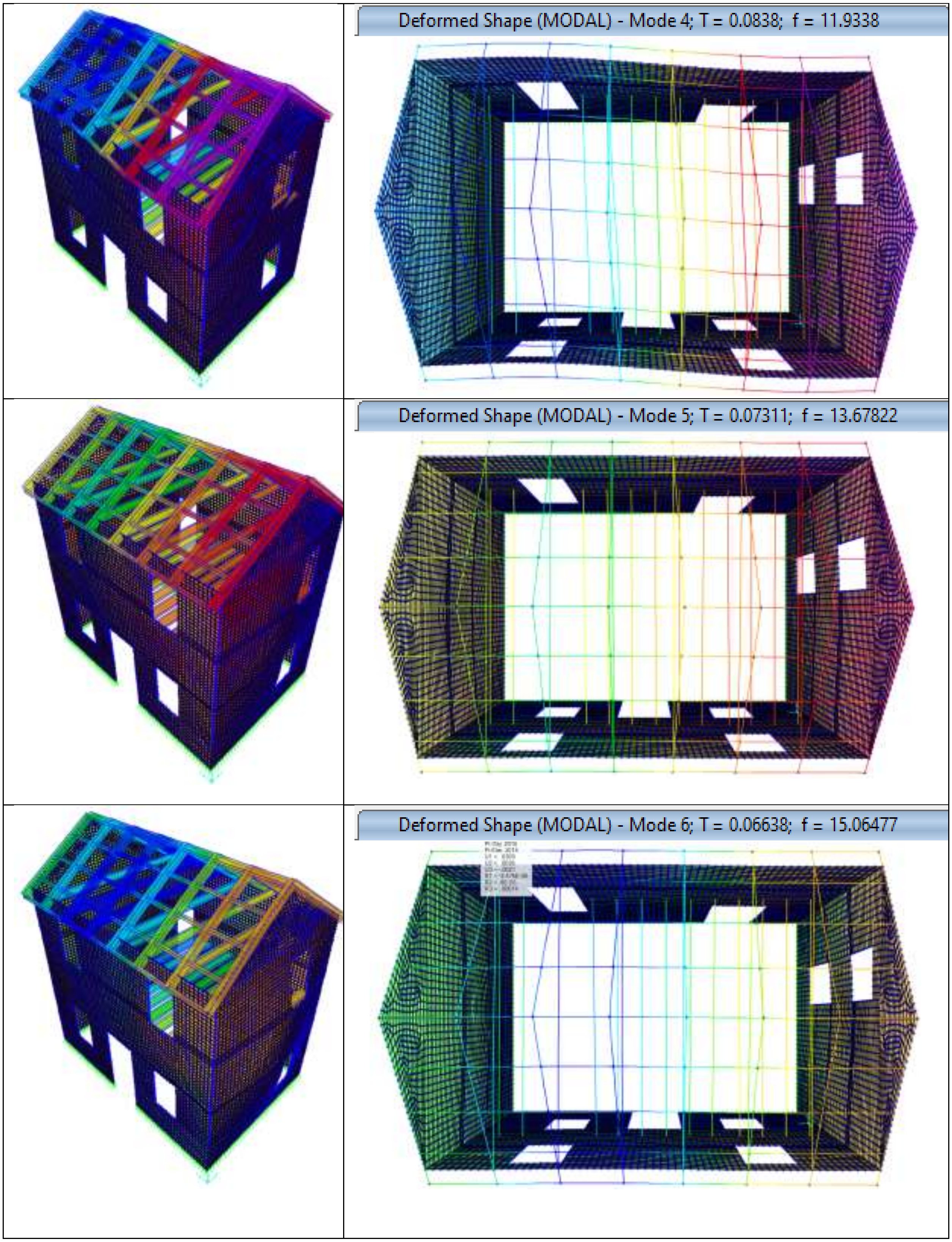

Half scale Shell model, X Direction

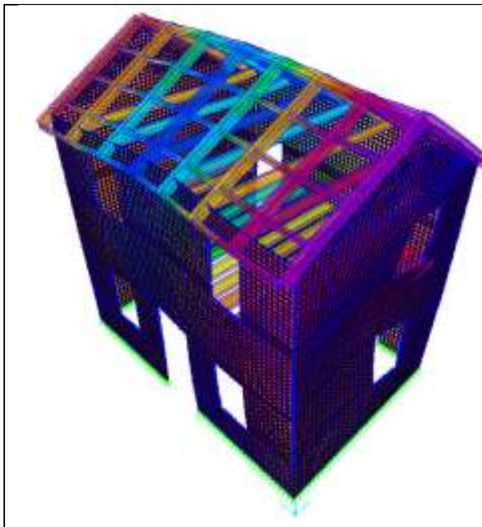	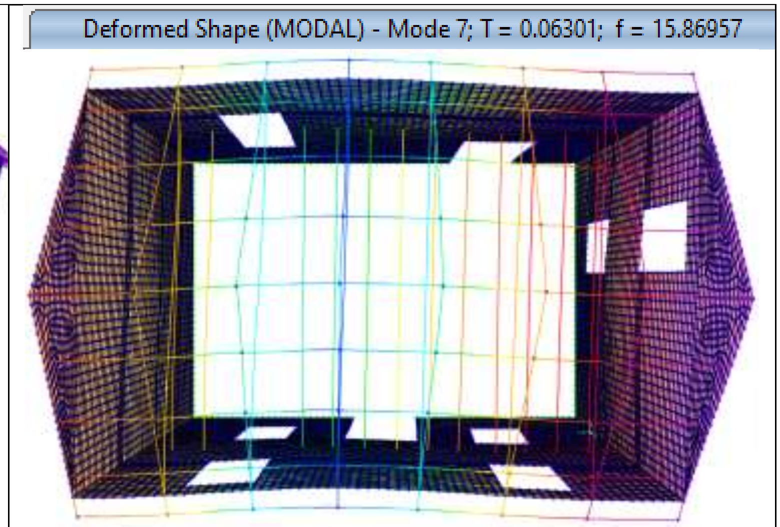
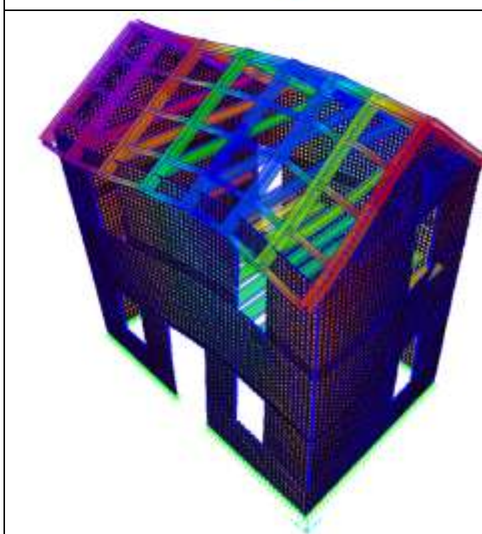	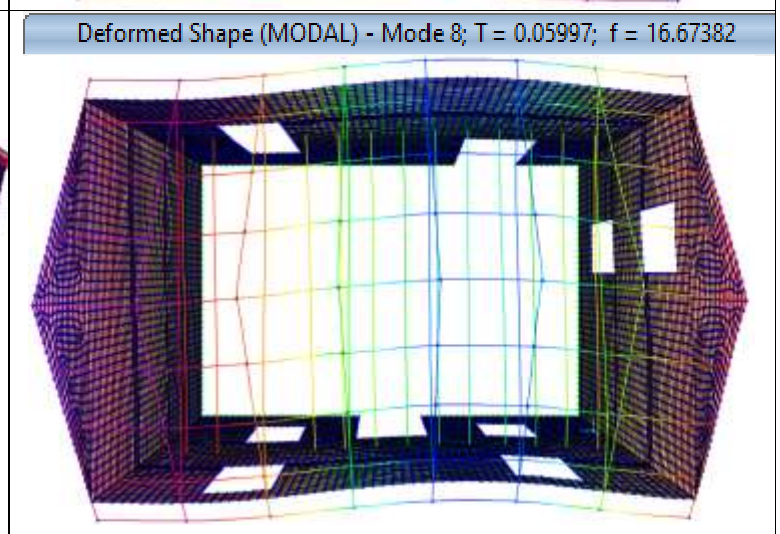
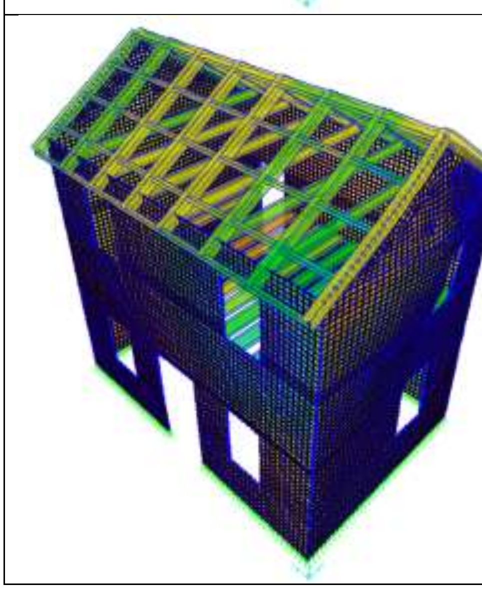	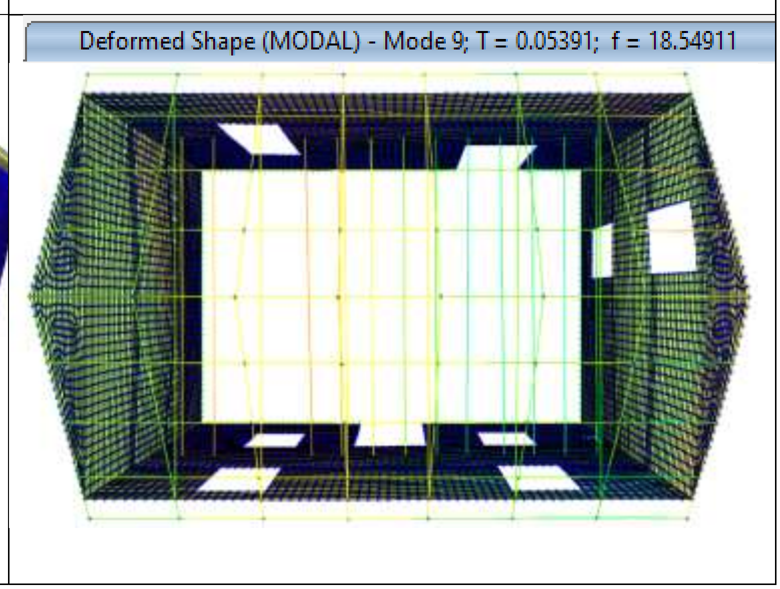

Half scale Shell model, X Direction

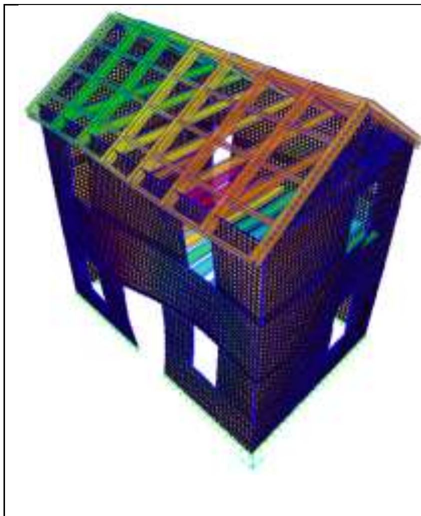

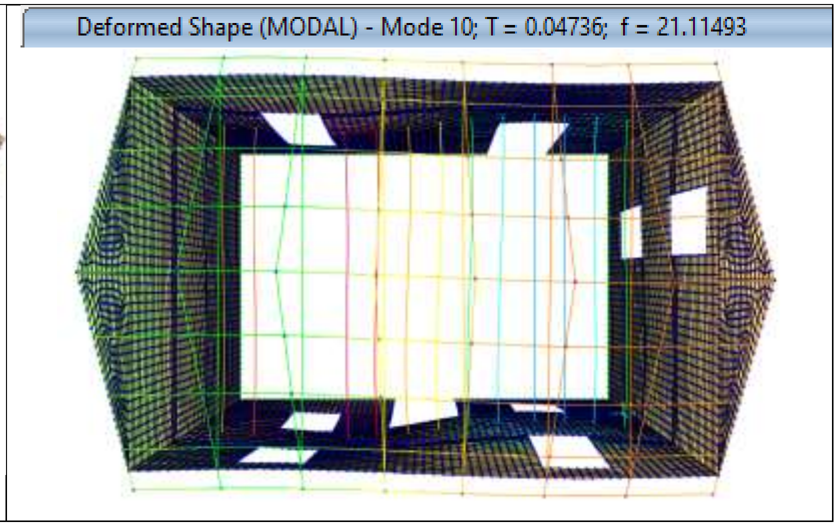

Figure B. 4. Half scale Shell model, Y Direction

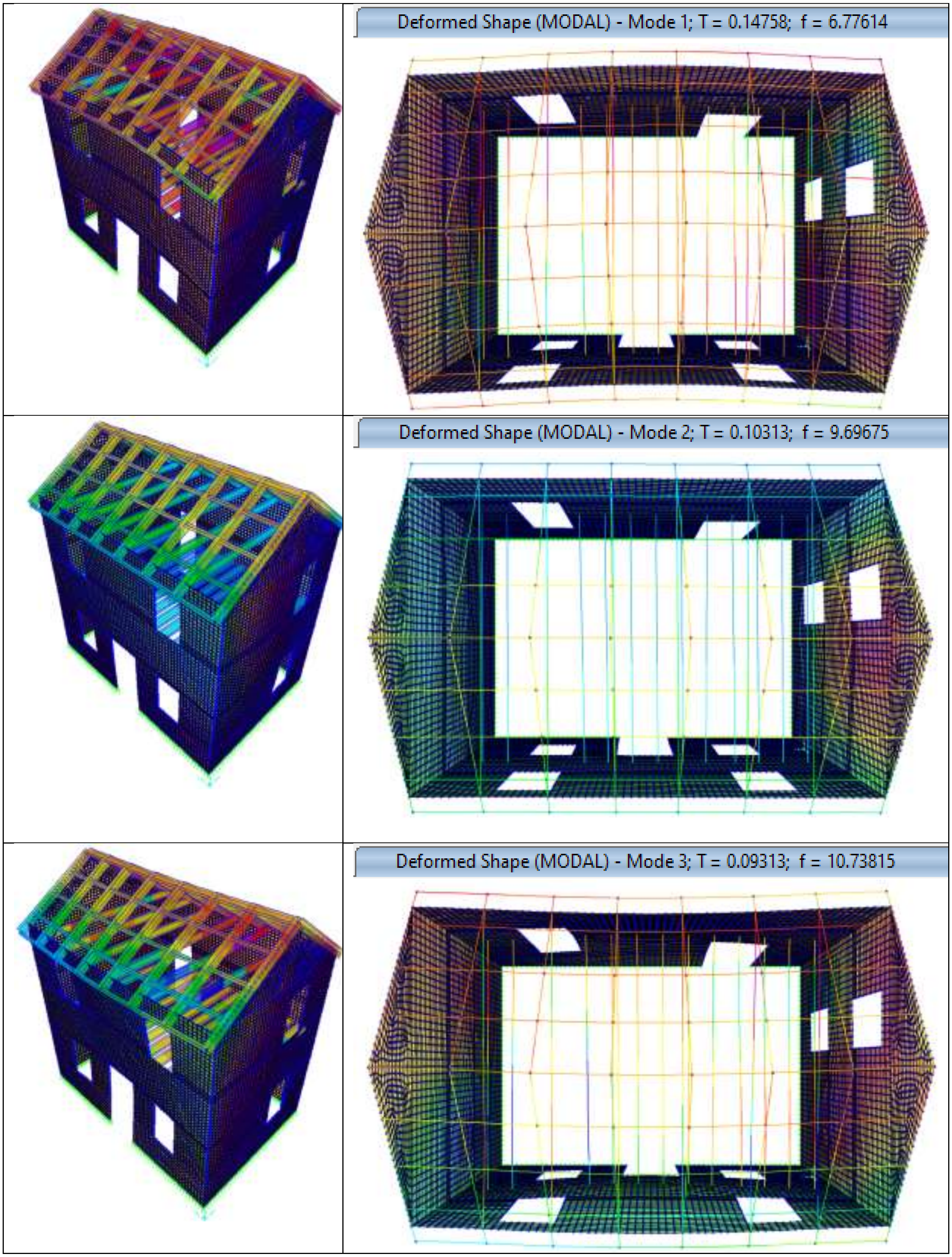

Half scale Shell model, Y Direction

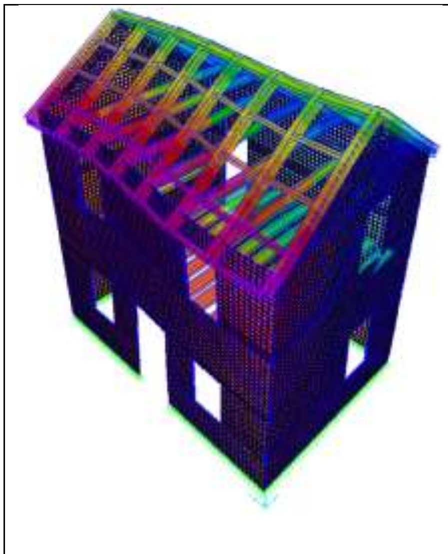

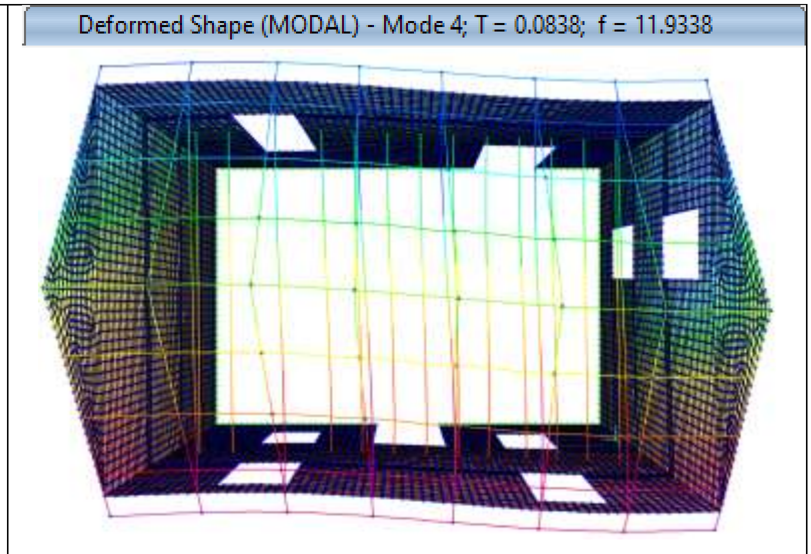

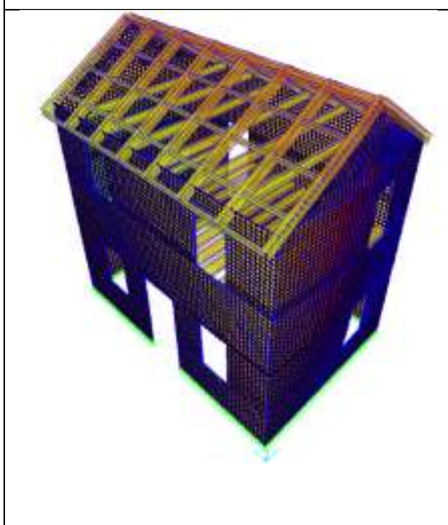

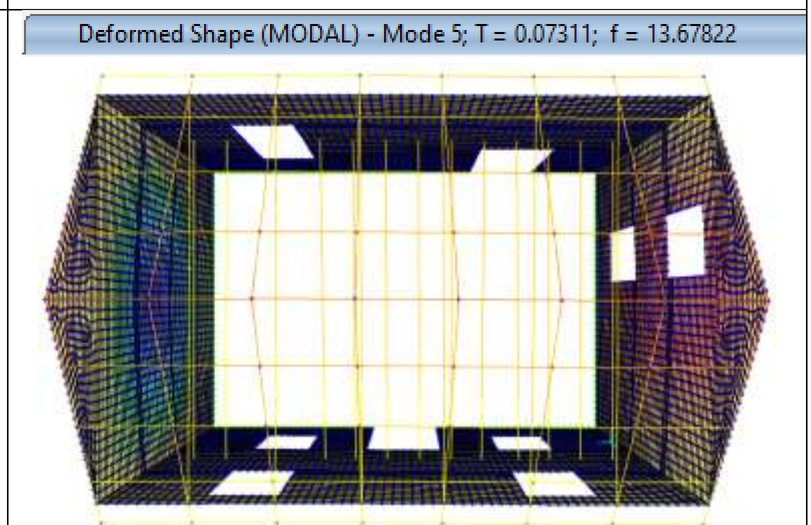

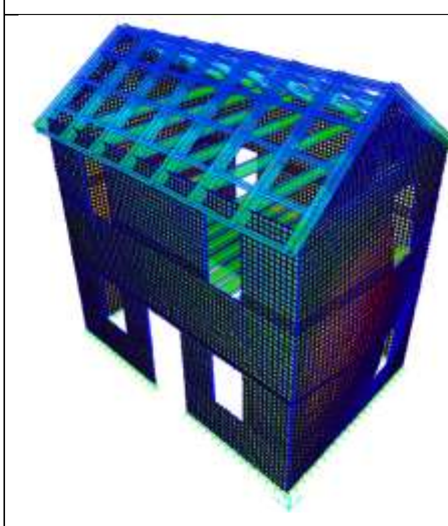

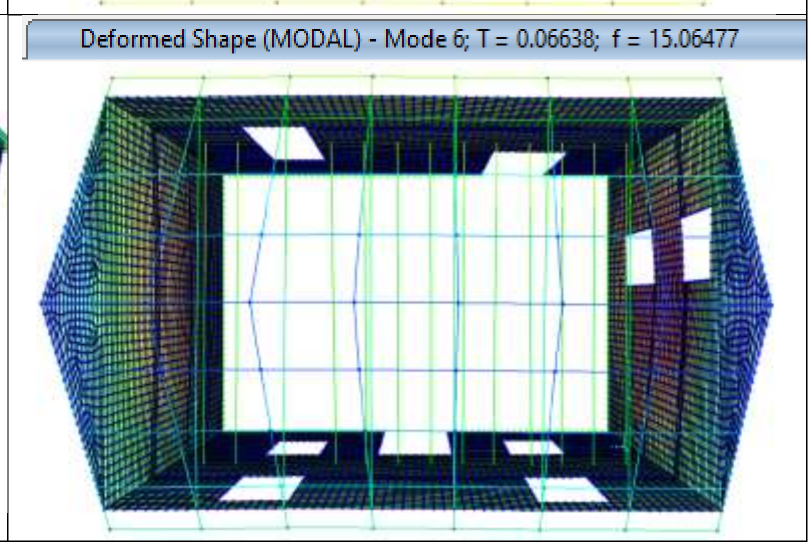

Half scale Shell model, Y Direction

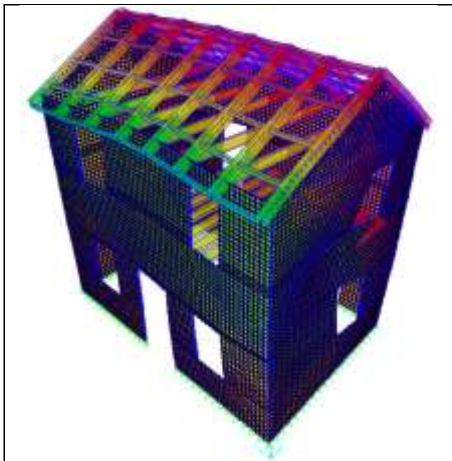

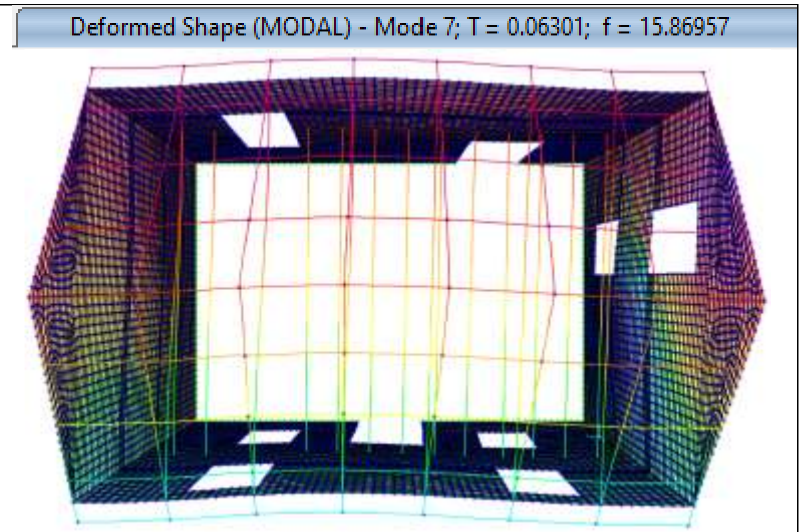

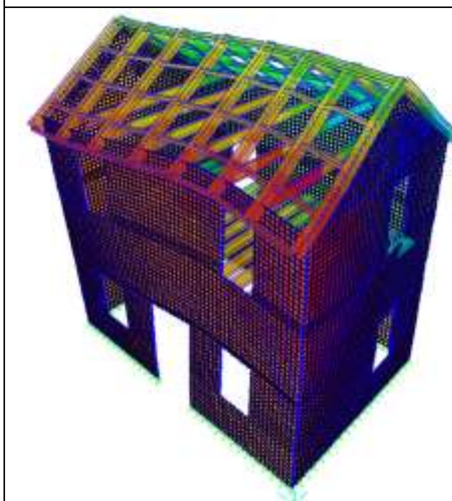

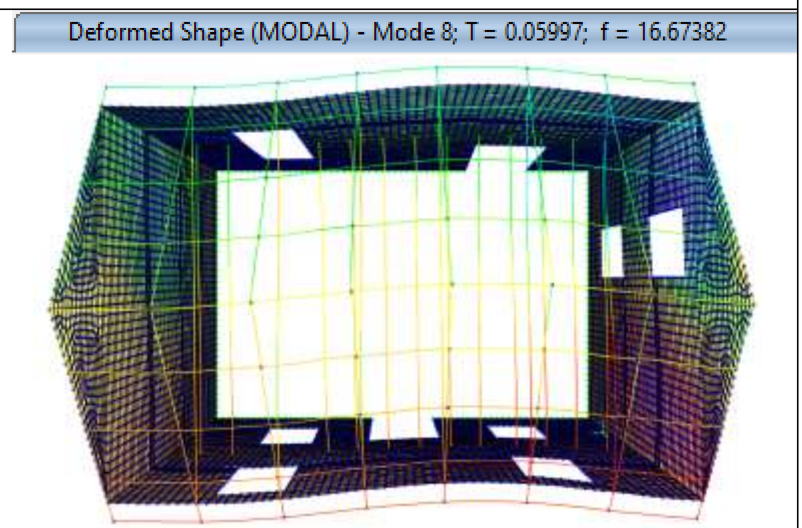

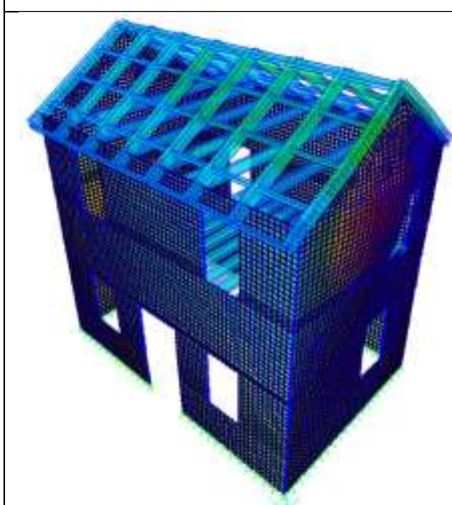

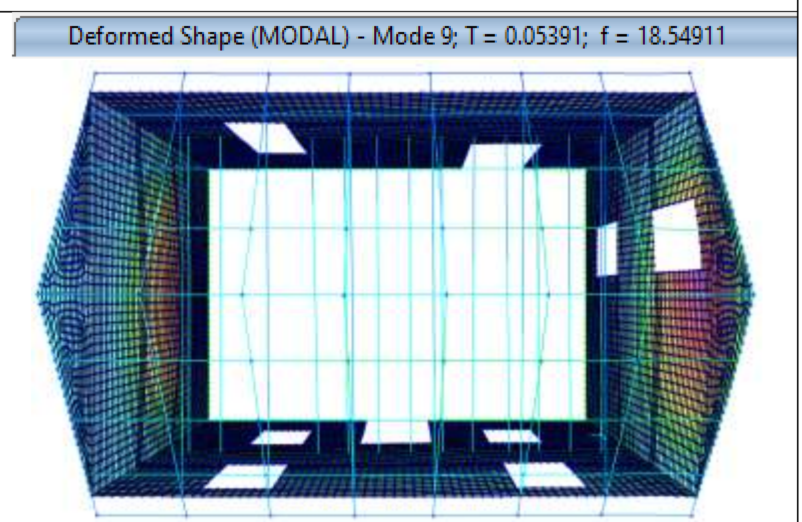

Half scale Shell model, Y Direction

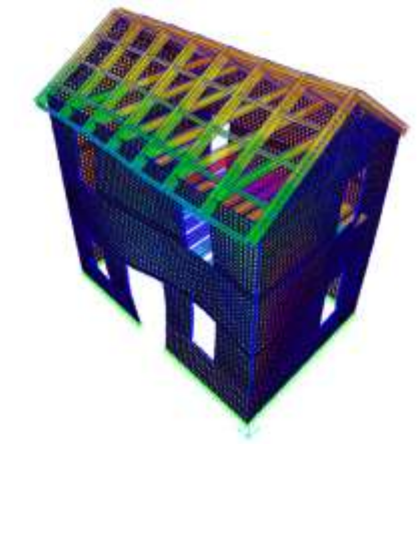

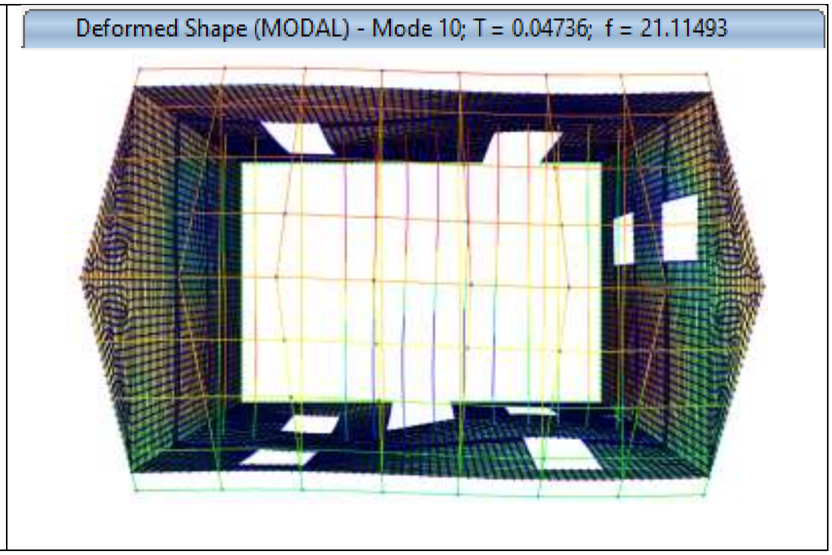

Figure B. 5. Full scale Shell model, X Direction

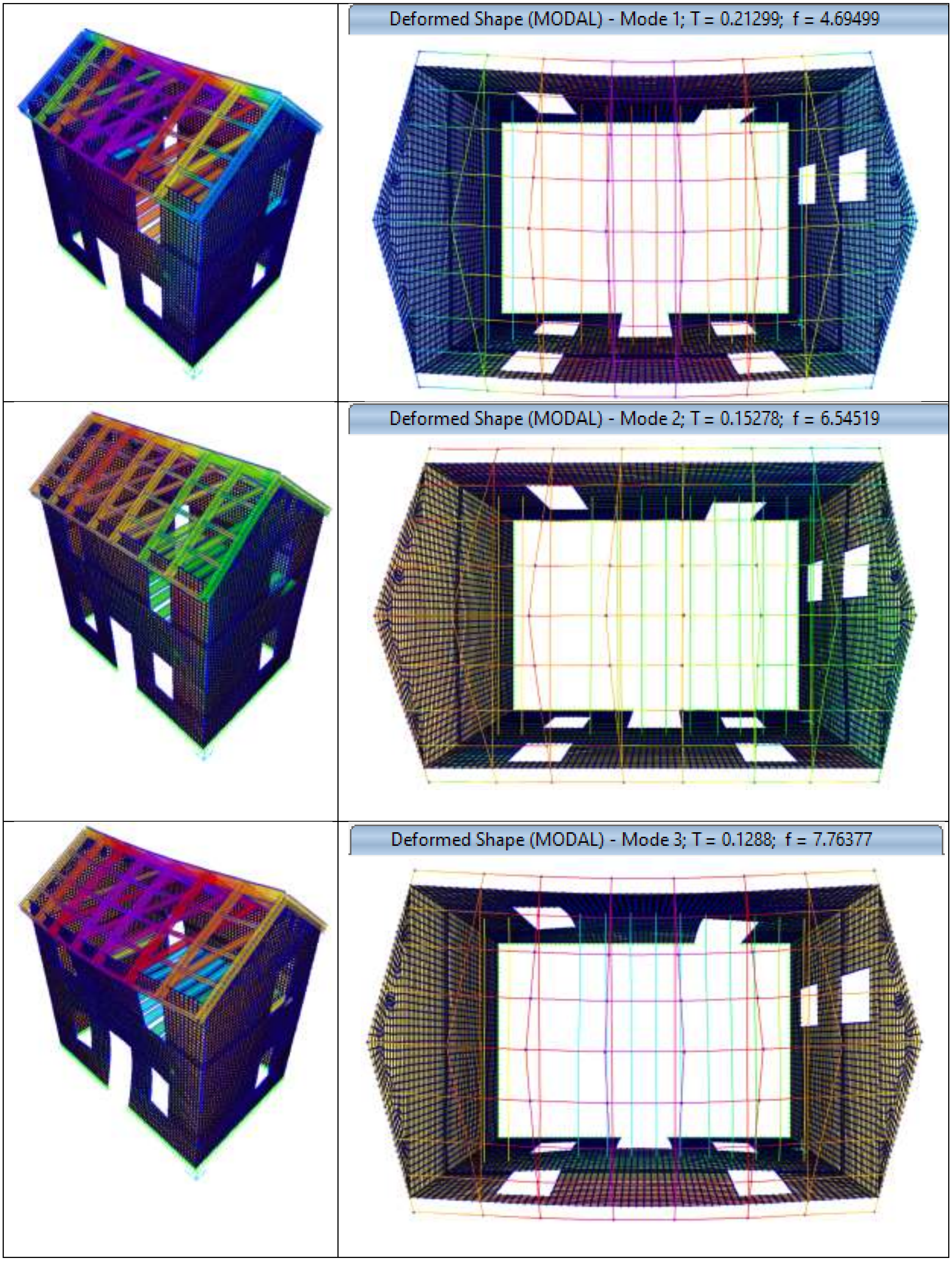

Full scale Shell model, X Direction

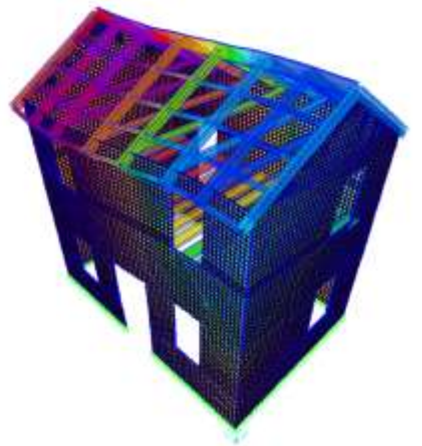

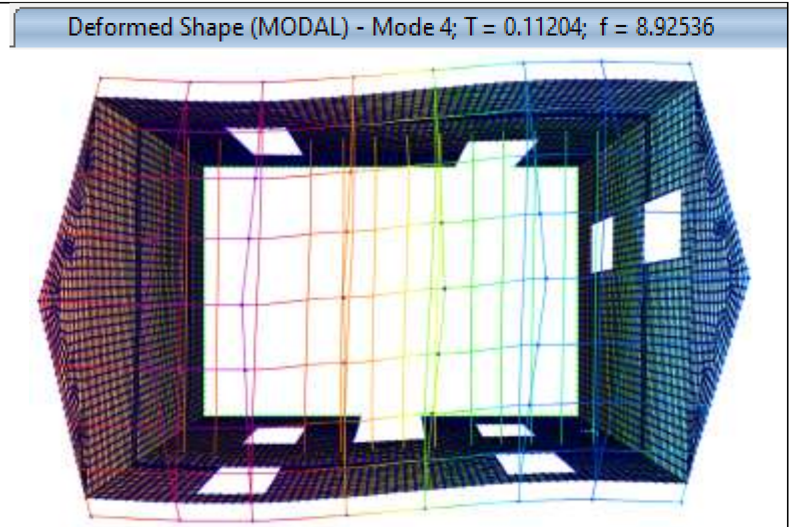

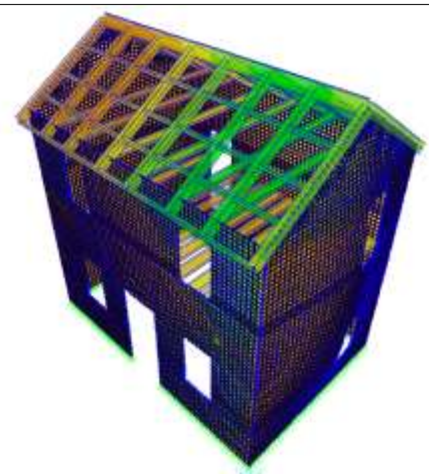

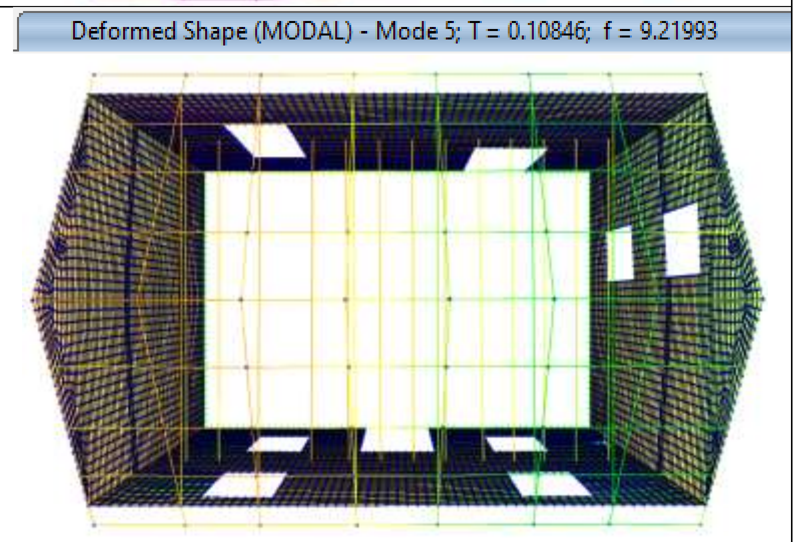

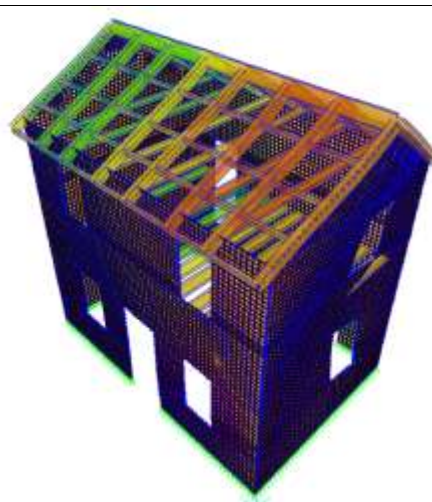

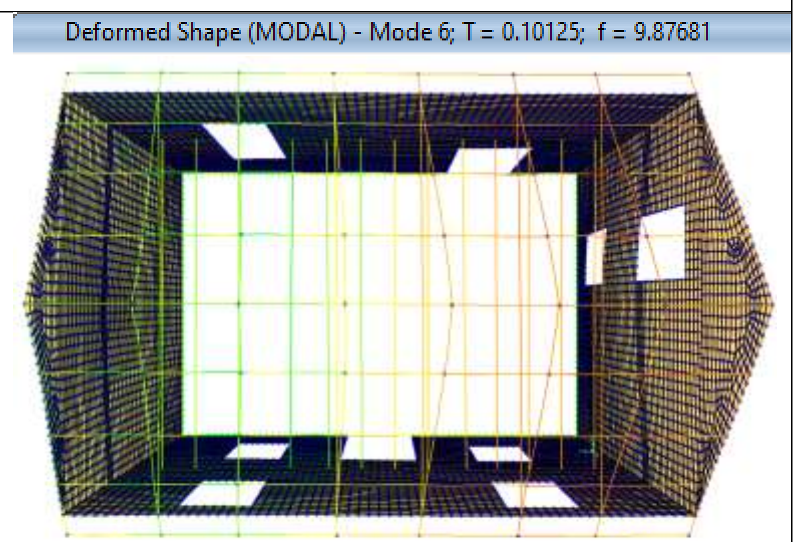

Full scale Shell model, X Direction

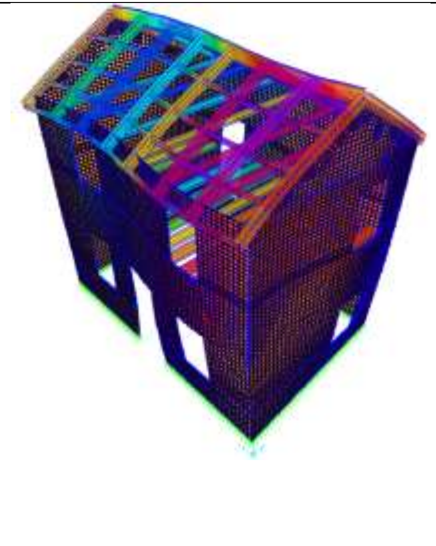

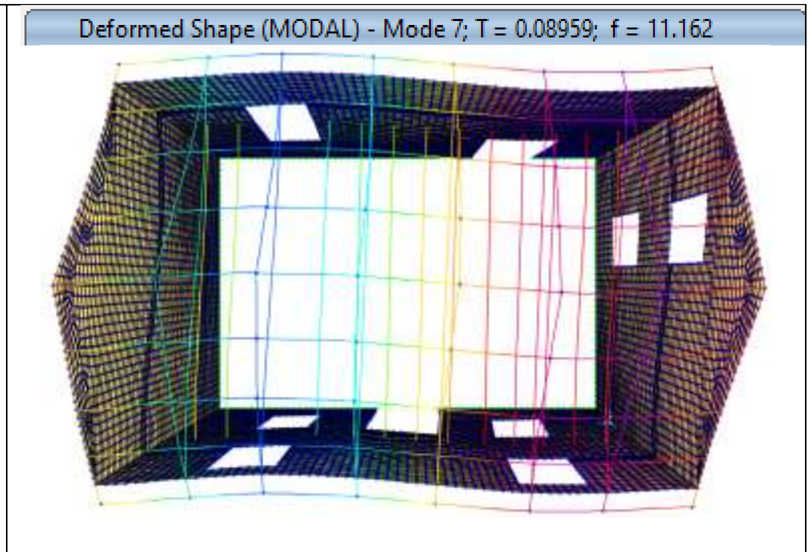

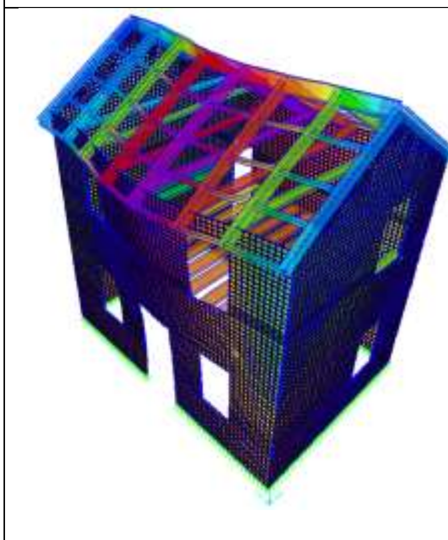

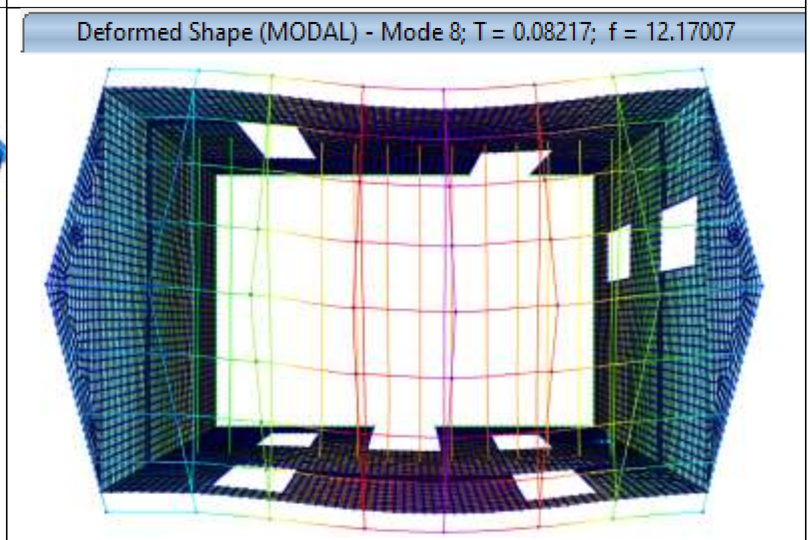

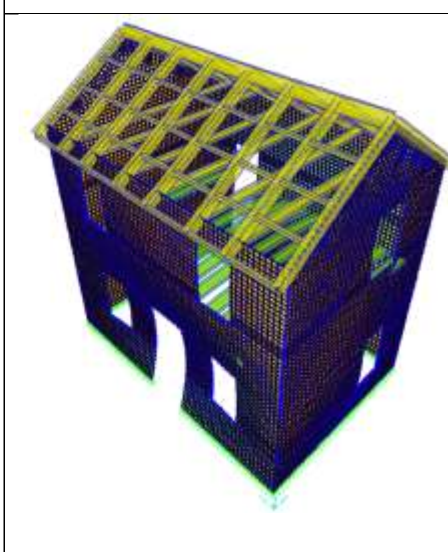

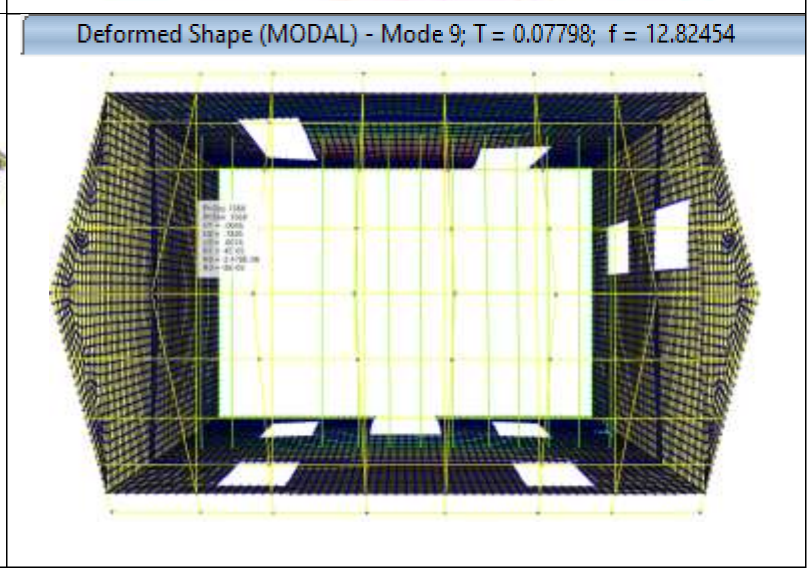

Full scale Shell model, X Direction

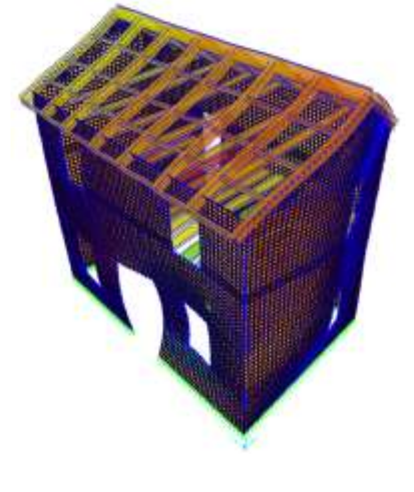

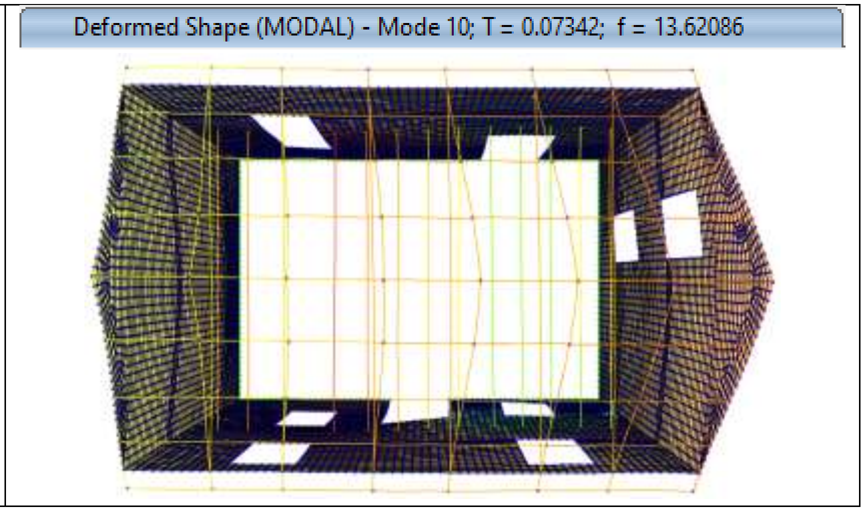

Figure B. 6. Full scale Shell model, Y Direction

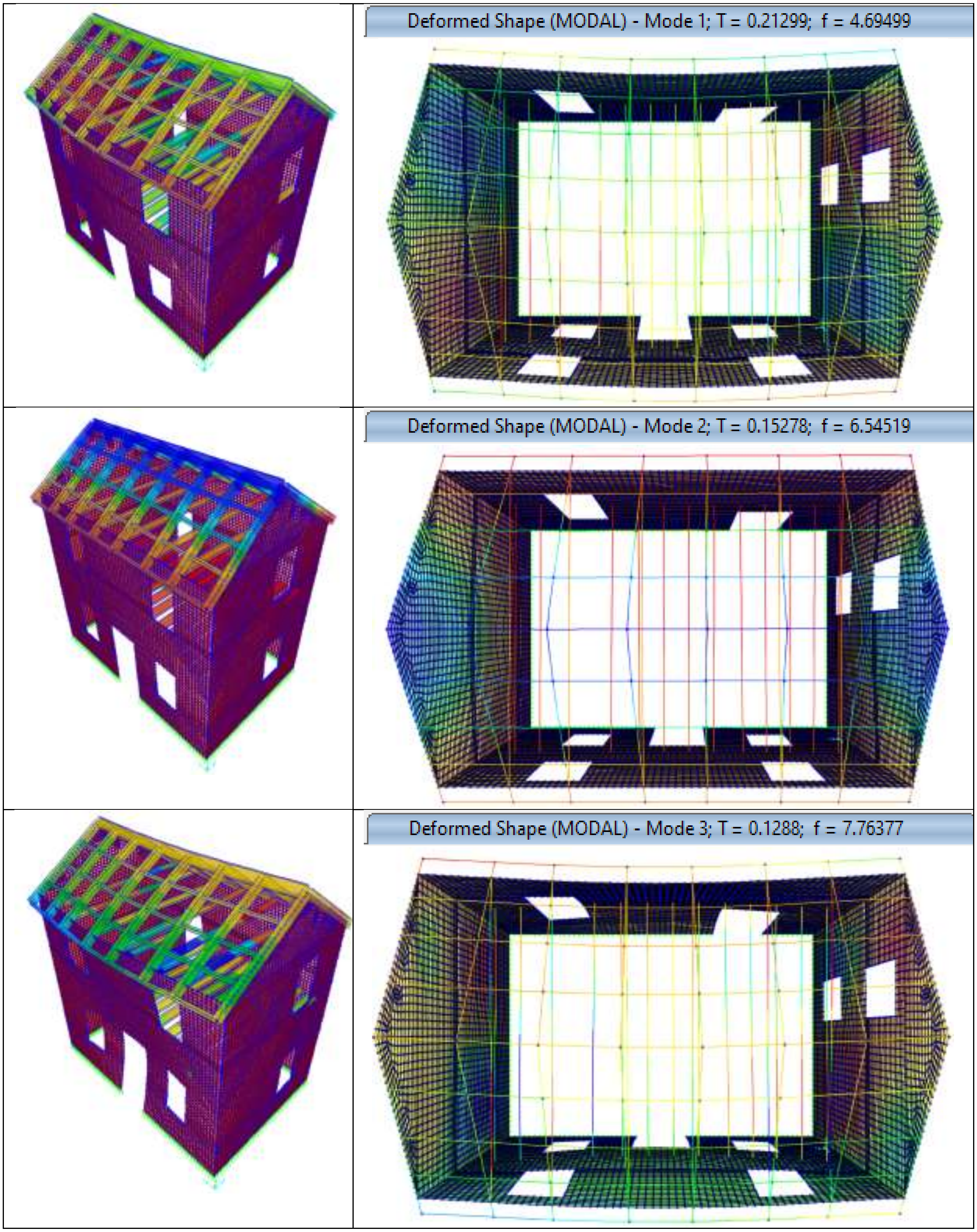

Full scale Shell model, Y Direction

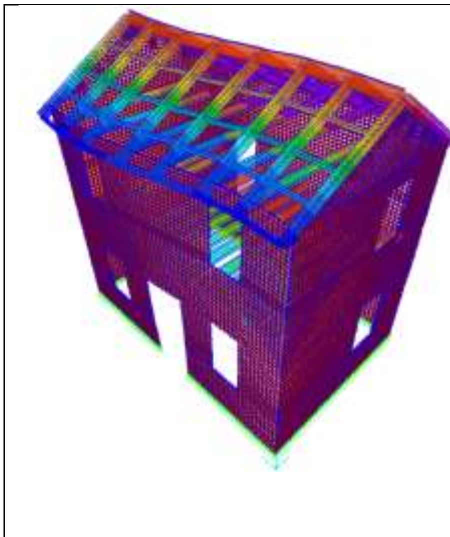

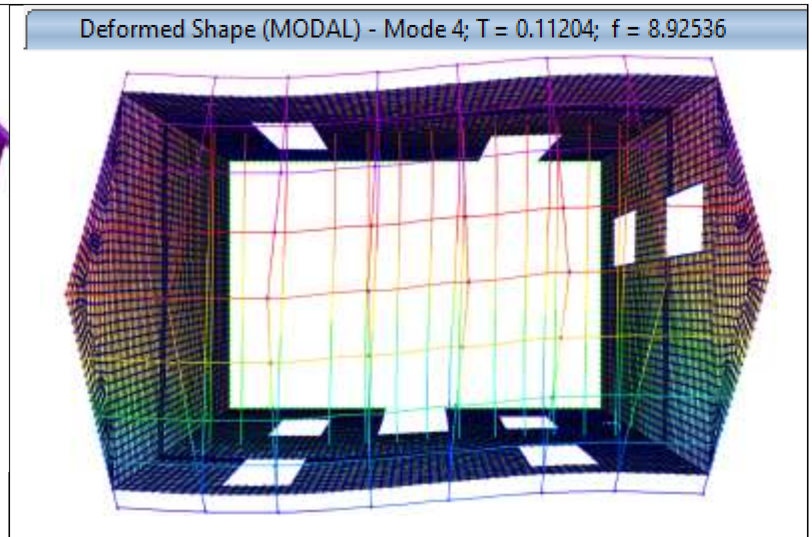

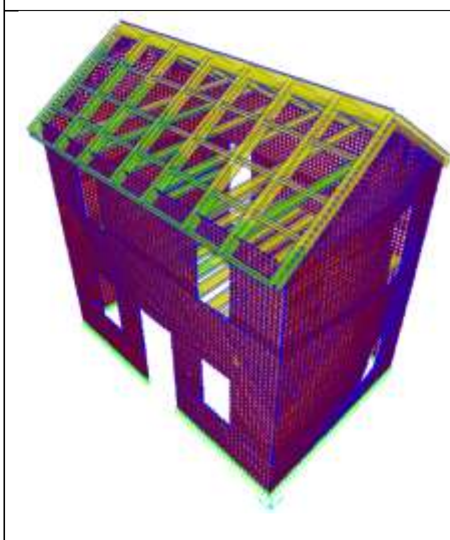

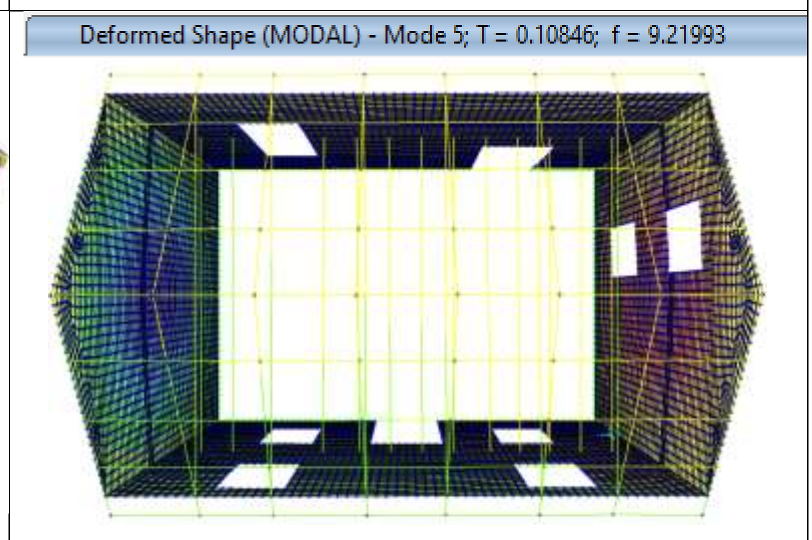

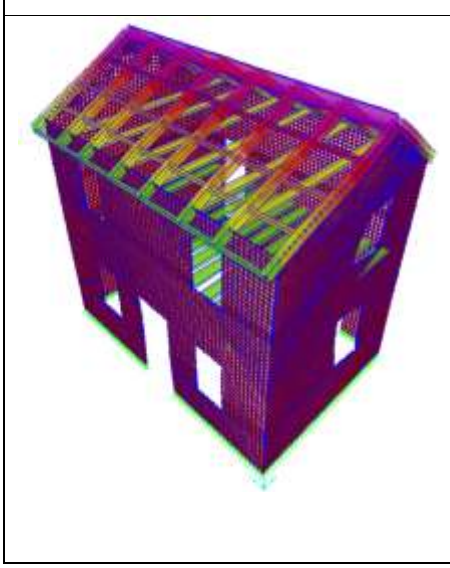

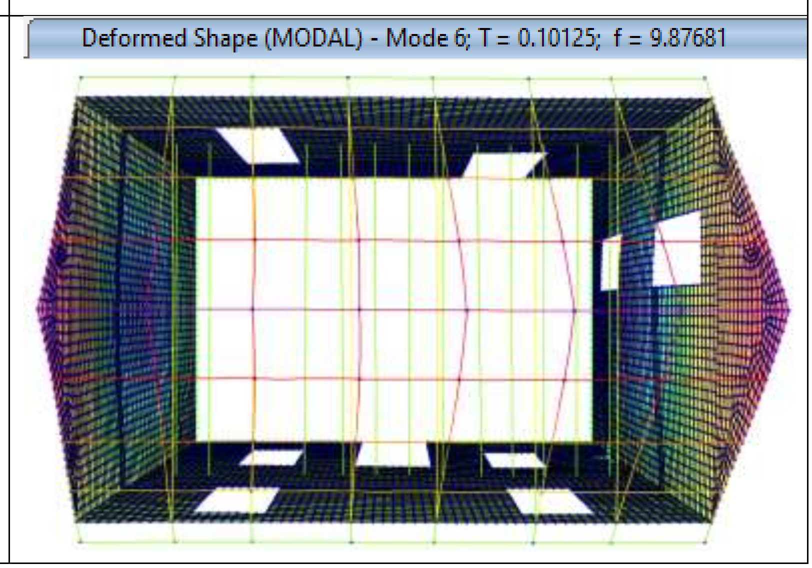

Full scale Shell model, Y Direction

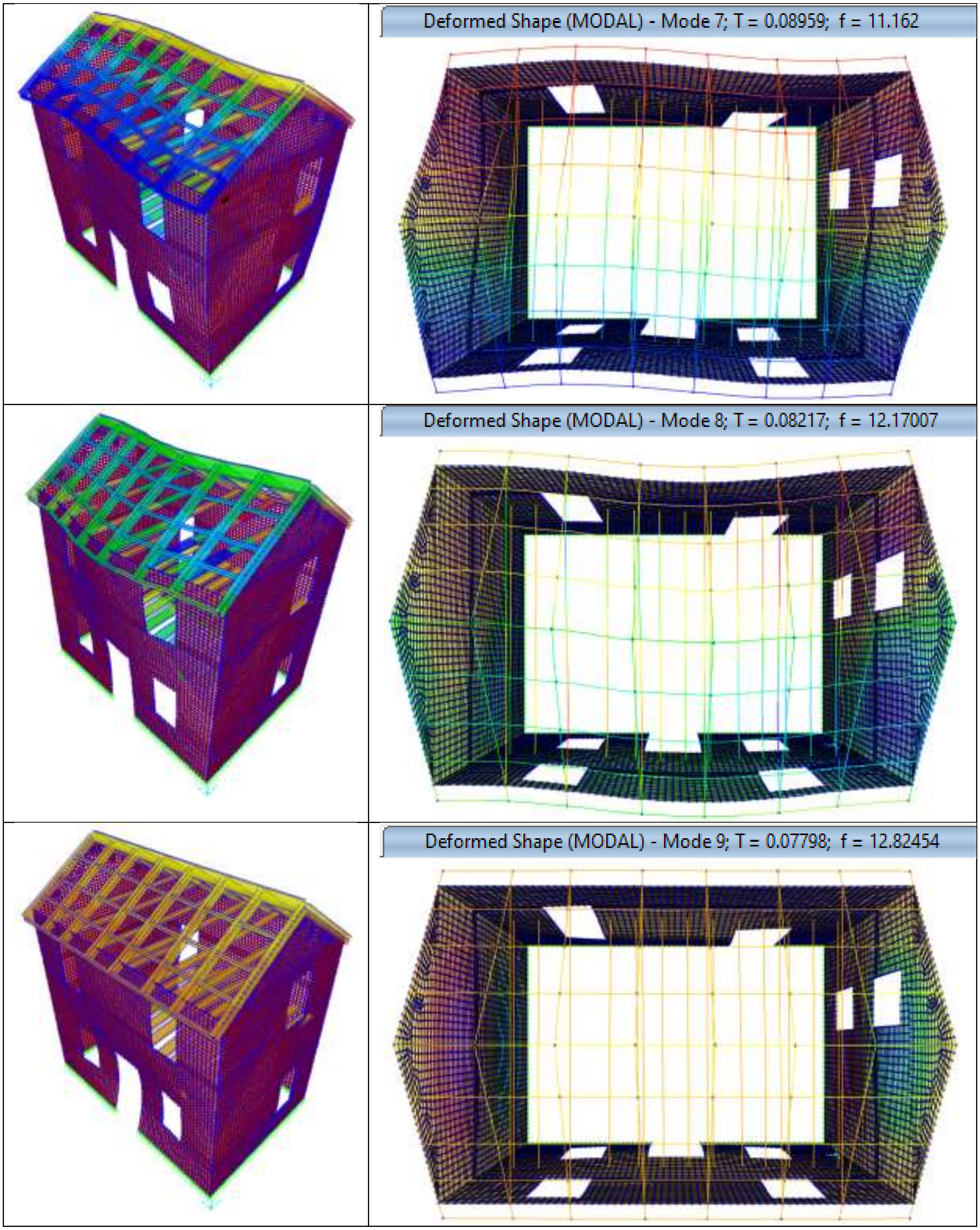

Full scale Shell model, Y Direction

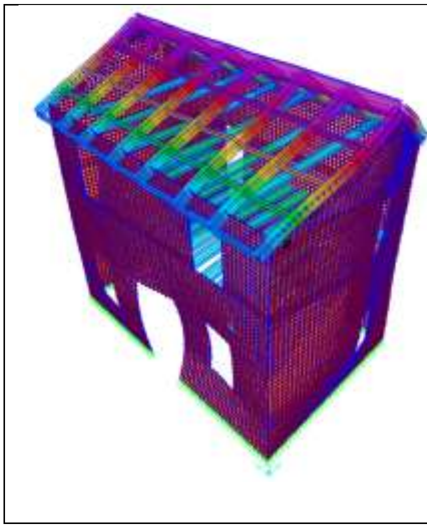

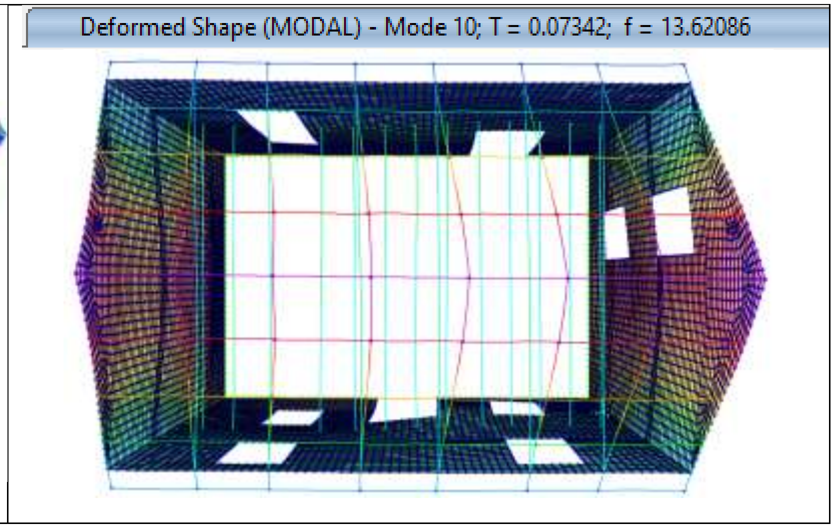

Appendix C: Modal Analysis Result

Table C. 1: Frame model half scale Modal Participating Mass Ratios E=840 MPa									
OutputCase	**StepType**	**StepNum**	**Period**	**UX**	**UY**	**UZ**	**SumUX**	**SumUY**	**SumUZ**
Text	Text	Unitless	Sec	Unitless	Unitless	Unitless	Unitless	Unitless	Unitless
MODAL	Mode	1	0.222703	0.005614	0.17	4.997E-07	0.005614	0.17	4.997E-07
MODAL	Mode	2	0.187699	0.52	0.004152	0.000003618	0.52	0.17	0.000004117
MODAL	Mode	3	0.13145	0.002254	0.29	0.000006788	0.53	0.46	0.00001091
MODAL	Mode	4	0.108986	0.001317	0.02341	1.524E-07	0.53	0.48	0.00001106
MODAL	Mode	5	0.106749	0.009588	0.001425	0.000006794	0.54	0.49	0.00001785
MODAL	Mode	6	0.096766	0.02614	0.12	0.00002141	0.56	0.61	0.00003926
MODAL	Mode	7	0.092324	0.17	0.005253	0.000002541	0.73	0.61	0.00004181
MODAL	Mode	8	0.090325	0.0006464	0.001282	6.516E-08	0.73	0.61	0.00004187
MODAL	Mode	9	0.083765	0.003327	0.003215	0.000004697	0.73	0.62	0.00004657
MODAL	Mode	10	0.079979	0.003972	0.15	0.00001404	0.74	0.77	0.00006061
MODAL	Mode	11	0.070061	0.0002332	0.00001177	0.00003235	0.8	0.78	0.0004952
MODAL	Mode	12	0.069299	0.0000191	0.0268	0.000003746	0.8	0.81	0.000499
MODAL	Mode	13	0.066228	0.00003086	0.02845	0.00002998	0.8	0.84	0.000529
MODAL	Mode	14	0.064108	0.006627	0.001845	0.000003867	0.8	0.84	0.0005328
MODAL	Mode	15	0.063356	0.0005434	0.002335	1.179E-08	0.8	0.84	0.0005328
MODAL	Mode	16	0.053803	0.00005008	0.001668	0.00001016	0.8	0.84	0.000543
MODAL	Mode	17	0.050702	0.000001574	0.00003679	0.00007911	0.8	0.84	0.0006221
MODAL	Mode	18	0.048646	0.002653	0.000002362	0.003655	0.81	0.84	0.004277
MODAL	Mode	19	0.045398	0.008638	0.00001972	0.0004476	0.81	0.84	0.004724
MODAL	Mode	20	0.043684	0.006886	0.00009596	0.0002537	0.82	0.84	0.004978

Table C. 2: Frame model half scale Modal Participating Mass Ratios E=840 MPa									
OutputCase	**StepType**	**StepNum**	**Period**	**RX**	**RY**	**RZ**	**SumRX**	**SumRY**	**SumRZ**
Text	Text	Unitless	Sec	Unitless	Unitless	Unitless	Unitless	Unitless	Unitless
MODAL	Mode	1	0.222703	0.02093	0.001553	0.000006718	0.02093	0.001553	0.000006718
MODAL	Mode	2	0.187699	0.0005115	0.12	0.006063	0.02144	0.12	0.006069
MODAL	Mode	3	0.13145	0.04422	0.000412	0.001575	0.06566	0.12	0.007644
MODAL	Mode	4	0.108986	0.01451	2.42E-05	0.0272	0.08017	0.12	0.03484

Table C. 2: Frame model half scale Modal Participating Mass Ratios E=840 MPa									
OutputCase	**StepType**	**StepNum**	**Period**	**RX**	**RY**	**RZ**	**SumRX**	**SumRY**	**SumRZ**
Text	Text	Unitless	Sec	Unitless	Unitless	Unitless	Unitless	Unitless	Unitless
MODAL	Mode	5	0.106749	0.002111	3.85E-05	0.45	0.08228	0.12	0.49
MODAL	Mode	6	0.096766	0.0126	0.000769	0.08334	0.09487	0.12	0.57
MODAL	Mode	7	0.092324	0.002753	0.03756	0.001825	0.09763	0.16	0.57
MODAL	Mode	8	0.090325	0.00485	4.46E-05	0.0003943	0.1	0.16	0.57
MODAL	Mode	9	0.083765	0.05061	0.000177	0.008131	0.15	0.16	0.58
MODAL	Mode	10	0.079979	0.01351	0.000798	0.09435	0.17	0.16	0.68
MODAL	Mode	11	0.070061	0.00001342	0.0001807	0.0005338	0.2	0.31	0.54
MODAL	Mode	12	0.069299	0.001971	0.0002723	0.007467	0.2	0.31	0.55
MODAL	Mode	13	0.066228	0.006695	0.0005537	0.003368	0.21	0.31	0.56
MODAL	Mode	14	0.064108	0.0004764	0.001055	0.16	0.21	0.31	0.71
MODAL	Mode	15	0.063356	0.0001656	0.01281	0.06239	0.21	0.32	0.78
MODAL	Mode	16	0.053803	0.0006453	0.00003639	0.0002106	0.21	0.32	0.78
MODAL	Mode	17	0.050702	0.0001337	0.02377	0.0000749	0.21	0.35	0.78
MODAL	Mode	18	0.048646	0.000001306	0.003478	0.000009203	0.21	0.35	0.78
MODAL	Mode	19	0.045398	0.0004082	0.009551	0.000431	0.21	0.36	0.78
MODAL	Mode	20	0.043684	0.00003171	0.004155	0.000005972	0.21	0.36	0.78

Table C. 3: Shell model half scale Modal Participating Mass Ratios E=840 MPa									
OutputCase	**StepType**	**StepNum**	**Period**	**UX**	**UY**	**UZ**	**SumUX**	**SumUY**	**SumUZ**
Text	Text	Unitless	Sec	Unitless	Unitless	Unitless	Unitless	Unitless	Unitless
MODAL	Mode	1	0.147577	0.57	2.278E-08	1.731E-09	0.57	2.278E-08	1.731E-09
MODAL	Mode	2	0.103127	0.000000302	0.67	0.0001099	0.57	0.67	0.0001099
MODAL	Mode	3	0.093126	0.005166	0.001378	0.000006231	0.58	0.68	0.0001161
MODAL	Mode	4	0.083796	0.004331	0.003299	0.00006814	0.58	0.68	0.0001843
MODAL	Mode	5	0.073109	0.000394	0.11	0.00003865	0.58	0.79	0.0002229
MODAL	Mode	6	0.06638	0.0034	0.0002418	0.000005936	0.58	0.79	0.0002288
MODAL	Mode	7	0.063014	0.06175	0.005056	0.00005891	0.65	0.79	0.0002878
MODAL	Mode	8	0.059974	0.19	0.0001156	0.00002581	0.84	0.79	0.0003136
MODAL	Mode	9	0.053911	0.0001883	0.08049	0.0006593	0.84	0.87	0.0009729
MODAL	Mode	10	0.04736	0.001359	0.0007663	8.761E-07	0.84	0.87	0.0009737
MODAL	Mode	11	0.045031	0.008489	0.0001178	0.00002256	0.85	0.87	0.0009963
MODAL	Mode	12	0.039084	0.0009942	0.000123	0.00001399	0.85	0.87	0.00101
MODAL	Mode	13	0.037052	0.00001308	0.002849	0.00008239	0.85	0.88	0.001093
MODAL	Mode	14	0.034896	0.004073	0.000006691	0.00008202	0.85	0.88	0.001175
MODAL	Mode	15	0.034517	0.002443	0.0000716	0.00004825	0.86	0.88	0.001223
MODAL	Mode	16	0.031149	0.005431	0.004962	0.001495	0.86	0.88	0.002718

Table C. 3: Shell model half scale Modal Participating Mass Ratios E=840 MPa									
OutputCase	**StepType**	**StepNum**	**Period**	**UX**	**UY**	**UZ**	**SumUX**	**SumUY**	**SumUZ**
Text	Text	Unitless	Sec	Unitless	Unitless	Unitless	Unitless	Unitless	Unitless
MODAL	Mode	17	0.03098	0.009649	0.001794	0.0001307	0.87	0.88	0.002849
MODAL	Mode	18	0.029665	0.0006529	0.01498	0.02205	0.87	0.9	0.0249
MODAL	Mode	19	0.029014	0.002662	0.001284	0.0699	0.88	0.9	0.09479
MODAL	Mode	20	0.028667	0.005574	0.0004442	0.47	0.88	0.9	0.57

Table C. 4: Shell model half scale Modal Participating Mass Ratios E=840 MPa									
OutputCase	**StepType**	**StepNum**	**Period**	**RX**	**RY**	**RZ**	**SumRX**	**SumRY**	**SumRZ**
Text	Text	Unitless	Sec	Unitless	Unitless	Unitless	Unitless	Unitless	Unitless
MODAL	Mode	1	0.147577	0.000004147	0.04235	0.001987	4.15E-06	0.04235	0.001987
MODAL	Mode	2	0.103127	0.05203	0.0003129	0.0008866	0.05203	0.04267	0.002874
MODAL	Mode	3	0.093126	0.0001116	0.15	9.333E-08	0.05214	0.19	0.002874
MODAL	Mode	4	0.083796	0.0006364	0.008584	0.12	0.05278	0.2	0.13
MODAL	Mode	5	0.073109	0.0003522	1.831E-05	0.01944	0.05313	0.2	0.15
MODAL	Mode	6	0.06638	0.08721	0.0005517	0.04733	0.14	0.2	0.19
MODAL	Mode	7	0.063014	0.01335	0.01121	0.34	0.15	0.21	0.53
MODAL	Mode	8	0.059974	0.0006714	0.06031	0.14	0.15	0.27	0.68
MODAL	Mode	9	0.053911	0.01289	5.795E-06	0.009499	0.17	0.27	0.69
MODAL	Mode	10	0.04736	0.0007859	4.736E-06	0.007537	0.17	0.27	0.69
MODAL	Mode	11	0.045031	0.0002125	0.00128	0.15	0.17	0.28	0.84
MODAL	Mode	12	0.039084	0.00001765	0.0004981	0.00004443	0.17	0.28	0.84
MODAL	Mode	13	0.037052	0.001448	0.0001183	0.0004108	0.17	0.28	0.84
MODAL	Mode	14	0.034896	0.000201	0.0396	0.000142	0.17	0.32	0.84
MODAL	Mode	15	0.034517	0.0001265	0.0002894	0.0001438	0.17	0.32	0.84
MODAL	Mode	16	0.031149	0.02912	0.004289	0.001864	0.2	0.32	0.84
MODAL	Mode	17	0.03098	0.007722	0.02932	0.005038	0.21	0.35	0.85
MODAL	Mode	18	0.029665	0.04092	0.002787	0.0002514	0.25	0.35	0.85
MODAL	Mode	19	0.029014	0.006862	0.00152	0.001329	0.25	0.35	0.85
MODAL	Mode	20	0.028667	0.05504	0.02502	0.00006305	0.31	0.38	0.85

Table C. 5: Shell model full scale Modal Participating Mass Ratios E=840 MPa									
OutputCase	**StepType**	**StepNum**	**Period**	**UX**	**UY**	**UZ**	**SumUX**	**SumUY**	**SumUZ**
Text	Text	Unitless	Sec	Unitless	Unitless	Unitless	Unitless	Unitless	Unitless
MODAL	Mode	1	0.212993	0.5	3.348E-07	5.254E-07	0.5	3.348E-07	5.254E-07
MODAL	Mode	2	0.152784	0.000005147	0.6	0.00001518	0.5	0.6	0.0000157

Table C. 5: Shell model full scale Modal Participating Mass Ratios E=840 MPa									
OutputCase	StepType	StepNum	Period	UX	UY	UZ	SumUX	SumUY	SumUZ
Text	Text	Unitless	Sec	Unitless	Unitless	Unitless	Unitless	Unitless	Unitless
MODAL	Mode	3	0.128803	0.008214	0.0002858	6.451E-07	0.51	0.6	0.00001635
MODAL	Mode	4	0.11204	0.0002198	0.000858	0.00005059	0.51	0.6	0.00006694
MODAL	Mode	5	0.108461	0.000003513	0.00007236	0.0001416	0.51	0.6	0.0002085
MODAL	Mode	6	0.101247	0.00001736	0.05493	0.000002187	0.51	0.66	0.0002107
MODAL	Mode	7	0.08959	0.01302	0.0002749	0.00002791	0.52	0.66	0.0002386
MODAL	Mode	8	0.082169	0.27	0.0000141	9.458E-08	0.79	0.66	0.0002387
MODAL	Mode	9	0.077976	0.002254	0.0007873	0.00004987	0.8	0.66	0.0002886
MODAL	Mode	10	0.073417	0.0005842	0.12	0.0001743	0.8	0.78	0.0004629
MODAL	Mode	11	0.070061	0.0002332	0.00001177	0.00003235	0.8	0.78	0.0004952
MODAL	Mode	12	0.069299	0.0000191	0.0268	0.000003746	0.8	0.81	0.000499
MODAL	Mode	13	0.066228	0.00003086	0.02845	0.00002998	0.8	0.84	0.000529
MODAL	Mode	14	0.064108	0.006627	0.001845	0.000003867	0.8	0.84	0.0005328
MODAL	Mode	15	0.063356	0.0005434	0.002335	1.179E-08	0.8	0.84	0.0005328
MODAL	Mode	16	0.053803	0.00005008	0.001668	0.00001016	0.8	0.84	0.000543
MODAL	Mode	17	0.050702	0.000001574	0.00003679	0.00007911	0.8	0.84	0.0006221
MODAL	Mode	18	0.048646	0.002653	0.000002362	0.003655	0.81	0.84	0.004277
MODAL	Mode	19	0.045398	0.008638	0.00001972	0.0004476	0.81	0.84	0.004724
MODAL	Mode	20	0.043684	0.006886	0.00009596	0.0002537	0.82	0.84	0.004978
MODAL	Mode	11	0.045031	0.0002125	0.00128	0.15	0.17	0.28	0.84
MODAL	Mode	12	0.039084	0.00001765	0.0004981	0.00004443	0.17	0.28	0.84
MODAL	Mode	13	0.037052	0.001448	0.0001183	0.0004108	0.17	0.28	0.84
MODAL	Mode	14	0.034896	0.000201	0.0396	0.000142	0.17	0.32	0.84
MODAL	Mode	15	0.034517	0.0001265	0.0002894	0.0001438	0.17	0.32	0.84
MODAL	Mode	16	0.031149	0.02912	0.004289	0.001864	0.2	0.32	0.84
MODAL	Mode	17	0.03098	0.007722	0.02932	0.005038	0.21	0.35	0.85
MODAL	Mode	18	0.029665	0.04092	0.002787	0.0002514	0.25	0.35	0.85
MODAL	Mode	19	0.029014	0.006862	0.00152	0.001329	0.25	0.35	0.85
MODAL	Mode	20	0.028667	0.05504	0.02502	0.00006305	0.31	0.38	0.85

Table C. 6: Shell model full scale Modal Participating Mass Ratios									
OutputCase	**StepType**	**StepNum**	**Period**	**RX**	**RY**	**RZ**	**SumRX**	**SumRY**	**SumRZ**
Text	Text	Unitless	Sec	Unitless	Unitless	Unitless	Unitless	Unitless	Unitless
MODAL	Mode	1	0.212993	0.000006387	0.0598	0.001604	6.39E-06	0.0598	0.001604
MODAL	Mode	2	0.152784	0.1	0.00008728	0.001365	0.1	0.05989	0.002969
MODAL	Mode	3	0.128803	0.000008831	0.15	0.00002118	0.1	0.21	0.00299
MODAL	Mode	4	0.11204	0.001884	0.001689	0.12	0.1	0.22	0.12
MODAL	Mode	5	0.108461	0.00003611	0.0001162	0.001122	0.1	0.22	0.12
MODAL	Mode	6	0.101247	0.07532	0.00002179	0.006672	0.18	0.22	0.13
MODAL	Mode	7	0.08959	6.786E-08	0.002006	0.4	0.18	0.22	0.52
MODAL	Mode	8	0.082169	0.00005925	0.08781	0.01802	0.18	0.31	0.54
MODAL	Mode	9	0.077976	0.0001232	0.000842	0.00005163	0.18	0.31	0.54
MODAL	Mode	10	0.073417	0.0192	0.0000296	0.0008525	0.2	0.31	0.54
MODAL	Mode	11	0.070061	0.00001342	0.0001807	0.0005338	0.2	0.31	0.54
MODAL	Mode	12	0.069299	0.001971	0.0002723	0.007467	0.2	0.31	0.55
MODAL	Mode	13	0.066228	0.006695	0.0005537	0.003368	0.21	0.31	0.56
MODAL	Mode	14	0.064108	0.0004764	0.001055	0.16	0.21	0.31	0.71
MODAL	Mode	15	0.063356	0.0001656	0.01281	0.06239	0.21	0.32	0.78
MODAL	Mode	16	0.053803	0.0006453	0.00003639	0.0002106	0.21	0.32	0.78
MODAL	Mode	17	0.050702	0.0001337	0.02377	0.0000749	0.21	0.35	0.78
MODAL	Mode	18	0.048646	0.000001306	0.003478	0.000009203	0.21	0.35	0.78
MODAL	Mode	19	0.045398	0.0004082	0.009551	0.000431	0.21	0.36	0.78
MODAL	Mode	20	0.043684	0.00003171	0.004155	0.000005972	0.21	0.36	0.78

Table C. 7: Frame model half scale Modal Participating Mass Ratios, after changing E									
OutputCase	**StepType**	**StepNum**	**Period**	**UX**	**UY**	**UZ**	**SumUX**	**SumUY**	**SumUZ**
Text	Text	Unitless	Sec	Unitless	Unitless	Unitless	Unitless	Unitless	Unitless
MODAL	Mode	1	0.115308	0.37	0.01149	0.000001414	0.37	0.01149	0.000001414
MODAL	Mode	2	0.098621	0.04897	0.15	3.87E-08	0.42	0.16	0.000001453
MODAL	Mode	3	0.063363	0.00421	0.21	0.00001019	0.42	0.37	0.00001165
MODAL	Mode	4	0.052305	0.002482	0.01933	4.523E-08	0.42	0.39	0.00001169
MODAL	Mode	5	0.049764	0.11	0.0003285	7.367E-08	0.54	0.39	0.00001177
MODAL	Mode	6	0.047374	0.00007879	0.003908	0.000004795	0.54	0.39	0.00001656
MODAL	Mode	7	0.041214	0.004201	0.02328	6.145E-07	0.54	0.41	0.00001718
MODAL	Mode	8	0.040935	0.001482	0.02053	1.223E-07	0.54	0.44	0.0000173
MODAL	Mode	9	0.038661	0.15	0.007933	0.00004963	0.69	0.44	0.00006693
MODAL	Mode	10	0.036926	0.001819	0.36	0.0001044	0.69	0.81	0.0001713
MODAL	Mode	11	0.032679	0.0001219	0.003783	3.497E-07	0.69	0.81	0.0001717
MODAL	Mode	12	0.032039	0.0006695	0.0009237	0.00002634	0.69	0.81	0.000198
MODAL	Mode	13	0.031577	0.00004879	0.006652	0.000001382	0.69	0.82	0.0001994

Table C. 7: Frame model half scale Modal Participating Mass Ratios, after changing E									
OutputCase	**StepType**	**StepNum**	**Period**	**UX**	**UY**	**UZ**	**SumUX**	**SumUY**	**SumUZ**
Text	Text	Unitless	Sec	Unitless	Unitless	Unitless	Unitless	Unitless	Unitless
MODAL	Mode	14	0.028942	0.02349	0.0004261	0.000004159	0.71	0.82	0.0002035
MODAL	Mode	15	0.027549	0.0000549	0.0002411	0.000007516	0.71	0.82	0.0002111
MODAL	Mode	16	0.026704	0.04822	0.000000565	0.000537	0.76	0.82	0.000748
MODAL	Mode	17	0.026448	0.01188	0.00001598	0.000119	0.77	0.82	0.000867
MODAL	Mode	18	0.025594	0.002381	0.00002586	0.0001718	0.78	0.82	0.001039
MODAL	Mode	19	0.024133	0.03927	0.00002044	0.0001862	0.82	0.82	0.001225
MODAL	Mode	20	0.022542	0.00007768	0.0006324	0.0003505	0.82	0.82	0.001576

Table C. 8: Frame model half scale Modal Participating Mass Ratios, after changing E									
OutputCase	**StepType**	**StepNum**	**Period**	**RX**	**RY**	**RZ**	**SumRX**	**SumRY**	**SumRZ**
Text	Text	Unitless	Sec	Unitless	Unitless	Unitless	Unitless	Unitless	Unitless
MODAL	Mode	1	0.115308	0.00179	0.08448	0.0000972	0.00179	0.08448	0.0000972
MODAL	Mode	2	0.098621	0.02222	0.00987	0.002037	0.02401	0.09435	0.002135
MODAL	Mode	3	0.063363	0.04332	6.269E-05	0.009031	0.06733	0.09441	0.01117
MODAL	Mode	4	0.052305	0.003452	0.003827	0.16	0.07079	0.09824	0.18
MODAL	Mode	5	0.049764	0.000227	0.04871	0.003011	0.07101	0.15	0.18
MODAL	Mode	6	0.047374	0.01681	0.001116	0.00494	0.08782	0.15	0.18
MODAL	Mode	7	0.041214	0.007939	0.0007314	0.03654	0.09576	0.15	0.22
MODAL	Mode	8	0.040935	0.001684	0.0002793	0.22	0.09744	0.15	0.44
MODAL	Mode	9	0.038661	0.00106	0.0395	0.04151	0.0985	0.19	0.48
MODAL	Mode	10	0.036926	0.01714	0.0004673	0.005651	0.12	0.19	0.48
MODAL	Mode	11	0.032679	0.005322	0.00000694	0.00272	0.12	0.19	0.49
MODAL	Mode	12	0.032039	0.02316	0.00003278	0.02715	0.14	0.19	0.51
MODAL	Mode	13	0.031577	0.007807	0.00006314	0.18	0.15	0.19	0.69
MODAL	Mode	14	0.028942	0.003195	0.004491	0.01093	0.16	0.19	0.7
MODAL	Mode	15	0.027549	0.0007232	0.00003174	0.02105	0.16	0.19	0.72
MODAL	Mode	16	0.026704	0.00007837	0.001133	0.007626	0.16	0.19	0.73
MODAL	Mode	17	0.026448	6.719E-06	0.003956	0.002878	0.16	0.2	0.73
MODAL	Mode	18	0.025594	0.00002234	0.001029	0.0007563	0.16	0.2	0.73
MODAL	Mode	19	0.024133	0.00004264	0.005216	0.05038	0.16	0.2	0.78
MODAL	Mode	20	0.022542	0.0006995	0.000413	0.0001083	0.16	0.21	0.78

Table C. 9: Shell model half scale, Modal Participating Mass Ratios, after changing E									
OutputCase	**StepType**	**StepNum**	**Period**	**UX**	**UY**	**UZ**	**SumUX**	**SumUY**	**SumUZ**
Text	Text	Unitless	Sec	Unitless	Unitless	Unitless	Unitless	Unitless	Unitless
MODAL	Mode	1	0.115477	0.51	0.000001693	1.313E-09	0.51	0.000001693	1.313E-09
MODAL	Mode	2	0.073112	0.00006267	0.61	0.0000834	0.51	0.61	0.0000834
MODAL	Mode	3	0.06946	0.02249	0.002256	0.00000368	0.53	0.62	0.00008708
MODAL	Mode	4	0.062009	0.005836	0.00707	0.00006471	0.53	0.62	0.0001518
MODAL	Mode	5	0.051287	0.0007246	0.15	0.00001575	0.53	0.77	0.0001675
MODAL	Mode	6	0.047189	0.002958	0.0003407	0.000001104	0.54	0.77	0.0001686
MODAL	Mode	7	0.044724	0.05054	0.007479	0.00003703	0.59	0.78	0.0002057
MODAL	Mode	8	0.043843	0.23	0.0001106	0.00001244	0.82	0.78	0.0002181
MODAL	Mode	9	0.037979	0.0008172	0.08617	0.0007161	0.82	0.87	0.0009343
MODAL	Mode	10	0.03538	0.003002	0.0002133	0.00001518	0.83	0.87	0.0009494
MODAL	Mode	11	0.033798	0.01544	0.00187	0.000001761	0.84	0.87	0.0009512
MODAL	Mode	12	0.027935	0.00002645	0.005639	0.000002986	0.84	0.87	0.0009542
MODAL	Mode	13	0.027225	0.001128	0.0003785	0.0001533	0.84	0.87	0.001107
MODAL	Mode	14	0.025208	0.0009518	0.00001234	0.0001145	0.84	0.87	0.001222
MODAL	Mode	15	0.024336	0.005269	0.00006684	0.0001026	0.85	0.87	0.001325
MODAL	Mode	16	0.023683	0.01956	0.00006285	0.00007039	0.87	0.87	0.001395
MODAL	Mode	17	0.022145	0.0009664	0.001729	0.000004354	0.87	0.88	0.001399
MODAL	Mode	18	0.021129	0.00003474	0.005932	0.003645	0.87	0.88	0.005045
MODAL	Mode	19	0.02071	0.00001298	0.01341	0.004251	0.87	0.9	0.009296
MODAL	Mode	20	0.019958	0.0005445	0.002167	0.16	0.87	0.9	0.17

Table C. 10: Shell model half scale, Modal Participating Mass Ratios, after changing E									
OutputCase	**StepType**	**StepNum**	**Period**	**RX**	**RY**	**RZ**	**SumRX**	**SumRY**	**SumRZ**
Text	Text	Unitless	Sec	Unitless	Unitless	Unitless	Unitless	Unitless	Unitless
MODAL	Mode	1	0.115477	1.202E-06	0.04464	0.001062	1.2E-06	0.04464	0.001062
MODAL	Mode	2	0.073112	0.05731	0.0003598	0.0001495	0.05731	0.045	0.001211
MODAL	Mode	3	0.06946	0.0002462	0.12	0.0001529	0.05755	0.17	0.001364
MODAL	Mode	4	0.062009	0.001457	0.007783	0.12	0.05901	0.18	0.12
MODAL	Mode	5	0.051287	0.002867	0.0001069	0.02155	0.06188	0.18	0.14
MODAL	Mode	6	0.047189	0.07116	0.0006145	0.04612	0.13	0.18	0.19
MODAL	Mode	7	0.044724	0.01045	0.01111	0.29	0.14	0.19	0.48
MODAL	Mode	8	0.043843	0.0004345	0.07623	0.04106	0.14	0.27	0.52

Table C. 10: Shell model half scale, Modal Participating Mass Ratios, after changing E									
OutputCase	**StepType**	**StepNum**	**Period**	**RX**	**RY**	**RZ**	**SumRX**	**SumRY**	**SumRZ**
Text	Text	Unitless	Sec	Unitless	Unitless	Unitless	Unitless	Unitless	Unitless
MODAL	Mode	9	0.037979	0.01898	0.00003559	0.003379	0.16	0.27	0.53
MODAL	Mode	10	0.03538	0.0001391	0.00181	0.06069	0.16	0.27	0.59
MODAL	Mode	11	0.033798	0.001448	0.002607	0.25	0.16	0.27	0.84
MODAL	Mode	12	0.027935	0.0004087	0.00008922	0.0007485	0.16	0.27	0.84
MODAL	Mode	13	0.027225	0.00001446	0.0003456	0.0000881	0.16	0.27	0.84
MODAL	Mode	14	0.025208	0.0002879	0.01759	0.0001383	0.17	0.29	0.84
MODAL	Mode	15	0.024336	0.00002796	0.008764	0.000149	0.17	0.3	0.84
MODAL	Mode	16	0.023683	7.934E-06	0.02796	0.000325	0.17	0.32	0.84
MODAL	Mode	17	0.022145	0.01209	0.00227	0.00007204	0.18	0.33	0.84
MODAL	Mode	18	0.021129	0.0168	0.02178	0.01151	0.19	0.35	0.85
MODAL	Mode	19	0.02071	0.0183	0.00007933	0.0008267	0.21	0.35	0.85
MODAL	Mode	20	0.019958	0.03445	0.00001153	0.000008482	0.25	0.35	0.85

Table C. 11: Shell model full scale, Modal Participating Mass Ratios, after changing E									
OutputCase	**StepType**	**StepNum**	**Period**	**UX**	**UY**	**UZ**	**SumUX**	**SumUY**	**SumUZ**
Text	Text	Unitless	Sec	Unitless	Unitless	Unitless	Unitless	Unitless	Unitless
MODAL	Mode	1	0.15908	0.46	3.617E-07	2.383E-07	0.46	3.617E-07	2.383E-07
MODAL	Mode	2	0.110722	1.193E-08	0.47	0.0000103	0.46	0.47	0.00001054
MODAL	Mode	3	0.092763	0.02178	0.0001188	1.988E-07	0.48	0.47	0.00001074
MODAL	Mode	4	0.079716	0.0008204	0.001117	0.00004625	0.48	0.47	0.00005699
MODAL	Mode	5	0.07319	0.0001464	0.18	2.316E-08	0.48	0.65	0.00005701
MODAL	Mode	6	0.072507	7.237E-07	0.003791	0.00009708	0.48	0.65	0.0001541
MODAL	Mode	7	0.061816	0.00271	0.00125	0.00003368	0.48	0.65	0.0001878
MODAL	Mode	8	0.05629	0.3	0.000102	0.000002133	0.78	0.65	0.0001899
MODAL	Mode	9	0.052343	0.004662	0.002408	0.0002094	0.78	0.65	0.0003993
MODAL	Mode	10	0.050331	0.0008456	0.09472	0.0001022	0.78	0.75	0.0005015
MODAL	Mode	11	0.048267	0.001383	0.02261	0.00001329	0.78	0.77	0.0005148
MODAL	Mode	12	0.047213	0.001941	4.754E-07	0.00002495	0.79	0.77	0.0005397
MODAL	Mode	13	0.044952	0.003209	0.004535	0.00002571	0.79	0.78	0.0005654
MODAL	Mode	14	0.044569	0.003199	0.05926	0.000039	0.79	0.83	0.0006044
MODAL	Mode	15	0.043869	0.003723	0.003671	0.000006965	0.8	0.84	0.0006114
MODAL	Mode	16	0.036316	0.00004344	0.001991	0.00001571	0.8	0.84	0.0006271
MODAL	Mode	17	0.035208	0.006962	0.00001014	0.001035	0.8	0.84	0.001663
MODAL	Mode	18	0.034146	0.0001943	0.000005299	0.006448	0.8	0.84	0.008111
MODAL	Mode	19	0.032309	0.01685	0.000000695	0.0004861	0.82	0.84	0.008597
MODAL	Mode	20	0.03181	0.000851	0.00009761	0.00002062	0.82	0.84	0.008617

Table C. 12: Shell model full scale, Modal Participating Mass Ratios, after changing E									
OutputCase	**StepType**	**StepNum**	**Period**	**RX**	**RY**	**RZ**	**SumRX**	**SumRY**	**SumRZ**
Text	Text	Unitless	Sec	Unitless	Unitless	Unitless	Unitless	Unitless	Unitless
MODAL	Mode	1	0.15908	0.0000042	0.06148	0.00116	4.2E-06	0.06148	0.00116
MODAL	Mode	2	0.110722	0.12	0.0000381	0.0006522	0.12	0.06152	0.001812
MODAL	Mode	3	0.092763	0.00001044	0.13	0.0001259	0.12	0.19	0.001938
MODAL	Mode	4	0.079716	0.002309	0.00169	0.11	0.12	0.19	0.11
MODAL	Mode	5	0.07319	0.02445	0.0000818	0.01709	0.14	0.19	0.13
MODAL	Mode	6	0.072507	0.0005922	0.00006528	0.001645	0.14	0.19	0.13
MODAL	Mode	7	0.061816	0.0001108	0.0003847	0.29	0.15	0.19	0.42
MODAL	Mode	8	0.05629	0.0002902	0.11	0.000105	0.15	0.3	0.42
MODAL	Mode	9	0.052343	0.00122	0.0008814	0.00002473	0.15	0.3	0.42
MODAL	Mode	10	0.050331	0.04087	0.0001076	0.0002245	0.19	0.3	0.42
MODAL	Mode	11	0.048267	0.007182	0.00007637	0.006799	0.19	0.3	0.43
MODAL	Mode	12	0.047213	0.00006642	0.0007183	0.003249	0.19	0.3	0.43
MODAL	Mode	13	0.044952	0.006753	0.002679	0.23	0.2	0.3	0.66
MODAL	Mode	14	0.044569	0.0009353	0.00001736	0.09825	0.2	0.3	0.76
MODAL	Mode	15	0.043869	0.0007143	0.01676	0.005267	0.2	0.32	0.77
MODAL	Mode	16	0.036316	0.00104	0.0001636	0.0008086	0.2	0.32	0.77
MODAL	Mode	17	0.035208	0.00005756	0.009167	0.000003318	0.2	0.33	0.77
MODAL	Mode	18	0.034146	6.451E-07	0.007933	0.00006169	0.2	0.33	0.77
MODAL	Mode	19	0.032309	0.0005153	0.02165	0.001243	0.2	0.36	0.77
MODAL	Mode	20	0.03181	0.001401	0.0005189	0.002803	0.21	0.36	0.77

Table C. 13: Modal Periods and Frequencies for a Full-Scale Shell Model without Timber Ceiling						
OutputCase	**StepType**	**StepNum**	**Period**	**Frequency**	**CircFreq**	**Eigenvalue**
Text	Text	Unitless	Sec	Cyc/sec	rad/sec	rad2/sec2
MODAL	Mode	1	0.159017	6.288626553	39.51260596	1561.24603
MODAL	Mode	2	0.110722	9.031637454	56.74745175	3220.27328
MODAL	Mode	3	0.092742	10.78264286	67.7493432	4589.973504
MODAL	Mode	4	0.079715	12.54476216	78.82106528	6212.760333
MODAL	Mode	5	0.07319	13.66304327	85.84743275	7369.78171
MODAL	Mode	6	0.072507	13.7918542	86.65677566	7509.396768
MODAL	Mode	7	0.061811	16.17822038	101.6507566	10332.87631
MODAL	Mode	8	0.056286	17.76644928	111.6298931	12461.23303
MODAL	Mode	9	0.052343	19.10473157	120.0385687	14409.25798
MODAL	Mode	10	0.05033	19.86890375	124.8400041	15585.02663
MODAL	Mode	11	0.048266	20.71868423	130.1793324	16946.65857
MODAL	Mode	12	0.047213	21.1807908	133.0828336	17711.04059

Table C. 13: Modal Periods and Frequencies for a Full-Scale Shell Model without Timber Ceiling						
OutputCase	**StepType**	**StepNum**	**Period**	**Frequency**	**CircFreq**	**Eigenvalue**
Text	Text	Unitless	Sec	Cyc/sec	rad/sec	rad2/sec2
MODAL	Mode	13	0.044951	22.24651152	139.7789543	19538.15606
MODAL	Mode	14	0.044569	22.43713223	140.9766596	19874.41855
MODAL	Mode	15	0.043868	22.79540878	143.2277775	20514.19626
MODAL	Mode	16	0.036316	27.5362981	173.0156637	29934.41987
MODAL	Mode	17	0.035208	28.40274341	178.4597001	31847.86454
MODAL	Mode	18	0.034146	29.28607884	184.0098603	33859.62868
MODAL	Mode	19	0.032308	30.95165055	194.474956	37820.50851
MODAL	Mode	20	0.03181	31.43658769	197.5219059	39014.90329

Table C. 14: Modal Periods and Frequencies for a Full-Scale Shell Model with Timber Ceiling in the Floor						
OutputCase	**StepType**	**StepNum**	**Period**	**Frequency**	**CircFreq**	**Eigenvalue**
Text	Text	Unitless	Sec	Cyc/sec	rad/sec	rad2/sec2
MODAL	Mode	1	0.14314	6.986157139	43.89531989	1926.799108
MODAL	Mode	2	0.111308	8.984085672	56.44867509	3186.45292
MODAL	Mode	3	0.086444	11.56821516	72.68523955	5283.144048
MODAL	Mode	4	0.075196	13.29855026	83.55725562	6981.814967
MODAL	Mode	5	0.073205	13.66029746	85.83018028	7366.819847
MODAL	Mode	6	0.071623	13.96195487	87.7255497	7695.77207
MODAL	Mode	7	0.062459	16.01052415	100.5970901	10119.77454
MODAL	Mode	8	0.055451	18.03390878	113.3103907	12839.24464
MODAL	Mode	9	0.052474	19.05702892	119.7388441	14337.39079
MODAL	Mode	10	0.048501	20.61833733	129.5488342	16782.90044
MODAL	Mode	11	0.046507	21.50205732	135.1014106	18252.39115
MODAL	Mode	12	0.044826	22.30836102	140.1675662	19646.94661
MODAL	Mode	13	0.043723	22.87147473	143.705714	20651.33222
MODAL	Mode	14	0.042901	23.30968509	146.4590709	21450.25945
MODAL	Mode	15	0.038584	25.91720176	162.8425813	26517.70629
MODAL	Mode	16	0.035007	28.56585194	179.4845412	32214.70052
MODAL	Mode	17	0.034409	29.06194235	182.6015691	33343.33305
MODAL	Mode	18	0.0325	30.76964281	193.3313676	37377.01771
MODAL	Mode	19	0.032213	31.0436855	195.0532286	38045.762
MODAL	Mode	20	0.031934	31.31440056	196.7541815	38712.20793

Table C. 15: Modal Periods and Frequencies for a Full-Scale Shell Model with Timber transverse flanges in floor and roof						
OutputCase	**StepType**	**StepNum**	**Period**	**Frequency**	**CircFreq**	**Eigenvalue**
Text	Text	Unitless	Sec	Cyc/sec	rad/sec	rad2/sec2
MODAL	Mode	1	0.138819	7.203621958	45.26169165	2048.620731
MODAL	Mode	2	0.111384	8.977954233	56.41015013	3182.105037
MODAL	Mode	3	0.080651	12.39906685	77.90563466	6069.287912
MODAL	Mode	4	0.074576	13.40910899	84.25191657	7098.385446
MODAL	Mode	5	0.073051	13.68900702	86.01056778	7397.81777
MODAL	Mode	6	0.071255	14.03417345	88.17931241	7775.591137
MODAL	Mode	7	0.063955	15.63592263	98.24339936	9651.765518
MODAL	Mode	8	0.055126	18.14036252	113.9792593	12991.27155
MODAL	Mode	9	0.054049	18.50180682	116.2502808	13514.12778
MODAL	Mode	10	0.048195	20.74923313	130.3712767	16996.66979
MODAL	Mode	11	0.044853	22.2952022	140.0848869	19623.77553
MODAL	Mode	12	0.044595	22.42404566	140.8944342	19851.2416
MODAL	Mode	13	0.043058	23.22470422	145.9251203	21294.14073
MODAL	Mode	14	0.042386	23.59245683	148.2357781	21973.84591
MODAL	Mode	15	0.03747	26.6880974	167.6862615	28118.68228
MODAL	Mode	16	0.034716	28.80494102	180.9867822	32756.21533
MODAL	Mode	17	0.033984	29.42575258	184.8874563	34183.37149
MODAL	Mode	18	0.032268	30.99012408	194.7166923	37914.59026
MODAL	Mode	19	0.031877	31.37036491	197.1058159	38850.70266
MODAL	Mode	20	0.029852	33.49807498	210.4746125	44299.56252

Table C. 16: Modal Periods And Frequencies for Installing timber cross beams in the roof						
OutputCase	**StepType**	**StepNum**	**Period**	**Frequency**	**CircFreq**	**Eigenvalue**
Text	Text	Unitless	Sec	Cyc/sec	rad/sec	rad2/sec2
MODAL	Mode	1	0.148508	6.733660131	42.3088344	1790.037468
MODAL	Mode	2	0.11061	9.040746838	56.8046877	3226.772545
MODAL	Mode	3	0.087394	11.44245039	71.89503615	5168.896223
MODAL	Mode	4	0.07777	12.85845535	80.79205776	6527.356596
MODAL	Mode	5	0.073491	13.60706963	85.49573999	7309.521557
MODAL	Mode	6	0.072135	13.86285157	87.10286527	7586.909139
MODAL	Mode	7	0.06303	15.86537424	99.68508629	9937.116429
MODAL	Mode	8	0.054829	18.23837646	114.595099	13132.03671
MODAL	Mode	9	0.053398	18.7271485	117.6661443	13845.32151
MODAL	Mode	10	0.050582	19.76972849	124.2168675	15429.83018
MODAL	Mode	11	0.048223	20.73689176	130.2937337	16976.45703
MODAL	Mode	12	0.046552	21.48119719	134.9703426	18216.99338
MODAL	Mode	13	0.044561	22.44133933	141.0030936	19881.87239

Table C. 16: Modal Periods And Frequencies for Installing timber cross beams in the roof						
OutputCase	StepType	StepNum	Period	Frequency	CircFreq	Eigenvalue
Text	Text	Unitless	Sec	Cyc/sec	rad/sec	rad2/sec2
MODAL	Mode	14	0.043138	23.18127037	145.6522174	21214.56844
MODAL	Mode	15	0.04055	24.66112247	154.9504024	24009.62719
MODAL	Mode	16	0.035768	27.95818391	175.6664504	30858.70178
MODAL	Mode	17	0.034765	28.76428155	180.7313112	32663.80686
MODAL	Mode	18	0.032129	31.1241131	195.5585701	38243.15435
MODAL	Mode	19	0.031641	31.60436747	198.5760973	39432.46643
MODAL	Mode	20	0.029894	33.45128757	210.1806386	44175.90082

Table C. 17 : Modal Participating Mass Ratios after Installing timber cross beams in the floor, scenario #1									
Output	StepType	StepNum	Period	UX	UY	UZ	SumUX	SumUY	SumUZ
Text	Text	Unitless	Sec	Unitless	Unitless	Unitless	Unitless	Unitless	Unitless
MODAL	Mode	1	0.14314	0.53	0.00006903	4.034E-07	0.53	0.00006903	4.034E-07
MODAL	Mode	2	0.111308	0.00007151	0.48	0.00001559	0.53	0.48	0.00001599
MODAL	Mode	3	0.086444	0.02512	0.00004862	0.0000115	0.55	0.48	0.00002749
MODAL	Mode	4	0.075196	0.005125	0.03568	0.00002547	0.56	0.51	0.00005297
MODAL	Mode	5	0.073205	0.00005409	0.17	0.00001232	0.56	0.68	0.00006529
MODAL	Mode	6	0.071623	0.0000312	0.00008391	0.0001466	0.56	0.68	0.0002119
MODAL	Mode	7	0.062459	0.02343	0.001751	0.00004262	0.58	0.68	0.0002545
MODAL	Mode	8	0.055451	0.21	0.000003306	1.428E-07	0.79	0.68	0.0002547
MODAL	Mode	9	0.052474	0.001048	0.13	0.0002751	0.8	0.81	0.0005298
MODAL	Mode	10	0.048501	0.0004037	0.003293	0.0001848	0.8	0.81	0.0007146
MODAL	Mode	11	0.046507	0.008515	0.0000383	6.137E-08	0.8	0.81	0.0007147
MODAL	Mode	12	0.044826	0.001362	0.03115	0.00005575	0.81	0.84	0.0007704
MODAL	Mode	13	0.043723	0.0009719	0.01238	0.000001066	0.81	0.86	0.0007715
MODAL	Mode	14	0.042901	0.0007795	0.00006044	0.00001223	0.81	0.86	0.0007837
MODAL	Mode	15	0.038584	0.0111	0.00001662	0.0001197	0.82	0.86	0.0009035
MODAL	Mode	16	0.035007	0.0002892	0.0008161	0.00001561	0.82	0.86	0.0009191
MODAL	Mode	17	0.034409	0.008814	0.000002931	0.0007928	0.83	0.86	0.001712
MODAL	Mode	18	0.0325	0.005897	0.00003694	0.008006	0.83	0.86	0.009718
MODAL	Mode	19	0.032213	0.001054	0.00009039	0.01271	0.83	0.86	0.02242
MODAL	Mode	20	0.031934	0.005953	0.00005623	0.003412	0.84	0.86	0.02584

Table C. 18: Modal Participating Mass Ratios after Installing timber cross beams in both the floor and roof structures scenario #2									
Output	StepType	StepNum	Period	UX	UY	UZ	SumUX	SumUY	SumUZ
Text	Text	Unitless	Sec	Unitless	Unitless	Unitless	Unitless	Unitless	Unitless
MODAL	Mode	1	0.138819	0.6	0.00002712	1.639E-07	0.6	0.00002712	1.639E-07
MODAL	Mode	2	0.111384	0.00006275	0.52	0.00001812	0.6	0.52	0.00001829
MODAL	Mode	3	0.080651	0.002409	0.0002228	0.00002977	0.61	0.52	0.00004806
MODAL	Mode	4	0.074576	0.002493	0.13	0.000001371	0.61	0.65	0.00004943
MODAL	Mode	5	0.073051	0.00112	0.07063	0.00001472	0.61	0.72	0.00006414
MODAL	Mode	6	0.071255	0.00001178	0.00000553	0.0002689	0.61	0.72	0.0003331
MODAL	Mode	7	0.063955	0.009513	0.003736	0.00003642	0.62	0.72	0.0003695
MODAL	Mode	8	0.055126	0.00008297	0.1	0.0002208	0.62	0.82	0.0005903
MODAL	Mode	9	0.054049	0.19	0.0005746	0.00001452	0.81	0.82	0.0006048
MODAL	Mode	10	0.048195	0.0003431	0.001416	0.0001159	0.81	0.83	0.0007207
MODAL	Mode	11	0.044853	0.002396	0.01083	0.000004385	0.81	0.84	0.0007251
MODAL	Mode	12	0.044595	0.002696	0.0164	0.00009605	0.81	0.85	0.0008211
MODAL	Mode	13	0.043058	0.00008995	0.005993	0.00003546	0.81	0.86	0.0008566
MODAL	Mode	14	0.042386	0.001174	0.0001679	0.00001448	0.82	0.86	0.0008711
MODAL	Mode	15	0.03747	0.009567	0.000001774	0.00001568	0.83	0.86	0.0008868
MODAL	Mode	16	0.034716	0.0000434	0.0006246	0.000001189	0.83	0.86	0.000888
MODAL	Mode	17	0.033984	0.006483	0.000001591	0.0002261	0.83	0.86	0.001114
MODAL	Mode	18	0.032268	0.00932	0.000008394	0.0001248	0.84	0.86	0.001239
MODAL	Mode	19	0.031877	0.009126	0.000002262	0.0004208	0.85	0.86	0.00166
MODAL	Mode	20	0.029852	0.0007304	0.00004632	0.06031	0.85	0.86	0.06196

Table C. 19: Modal Participating Mass Ratios After adding the transverse flanges to the roof scenario #3									
Output	**StepType**	**StepNum**	**Period**	**UX**	**UY**	**UZ**	**SumUX**	**SumUY**	**SumUZ**
Text	Text	Unitless	Sec	Unitless	Unitless	Unitless	Unitless	Unitless	Unitless
MODAL	Mode	1	0.148508	0.54	0.00001169	1.404E-07	0.54	0.00001169	1.404E-07
MODAL	Mode	2	0.11061	0.000001588	0.5	0.00001222	0.54	0.5	0.00001236
MODAL	Mode	3	0.087394	0.002709	0.00007795	0.000001587	0.55	0.5	0.00001395
MODAL	Mode	4	0.07777	0.0001883	0.004353	0.00003543	0.55	0.51	0.00004938
MODAL	Mode	5	0.073491	0.0001081	0.17	0.000000508	0.55	0.68	0.00004988
MODAL	Mode	6	0.072135	0.000003373	0.0004916	0.0001997	0.55	0.68	0.0002496
MODAL	Mode	7	0.06303	0.00205	0.001827	0.00002432	0.55	0.69	0.0002739
MODAL	Mode	8	0.054829	0.24	0.00222	1.232E-07	0.79	0.69	0.000274
MODAL	Mode	9	0.053398	0.009167	0.11	0.0001772	0.8	0.79	0.0004512
MODAL	Mode	10	0.050582	0.000124	0.002417	0.000001255	0.8	0.8	0.0004525
MODAL	Mode	11	0.048223	0.000001236	0.006505	0.00000166	0.8	0.8	0.0004542
MODAL	Mode	12	0.046552	0.00008595	0.000001027	0.00007143	0.8	0.8	0.0005256
MODAL	Mode	13	0.044561	0.000006348	0.03644	0.00002349	0.8	0.84	0.0005491

Table C. 19: Modal Participating Mass Ratios After adding the transverse flanges to the roof scenario #3									
Output	**StepType**	**StepNum**	**Period**	**UX**	**UY**	**UZ**	**SumUX**	**SumUY**	**SumUZ**
MODAL	Mode	14	0.043138	0.004025	0.003379	0.00001639	0.8	0.84	0.0005655
MODAL	Mode	15	0.04055	0.002543	0.0002025	0.00004839	0.8	0.84	0.0006139
MODAL	Mode	16	0.035768	0.00008126	0.00128	0.00000411	0.8	0.85	0.000618
MODAL	Mode	17	0.034765	0.004236	0.000007473	0.00004949	0.81	0.85	0.0006675
MODAL	Mode	18	0.032129	0.02407	0.000001866	0.00001558	0.83	0.85	0.000683
MODAL	Mode	19	0.031641	0.00006911	0.00001498	0.00008786	0.83	0.85	0.0007709
MODAL	Mode	20	0.029894	0.00004038	0.00004916	0.001416	0.83	0.85	0.002187

Table C. 20: Modal Participating Mass Ratios after adding diagonal braces to the floor (scenario #1)									
Output	**StepType**	**Num**	**Period**	**UX**	**UY**	**UZ**	**SumUX**	**SumUY**	**SumUZ**
Text	Text	Unitless	Sec	Unitless	Unitless	Unitless	Unitless	Unitless	Unitless
MODAL	Mode	1	0.153855	0.45	0.00003782	2.984E-08	0.45	0.00003782	2.984E-08
MODAL	Mode	2	0.109756	0.000007811	0.47	0.0000146	0.45	0.47	0.00001463
MODAL	Mode	3	0.091517	0.01971	0.00007654	3.936E-09	0.47	0.47	0.00001464
MODAL	Mode	4	0.072794	0.0002623	0.2	0.000003392	0.47	0.67	0.00001803
MODAL	Mode	5	0.070281	0.005853	0.00529	0.00003951	0.48	0.67	0.00005753
MODAL	Mode	6	0.07001	0.001957	0.00181	0.00001709	0.48	0.68	0.00007463
MODAL	Mode	7	0.057776	0.31	0.00001958	6.355E-07	0.79	0.68	0.00007526
MODAL	Mode	8	0.05232	0.002827	0.007307	0.0001897	0.79	0.68	0.000265
MODAL	Mode	9	0.051166	0.0007817	0.09529	0.00001873	0.79	0.78	0.0002837
MODAL	Mode	10	0.049665	0.0004432	0.001578	0.0001161	0.79	0.78	0.0003998
MODAL	Mode	11	0.047173	0.00126	0.002666	0.00001448	0.79	0.78	0.0004143
MODAL	Mode	12	0.046178	0.00002263	0.0146	0.00004875	0.79	0.8	0.0004631
MODAL	Mode	13	0.04542	0.004475	0.002824	0.00006907	0.8	0.8	0.0005322
MODAL	Mode	14	0.044595	0.002097	0.04102	0.00001643	0.8	0.84	0.0005486
MODAL	Mode	15	0.043781	0.003593	0.003432	0.00003295	0.8	0.85	0.0005815
MODAL	Mode	16	0.036075	0.000009916	0.001543	0.00001474	0.8	0.85	0.0005963
MODAL	Mode	17	0.034639	0.005404	0.00000331	0.004638	0.81	0.85	0.005234
MODAL	Mode	18	0.03365	0.001197	0.0000103	0.002939	0.81	0.85	0.008173
MODAL	Mode	19	0.031855	0.0179	0.00001619	0.0003202	0.83	0.85	0.008493
MODAL	Mode	20	0.030787	0.00137	0.00005843	0.00001791	0.83	0.85	0.008511

Table C. 21: Modal Participating Mass Ratios after adding diagonal braces to the roof (scenario #2)									
Output	**StepType**	**Num**	**Period**	**UX**	**UY**	**UZ**	**SumUX**	**SumUY**	**SumUZ**
Text	Text	Unitless	Sec	Unitless	Unitless	Unitless	Unitless	Unitless	Unitless
MODAL	Mode	1	0.154666	0.46	0.000041	5.063E-08	0.46	0.000041	5.063E-08
MODAL	Mode	2	0.107164	0.000002077	0.53	0.00002223	0.46	0.53	0.00002228

Table C. 21: Modal Participating Mass Ratios after adding diagonal braces to the roof (scenario #2)									
Output	**StepType**	**Num**	**Period**	**UX**	**UY**	**UZ**	**SumUX**	**SumUY**	**SumUZ**
Text	Text	Unitless	Sec	Unitless	Unitless	Unitless	Unitless	Unitless	Unitless
MODAL	Mode	3	0.091921	0.01194	0.0001111	4.974E-08	0.47	0.53	0.00002233
MODAL	Mode	4	0.072473	0.00014	0.15	0.000000563	0.47	0.67	0.00002289
MODAL	Mode	5	0.071945	0.000007935	0.003213	0.00008871	0.47	0.68	0.0001116
MODAL	Mode	6	0.067886	0.01846	0.002609	2.095E-07	0.49	0.68	0.0001118
MODAL	Mode	7	0.059978	0.29	0.00001715	2.383E-08	0.79	0.68	0.0001118
MODAL	Mode	8	0.052724	0.002505	0.07892	0.0001992	0.79	0.76	0.000311
MODAL	Mode	9	0.052082	0.00006281	0.01026	0.00006271	0.79	0.77	0.0003738
MODAL	Mode	10	0.048857	0.001444	0.02531	0.00004767	0.79	0.79	0.0004214
MODAL	Mode	11	0.047695	0.00159	0.0001942	0.000008804	0.79	0.79	0.0004302
MODAL	Mode	12	0.046762	0.0002495	0.0001903	0.00002101	0.79	0.79	0.0004512
MODAL	Mode	13	0.044547	0.0009071	0.04283	0.00004748	0.79	0.84	0.0004987
MODAL	Mode	14	0.043798	0.005443	0.003301	0.000003092	0.8	0.84	0.0005018
MODAL	Mode	15	0.037782	0.0004823	0.0002499	0.00008374	0.8	0.84	0.0005856
MODAL	Mode	16	0.036285	0.000001125	0.00176	0.00002461	0.8	0.84	0.0006102
MODAL	Mode	17	0.034758	0.0009813	0.000002085	0.002672	0.8	0.84	0.003282
MODAL	Mode	18	0.034081	0.001133	0.000007223	0.004993	0.8	0.84	0.008276
MODAL	Mode	19	0.032003	0.01815	0.00001818	0.0006205	0.82	0.84	0.008896
MODAL	Mode	20	0.030903	0.0006627	0.00008226	0.00005765	0.82	0.84	0.008954

Table C. 22: Modal Periods And Frequencies after adding diagonal braces to the roof (scenario #2)						
OutputCase	**StepType**	**StepNum**	**Period**	**Frequency**	**CircFreq**	**Eigenvalue**
``Text	Text	Unitless	Sec	Cyc/sec	rad/sec	rad2/sec2
MODAL	Mode	1	0.154666	6.465531089	40.62412994	1650.319934
MODAL	Mode	2	0.107164	9.331466072	58.63133052	3437.632919
MODAL	Mode	3	0.091921	10.87886285	68.35391122	4672.257179
MODAL	Mode	4	0.072473	13.79816399	86.69642125	7516.269457
MODAL	Mode	5	0.071945	13.89953048	87.33332568	7627.109775
MODAL	Mode	6	0.067886	14.73052271	92.55460387	8566.354698
MODAL	Mode	7	0.059978	16.67286352	104.7586911	10974.38336
MODAL	Mode	8	0.052724	18.96661174	119.1707362	14201.66437
MODAL	Mode	9	0.052082	19.20044773	120.6399711	14554.00262
MODAL	Mode	10	0.048857	20.46806146	128.604623	16539.14907
MODAL	Mode	11	0.047695	20.9666295	131.7372184	17354.69471
MODAL	Mode	12	0.046762	21.38474992	134.3643465	18053.77761
MODAL	Mode	13	0.044547	22.44844187	141.0477201	19894.45936
MODAL	Mode	14	0.043798	22.83202213	143.457826	20580.14783
MODAL	Mode	15	0.037782	26.46747369	166.3000418	27655.70391
MODAL	Mode	16	0.036285	27.5592294	173.1597452	29984.29736

MODAL	Mode	17	0.034758	28.77045177	180.7700799	32677.82178
MODAL	Mode	18	0.034081	29.34200186	184.3612349	33989.06495
MODAL	Mode	19	0.032003	31.24693542	196.3302856	38545.58103
MODAL	Mode	20	0.030903	32.35981147	203.322692	41340.11708

Table C. 23: Modal Participating Mass Ratios after adding diagonal braces to the floor and roof (scenario #3)

Output	StepType	Step	Period	UX	UY	UZ	SumUX	SumUY	SumUZ
Text	Text	Unitless	Sec	Unitless	Unitless	Unitless	Unitless	Unitless	Unitless
MODAL	Mode	1	0.152454	0.45	0.00006296	9.036E-10	0.45	0.00006296	9.036E-10
MODAL	Mode	2	0.107258	0.0000038	0.53	0.00002263	0.45	0.53	0.00002263
MODAL	Mode	3	0.091277	0.01441	0.00009055	2.655E-10	0.47	0.53	0.00002263
MODAL	Mode	4	0.072058	0.0003274	0.17	0.000001446	0.47	0.69	0.00002408
MODAL	Mode	5	0.069671	0.000003537	0.000001404	0.00003762	0.47	0.69	0.0000617
MODAL	Mode	6	0.067654	0.03234	0.004612	7.081E-08	0.5	0.7	0.00006177
MODAL	Mode	7	0.060858	0.29	0.00001732	5.318E-07	0.79	0.7	0.0000623
MODAL	Mode	8	0.052895	0.001581	0.08542	0.0001952	0.79	0.78	0.0002575
MODAL	Mode	9	0.052022	0.0001316	0.01203	0.00005207	0.79	0.8	0.0003096
MODAL	Mode	10	0.048082	0.003724	0.007576	0.00002238	0.79	0.8	0.000332
MODAL	Mode	11	0.04743	0.0003234	0.003685	8.137E-08	0.8	0.81	0.0003321
MODAL	Mode	12	0.046704	0.0001366	0.0003103	0.000006403	0.8	0.81	0.0003385
MODAL	Mode	13	0.044572	0.0007598	0.03614	0.00004118	0.8	0.84	0.0003796
MODAL	Mode	14	0.043787	0.0052	0.002908	0.00001094	0.8	0.85	0.0003906
MODAL	Mode	15	0.036104	1.14E-08	0.001622	0.00002121	0.8	0.85	0.0004118
MODAL	Mode	16	0.034588	0.002246	0.00000036	0.005265	0.8	0.85	0.005677
MODAL	Mode	17	0.033596	7.576E-08	0.00001682	0.002719	0.8	0.85	0.008396
MODAL	Mode	18	0.031879	0.01908	0.000001816	0.0002494	0.82	0.85	0.008645
MODAL	Mode	19	0.031566	0.001572	0.0001386	0.0004566	0.82	0.85	0.009102
MODAL	Mode	20	0.030679	0.00196	0.0002268	0.00007032	0.83	0.85	0.009172

Table C. 24: Modal Periods And Frequencies after adding diagonal braces to the floor and roof (scenario #3)

OutputCase	StepType	StepNum	Period	Frequency	CircFreq	Eigenvalue
Text	Text	Unitless	Sec	Cyc/sec	rad/sec	rad2/sec2
MODAL	Mode	1	0.152454	6.559334945	41.21351695	1698.55398
MODAL	Mode	2	0.107258	9.323333241	58.58023043	3431.643397
MODAL	Mode	3	0.091277	10.95567857	68.83655859	4738.471799
MODAL	Mode	4	0.072058	13.87766555	87.19594427	7603.132698
MODAL	Mode	5	0.069671	14.35324409	90.18409237	8133.170516
MODAL	Mode	6	0.067654	14.7810057	92.87179784	8625.170835
MODAL	Mode	7	0.060858	16.43175579	103.2437666	10659.27533

MODAL	Mode	8	0.052895	18.90537011	118.7859437	14110.10042
MODAL	Mode	9	0.052022	19.22263909	120.7794035	14587.6643
MODAL	Mode	10	0.048082	20.79794981	130.6773726	17076.57572
MODAL	Mode	11	0.04743	21.08368605	132.4727064	17549.01794
MODAL	Mode	12	0.046704	21.41140184	134.5318054	18098.80667
MODAL	Mode	13	0.044572	22.43552394	140.9665544	19871.56946
MODAL	Mode	14	0.043787	22.83770172	143.4935119	20590.38795
MODAL	Mode	15	0.036104	27.69764324	174.0294251	30286.24079
MODAL	Mode	16	0.034588	28.91181807	181.6583105	32999.74178
MODAL	Mode	17	0.033596	29.76534024	187.0211485	34976.90997
MODAL	Mode	18	0.031879	31.36812535	197.0917443	38845.15567
MODAL	Mode	19	0.031566	31.67922287	199.0464277	39619.48037
MODAL	Mode	20	0.030679	32.5958731	204.8059109	41945.46115

Table C. 25: Modal Participating Mass Ratios after installing Steel rods to the first floor (scenario #1)

Output	**Type**	**Step**	**Period**	**UX**	**UY**	**UZ**	**SumUX**	**SumUY**	**SumUZ**
Text	Text	Unitless	Sec	Unitless	Unitless	Unitless	Unitless	Unitless	Unitless
MODAL	Mode	1	0.488955	1.261E-09	2.668E-09	0.0006512	1.261E-09	2.668E-09	0.0006512
MODAL	Mode	2	0.15623	0.46	0.00001065	1.835E-07	0.46	0.00001066	0.0006514
MODAL	Mode	3	0.10986	0.00000189	0.47	0.00001261	0.46	0.47	0.000664
MODAL	Mode	4	0.092152	0.01689	0.0001055	3.811E-08	0.48	0.47	0.0006641
MODAL	Mode	5	0.074396	0.002727	0.004558	0.00003669	0.48	0.48	0.0007008
MODAL	Mode	6	0.073145	0.0001813	0.18	0.000000762	0.48	0.65	0.0007015
MODAL	Mode	7	0.072141	9.001E-07	0.0008217	0.00008521	0.48	0.66	0.0007867
MODAL	Mode	8	0.057474	0.03254	0.00001715	0.00005526	0.51	0.66	0.000842
MODAL	Mode	9	0.056619	0.27	0.00002648	0.000009894	0.78	0.66	0.0008519
MODAL	Mode	10	0.052307	0.003561	0.003	0.0001962	0.78	0.66	0.001048
MODAL	Mode	11	0.050515	0.0008757	0.09499	0.00009605	0.78	0.75	0.001144
MODAL	Mode	12	0.04787	0.0001994	0.02092	0.00002392	0.78	0.77	0.001168
MODAL	Mode	13	0.047113	0.001935	0.0003043	0.00001033	0.79	0.78	0.001178
MODAL	Mode	14	0.044894	0.002792	0.008033	0.00003175	0.79	0.78	0.00121
MODAL	Mode	15	0.044481	0.003825	0.05122	0.00003177	0.79	0.83	0.001242
MODAL	Mode	16	0.043811	0.003568	0.004576	0.000009459	0.8	0.84	0.001251
MODAL	Mode	17	0.036286	0.00001728	0.001913	0.00001394	0.8	0.84	0.001265
MODAL	Mode	18	0.03478	0.004389	0.00001074	0.002458	0.8	0.84	0.003724
MODAL	Mode	19	0.034067	0.0001088	0.000008047	0.004843	0.8	0.84	0.008567
MODAL	Mode	20	0.0321	0.01885	0.000007636	0.0005435	0.82	0.84	0.009111

Table C. 26: Modal Periods and Frequencies after installing Steel rods to the first floor (scenario #1)						
OutputCase	**StepType**	**StepNum**	**Period**	**Frequency**	**CircFreq**	**Eigenvalue**
Text	Text	Unitless	Sec	Cyc/sec	rad/sec	rad2/sec2
MODAL	Mode	1	0.488955	2.045179659	12.85024278	165.1287396
MODAL	Mode	2	0.15623	6.400811221	40.21748302	1617.44594
MODAL	Mode	3	0.10986	9.102514985	57.19278841	3271.015046
MODAL	Mode	4	0.092152	10.85160192	68.18262573	4648.870451
MODAL	Mode	5	0.074396	13.44155262	84.45576594	7132.7764
MODAL	Mode	6	0.073145	13.6713861	85.89985227	7378.784621
MODAL	Mode	7	0.072141	13.86170521	87.09566248	7585.654422
MODAL	Mode	8	0.057474	17.39916812	109.3221975	11951.34286
MODAL	Mode	9	0.056619	17.66176676	110.9721534	12314.81883
MODAL	Mode	10	0.052307	19.11789816	120.1212969	14429.12596
MODAL	Mode	11	0.050515	19.79600835	124.3819888	15470.87915
MODAL	Mode	12	0.04787	20.8900865	131.2562846	17228.21224
MODAL	Mode	13	0.047113	21.22534996	133.362807	17785.6383
MODAL	Mode	14	0.044894	22.27492169	139.9574607	19588.0908
MODAL	Mode	15	0.044481	22.48158238	141.2559481	19953.24287
MODAL	Mode	16	0.043811	22.82553333	143.4170556	20568.45184
MODAL	Mode	17	0.036286	27.55851461	173.1552541	29982.74202
MODAL	Mode	18	0.03478	28.75238583	180.6565682	32636.79563
MODAL	Mode	19	0.034067	29.35377963	184.4352369	34016.3566
MODAL	Mode	20	0.0321	31.15296204	195.7398333	38314.08236

Table C. 27: Modal Participating Mass Ratios after installing Steel rods to the roof (scenario #2)									
Output	**Type**	**Step**	**Period**	**UX**	**UY**	**UZ**	**SumUX**	**SumUY**	**SumUZ**
Text	Text	Unitless	Sec	Unitless	Unitless	Unitless	Unitless	Unitless	Unitless
MODAL	Mode	1	0.488955	1.09E-09	1.029E-11	0.0006519	1.09E-09	1.029E-11	0.0006519
MODAL	Mode	2	0.156175	0.46	0.00001891	1.182E-07	0.46	0.00001891	0.0006521
MODAL	Mode	3	0.109765	0.000004606	0.47	0.00001479	0.46	0.47	0.0006668
MODAL	Mode	4	0.092163	0.01678	0.0000983	5.297E-08	0.48	0.47	0.0006669
MODAL	Mode	5	0.07321	0.00001213	0.18	1.409E-07	0.48	0.66	0.000667
MODAL	Mode	6	0.072378	0.00001838	0.001375	0.00009747	0.48	0.66	0.0007645
MODAL	Mode	7	0.069766	0.005528	0.0001444	0.00001071	0.48	0.66	0.0007752
MODAL	Mode	8	0.056776	0.3	0.00009091	4.723E-07	0.78	0.66	0.0007757
MODAL	Mode	9	0.053525	0.001541	0.01208	0.000009365	0.78	0.67	0.0007851
MODAL	Mode	10	0.052306	0.003203	0.002263	0.0002004	0.78	0.67	0.0009855
MODAL	Mode	11	0.049964	0.0001575	0.08128	0.0001453	0.78	0.75	0.001131
MODAL	Mode	12	0.048042	0.0002405	0.02176	0.00001508	0.78	0.77	0.001146

MODAL	Mode	13	0.047088	0.001447	0.0003999	0.0000121	0.79	0.78	0.001158
MODAL	Mode	14	0.044597	0.0001983	0.05914	0.00007243	0.79	0.83	0.00123
MODAL	Mode	15	0.043935	0.009712	0.0001595	3.986E-08	0.8	0.83	0.00123
MODAL	Mode	16	0.043594	0.0003588	0.004202	0.00002606	0.8	0.84	0.001256
MODAL	Mode	17	0.036297	0.00001313	0.00194	0.00001852	0.8	0.84	0.001275
MODAL	Mode	18	0.034783	0.004232	0.00001067	0.002421	0.8	0.84	0.003696
MODAL	Mode	19	0.034073	0.0001325	0.00000889	0.004985	0.8	0.84	0.008681
MODAL	Mode	20	0.032114	0.01774	0.000001257	0.0004872	0.82	0.84	0.009168

Table C. 28: Modal Periods And Frequencies after installing Steel rods to the roof (scenario #2)

OutputCase	StepType	StepNum	Period	Frequency	CircFreq	Eigenvalue
Text	Text	Unitless	Sec	Cyc/sec	rad/sec	rad2/sec2
MODAL	Mode	1	0.488955	2.045176768	12.85022462	165.1282728
MODAL	Mode	2	0.156175	6.403074085	40.23170101	1618.589766
MODAL	Mode	3	0.109765	9.110400674	57.24233566	3276.684992
MODAL	Mode	4	0.092163	10.85037999	68.17494816	4647.823557
MODAL	Mode	5	0.07321	13.65935753	85.82427451	7365.806096
MODAL	Mode	6	0.072378	13.81644288	86.81127091	7536.196758
MODAL	Mode	7	0.069766	14.3336073	90.06071079	8110.931628
MODAL	Mode	8	0.056776	17.6132276	110.6671729	12247.22316
MODAL	Mode	9	0.053525	18.68280743	117.3875411	13779.83481
MODAL	Mode	10	0.052306	19.11840239	120.124465	14429.88709
MODAL	Mode	11	0.049964	20.01426581	125.7533409	15813.90274
MODAL	Mode	12	0.048042	20.81507536	130.7849757	17104.70987
MODAL	Mode	13	0.047088	21.23678283	133.4346419	17804.80365
MODAL	Mode	14	0.044597	22.42289537	140.8872067	19849.20501
MODAL	Mode	15	0.043935	22.7609071	143.010997	20452.14528
MODAL	Mode	16	0.043594	22.93888674	144.1292761	20773.24824
MODAL	Mode	17	0.036297	27.55017257	173.1028395	29964.59305
MODAL	Mode	18	0.034783	28.74989161	180.6408966	32631.13351
MODAL	Mode	19	0.034073	29.34901426	184.4052951	34005.31288
MODAL	Mode	20	0.032114	31.13924715	195.6536602	38280.35473

Table C. 29: Modal Participating Mass Ratios after installing Steel rods to the floor and roof. (scenario #3)

Output	Type	Step	Period	UX	UY	UZ	SumUX	SumUY	SumUZ
Text	Text	Unitless	Sec	Unitless	Unitless	Unitless	Unitless	Unitless	Unitless
MODAL	Mode	1	0.488955	1.536E-09	7.044E-11	0.0003875	1.536E-09	7.044E-11	0.0003875
MODAL	Mode	2	0.488955	7.014E-10	2.756E-09	0.000914	2.238E-09	2.826E-09	0.001301

Table C. 29: Modal Participating Mass Ratios after installing Steel rods to the floor and roof. (scenario #3)									
Output	**Type**	**Step**	**Period**	**UX**	**UY**	**UZ**	**SumUX**	**SumUY**	**SumUZ**
Text	Text	Unitless	Sec	Unitless	Unitless	Unitless	Unitless	Unitless	Unitless
MODAL	Mode	3	0.156137	0.46	0.00002676	1.065E-07	0.46	0.00002676	0.001302
MODAL	Mode	4	0.109728	0.00000583	0.47	0.00001481	0.46	0.47	0.001316
MODAL	Mode	5	0.092153	0.01677	0.0000951	1.994E-08	0.48	0.47	0.001316
MODAL	Mode	6	0.073165	0.00003653	0.18	3.572E-08	0.48	0.66	0.001316
MODAL	Mode	7	0.07214	0.00000319	0.0007985	0.00008359	0.48	0.66	0.0014
MODAL	Mode	8	0.06915	0.006025	0.001176	0.000006477	0.48	0.66	0.001407
MODAL	Mode	9	0.056807	0.3	0.00007583	7.041E-07	0.78	0.66	0.001407
MODAL	Mode	10	0.05231	0.00355	0.00388	0.0001928	0.78	0.66	0.0016
MODAL	Mode	11	0.05113	0.00139	0.07743	0.00001092	0.79	0.74	0.001611
MODAL	Mode	12	0.048971	0.0005255	0.007873	0.00009568	0.79	0.75	0.001707
MODAL	Mode	13	0.047681	0.0001268	0.0246	0.00007033	0.79	0.77	0.001777
MODAL	Mode	14	0.046933	0.0007601	0.004442	5.537E-08	0.79	0.78	0.001777
MODAL	Mode	15	0.044597	0.0003193	0.06037	0.00007176	0.79	0.84	0.001849
MODAL	Mode	16	0.043885	0.007622	0.001519	0.000001368	0.79	0.84	0.00185
MODAL	Mode	17	0.043073	0.001959	0.001248	0.00006892	0.8	0.84	0.001919
MODAL	Mode	18	0.036285	0.00001525	0.001901	0.00001474	0.8	0.84	0.001934
MODAL	Mode	19	0.034786	0.004268	0.00001011	0.002432	0.8	0.84	0.004365
MODAL	Mode	20	0.034069	0.0001302	0.000007793	0.004865	0.8	0.84	0.00923

Table C. 30: Modal Periods and Frequencies after installing Steel rods to the floor and roof						
OutputCase	**StepType**	**StepNum**	**Period**	**Frequency**	**CircFreq**	**Eigenvalue**
Text	Text	Unitless	Sec	Cyc/sec	rad/sec	rad2/sec2
MODAL	Mode	1	0.488955	2.045176761	12.85022457	165.1282716
MODAL	Mode	2	0.488955	2.045179828	12.85024384	165.1287669
MODAL	Mode	3	0.156137	6.404632789	40.24149464	1619.377891
MODAL	Mode	4	0.109728	9.113432972	57.26138814	3278.866572
MODAL	Mode	5	0.092153	10.85157037	68.18242752	4648.843422
MODAL	Mode	6	0.073165	13.66770144	85.87670089	7374.807756
MODAL	Mode	7	0.07214	13.86184636	87.09654941	7585.808919
MODAL	Mode	8	0.06915	14.46126171	90.86278713	8256.046084
MODAL	Mode	9	0.056807	17.60340849	110.6054776	12233.57167
MODAL	Mode	10	0.05231	19.11688811	120.1149505	14427.60133
MODAL	Mode	11	0.05113	19.55812432	122.8873193	15101.29325
MODAL	Mode	12	0.048971	20.42023137	128.3040977	16461.94149
MODAL	Mode	13	0.047681	20.97288831	131.7765437	17365.05747
MODAL	Mode	14	0.046933	21.30705374	133.876167	17922.82808
MODAL	Mode	15	0.044597	22.42290007	140.8872363	19849.21335

Table C. 30: Modal Periods and Frequencies after installing Steel rods to the floor and roof						
OutputCase	**StepType**	**StepNum**	**Period**	**Frequency**	**CircFreq**	**Eigenvalue**
Text	Text	Unitless	Sec	Cyc/sec	rad/sec	rad2/sec2
MODAL	Mode	16	0.043885	22.78679392	143.1736487	20498.69369
MODAL	Mode	17	0.043073	23.21653467	145.8737895	21279.16248
MODAL	Mode	18	0.036285	27.5594847	173.1613493	29984.8529
MODAL	Mode	19	0.034786	28.74682111	180.6216041	32624.16385
MODAL	Mode	20	0.034069	29.35182584	184.4229609	34011.8285

Table C. 31: Modal Participating Mass Ratios for repointing the shell model full scale									
Output	**Type**	**Num**	**Period**	**UX**	**UY**	**UZ**	**SumUX**	**SumUY**	**SumUZ**
Text	Text	Unitless	Sec	Unitless	Unitless	Unitless	Unitless	Unitless	Unitless
MODAL	Mode	1	0.091713	0.41	1.344E-08	6.004E-08	0.41	1.344E-08	6.004E-08
MODAL	Mode	2	0.064918	9.932E-07	0.31	0.000005582	0.41	0.31	0.000005642
MODAL	Mode	3	0.051037	0.04011	0.00001654	7.354E-11	0.45	0.31	0.000005642
MODAL	Mode	4	0.042915	0.001197	0.008561	0.000032	0.45	0.31	0.00003764
MODAL	Mode	5	0.039271	0.0002448	0.31	0.000005453	0.45	0.62	0.0000431
MODAL	Mode	6	0.037457	0.00002064	0.003351	0.00001255	0.45	0.63	0.00005564
MODAL	Mode	7	0.032717	0.0007662	0.002927	0.00004623	0.45	0.63	0.0001019
MODAL	Mode	8	0.028909	0.27	0.0001229	0.00003761	0.72	0.63	0.0001395
MODAL	Mode	9	0.02725	0.008691	0.001594	0.001532	0.73	0.63	0.001671
MODAL	Mode	10	0.02707	0.01312	0.001541	0.00001601	0.74	0.63	0.001687
MODAL	Mode	11	0.025539	0.006906	0.09024	0.000008391	0.75	0.72	0.001696
MODAL	Mode	12	0.025433	0.003594	0.01364	0.00008108	0.75	0.74	0.001777
MODAL	Mode	13	0.02435	0.0001214	0.0007787	0.001002	0.75	0.74	0.002779
MODAL	Mode	14	0.023341	0.009087	0.002916	3.658E-08	0.76	0.74	0.002779
MODAL	Mode	15	0.022997	0.03684	0.0004127	0.0000042	0.8	0.74	0.002783
MODAL	Mode	16	0.022794	0.00006072	0.08882	0.0001507	0.8	0.83	0.002934
MODAL	Mode	17	0.0214	0.0001115	1.042E-07	0.01367	0.8	0.83	0.0166
MODAL	Mode	18	0.021161	0.000005076	0.0002421	0.00004232	0.8	0.83	0.01664
MODAL	Mode	19	0.020664	0.001144	0.00306	0.00005484	0.8	0.83	0.0167
MODAL	Mode	20	0.01983	0.0006423	5.106E-07	0.000003248	0.8	0.83	0.0167

Table C. 32: Modal Periods and Frequencies for repointing the shell model full scale						
OutputCase	**StepType**	**StepNum**	**Period**	**Frequency**	**CircFreq**	**Eigenvalue**
Text	Text	Unitless	Sec	Cyc/sec	rad/sec	rad2/sec2
MODAL	Mode	1	0.091713	10.90362772	68.50951349	4693.553439
MODAL	Mode	2	0.064918	15.40396725	96.78598069	9367.526058

Table C. 32: Modal Periods and Frequencies for repointing the shell model full scale						
OutputCase	**StepType**	**StepNum**	**Period**	**Frequency**	**CircFreq**	**Eigenvalue**
Text	Text	Unitless	Sec	Cyc/sec	rad/sec	rad2/sec2
MODAL	Mode	3	0.051037	19.59380081	123.1114813	15156.43684
MODAL	Mode	4	0.042915	23.30202608	146.4109479	21436.16567
MODAL	Mode	5	0.039271	25.464372	159.997368	25599.15777
MODAL	Mode	6	0.037457	26.69759524	167.7459382	28138.69978
MODAL	Mode	7	0.032717	30.56479666	192.0442813	36881.00598
MODAL	Mode	8	0.028909	34.59117066	217.3427353	47237.86458
MODAL	Mode	9	0.02725	36.69774384	230.5787249	53166.54838
MODAL	Mode	10	0.02707	36.94190797	232.1128534	53876.37669
MODAL	Mode	11	0.025539	39.1552987	246.0199975	60525.83918
MODAL	Mode	12	0.025433	39.31957009	247.052145	61034.76237
MODAL	Mode	13	0.02435	41.06858022	258.0414998	66585.41564
MODAL	Mode	14	0.023341	42.84257967	269.1878671	72462.10778
MODAL	Mode	15	0.022997	43.48387977	273.2172745	74647.67906
MODAL	Mode	16	0.022794	43.87207701	275.6563897	75986.44517
MODAL	Mode	17	0.0214	46.72821419	293.6020288	86202.15132
MODAL	Mode	18	0.021161	47.25643338	296.9209279	88162.03743
MODAL	Mode	19	0.020664	48.39304124	304.0624457	92453.97089
MODAL	Mode	20	0.01983	50.42868367	316.8527643	100395.6742

Table C. 33: Modal Participating Mass Ratios after concrete shotcrete on side									
Output	**StepType**	**Step**	**Period**	**UX**	**UY**	**UZ**	**SumUX**	**SumUY**	**SumUZ**
Text	Text		Sec	Unitless	Unitless	Unitless	Unitless	Unitless	Unitless
MODAL	Mode	1	0.098394	0.48	0.0002013	0.00000164	0.48	0.0002013	0.00000164
MODAL	Mode	2	0.064948	0.000005128	0.57	0.00009104	0.48	0.57	0.00009267
MODAL	Mode	3	0.059995	0.0004475	0.0213	0.0001368	0.48	0.59	0.0002295
MODAL	Mode	4	0.054404	0.03154	0.0002464	0.04684	0.51	0.59	0.04707
MODAL	Mode	5	0.04449	0.0007926	0.16	0.01042	0.51	0.75	0.05749
MODAL	Mode	6	0.042786	0.19	0.002219	0.0002732	0.7	0.76	0.05776
MODAL	Mode	7	0.039038	0.01568	0.0009246	0.0002433	0.71	0.76	0.058
MODAL	Mode	8	0.03668	0.01397	0.00008931	0.001591	0.73	0.76	0.05959
MODAL	Mode	9	0.030756	0.0009332	0.002377	0.02425	0.73	0.76	0.08384
MODAL	Mode	10	0.030623	0.002291	0.001966	0.003296	0.73	0.76	0.08714
MODAL	Mode	11	0.029071	0.01996	0.006609	0.003446	0.75	0.77	0.09059
MODAL	Mode	12	0.0284	2.274E-07	0.004542	0.012	0.75	0.77	0.1
MODAL	Mode	13	0.027543	0.008095	0.001985	0.11	0.76	0.77	0.22
MODAL	Mode	14	0.024734	0.0003307	0.02309	0.001175	0.76	0.8	0.22

Table C. 33: Modal Participating Mass Ratios after concrete shotcrete on side									
Output	StepType	Step	Period	UX	UY	UZ	SumUX	SumUY	SumUZ
Text	Text		Sec	Unitless	Unitless	Unitless	Unitless	Unitless	Unitless
MODAL	Mode	15	0.024591	0.008857	0.0037	0.07889	0.77	0.8	0.3
MODAL	Mode	16	0.023502	0.01181	0.003042	0.0004114	0.78	0.8	0.3
MODAL	Mode	17	0.023453	0.004545	0.01736	0.03572	0.79	0.82	0.33
MODAL	Mode	18	0.02177	0.00001635	0.001486	0.008188	0.79	0.82	0.34
MODAL	Mode	19	0.021076	0.001937	0.001129	0.17	0.79	0.82	0.51
MODAL	Mode	20	0.02095	0.0003322	0.0002312	0.01527	0.79	0.82	0.53

Table C. 34: Modal Periods and Frequencies after concrete shotcrete one side						
OutputCase	StepType	StepNum	Period	Frequency	CircFreq	Eigenvalue
Text	Text	Unitless	Sec	Cyc/sec	rad/sec	rad2/sec2
MODAL	Mode	1	0.098394	10.1631872	63.85718847	4077.74052
MODAL	Mode	2	0.064948	15.39694044	96.74182996	9358.981664
MODAL	Mode	3	0.059995	16.66805803	104.7284973	10968.05815
MODAL	Mode	4	0.054404	18.38110753	115.4919048	13338.38006
MODAL	Mode	5	0.04449	22.47703337	141.2273658	19945.16886
MODAL	Mode	6	0.042786	23.37231733	146.8526008	21565.68637
MODAL	Mode	7	0.039038	25.61621162	160.9514045	25905.3546
MODAL	Mode	8	0.03668	27.26260969	171.2960286	29342.32942
MODAL	Mode	9	0.030756	32.51369322	204.2895595	41734.22413
MODAL	Mode	10	0.030623	32.65533766	205.1795378	42098.64272
MODAL	Mode	11	0.029071	34.39904957	216.1356028	46714.59882
MODAL	Mode	12	0.0284	35.21109622	221.2378424	48946.18293
MODAL	Mode	13	0.027543	36.30736951	228.1259306	52041.44023
MODAL	Mode	14	0.024734	40.43056375	254.0327241	64532.62493
MODAL	Mode	15	0.024591	40.66516088	255.5067413	65283.69487
MODAL	Mode	16	0.023502	42.54968203	267.3475369	71474.70551
MODAL	Mode	17	0.023453	42.63932842	267.9108019	71776.19775
MODAL	Mode	18	0.02177	45.93509509	288.6187145	83300.76239
MODAL	Mode	19	0.021076	47.44835624	298.1268147	88879.59767
MODAL	Mode	20	0.02095	47.73370289	299.9197007	89951.82685

Table C. 35: Modal Participating Mass Ratios after concrete shotcrete both side of the wall									
Output	Step	Num	Period	UX	UY	UZ	SumUX	SumUY	SumUZ
Text	Text		Sec	Unitless	Unitless	Unitless	Unitless	Unitless	Unitless
MODAL	Mode	1	0.055142	0.54	0.00003448	9.926E-07	0.54	0.00003448	9.926E-07

Table C. 35: Modal Participating Mass Ratios after concrete shotcrete both side of the wall									
Output	**Step**	**Num**	**Period**	**UX**	**UY**	**UZ**	**SumUX**	**SumUY**	**SumUZ**
Text	Text		Sec	Unitless	Unitless	Unitless	Unitless	Unitless	Unitless
MODAL	Mode	2	0.045	2.032E-08	0.59	3.965E-08	0.54	0.59	0.000001032
MODAL	Mode	3	0.036917	0.0006933	0.002015	0.00003452	0.54	0.59	0.00003555
MODAL	Mode	4	0.028135	0.04115	0.008804	0.0154	0.58	0.6	0.01544
MODAL	Mode	5	0.027473	0.003949	0.15	0.0007125	0.59	0.75	0.01615
MODAL	Mode	6	0.02542	0.069	0.03333	0.0005244	0.65	0.79	0.01668
MODAL	Mode	7	0.025007	0.11	0.01869	0.0005075	0.76	0.81	0.01718
MODAL	Mode	8	0.023718	0.0005612	0.0002692	0.0003254	0.76	0.81	0.01751
MODAL	Mode	9	0.021913	0.0003649	0.0007698	0.00001965	0.76	0.81	0.01753
MODAL	Mode	10	0.020862	0.0005789	3.916E-07	0.0006414	0.76	0.81	0.01817
MODAL	Mode	11	0.020292	0.02413	0.0001101	0.01426	0.79	0.81	0.03243
MODAL	Mode	12	0.019724	0.00003301	0.000001465	5.103E-07	0.79	0.81	0.03243
MODAL	Mode	13	0.019552	0.001246	0.00001157	0.00873	0.79	0.81	0.04116
MODAL	Mode	14	0.018816	0.0002029	0.000002036	0.00003783	0.79	0.81	0.0412
MODAL	Mode	15	0.018611	0.0009375	0.0001161	0.001436	0.79	0.81	0.04264
MODAL	Mode	16	0.018273	0.000001342	0.000000213	9.183E-07	0.79	0.81	0.04264
MODAL	Mode	17	0.017568	0.0009704	0.004584	0.003695	0.79	0.81	0.04633
MODAL	Mode	18	0.016394	0.0004502	0.001204	0.002728	0.79	0.81	0.04906
MODAL	Mode	19	0.016263	0.0001261	0.0002013	0.006356	0.79	0.81	0.05541
MODAL	Mode	20	0.016037	0.002717	0.0003949	0.02055	0.8	0.81	0.07597

Table C. 36: Modal Periods and Frequencies after concrete shotcrete both side of the wall						
OutputCase	**StepType**	**StepNum**	**Period**	**Frequency**	**CircFreq**	**Eigenvalue**
Text	Text	Unitless	Sec	Cyc/sec	rad/sec	rad2/sec2
MODAL	Mode	1	0.055142	18.13485787	113.9446725	12983.38839
MODAL	Mode	2	0.045	22.22221742	139.62631	19495.50645
MODAL	Mode	3	0.036917	27.08747605	170.1956315	28966.55298
MODAL	Mode	4	0.028135	35.54320352	223.3245341	49873.84753
MODAL	Mode	5	0.027473	36.39917078	228.7027351	52304.94102
MODAL	Mode	6	0.02542	39.33873747	247.1725773	61094.28294
MODAL	Mode	7	0.025007	39.98806968	251.2524519	63127.79457
MODAL	Mode	8	0.023718	42.1621363	264.9125153	70178.64078
MODAL	Mode	9	0.021913	45.63590546	286.7388507	82219.16849
MODAL	Mode	10	0.020862	47.93382723	301.177119	90707.65699
MODAL	Mode	11	0.020292	49.28115218	309.6426113	95878.54673
MODAL	Mode	12	0.019724	50.6997612	318.5559947	101477.9217
MODAL	Mode	13	0.019552	51.14436005	321.3494916	103265.4958
MODAL	Mode	14	0.018816	53.14693879	333.9320649	111510.624

Table C. 36: Modal Periods and Frequencies after concrete shotcrete both side of the wall						
OutputCase	**StepType**	**StepNum**	**Period**	**Frequency**	**CircFreq**	**Eigenvalue**
Text	Text	Unitless	Sec	Cyc/sec	rad/sec	rad2/sec2
MODAL	Mode	15	0.018611	53.73231897	337.610117	113980.5911
MODAL	Mode	16	0.018273	54.72497727	343.8471731	118230.8785
MODAL	Mode	17	0.017568	56.92197642	357.6513259	127914.4709
MODAL	Mode	18	0.016394	60.99897904	383.2678889	146894.2746
MODAL	Mode	19	0.016263	61.48999211	386.3530149	149268.6522
MODAL	Mode	20	0.016037	62.35626688	391.7959799	153504.0899

Table C. 37: Modal Participating Mass Ratios Shell model nonlinear analysis lateral pushover results (X&Y)									
Output	**Type**	**Num**	**Period**	**UX**	**UY**	**UZ**	**SumUX**	**SumUY**	**SumUZ**
Text	Text	Unitless	Sec	Unitless	Unitless	Unitless	Unitless	Unitless	Unitless
MODAL	Mode	1	0.104791	0.4	6.586E-07	4.275E-08	0.4	6.586E-07	4.275E-08
MODAL	Mode	2	0.072929	1.953E-08	0.31	0.000003208	0.4	0.31	0.000003251
MODAL	Mode	3	0.058114	0.0282	0.00002458	1.078E-08	0.43	0.31	0.000003262
MODAL	Mode	4	0.047649	0.001566	0.02801	0.00001797	0.43	0.34	0.00002123
MODAL	Mode	5	0.046276	0.0004118	0.11	0.000006936	0.43	0.45	0.00002816
MODAL	Mode	6	0.045523	0.00007552	0.11	1.333E-07	0.43	0.57	0.0000283
MODAL	Mode	7	0.036411	0.001441	0.000003069	0.00002327	0.43	0.57	0.00005156
MODAL	Mode	8	0.032727	0.01829	0.000631	0.0004849	0.45	0.57	0.0005365
MODAL	Mode	9	0.031449	0.25	0.00007609	0.000003633	0.7	0.57	0.0005401
MODAL	Mode	10	0.030755	0.02501	0.00641	0.000000955	0.73	0.57	0.0005411
MODAL	Mode	11	0.029887	0.01125	0.0001257	0.0001259	0.74	0.57	0.000667
MODAL	Mode	12	0.02895	0.006685	0.06188	0.00003834	0.74	0.63	0.0007053
MODAL	Mode	13	0.028053	0.0005539	0.009385	0.0004838	0.74	0.64	0.001189
MODAL	Mode	14	0.026946	0.0007522	0.16	0.00002292	0.74	0.8	0.001212
MODAL	Mode	15	0.025782	0.002761	0.007433	0.002461	0.75	0.81	0.003673
MODAL	Mode	16	0.02534	0.004923	0.01789	0.000295	0.75	0.83	0.003968
MODAL	Mode	17	0.024086	0.04264	0.00001213	0.00004206	0.79	0.83	0.00401
MODAL	Mode	18	0.023242	0.001218	0.002201	0.000002527	0.8	0.83	0.004013
MODAL	Mode	19	0.021743	0.0005995	0.0001937	0.000007557	0.8	0.83	0.004021
MODAL	Mode	20	0.021371	0.00006143	0.0003475	0.000004518	0.8	0.83	0.004025

Table C. 38: Modal Participating Mass Ratios Shell model nonlinear analysis lateral pushover results (Z)									
Output	**Type**	**Num**	**Period**	**RX**	**RY**	**RZ**	**SumRX**	**SumRY**	**SumRZ**
Text	Text	Unitless	Sec	Unitless	Unitless	Unitless	Unitless	Unitless	Unitless
MODAL	Mode	1	0.104791	5.195E-07	0.05746	0.0007598	5.2E-07	0.05746	0.0007598

Table C. 38: Modal Participating Mass Ratios Shell model nonlinear analysis lateral pushover results (Z)									
Output	**Type**	**Num**	**Period**	**RX**	**RY**	**RZ**	**SumRX**	**SumRY**	**SumRZ**
Text	Text	Unitless	Sec	Unitless	Unitless	Unitless	Unitless	Unitless	Unitless
MODAL	Mode	2	0.072929	0.13	0.00002226	0.0002146	0.13	0.05748	0.0009744
MODAL	Mode	3	0.058114	0.00001795	0.12	0.00008181	0.13	0.17	0.001056
MODAL	Mode	4	0.047649	0.002076	0.001278	0.1	0.13	0.18	0.1
MODAL	Mode	5	0.046276	0.004608	4.352E-07	0.01442	0.14	0.18	0.12
MODAL	Mode	6	0.045523	0.004551	0.0002426	0.01765	0.14	0.18	0.13
MODAL	Mode	7	0.036411	0.0003245	0.0005133	0.11	0.14	0.18	0.24
MODAL	Mode	8	0.032727	0.0008687	0.008588	0.002094	0.14	0.18	0.25
MODAL	Mode	9	0.031449	0.00008188	0.09014	0.01929	0.14	0.27	0.27
MODAL	Mode	10	0.030755	0.004274	0.006903	0.008217	0.15	0.28	0.27
MODAL	Mode	11	0.029887	0.000356	0.0001094	0.001559	0.15	0.28	0.28
MODAL	Mode	12	0.02895	0.05893	0.000697	0.01039	0.21	0.28	0.29
MODAL	Mode	13	0.028053	0.01008	0.03517	9.597E-07	0.22	0.32	0.29
MODAL	Mode	14	0.026946	1.892E-06	0.0004979	0.01631	0.22	0.32	0.3
MODAL	Mode	15	0.025782	0.001775	0.002042	0.01839	0.22	0.32	0.32
MODAL	Mode	16	0.02534	0.004086	0.002002	0.32	0.22	0.32	0.64
MODAL	Mode	17	0.024086	0.0002147	0.006789	0.007218	0.22	0.33	0.64
MODAL	Mode	18	0.023242	0.0003878	0.000239	0.05408	0.22	0.33	0.7
MODAL	Mode	19	0.021743	0.002309	0.000009676	0.04747	0.23	0.33	0.75
MODAL	Mode	20	0.021371	0.00002933	0.00001402	0.006034	0.23	0.33	0.75

Table C. 39: Modal Periods And Frequencies FARAME model with hinges and E=840						
OutputCase	**StepType**	**StepNum**	**Period**	**Frequency**	**CircFreq**	**Eigenvalue**
Text	Text	Unitless	Sec	Cyc/sec	rad/sec	rad2/sec2
MODAL	Mode	1	0.222527	4.493832588	28.23558289	797.248141
MODAL	Mode	2	0.183018	5.463958076	34.3310611	1178.621756
MODAL	Mode	3	0.130589	7.657613876	48.11420699	2314.976914
MODAL	Mode	4	0.108918	9.181185299	57.68708857	3327.800188
MODAL	Mode	5	0.105118	9.513095813	59.77254384	3572.756997
MODAL	Mode	6	0.095837	10.43439045	65.56120875	4298.272093
MODAL	Mode	7	0.091549	10.92308372	68.63175917	4710.318366
MODAL	Mode	8	0.090321	11.07158988	69.56485084	4839.268472
MODAL	Mode	9	0.083099	12.03389459	75.61118966	5717.052001
MODAL	Mode	10	0.078835	12.68478909	79.70088043	6352.230341
MODAL	Mode	11	0.077492	12.90448991	81.0813014	6574.177437
MODAL	Mode	12	0.061437	16.27681136	102.270222	10459.1983
MODAL	Mode	13	0.058292	17.1550639	107.7884455	11618.34898
MODAL	Mode	14	0.054431	18.37182449	115.4335777	13324.91087

Table C. 39: Modal Periods And Frequencies FARAME model with hinges and E=840						
OutputCase	**StepType**	**StepNum**	**Period**	**Frequency**	**CircFreq**	**Eigenvalue**
Text	Text	Unitless	Sec	Cyc/sec	rad/sec	rad2/sec2
MODAL	Mode	15	0.051511	19.41337744	121.9778479	14878.59537
MODAL	Mode	16	0.048411	20.65662047	129.7893742	16845.28166
MODAL	Mode	17	0.04467	22.3863397	140.6575207	19784.53812
MODAL	Mode	18	0.043195	23.15070705	145.4601824	21158.66466
MODAL	Mode	19	0.042951	23.28213781	146.2859862	21399.58976
MODAL	Mode	20	0.042118	23.7429833	149.1815638	22255.13898

Table C. 40: Modal Participating Mass Ratios frame model with hinges and E=840									
Case	**Type**	**StepNum**	**Period**	**UX**	**UY**	**UZ**	**SumUX**	**SumUY**	**SumUZ**
Text	Text	Unitless	Sec	Unitless	Unitless	Unitless	Unitless	Unitless	Unitless
MODAL	Mode	1	0.222527	0.004156	0.16	4.536E-07	0.004156	0.16	4.536E-07
MODAL	Mode	2	0.183018	0.52	0.00351	0.000003828	0.53	0.17	0.000004282
MODAL	Mode	3	0.130589	0.002494	0.28	0.000006566	0.53	0.45	0.00001085
MODAL	Mode	4	0.108918	0.0006924	0.02275	2.526E-08	0.53	0.47	0.00001087
MODAL	Mode	5	0.105118	0.009603	0.003713	0.000008367	0.54	0.47	0.00001924
MODAL	Mode	6	0.095837	0.02727	0.13	0.00002087	0.57	0.6	0.00004011
MODAL	Mode	7	0.091549	0.16	0.005513	0.00000155	0.72	0.6	0.00004166
MODAL	Mode	8	0.090321	0.00113	0.001265	7.443E-08	0.72	0.61	0.00004174
MODAL	Mode	9	0.083099	0.003792	0.00005168	0.000003405	0.73	0.61	0.00004514
MODAL	Mode	10	0.078835	0.004681	0.16	0.00002039	0.73	0.77	0.00006553
MODAL	Mode	11	0.077492	0.0772	0.004401	0.00001058	0.81	0.77	0.0000761
MODAL	Mode	12	0.061437	0.003025	0.0003937	7.122E-07	0.81	0.77	0.00007681
MODAL	Mode	13	0.058292	0.005102	0.000009482	0.000004505	0.82	0.77	0.00008132
MODAL	Mode	14	0.054431	0.0001795	0.00004834	0.0000124	0.82	0.77	0.00009372
MODAL	Mode	15	0.051511	0.0008436	0.00003838	0.000008889	0.82	0.77	0.0001026
MODAL	Mode	16	0.048411	0.02059	0.00001009	0.0000795	0.84	0.78	0.0001821
MODAL	Mode	17	0.04467	0.0001884	0.0002436	0.00006374	0.84	0.78	0.0002459
MODAL	Mode	18	0.043195	0.0003641	0.0003639	0.0004391	0.84	0.78	0.000685
MODAL	Mode	19	0.042951	0.00009731	0.0003249	0.00001104	0.84	0.78	0.000696
MODAL	Mode	20	0.042118	6.24E-08	0.0006133	0.001368	0.84	0.78	0.002064